Master's thesis

NTNU
Norwegian University of Science and Technology
Faculty of Natural Sciences
Department of Chemistry

Monica Eian Løberg

Synthesis of Phenothiazine Dyes Containing Thiophene and Diketopyrrolopyrrole pi-Bridge for Use in DSSCs

Master's thesis in Chemical Engineering and Biotechnology
Supervisor: Bård Helge Hoff, Audun Formo Buene
June 2019

NTNU
Kunnskap for en bedre verden

Monica Eian Løberg

Synthesis of Phenothiazine Dyes Containing Thiophene and Diketopyrrolopyrrole pi-Bridge for Use in DSSCs

Master's thesis in Chemical Engineering and Biotechnology
Supervisor: Bård Helge Hoff, Audun Formo Buene
June 2019

Norwegian University of Science and Technology
Faculty of Natural Sciences
Department of Chemistry

NTNU
Norwegian University of
Science and Technology

Preface

This master thesis has been carried out at the Department of Chemistry at NTNU (Trondheim) during the spring of 2019. This thesis is built on the specialization project carried out in the autumn of 2018.

I would like to thank my supervisors, Professor Bård Helge Hoff and PhD Candidate Audun Formo Buene. Your insight in the field of DSSCs has been crucial for this thesis, as well as your practical knowledge and motivational conversations. I would also like to thank PhD Candidate David Moe Almenningen and post doc. Amsalu Efrem for all help concerning laboratory work and theoretical questions. Additionally, I am grateful to department Engineer Roger Aarvik for supplying the chemicals, PhD Susana Villa Gonzalez for MS analysis and Senior Engineer Torun Margareta Melø for guidance regarding NMR. To the members of the solar cell laboratory, thank you for all the good conversations, both professional and non-academic.

Lastly I would like to thank my family and friends, and specially Marius Reed for the support and motivation.

Abstract

Dye-sensitized solar cells (DSSCs) is an emerging new photovoltaic (PV) technology, allowing solar cells to be semi-transparent, flexible and of tuneable colour. Under ambient light conditions, DSSCs have out-performed most other long established PV technologies. Hot applications of DSSCs include building integration and powering an increasing number of devices in the Internet of Things (IoT).

Our group at NTNU has initially focused on phenothiazine based dyes. A method to lower the band gap and increase light harvest is to incorporate electron deficient units into the conjugated system. This thesis presents chemistry to synthesize three novel phenothiazine dyes containing one (**MEL1**) or two thiophenes (**MEL2**) or diketopyrrolopyrrole (**MEL3**) as part of the π-bridge. After a four-step synthesis, **MEL1** and **MEL2** were synthesized in a total yield of 44% and 20%, respectively. The novel dye **MEL3** was synthesized in a five-step synthesis, and had the most red-shifted adsorption spectra of the three dyes.

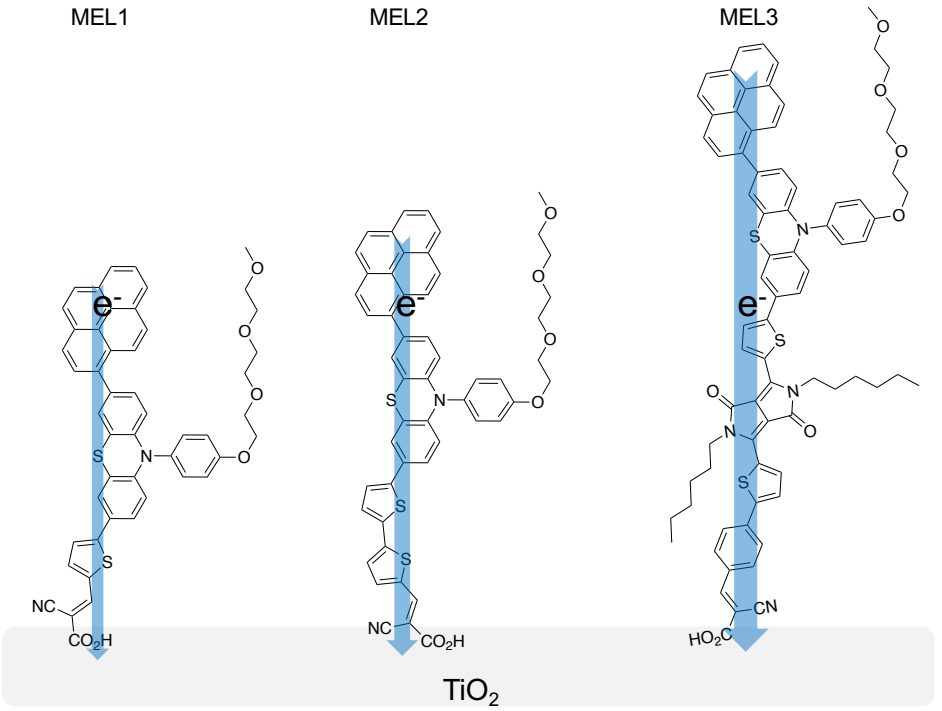

Sammendrag

Fargestoff-solceller er nye og voksende fotovoltaiske teknologier som gjør at solceller kan være halvtransparente, fleksible og av justerbar farge. Disse solcellene har utkonkurrert de fleste andre etablerte fotovoltaiske teknologier under naturlige lysforhold. Noen av bruksområdene til fargestoff-solcellene er bygningsintegrasjon og strøm til gjenstander i tingenes internett.

Vår forskningsgruppe på NTNU har forsket på fenotiazin-baserte fargestoffer. En metode for å senke båndgapsenergien og øke lysinnsamlingen er ved å lage fargestoff med elektronfattige enheter i det konjugerte systemet. Denne masteravhandlingen presenterer syntesen av tre nye fenotiazin fargestoffer som inneholder en (**MEL1**) eller to (**MEL2**) tiofener eller diketopyrrolopyrrole (**MEL3**) som en del av π-broen. Etter en firetrinns syntese ble **MEL1** og **MEL2** syntetisert med et totalt utbytte på henholdsvis 44% og 20%. Fargestoffet **MEL3** ble syntetisert med en femtrinns syntese, og hadde det mest rødskiftede adsorpsjonsspekteret av de tre fargestoffene.

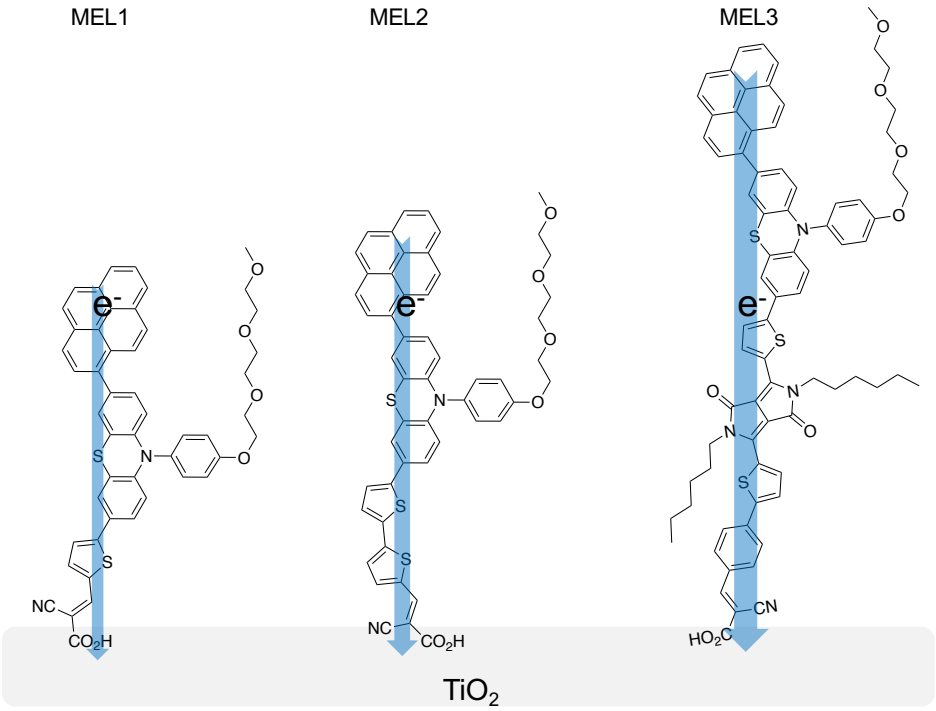

Table of Contents

List of Tables

List of Figures

List of Schemes

Numbered Compounds

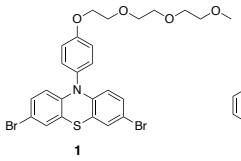

1

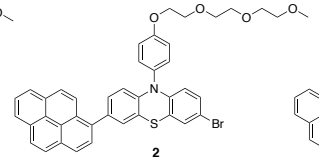

2

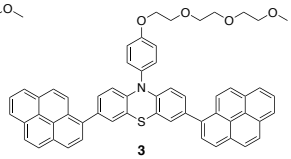

3

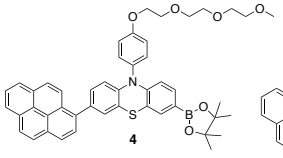

4

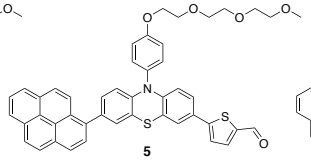

5

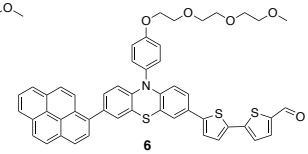

6

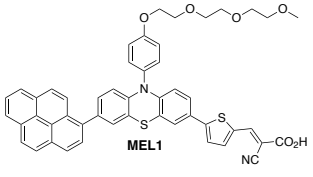

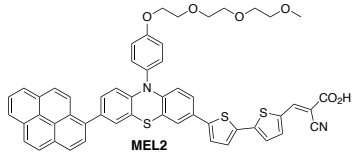

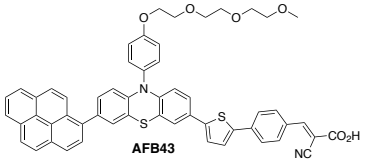

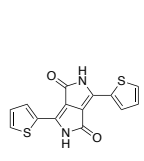

7

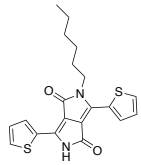

8

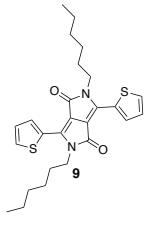

9

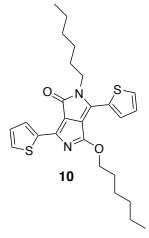

10

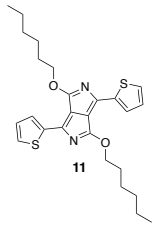

11

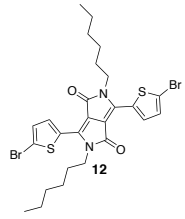

12

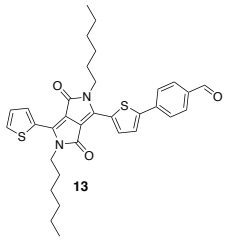

13

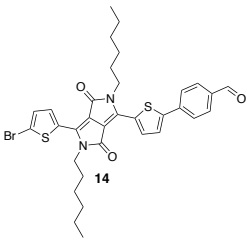

14

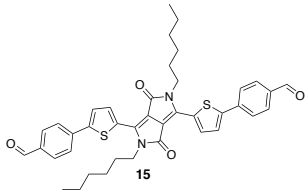

15

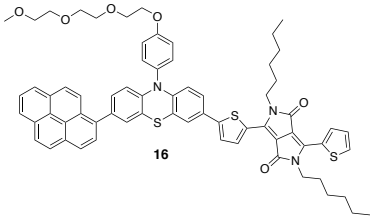

16

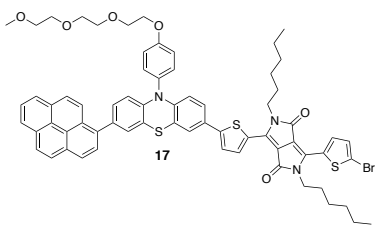

17

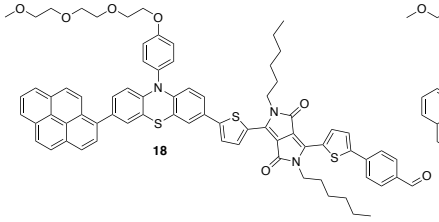

18

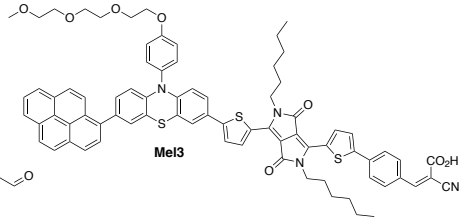

Mel3

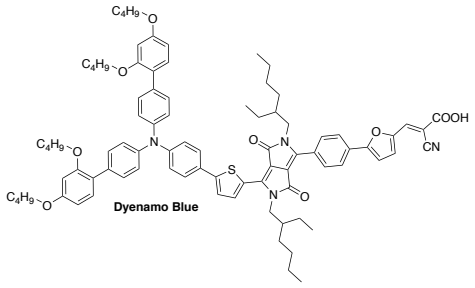

Dyenamo Blue

Abbreviations and Symbols

δ	Chemical Shift
^{1}H NMR	Proton Nuclear Magnetic Resonance
^{13}C NMR	Carbon Nuclear Magnetic Resonance
CB	Conduction Band
CMD	Concerted Metalation Deprotopnation
d	Doublet
DCM	Dichloromethane
DMF	Dimetylformamid
DMSO	Dimethyl Sulfoxide
DPP	Diketopyrrolopyrrole
DSSC	Dye-Sensitized Solar Cell
E^{+}	Electrophile
e^{-}	Electron
E_f	Fermi Level
E_{0-0}	Band Gap Energy
EAS	Electrophilic Aromatic Substitution
eq.	Equivalents
EWG	Electron Withdrawing Group
FF	Fill Factor

FTO	Fluorine-Doped Tin Oxide
h	Hours
HRMS	High Resolution Mass Spectrometry
IoT	Internet of Things
J	Coupling Constant [Hz]
J	Electric Current
J_{sc}	Short Circuit Current
L	Ligand
LHE	Light Harvesting Efficiency
m	Medium
m	Multiplet
m_p	Melting Point
MS	Mass Spectrometry
NMR	Nuclear Magnetic Resonance
Nu^-	Nucleophile
P	Power
P_{in}	Density of Incident Light
P_{max}	Maximum Power Point
PCE	Solar to Electical Energy Conversion Efficiency
ppm	Parts per Million
PV	Photovoltaic
R_f	Retention factor
r.t.	Room Temperature
s	Singlet
s	Strong
SPhos	2-Dicyclohexylphosphino-2,6-dimethoxybiphenyl
t	Triplet
TCO	Transparent Conductive Oxide
td	Triplet of Doublet
TEOME	Triethylene Oxide Methyl Ether
TM	Target Molecule

V	Voltage
V_m	Voltage at Maximum Power Point
V_{oc}	Open Circuit Voltage
VB	Valence Band
w	Weak
X	Halide
XPhos	2-Dicyclohexylphosphino-2,4,6-triisopropylbiphenyl

Chapter 1

Introduction

In recent years, dye-sensitized solar cells (DSSCs) has become an emerging photovoltaic technology allowing for harvesting of solar energy.[1] Under ambient light conditions DSSCs have out-performed most other long established PV technologies.[2] Dye-sensitized solar cells (DSSCs) profit from being flexible, semi-transparent and of tuneable colour.[3] The focus area for DSSCs are, among others, building integration and powering an increasing number of devices in the Internet of Things (IoT).[4,5] One of the leading DSSC-dyes is N719 based on a Ru-complex, with a solar-energy-to-electricity conversion efficiency of 11%.[6,7] Recently fully organic, metal-free, dyes have shown great progress in the field of DSSCs.[8]

1.1 Background and Aims

The worlds population is growing and together with higher standards of living this creates a great demand of energy. The energy consumption growth form 2016 to 2017 was 2.2%, and is expected to increase each year.[9] More energy must be produced and preferably in a sustainable way from renewable energy sources, which covered 40% of the global energy consumption in 2018.[10] The use of these energy sources is rising and the renewable power growth in 2017 was 17% from the year before.[9]

According to the International Energy Agency[10] solar photovoltaics (PV) will be the fastest growing energy source in the following years. A way to provide more

energy is to make the solar cells more efficient. Many strategies could be used to achieve this goal. Dye-sensitized solar cells (DSSCs) can be tuned to adsorb light energy in varied wavelengths and can result in a wider light adsorption range. This is due to a large selection of conjugated systems that can be combined.

Phenothiazine-based dyes have been the main focus in our group at NTNU. Electron deficient units can be incorporated into the conjugated system, to lower the band gap and increase light harvest. This thesis presents synthesis of phenothiazine dyes containing one or two thiophenes, or thiophenes together with diketopyrrolopyrrole (DPP) as part of the π-bridge. The phenothiazine-based dyes have shown qualities suited for dye-sensitized solar cells.[1] All the dyes in the **MEL**-series have a donor - π-bridge - acceptor system. The use of DPP in photovoltaics has yielded the first high-performance blue DSSC, with a power conversion efficiency above 10%.[5] Blue dyes have also shown an excellent ability of absorbing the incident photons in the red and near-infrared range.[11] Dyes made of DPPs can become blue, and the color itself is desirable for building integration.

1.2 Solar Cells

A solar cell is a device that converts light directly into electricity. This section will first present a short introduction to general photovoltaics, then the traditional silicon based solar cells. Thereafter, dye-sensitized solar cells and their energic considerations and requirements will be presented, and lastly the design of target molecules for this thesis.

1.2.1 Working Principles

In most of the renewable energy sources mechanical energy is converted to electrical energy, such as for wind and hydroelectric power plants. Solar cells use photon energy, which are particles of light, to excite electrons so that they can be used in an external circuit to make electricity.[12] The light creates mobile charge-particles in a semiconductor which can separate the charges.[13] This charge separation allows for transportation to the external circuit and thus generation of electric current.

Organic DSSCs work fundamentally different than traditional inorganic silicon solar cells.[14] The inorganic solar cells have a direct generation of the electron-hole pair. In DSSCs the electron has to be injected into a semiconductor, and after a migration through the external circuit, the electron is re-introduced into the cell

on a metal electrode. The electron is flowing from the electrode into an electrolyte and back to the dye where the dye reverts to its ground state.

Generally, for all kinds of PV devices, under open circuit there is no current, where the potential is called V_{oc}. This value together with the short circuit current, J_{sc}, represent the absolute maximum values of the current and voltage for the solar cell. In order to get the maximum power from the solar cell, the values of J and V must be chosen so that P = I·V is maximized, as shown in Figure 1.1.

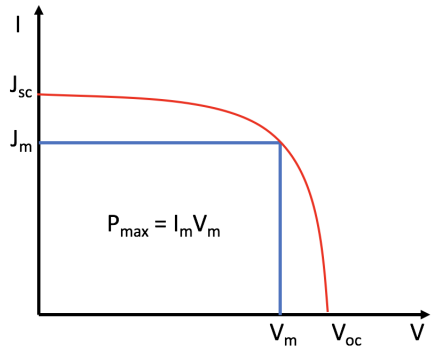

Figure 1.1: Illustrates the IV-curve (red) of a solar cell. In addition, the values of I and V which maximize the area (power) are highlighted (blue curve) to show that the real values of I and V are smaller than J_{sc} and V_{oc}, respectively. J_m and V_m are the maximum/optimized values.

The power, P, is the ultimate measurement of how good a solar cell is, and should be as high as possible. The fill factor, FF, is a measure of how ideal a solar cell is.[12]

$$FF = \frac{J_m \cdot V_m}{J_{sc} \cdot V_{oc}}$$

Where J_m and V_m is the current and voltage, respectively, of the maximum power point, P_{max}. The performance of the cell is often given by the solar-to-electrical energy conversion efficiency (PCE), also called the power conversion efficiency.[15]

$$PCE = \frac{J_{sc} \cdot V_{oc} \cdot FF}{P_{in}}$$

Where P_{in} is the intensity of incident light.

1.2.2 Silicon Solar Cells

An important feature of the silicon solar cell is the band gap, which corresponds to the energy difference between the valence band (VB) and the conduction band (CB). Electrons are excited from the VB to the CB if an energy equivalent to or larger than the band gap is provided. Another crucial part of the solar cell are the semiconductor layers. This is where electrons are freed and current is created. There are two different classifications of semiconductors, *p*-type or *n*-type,[16] as presented in Figure 1.2.

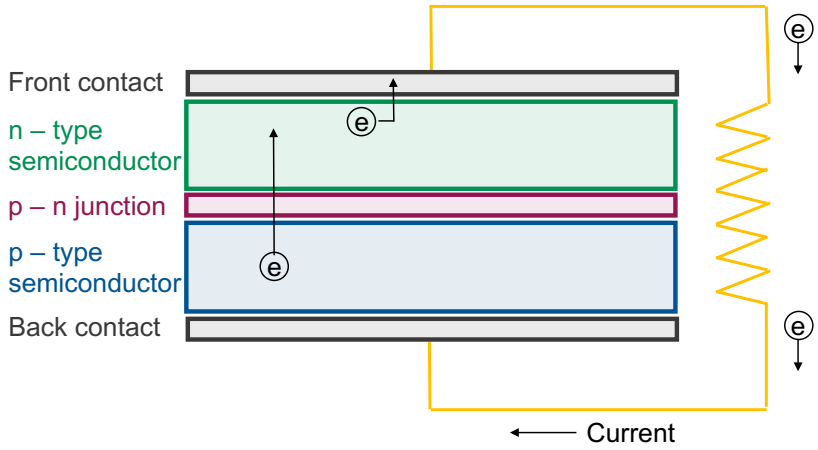

Figure 1.2: The silicon-based PV cell.[17]

A *pn*-junction is created by doping the two sides of the semiconductor with *n*- and *p*-type on each side. By doping a semiconductor, the Fermi level, Ef, is shifted towards the VB for *p*-type, and CB for *n*-type.[12] Because the two sides of the semiconductor are in thermal equilibrium, the Fermi level of the entire semiconductor must be equal, thus creating a potential difference between the two doped sides. This potential difference creates an electric field from the *n*-side to the *p*-side.[18] As a consequence, any electrons excited on the *p*-side will be transported through the *pn*-junction and end up on the *n*-side while a hole will remain on the *p*-side.[19] The separation of the electron-hole pair by an electric field increases their lifetime, making the time required for transport of the electrons to an external circuit sufficient to take advantage of its energy.

1.2.3 Dye-Sensitized Solar Cells

The dye-sensitized solar cell is a type of thin film solar cell, and can be considered to be a technology between the second and third generation solar cells.[15,20] The DSSCs, also referred to as Grätzel cells,[21] vary a lot from each other in architecture, but they have some common operating principles, as shown in Figure 1.3. The DSSC main components are the semiconducting metal oxide material, electrolyte, dye-materials and counter-electrode.[20] The main difference from silicon based solar cells is the charge separation process, where the generated exciton injects an electron to the semiconductor for DSSCs.

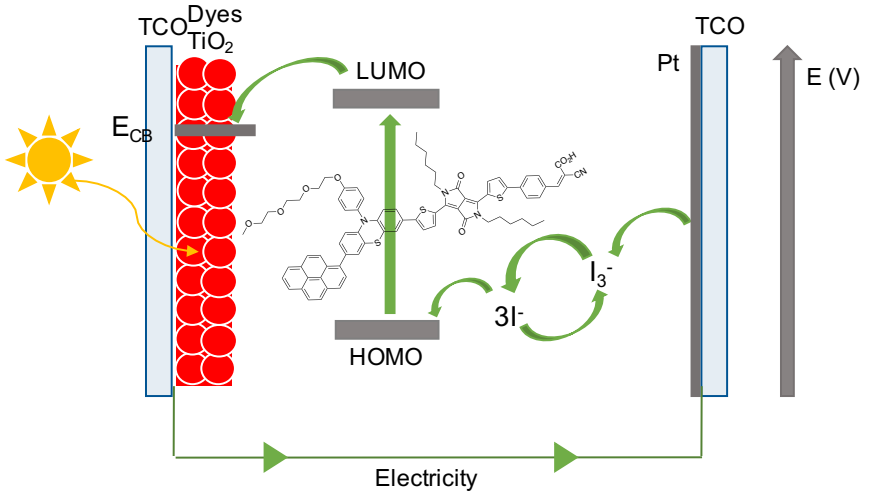

Figure 1.3: Energetic diagram of *n*-type DSSC.[22]

The light goes through the transparent conductive oxide (TCO) first. The TCO works as an anode, and the most common type of TCO is fluorine-doped tin oxide (FTO). Attached to the anode is the nano-crystalline oxide semiconductor, TiO_2. This type of semiconductor, TiO_2, proposed in 1991, is still the most used semiconductor in DSSCs.[3,23] The dyes can then be loaded onto the nano-crystalline oxide semiconductor. Ideally, the dyes will form a monolayer on the film. The dyes inject electrons to the semiconductor when photoexcitation occurs. Then the is in its oxidized form and is regenerated by the electrolyte, containing iodine in the anionic forms I^- and I_3^-. This is the most used electrolyte, due to its slow recombination rate with injected electrons and fast diffusion properties.[24,25] Electrolytes with Co(II)/Co(III) and Co(I)/Co(II) have also shown to be promising, and have the advantage over Iodide-couple due to their non-volatility, non-toxicity and

higher open-circuit voltage.[18,26,27] The higher open-circuit voltage is caused by their more positive redox potential. A counter electrode, the cathode, is at the bottom of the solar cell, and normally contains platinum, Pt, and TCO. The electron that was donated to the semiconductor will be transported to an external circuit via the TCO-anode.

The optimization of the DSSC can be done in different ways. For changing the charge transport, the electrolyte or semiconductor can be modified, and the dyes for changes in spectral properties. Despite the different working principles of the silicon solar cells and DSSCs, the DSSCs can also be divided into *p*- and *n*-type. The process described above is an *n*-type solar cell. In contrast, the *p*-type DSSCs have the dyes and semicondutor on the catode, and injects electrons to the electrolyte.[28,29]

1.2.4 Energic Consideration of Dyes in DSSC

In order for the dye to work in a DSSC, they have to absorb photons from the sun-light. The light harvesting efficiency (LHE) is a measure of the absorption as a function of the concentration of the dye-molecules absorbed onto the TiO_2 surface, extinction coefficient and the adsorption range of the dye.[22] The dye should be panchromatic, meaning that the dye is sensitive to all wavelengths of visible light. Preferably, also for some wavelengths near the infrared light.[30]

To be able to inject an electron into the TiO_2 a charge separation process has to take place.[31] The charge separation energy is proportional to the exciton binding energy, which depends on both the geometry of the dye and the electronic structure. The driving force for electron injection is defined as the difference between the LUMO level of the dye and the semiconductors conduction band, as shown in Figure 1.3.[22] To be thermodynamically possible, the LUMO level has to be above the TiO_2 conducting band. The energy difference, E_{0-0}, between the HOMO and LUMO level of the dye is one of the driving forces for excitation of electrons.

The band gap energy, E_{0-0}, of the sensitizers can be estimated from the adsorption spectra. This is done by drawing a tangent in the inflection point to the right of the absorption maxima. The intersection between this tangent and the x-axis reveals the absorption onset wavelength, λ, that is used to calculate the band gap energy, E_{0-0} [eV]:

$$E_{0-0} = \frac{h \cdot c}{\lambda}$$

1.2.5 Dye Design for DSSCs

In the case of a light absorbing dye, many considerations regarding the design have to be made. The following criteria for a dye have been suggested:[20,32]

- The visible region and even part of the near-infrared spectrum should be covered in the dyes absorption spectrum.
- The absorbing dye must have an anchoring group to strongly bind to the semiconductor surface. This group could be -COOH, -H_2PO_3, -SO_3H, etc.
- The LUMO level of the sensitizer should be higher in energy than the conduction band of the metal oxide. This ensures an efficient transfer between the excited dye and the CB.
- The HOMO level of the sensitizer has to be more positive than the redox potential of the electrolyte in order to get regeneration of the dye.
- The sensitizers have to be thermally, photo- and electrochemically stable.
- Must be soluble in common organic solvents compatible with electrolytes.

Organic sensitizers are in most cases based on a donor, a π-bridge and an acceptor (D-π-A) architecture, as shown in Figure 1.4. The backbone of this dye is phenothiazine, which works as an electron donor. Thiophene is the π-bridge and cyanoacrylic acid is the electron acceptor/anchoring group. These three parts are

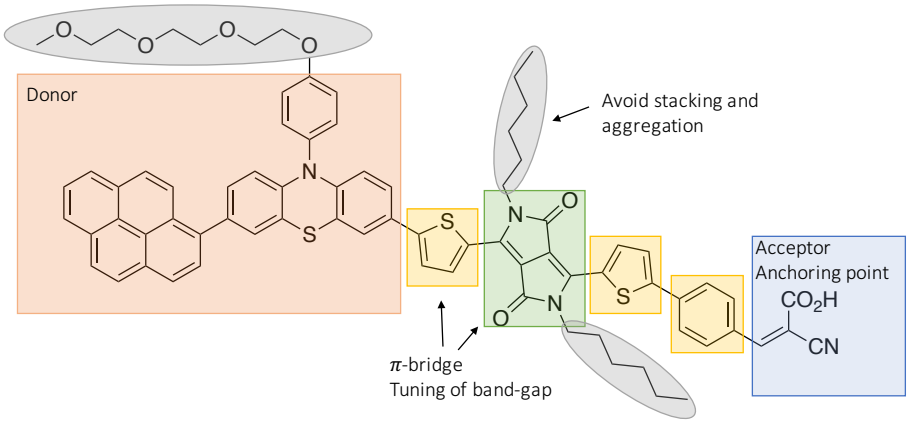

Figure 1.4: Design concept for new dyes, which should include a donor, a π-bridge and an acceptor, with **MEL3** as an example.

all what is needed to make a dye, but in order to increase the efficiency, some extra components could be added. The aromatic group pyrene is added as an auxiliary donor and the hexyl and the triethylene oxide methyl ether (TEOME) chain as anti aggregation components. Diketopyrrolopyrrole (DPP) extends the conjugation of the π-bridge by introducing an electron withdrawing group (EWG). Incorporation of an electron-deficient group reduces the energy gap of the dyes and broadly extends the spectral coverage.[33] Cyanoacrylic acid is one of the most common anchoring groups in DSSCs, but a large selection of other anchoring groups can also be used.[34,35]

The largest difference between **MEL3** and the two more simple dyes **MEL1** and **MEL2**, is the DPP-unit. This unit has been evaluated in other dyes used in DSSCs.[5] The addition of DPP makes the dye blue, unlike the red dyes **MEL1** and **MEL2**. Blue DSSCs have an excellent ability of absorbing the incident photons in the red and near-infrared range.[11] Dyes based on the DPP-unit have shown good efficiency in the cobalt electrolyte system, $[Co(bpy)3]^{3+/2+}$,[5] which has the advantages of non-volatility and non-toxicity. The dye displayed in Figure 1.5 was used in a DSSC with the previous mentioned electrolyte, and gave an energy conversion efficiency of 10.1%. Another DPP-based dye is the **Dyenamo Blue**, with an energy conversion efficiency of 7.3% and an adsorption maxima at 584 nm (49 000 $M^{-1}cm^{-1}$, in DCM).[36,37] The DPP-unit has been attached to a simpler phenothiazine donor group in a research done by Zang *et al*.[38] This resulted in a efficiency of 5.2% with a diphenyl-DPP.

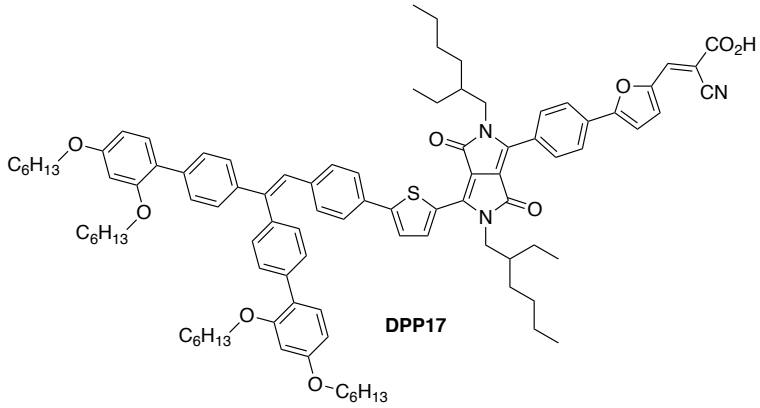

Figure 1.5: The dye **DPP-17** dye with a DPP-unit performed a PCE above 10%.[5]

The first phenothiazine dye for DSSC was developed in 2007.[39] Since then it has been shown that phenothiazine-based dyes are truly promising.[40] Phenothiazine is electron donating, with its electron rich heteroatoms. The research group at

NTNU has developed many DSSCs with phenothiazine.[41] Two of the dyes are **AFB-19** and **AFB-31** made by Buene and Boholm with a power conversion efficiency of 5.00% for both dyes.[41,42] **AFB-19** showed a molar extinction coefficient of 24 450 $M^{-1}cm^{-1}$ at absorption 441 nm. A molar extinction coefficient of 19 844 $M^{-1}cm^{-1}$ at 454 nm was seen for **AFB-31**.

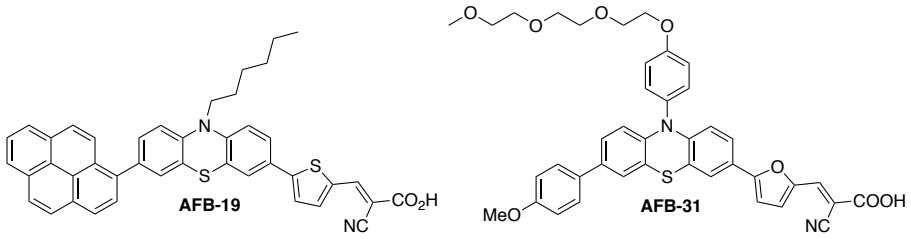

Figure 1.6: Two phenothiazine dyes, **AFB-19** (PCE = 5.00%) and **AFB-31** (PCE = 5.00%), synthesized by Buene and Boholm.[41,42]

1.2.6 The Diketopyrrolopyrrole Unit

The DPP-chromophore was first discovered in 1974 by Farnum *et al.*,[43] as a by-product. The DPP has shown to be easily synthesized, strongly absorbing and thermally stable.[44] The first DPP-based small-molecule dye for use in DSSCs was reported in 2010.[6] The DPP-unit as photovoltaic materials has been intensively explored since then.[45] By functionalizing the DPP-unit it can be tuned towards many different colors, from orange-yellow via blue-red to violet. This can be accomplished by exchanging the substituents in the *para*- and *meta*-position of the aromatic group attached to the DPP chromophore.[46]

The incorporation of the DPP chromophore in a dye can lead to high absorbance and emittance in the visible and near infrared region.[47] This is due to the tuning of the HOMO and LUMO energy levels which can be conveniently accomplished by alternating the π-conjugated systems, indicated by electrochemical measurements.[6] The integration of the DPP-unit with an electron donating unit, in this case phenothiazine, can give rise to compounds with low band gaps. Band gaps of DPP-based materials as low as 1.13 eV have been reported.[48]

The DPP-unit is complex, and has many reactive centers. An overview of the potential reactivity of the DPP is presented in Figure 1.7.[49]

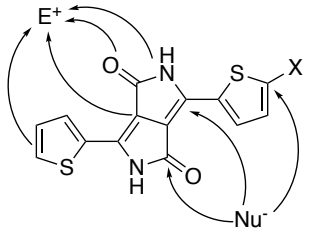

Figure 1.7: Potentially reactive centers for DPP derivatives, where E^+ is electrophile, Nu^- is nucleophile and X is halide.[49]

1.2.7 Target Molecules

The target molecules for this master thesis are the three novel dyes **MEL1**, **MEL2** and **MEL3** shown in Figure 1.8. They all have the phenothiazine, pyrene, thiophene and triethylene oxide methyl ether (TEOME) chain in common, which is inspired by Buenes dyes **AFB-19** and **AFB-31**,[41,42] displayed in Section 1.2.6. **MEL3** has a DPP-group similar to the ones in **DPP-17** and **Dyenamo Blue**.

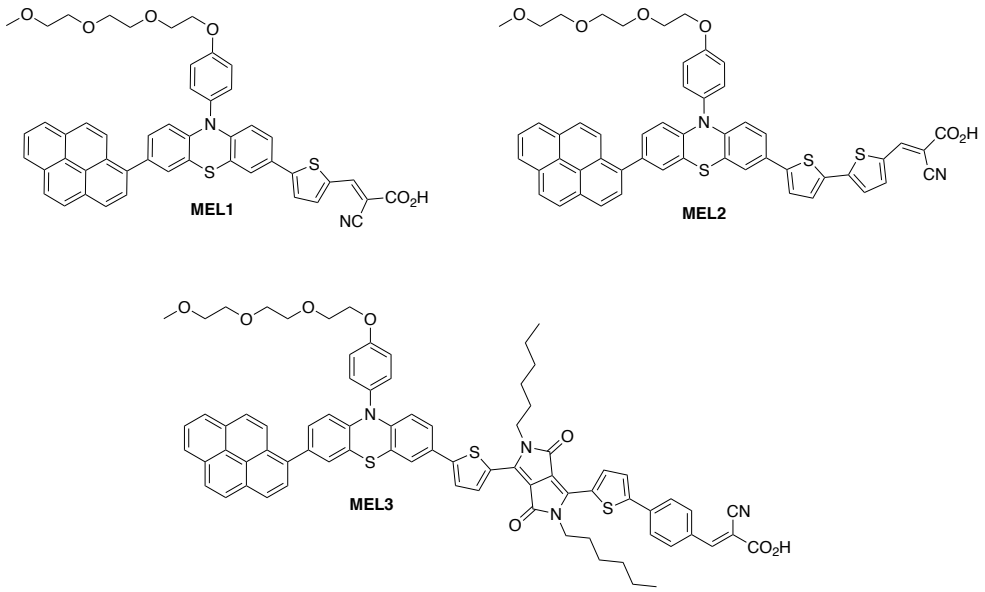

Figure 1.8: The target molecules are the three phenothiazine-based dyes **MEL1**, **MEL2** and **MEL3**.

The dyes **MEL1** and **MEL2** only differ from each other by one thiophene. The dyes have a (D‘-D-π-A) and (D‘-D-π-π-A)-system, respectively. **MEL3** has a

DPP-unit between the two thiophenes and a phenyl, that differs from **MEL2**. The phenothiazine has a pyrene attached to increase the donor quality of the dye.[42] The reason for attaching a TEOME-group and hexyl groups is to decrease the ability for the dyes to stack and aggregate.[50] The TEOME-chain, together with the phenyl group, is electron-rich and can increase both the solubility and donor quality additionally. The thiophene groups lower the charge recombination, and improve the absorption of the light by red-shifting the absorption spectrum.[51] The DPP component is electron withdrawing. The aim of adding this EWG is to cover more of the visible and near-infrared region of the adsorption spectra, then lower the band gap energy. The anchoring group is a cyanoacrylic acid group that absorbs well to the semiconductor material, and allows electron injection into TiO_2. A proposed retrosynthesis of target molecule **MEL1** and **MEL3** is presented in Schemes 1.1, 1.2 and 1.3. A similar retrosynthesis can be used for **MEL2**, as described for **MEL1**.

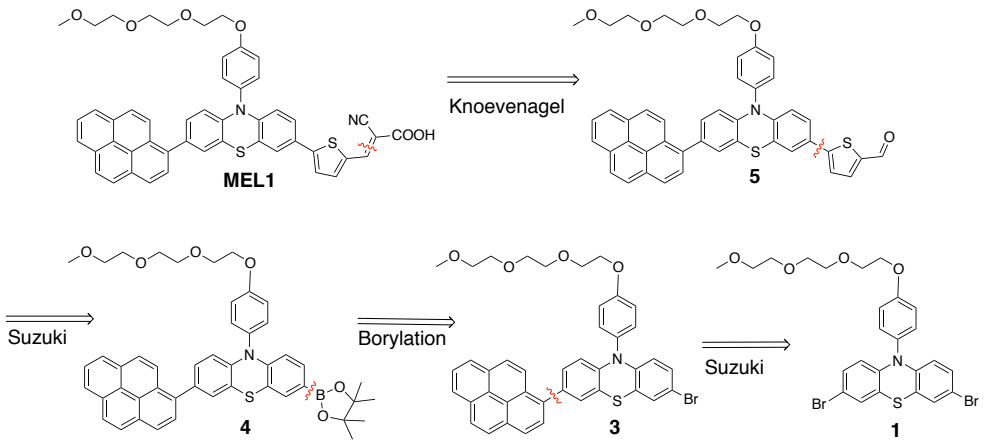

Scheme 1.1: A proposed retrosynthetic route for **MEL1**. **MEL2** has a largely similar retrosynthetic route.

The brominated phenothiazine **1** was synthesized in the specialization project. The first step described in this thesis towards the target molecules **MEL1** and **MEL2** is the Suzuki-Miyaura cross-coupling from the symmetric phenothiazine-backbone **1** to a monosubstituted pyrene compound **3**. The Suzuki-Miyaura is followed by borylation to make the boronate functionalized derivative **4**, before one more Suzuki to yield the aldehyde **5**. The last step toward the dye is the Knoevenagel condensation to form the cyanoacrylic acid **MEL1**. The total route is a linear four-step synthesis.

Synthesis of **MEL3** could be carried out in a convergent strategy. The synthetic route for the phenothiazine donor group **4** is previous described. Two proposed retrosyntheses for the dye **MEL3** will be presented, retrosyntheses A and B, where A, as shown in Scheme 1.2, will be presented first. The first step towards the DPP building-block is an alkylation to form the alkylated derivative **9** of the commercially available dithiophene-DPP **7**. The next synthesis is a NBS bromination, where bromines are introduced on both sides of the DPP **12**. A Suzuki-Miyaura cross-coupling can be used to introduce a benzaldehyde on one side of the DPP **14**, before one more Suzuki-Miyaura reaction binds the DPP aldehyde **14** with the donor group **4** to form the donor-π-bridge system **18**. The last step is the same as previous described for the two other dyes **MEL1** and **MEL2**, a Knoevenagel condensation to yield target dye **MEL3**, in a seven-step synthesis.

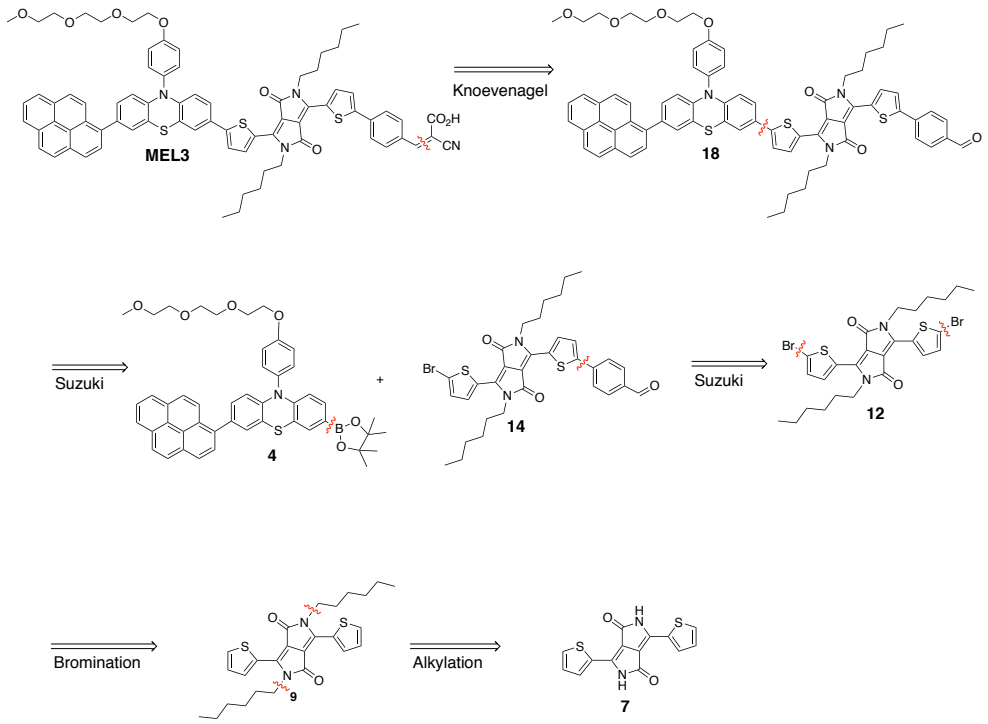

Scheme 1.2: The proposed retrosynthetic route A for **MEL3**.

The retrosynthesis route B is presented in Scheme 1.3. This is a shorter route, with only five step, and uses the direct arylation instead of Suzuki-Miyaura cross-coupling. The synthesis of the alkylated dithiophene **9** and the phenothiazine donor group **2** are previous described. To carry out the π-bridge **13** a direct arylation takes place from the alkylated DPP **9**. Another direct arylation between the

phenothiazine-based compound **2** and the DPP-aldehyde **13** yields the dye precursor **18**. As described for the other dyes, the last step is Knoevenagel condensation to form the target dye **MEL3**.

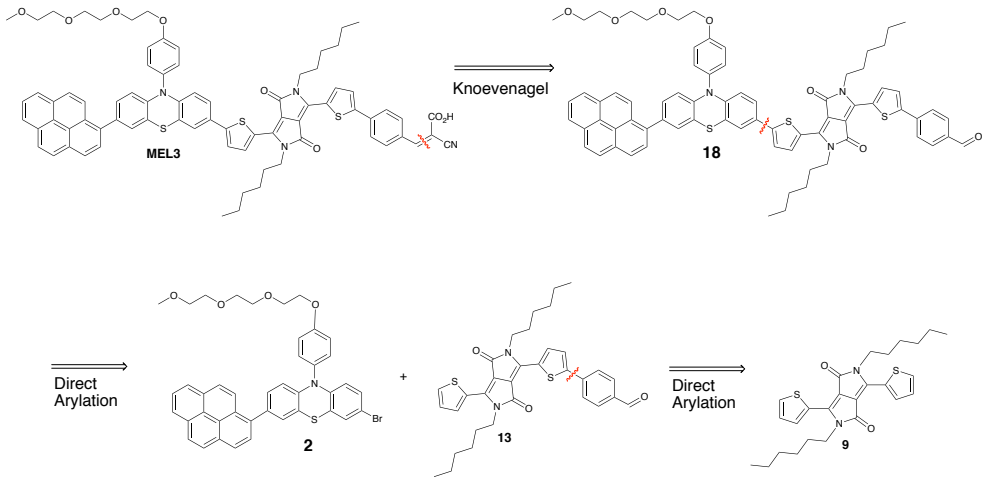

Scheme 1.3: The proposed retrosynthetic route B for **MEL3**.

1.3 Synthesis

1.3.1 Suzuki-Miyaura Cross-Coupling

The Suzuki-Miyaura cross-coupling creates a new carbon-carbon bond from an organoboron compound and aryl/vinyl halide,[52] and is considered one of the most versatile methods for carbon-carbon bond formation.[53] The reaction can be considered as a nucleophilic substitution of halide atoms with various carbon nucleophiles.[54] This method can use mild reaction conditions, water can be used as solvent and some of the by-products are water soluble, these are some of the advantages to the Suzuki-Miyaura cross-coupling. Other advantages are the availability of many boronic acids and the method tolarates a variety of functional groups in the starting material, due to the generally high chemo- and regioselectivity.[55] Some common by-products of the Suzuki reaction are the reduced product and homocoupling of arylboronic acid through an electroreductive or electrooxidative reaction.[56,57] A proposed mechanism for the palladium-catalyzed reaction is shown in Scheme 1.4.

Mechanism

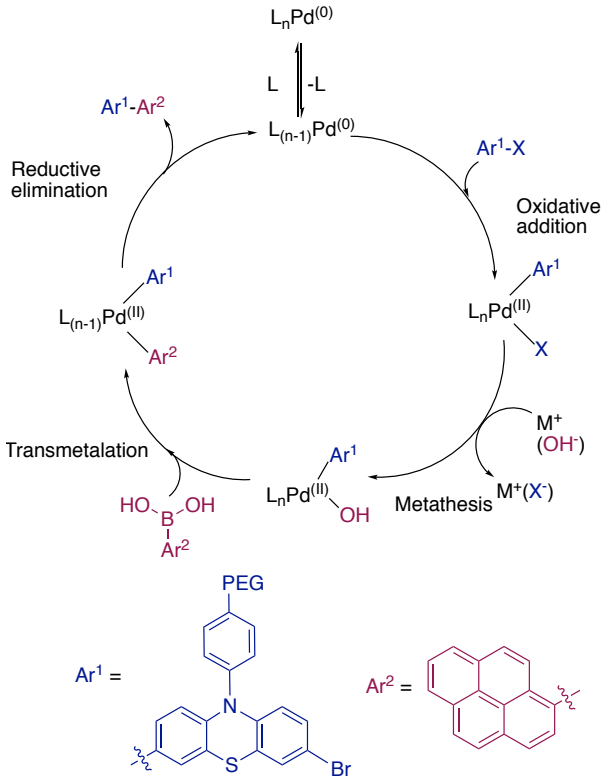

Scheme 1.4: Proposed mechanism for Suzuki-Miyaura cross-coupling between the symmetric phenothiazine **1** and a pyreneboronic acid to form the monosubstituted phenothiazine **2**.[58]

The suggested mechanism for Suzuki-Miyaura cross coupling proceeds trough a four step cycle, oxidative addition, metathesis, transmetalation and reductive elimination.

1. **Oxidative addition** is in most cases the rate determining step of the catalytic cycle.[58] This step breakes the carbon-halogen bond, allowing two new bonds to form with the palladium complex, resulting in oxidized palladium from Pd(0) to Pd(II). The result of this transformation is a reduced electron density of the metal. Electron rich ligands, L, stabilizes the Pd(II).[59]

2. **Metathesis** is the step where the halide exchanges with a base, to give a more reactive Pd-complex in the next step.

3. **Transmetalation** is the reaction where reactive groups are transferred from one metal to another, or more specific in the case of Suzuki-Miyaura, from the Pd complex to organoboron. The base that was added in the previous step, metathesis, is now exchanged with an aryl specie.[60]

4. **Reductive elimination** is the last step where the two aryl species on the Pd-complex are eliminated. This regenerates the active Pd(0) catalyst, and forms a bond between the two aryl units.[61]

The Suzuki cross-coupling reaction is frequently used, but the mechanism is not fully understood.[59] Oxidative addition was earlier reported as the rate determining step,[62] but research indicates that the reactivity is more complex and depends on many factors.[63] Electron withdrawing groups, EWG, in the aryl halide compound will increase the rate of oxidative addition, owing to the weakening of the C-X bond.[64]

Suzuki-Miyaura cross-coupling can also be used to synthesis DPP-based π-conjugated systems,[54] there the DPP-unit is an EWG and preferably the aryl halide. The two electronwithdrawing amide in DPP can facilitate nucleophilic aromatic substiution in the absence of palladium catalyst.[65]

Catalyst and Ligands

There are a large number of possible variables in a Suzuki-Miyaura reaction, such as metal source, ligand, base, solvent, temperature, etc.[66] The metal/ligand systems that facilitate the Suzuki-Miyaura cross-coupling with different electrophiles are the parameters that have been the most extensively studied.[67] Palladium is the most widely used metal as catalyst, with a choice between Pd(0) (Pd/C, Pd/Al_2O_3, $Pd_2(dba)_3$) or Pd(II) ($PdCl_2$, $Pd(OAc)_2$).[67] The catalytic species can be formed *in situ* using the Pd(0) source and a necessary ligand or a preformed catalyst can be introduced using the Pd(II). Careful choice of ligand can facilitate two of the four steps of the catalytic cycle, shown in Scheme 1.4. The use of electron donating ligands can increase the electron density around the metal, and accelerate the oxidative addition. If a bulky ligand is present, it helps the elimination step.[68] An overview of their impact on the efficacy of catalysts using these ligands are shown in Figure 1.9.

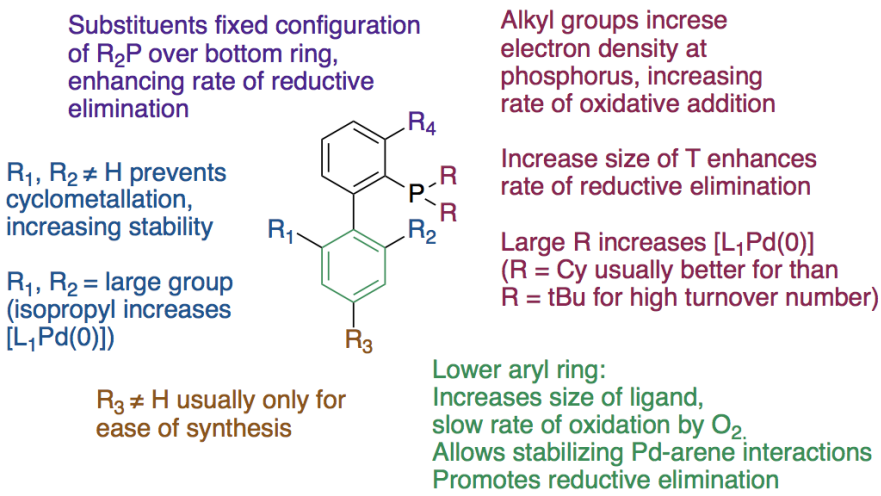

Figure 1.9: Structural features of dialkylbiarylphosphines ligands and their impact on catalysis.[69]

Some common dialkylbiarylphosphine ligands, L, are shown in Figure 1.10, where all are bulky, electron-rich and monodentate (only one donor atom used to bond to the central metal atom or ion).[69]

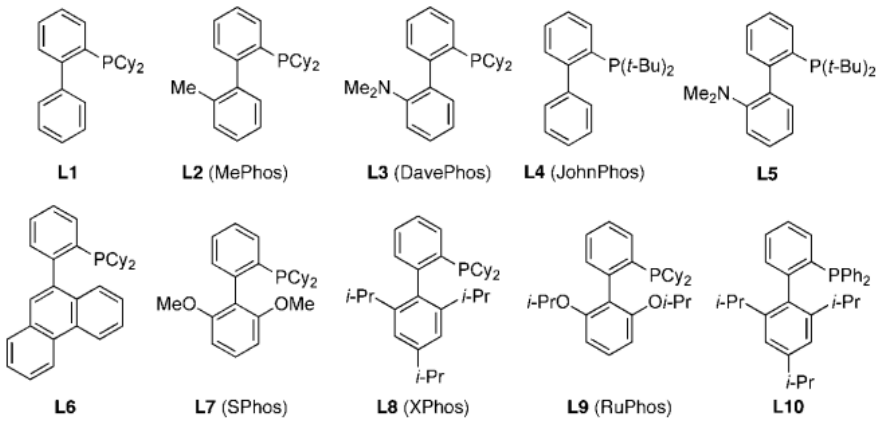

Figure 1.10: Common ligands in Suzuki-Miyaura cross-coupling reactions.[69]

1.3.2 Borylation

Pd-catalyzed borylation allows pinacolborane and aryl halides to react and form an arylboron compounds. This reaction has proved to be a powerful tool, due to the introducing of a Suzuki-Miyaura reactive group.[70] Borylation needs base and tetiary amine, Et_3N is especially important since it favours boron-carbon bond synthesis.[71] A proposed mechanism is shown in Scheme 1.5.

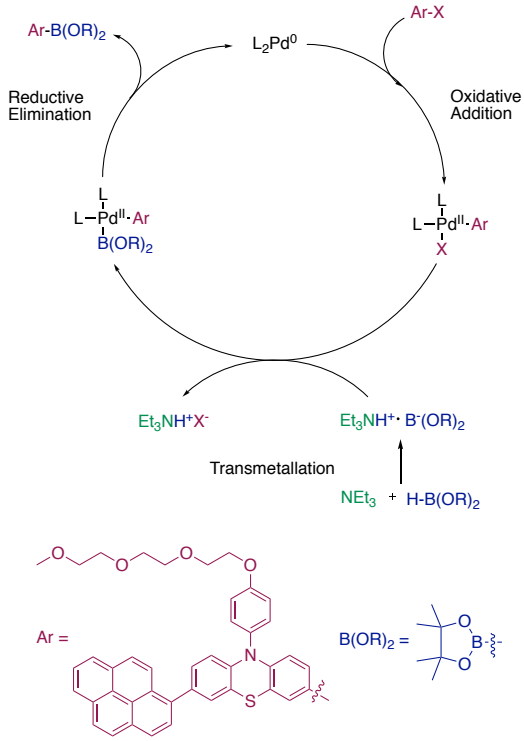

Scheme 1.5: Proposed mechanism for Pd-catalyzed borylation between the phenothiazine **2** and pinacolborane to form the borylated product **4**.[72,73]

The mechanism for Pd-catalyzed borylation has similarities with the Suzuki-Miyaura cross-coupling mechanism, and consists of oxidative addition, transmetalation and reductive elimination. The mechanism suggest that the boride acts as the active transmetalating anion, resulting in the interaction between triethylamine and pinacolborane, which forms an ion pair.[72]

1.3.3 Knoevenagel Condensation

The Knoevenagel condensation synthesizes an α,β-unsaturated compound by an amine catalyzed reaction of aldehydes/ketones and a carbon nucleophile.[52] This reaction is an important tool for introducing the anchoring group in the organic dyes for use in DSSCs.[35,74,75] The Knoevenagel condensation proceeds through a general base-catalyzed Aldol condensation. A proposed mechanism is displayed in Scheme 1.6. The amine reacts with the carbonyl group, in this case an aldehyde, and forms an iminium. The iminium and cyanoacetic acid react by a base-catalyzed reaction to form a C=C bond, where an α,β-unsaturated compound is formed.

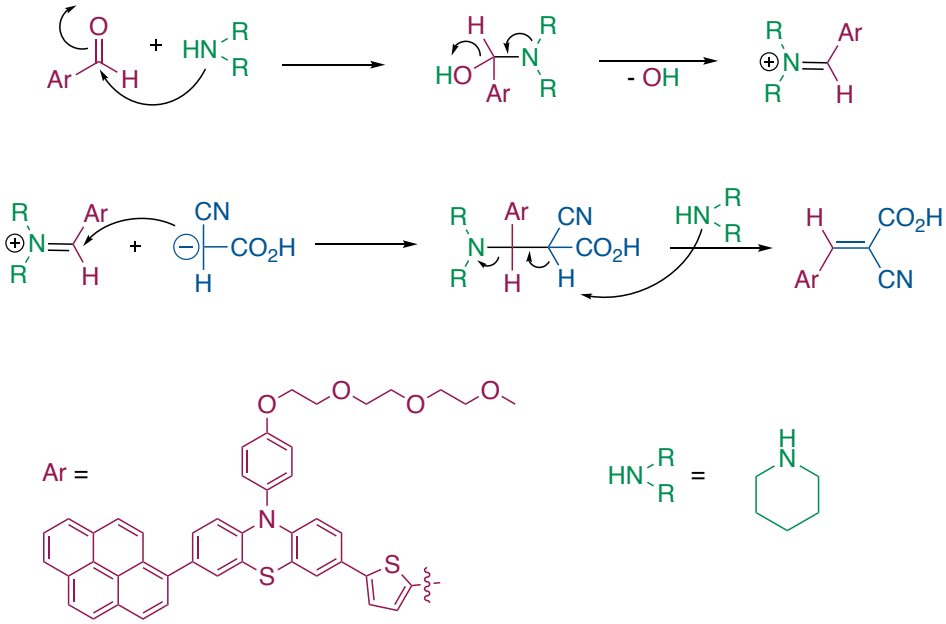

Scheme 1.6: Proposed mechanism for Knoevenagel condensation between the aldehyde **5** and cyanoacetic acid to furnish the dye **MEL1**.[52,58,76]

1.3.4 Amide Alkylation

Amides have two possible nucleophiles, oksygen and nitrogen. Typical alkylation agents are alkyl halides.[52] The amide alkylation, a type of nucleophilic aliphatic substitution, yields a higher substituted amide. The S_N2 mechanism for the alkylation is presented in Scheme 1.7.[52] The DPP-unit is usually alkylated to improve the solubility.[77]

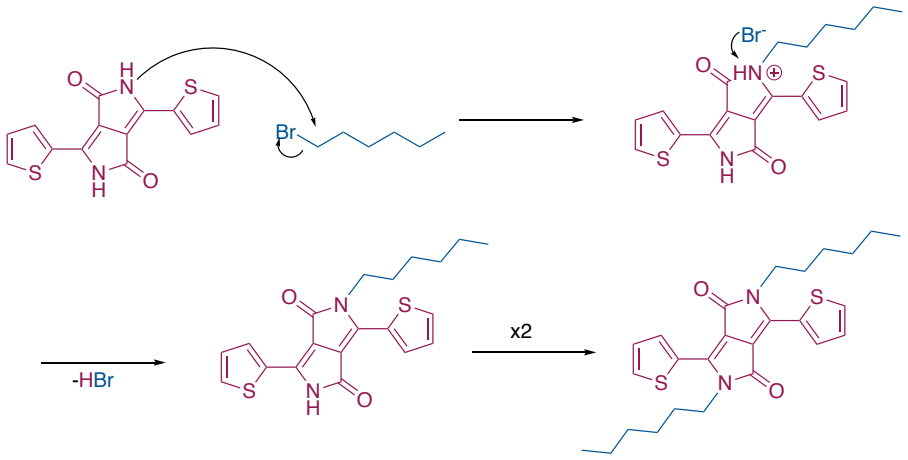

Scheme 1.7: Proposed mechanism for amide alkylation where hexyl is added to the DPP-nitrogen at coumpound **7**, to form product **9**.[52]

In 2010, it was assumed that the alkylation only occurs on the nitrogen.[78] One year after it was reported that *N,N*-, *N,O*- and *O,O*-alkylation occurs, with low selectivity.[77,79] The reason for this observation is influenced by the delocalization of the π-electrons along the O-C-N bonds, as shown in Scheme 1.8.[80]

The ratio of *O*- and *N*-alkylation depends on the reaction conditions, such as the reactivity of the alkylating agent and the reaction temperature. In a study by Mijin *et al.*,[80] was it found that the *N*-alkylation was more present than the *O*-alkylation when the alkylation agent was alkyl halide. The research indicated that the conversion of the reaction was low, and and the size of the alkyl-group does not influence the degree of conversion. On the other hand, research done by Zhao *et al.*[77] showed that the selectivety of the *N,N-*/*N,O-*/*O,O*-isomers varied with different alkyl reagents. The relative amount of the isomers for 2-ethylhexyl was 36/28/11, and 63/17/trace for octyl.

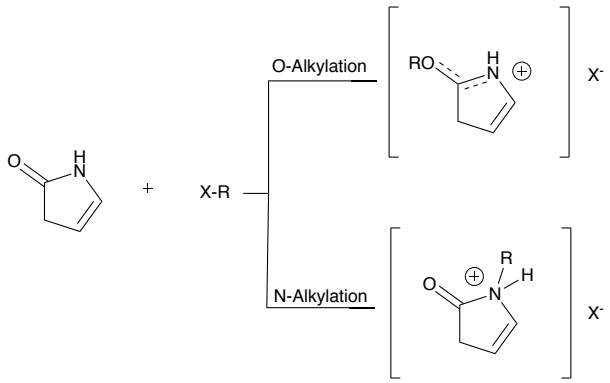

Scheme 1.8: *O*- and *N*-alkylation of amides.[80]

1.3.5 NBS Bromination

Bromination of aromatic compounds often occurs through an electrophilic aromatic substitution, EAS.[52] Lewis acid is normally needed to achieve desirable rates when adding halogens to aromatic compounds, but NBS or NCS (Br^+/Cl^+ source) can halogenate moderately active aromates without Lewis acid. The NBS bromination of thiophenes in acetic acid is considered to have a high degree of conversion.[81] Scheme 1.9 shows a proposed mechanism for the NBS bromination.[52]

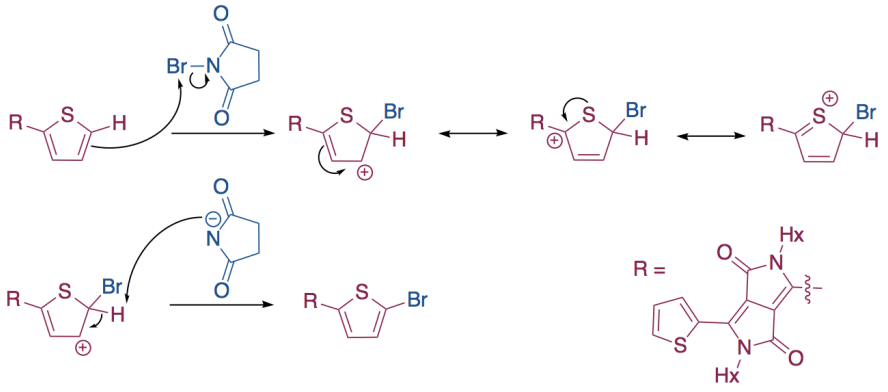

Scheme 1.9: Proposed mechanism for EAS with NBS and thiophene on DPP.[52] The bromination was done on both sides of the DPP-unit, to synthesize the dibrominated dithiophene-DPP **12**.

1.3.6 Direct Arylation

Direct arylation is a convenient way of synthesizing biaryl compounds, where one of the aryls is a privileged heteroaryl.[82,83] This palladium-catalyzed arylation is a valuable and efficient emerging alternative to the established metal-catalyzed cross-coupling, such as the previous described Suzuki-Miyaura.[84] Thiophenes are easily coupled in the direct arylation, without any adjustments.[85] This reaction is an environmentally benign and atom-efficient pathway for synthesis of π-conjugated systems.[86] The mechanism proceeds *via* activation of the C-H bond in a transmetalation catalytic cycle to form the C-C bond, as shown in Scheme 1.10.[86]

The exact mechanism of the direct C-H arylation is not known, but there has been established an agreement on pathway A or B when pivalic acid is present, as shown in Scheme 1.10.[86,87,89] In pathway A, the pivalic acid interacts reversibly with the Pd-catayst, while in pathway B the pivalic acid is bound to palladium throughout the catalytic cycle. Pathway A has large similarities with the Suzuki-Miyaura cross-coupling, described in Section 1.3.1, and other Pd-catalyzed cross-coupling mechanisms. Both the reductive elimination and oxidative addition are quite similar, what differs is the addition of the second aryl-compound to the Pd-catalyst, called the concerted metalation deprotonation (CMD). Both aryl-compounds bind directly to the Pd-catalyst, which prevents formation of the unstable Aryl-Pd-R complex between the metathesis and transmetalation step in the Suzuki-Miyaura reaction. Research on the CMD step done by Biswas *et al*.[87] showed that cleavage of the C-H bond occurs when an oxygen from the pivalic acid decoordinates from the Pd-centre, while the aryl-C still coordinates with Pd. The pivalic acid can then easily form an O-H bond with the aryl-H.

In the mechanism described in Scheme 1.10, the deprotonation occurs on the DPP-compound **9**. It is also possible to brominate the DPP and deprotonate the benzaldehyde instead. The possibility for *ortho*-addition on benzalehyde is present, and this method is possibly a convinient solution for polymerization.[90] Direct arylation can also be used for combining the phenothiazine-donor **2** and the DPP π-bridge **13** from this reaction.

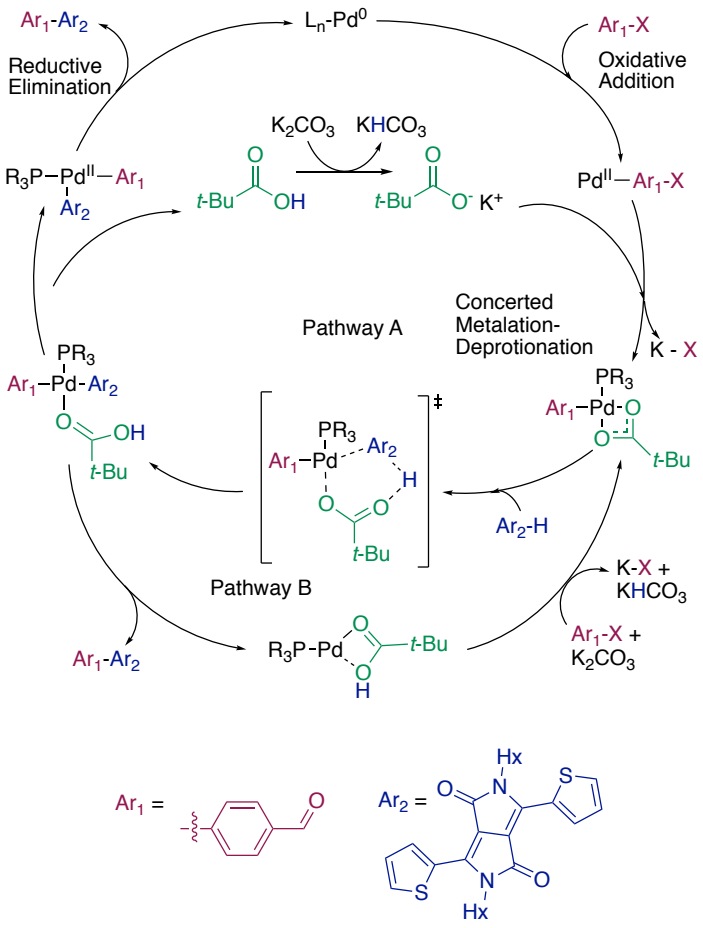

Scheme 1.10: Proposed mechanism for Pd-catalyzed direct arylation between dithiophene-DPP **9** and benzaldehyde to form the DPP-based aldehyde **13**, with assistance of pivalic acid.[86–88]

Chapter 2

Results and Discussion

2.1 General

The aim of this master project was to synthesize the three novel dyes **MEL1**, **MEL2** and **MEL3**, displayed in Figure 2.1. The syntheses of **MEL1** and **MEL2** are presented in Section 2.2.1 - 2.2.4, and **MEL3** is covered in Section 2.2.5 - 2.2.9. Detailed information about the syntheses can be found in Section 5.2 Synthesis. The photophysical properties of the dyes in the **MEL**-series are presented in Section 2.3.

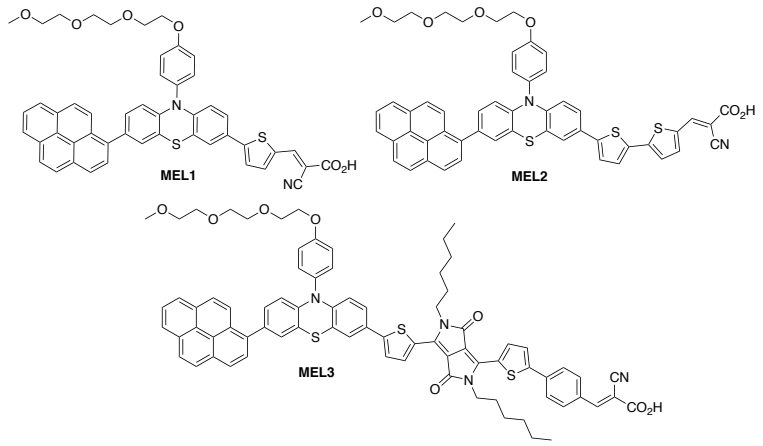

Figure 2.1: The target sensitizers synthesized during this master project.

2.2 Synthesis

2.2.1 Suzuki-Miyaura Cross-Coupling on Phenothiazine

Compound **2** was synthesized with a Suzuki-Miyaura cross-coupling between the brominated phenothiazine **1** and the commercially available pyrene-1-boronic acid, as shown in Figure 2.1.[91] The catalyst-system described by Knapp *et al.*[92] was used in this reaction.

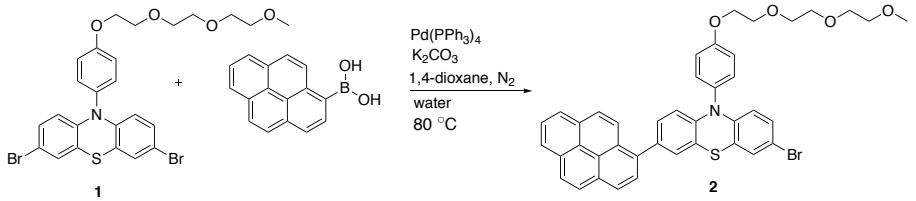

Scheme 2.1: The phenothiazine compound **1** reacted with pyrene-1-boronic acid in a Suzuki cross-coupling to form product **2**.

It was expected that the reaction would form three different products, mono-substituted **2**, di-substituted **3** and the homocoupled pyrene, together with an appreciable amount of starting material **1**. The statistically relative amounts of the unsubstituted, mono-substituted and di-substituted pyrene are respectively 1/2/1, using one equivalent of pyrene-1-boronic acid. Higher amounts of the pyrene-1-boronic acid can form more of the mono-substituted **2**, but also the di-substituted **3**. The reaction was run for 6 hours with 1.1 equivalents of pyrene-1-boronic acid, and all of the mentioned expected compounds were observed. The main challenge with this reaction is the purification, due to the equal polarity of the three phenothiazine-containing compounds, mainly caused by the triethylene oxide methyl ether (TEOME) chain. The Et_2O eluent-system showed best separation, with R_f-values of 0.24, 0.29 and 0.35. The donor building block **2** was synthesized in a yield of 54%, which is a significant improvement from the 19% yield obtained in the specialization project.[91] The high yield can be due to a more ideal amount of pyrene-1-boronic acid and an careful purification process with a large total load of silica on a relatively small amount of crude material.

2.2.2 Borylation of Phenothiazine

A boronate ester was introduced to the phenothiazine compound **2** by a Pd-catalyzed borylation to give compound **4**. The conditions used were inspired by Murata *et al.*,[93] but with another catalyst-system. The reaction is presented in Scheme 2.2.

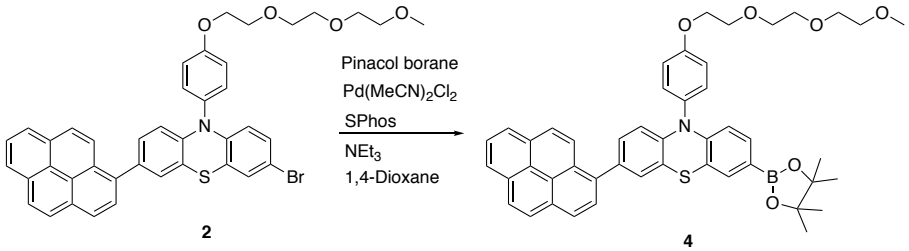

Scheme 2.2: Borylation of the donor molecule **2** to the boronate-functionalized compound **4**.

The borylation reaction was fast, as it was stirred for only 3 hours. Due to the instability on silica, the crude was only semi-purified with a celite plug. ^{1}H NMR indicated that pinacolborane was the only impurity with δ_H 7.92 and 1.17 ppm, and δ_C 81.8 and 24.9 ppm. The borylated phenothiazine **4** was carried out in a 94% yield (included the pinacolborane).

2.2.3 Suzuki-Miyaura Cross-Coupling Between Phenothiazine and Thiophene Aldehydes

The Suzuki-Miyaura cross-coupling between phenothiazine **4** and thiophene aldehydes was carried out with the same conditions as previously described in Section 2.2.1. The reactions are presented in Scheme 2.3.

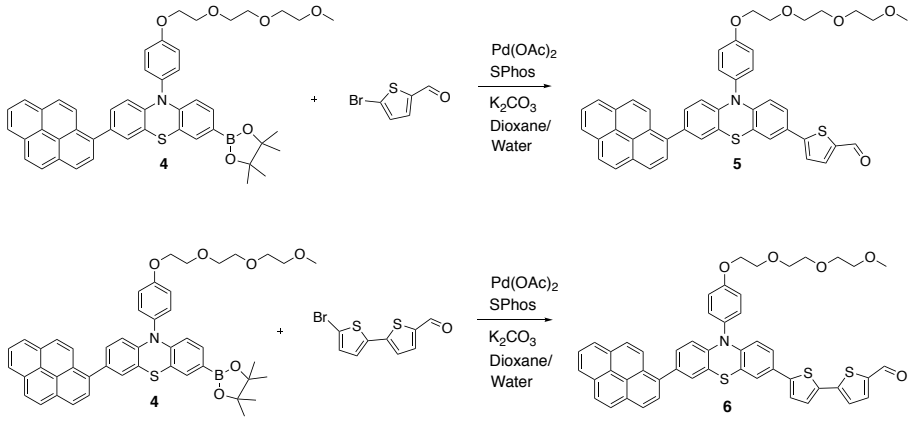

Scheme 2.3: Suzuki-Miyaura cross-coupling of the borylated compound **4** to form the donor-π-bridge systems **5** and **6**.

Both reactions to form the products **5** and **6** were run at 80 °C for 18 and five hours, respectively. This prepared the products **5** and **6** with a large difference in yield, 93% and 55%, respectively. The main inequality between the two reactions was the purification with silica gel chromatography. For compound **6** an EtOAc eluent was used, and an 1:1 Et_2O:EtOAc eluent-system for **5**. TLC did not show a better separation for the Et_2O:EtOAc eluent-system than for EtOAc. It is still possible that the Et_2O is a better eluent, due to the ether chains (TEOME) in the compounds **4**, **5** and **6**.

2.2.4 Knoevenagel Condensation to the Dyes MEL1 and MEL2

The Knoevenagel condensations displayed in Scheme 2.4 were used to derive the two target dyes **MEL1** and **MEL2**.

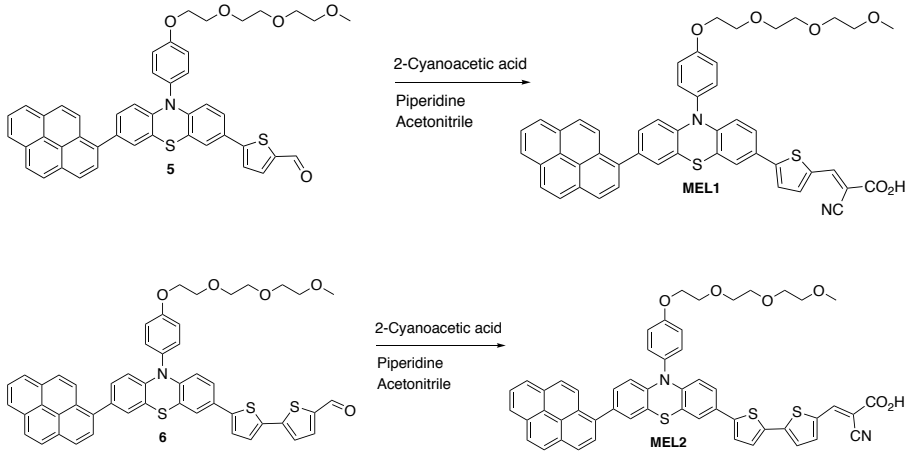

Scheme 2.4: Knoevenagel condensations to yield the target sensitizers **MEL1** and **MEL2**.

The Knoevenagel condensation is usually the last step in the synthesis of dyes, and it is expected to show high degree of conversion from this reactions.[74] A change in color from orange to red occured only minutes after the reactions were started. After 2 hours at reflux, both reactions showed full conversion, which was detected by TLC. The purification was performed with silica gel chromatography column with a gradient eluent system (DCM - DCM:MeOH). The products were not eluted in the DCM eluent, which makes all the impurities leave the column before addition of MeOH and following elution of the dyes **MEL1** and **MEL2**. The **MEL1** sensitizer was carried out from the Knoevenagel condensation in 94% yield, while the **MEL2** was synthesized in a yield of 72%.

2.2.5 Alkylation of Diketopyrrolopyrrole

In order to try other π-bridges, the diketopyrrolopyrrole (DPP) unit with thiophenes **7** was used. This extended π-conjugated bridge can hopefully reduce the band gap energy and increase the molar extinction coefficient, in order to get more efficient dyes. The absorption maxima is also expected to be more red-shifted for this dye than for the **MEL1** and **MEL2** dyes. This can result in adsorption of other parts of the visible-wavelengths. The incorporation of the DPP-unit can be done on similar dyes as the previous described **MEL1** and **MEL2**, as shown in Scheme 2.5.

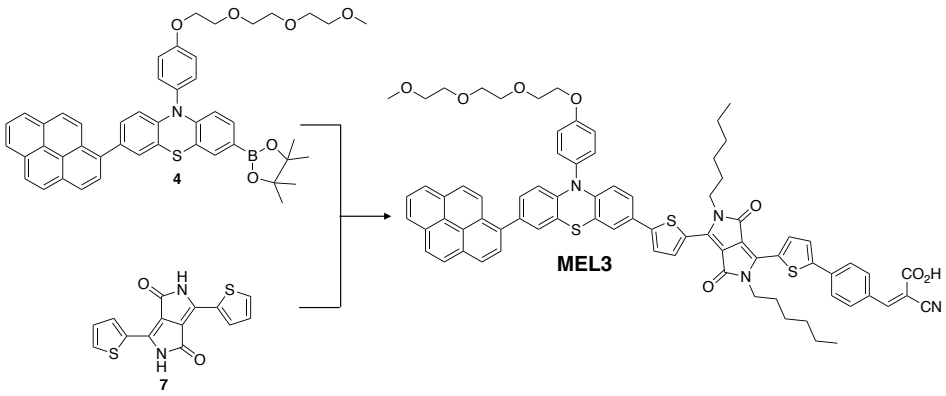

Scheme 2.5: The dye **MEL3** can be synthesized from phenothiazine **4** and DPP **9**.

The procedure for the amide alkylation was inspired by Vakuliuk *et al.*[94] The reaction was promising, as it had a yield of 79%. The method used the commercially available DPP **7** and potassium carbonate in DMF. They purified the product with re-crystallization. Additionally, the method employed $Bu_4N^+HSO_4^-$ and the alkylated agent was added in one portion. This differs from most of the other reaction done with this particularly system.[95–97] The reaction conditions are shown in Scheme 2.6.

Table 2.1 displays some relative amounts of mono-alkylated and *N,O*-dialkylated DPP **9** in the crude material, which were detected by ^{1}H NMR (400 MHz, $CDCl_3$). The un-alkylated compound **7** is not mentioned due to its insolubility in $CDCl_3$. The *O,O*-dialkylated **11** is also left out, due to only trace amounts were detected.

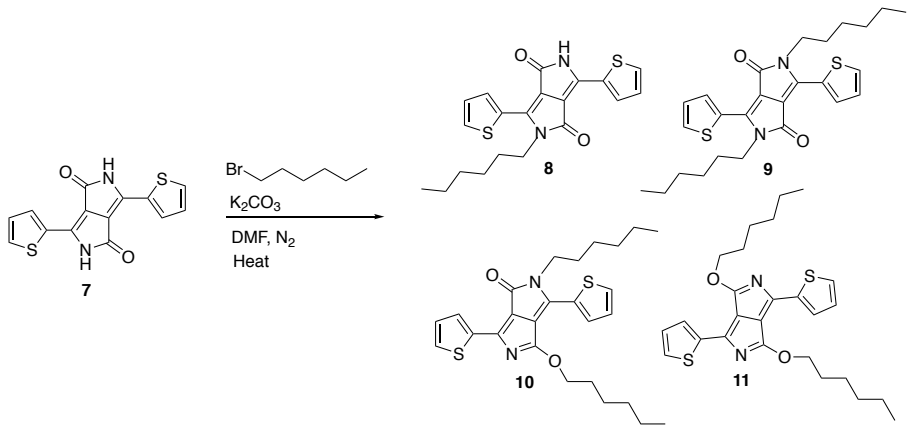

Scheme 2.6: Reaction conditions for amide alkylation of DPP **7** to form the alkylated derivate **9**.

Four out of eleven reactions (*Entry 1-4*), shown in Table 2.1, were performed with $Bu_4N^+HSO_4^-$ present. No clear difference was seen between the reactions with or without this phase transfer catalyst. The reaction time was varied between 3-25 hours, where the majority were between 20-25 hours. The experiment with reaction time of 3 hours (*Entry 1*) had a higher amount of the mono-N-alkylated product than the reactions with a longer reaction-time. The amount of *N,O*-dialkylated **10** was more or less the same as for the reaction with a longer reaction time. Therefore, the reaction time does not seem to affect the amount of *N,O*-dialkylated **10** equally as much. No significant difference was found between the 14 hour reaction (*Entry 10*) and the majority of reactions at 20-25 hours. This indicates that a reaction-time of approximately 14 hours or longer is mandatory for low yield of mono-alkylated DPP **10**, hence higher yield of *N,N*-dialkylated **9**.

Some variation of the temperature was also tested. An increase in temperature from 120 °C to 140 °C decreased the amount of *N,O*-dialkylated **10** from an average of 18% to 3%. The difference from 140 °C to 155 °C was not significant. This indicates that a high temperature, 140 °C, is required for *N-N* selection of the alkylation, but increasing above 140 °C would most likely have no effect.

The purification methods used were crystallization/re-crystallization or silica gel chromatography, as showed in Table 2.1. Some of the reactions were purified in many steps, but only the first step is presented in the table. The method described initially in this section suggested re-crystallization, with precipitation from cold DMF and re-crystallization with DCM and hexane. This was done for a reaction of 750 mg (*Entry 2*), in a yield of 11%. This purification method was supposed to be used for another reaction of 100 mg scale (*Entry 5*), but the product was

Table 2.1: Summary of alkylation reactions and purification. Hx is short for hexane. Purification and yields in this table are the first purification step.

Entry	Scale [mg]	Heat [°C]	Time [h]	Crude [%]		Purification		Yield [%]
				8[a]	**10**[b]	Cryst[c]	Chrom.[d]	
1	100	120	3	27	18	-	$CHCl_3$:Hx 7:3	11
2	750	120	25	2	22	DMF (DCM/Hx)	-	9
3	150	120	25	4	19	-	-	-
4	100	120	24	7	20	-	-	-
5	100	120	24	6	18	DMF	-	31
6	100	120	24	7	9	-	Hx:EtOAc 9:1	46
7	100	140	24	7	5	-	-	-
8	1000	140	24	6	4	DMF	-	31
9	1000	140	21	6	3	-	Hx:EtOAc 9:1	10
10	2000	140	14	4	2	DMF	-	43
11	2000	155	20	7	3	DMF	-	46

[a] *N*-monoalkylated **8**.
[b] *N,O*-dialkylated **10**.
[c] Crystallization (re-crystallization).
[d] Silica gel chromatography column.

pure after the precipitation from cold DMF, which was determined with ^{1}H NMR. This increased the yield to 31%. The exact same yield was obtained for a 1 000 mg scale (*Entry 8*) using the same crystallization conditions. Some more product could probably be isolated, due to 'bumping' while evaporation *in vacuo*. Two more reactions were purified with DMF crystallization (*Entry 10, 11*), which gave the pure *N,N*-dialkylated DPP **9** in a 43% and 46% yield. This indicates that crystallization is easier with a larger scale, which was expected. Only the *N,N*-dialkylated DPP **9** precipitated from cold DMF, meaning that crystallization is suficient purification for this particular system, and there is no need for re-crystallization.

The product **9** was isolated by silica gel chromatography following three of the reactions (*Entry 1, 6, 9*). The mono-alkylated compound **8** is effortless to sep-

arate from the di-alkylated compounds, due to its hydrophilic properties. 7:3 $CHCl_3$:hexane and 9:1 hexane:EtOAc were used as eluent-systems. The reaction with eluent system $CHCl_3$:hexane (*Entry 1*) had a large amount of mono-alkylated and *N,O*-dialkylated **10** in the crude material, and therefore only 11% was isolated of *N,N*-dialkylated product **9**. The two other reactions in a 100 mg (*Entry 6*) and 1 000 mg scale (*Entry 9*) which were purified by silica gel chromatography with eluent-system hexane:EtOAc had a yield of 46% (39 g silica) and 10% (102 g silica), respectively. ^{1}H NMR of the crude materials showed 16% of mono- and *N,O*-dialkylated of the 100 mg scale reaction, and 9% for the 1 000 mg scale. This argues for chromatography as purification method for relatively small scale reactions, and precipitation by crystallization for large scales.

One of the 2 g scales (*Entry 10*) had a crude containing 4% monoalkylated and 2% *N,O*-alkylated. This reaction was first purified with crystallization yielding 43% *N,N*-alkylated **9**, as previous described. The mother-liquor was purified with chromatography (104 g silica, hexane:EtOAc, 9:1), which resulted in a total yield of 52% of the *N,N*-dialkylated DPP **9**.

It has been reported that placing the branching point away from the nitrogen on DPP has increased the solubility compared to a linear alkyl, while maintaining their electronic properties.[98,99] This can reduce some of the solubility challenges, and may improve the alkylation and following reactions and purifications.

Formation of Mono-Alkylated Relative to *N,N*-Alkylated

An alkylation experiment with 120 °C was run in order to get a better under-

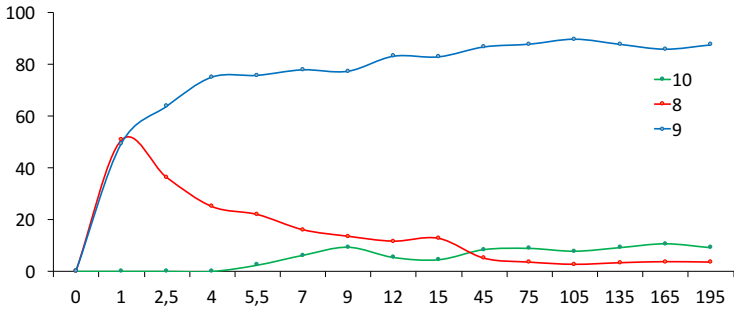

Figure 2.2: Formation of mono-alkylated **8** and *N,O*-alkylated **10** relative to *N,N*-alkylated **9**.

standing of the time-dependence formation of the *N*-monoalkylated **8** and *N,O*-dialkylated **10** relative to the *N,N*-dialkylated **9**, as displayed in Figure 2.2. Samples from the reaction were analyzed with ^{1}H NMR (400 MHz, $CDCl_3$).

As mentioned previously, the starting material, non alkylated **7**, is not soluble in chloroform, and was therefore not detected in the ^{1}H NMR-analysis. After only one minutes, there was formation of both mono- **8** and *N,N*-alkylated DPP **9**, with slightly more of the mono-alkylated molecule **8**. The *N,N*-dialkylated product **9** continues rapidly formation after the first minute, in line with the decreasing amount of mono-alkylated compound **8**. The formation of *N,O*-dialkylated **10** follows the same trend as shown for *N,N*-dialkylated **9**, but in smaller quantities.

2.2.6 NBS Bromination of Diketopyrrolopyrrole

The procedure for bromination of DPP was inspired by Sun *et al*.[100] The method uses NBS in $CHCl_3$ and acetic acid, as shown in Scheme 2.7 They carried out the brominated reaction in 77% yield.

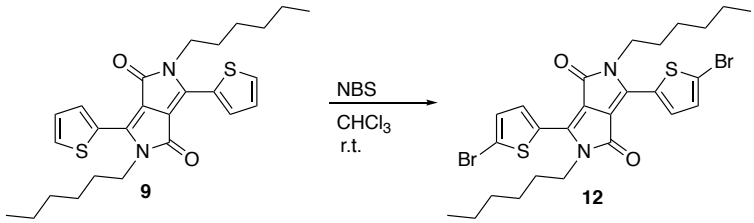

Scheme 2.7: NBS bromination of the DPP compound **9** to afford the brominated derivative **12**.

As the bromination is an electrophilic aromatic substitution (EAS) reaction, and sulfur (an electron donating atom) is attached to the aromatic, is it expected that the addition of bromine will occur in the position next to the sulfur, as shown in Scheme 2.7. Bromination in this position was obtained and no other brominated derivatives were observed. The reaction was followed with ^{1}H NMR, that revealed the importance of long reaction time, 15 hours, to achieve full conversion. The reaction was run three times at room temperature in the dark, in scales of 200 mg, 500 mg and 700 mg, and the crude was not purified for any of the reactions. The yield of the di-brominated product **12** was assumed 99% in all reaction. ^{1}H NMR-analysis predicted more than 98% pure product.

2.2.7 Suzuki-Miyaura Cross-Coupling on the DPP-Unit

The introduction of bromine in the previous mentioned reaction was done in order to react the product **12** further in a Suzuki-Miyaura cross coupling, to form the monosubstituted **14**. Six different experiments are summarized in Table 2.2. This table shows a variation of reaction time, catalyst, ligand and their relative amounts, analyzed with ^{1}H NMR. Notice that the table referres to the dehalogenated product **13**, and not target product **14**. The fixed conditions are shown in Scheme 2.8.

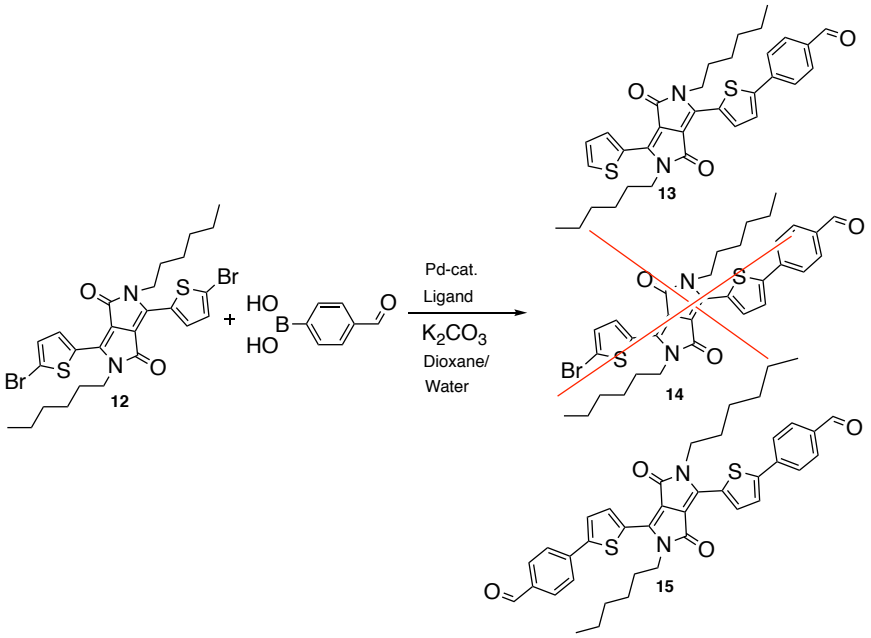

Scheme 2.8: Suzuki-Miyaura cross coupling on the dithiophene DPP **12** in an attempt to form the DPP-based aldehyde **14**.

The first experiment (*Entry 1*) with $Pd(OAc)_2$ and SPhos showed no conversion after 9 hours. In an attempt to get the disubstituted product **14**, an extra load of 4-formylphenylboronic acid (total 3 eq.) and catalyst/ligand were added to the reaction. After a total of 26 hours, 8% of both mono- and di-substituted product were formed, in addition to 23% of an unknown by-product. An experiment with the same start conditions was performed (*Entry 2*), to exclude the opportunity of human inaccuracy. This experiment had no conversion after 17 hours, and another reaction with a larger amount of catalyst and ligand was run (*Entry 3*). This resulted in a 6% conversion to the monosubstututed product **13** and 17% to the disubstituted **15**, and only trace amounts of the unknown by-product. In an attempt

Table 2.2: Summary of Suzuki cross coupling experiments on DPP, with varied catalyst and ligand. One unknown compound was also present, but is not included in this table.

Entry	Time [h]	Catalyst	(Eq.)	Ligand	(Eq.)	S[a] [%]	13 [%]	15 [%]
1	26	Pd(OAc)	(0.06)	SPhos	(0.10)	61	8	8
2	17	Pd(OAc)	(0.03)	SPhos	(0.06)	100	0	0
3	17	Pd(OAc)	(0.04)	SPhos	(0.08)	76	6	17
4	1	Pd(OAc)	(0.04)	XPhos	(0.08)	70	18	10
5	48	$Pd(dppf)Cl_2$	(0.06)	-	-	63	0	0
6	5	$Pd(PPh_3)_4$	(0.03)	-	-	94	0	6

[a] Starting material, 4-formylphenylboronic acid. Detected with ^{1}H NMR-analysis.

to decrease the amount of the disubstituted **15**, an experiment with with a reaction time of only one hour and another ligand, XPhos, was performed (*Entry 4*). A larger amount of the monosubstituted **13** was obtained, 18% out of a conversion of 30%.

All the described reactions above were run with the same catalyst. A reaction with the highly active palladium-catalyst $Pd(dppf)Cl_2$ showed no formation of either mono- or di-substituted product, even at a long reaction time of 48 hours. The catalyst $Pd(PPh_3)_4$ has been used on a similar compound,[101] but resulted in 6% conversion to the disubstituted compound.

None of the previous mentioned reaction showed the wanted halogenated product **14**, but instead the reduced product **13**. This indicates that the oxidative addition step is active. The reduction can occur from the unstable Aryl-Pd-R complex in the metathesis step, as mentioned in section 1.3.6.

The Suzuki-Miyaura cross-coupling was also used as a tool to bind the DPP unit **12** with the phenothiazine donor-group **4**, as shown in Scheme 2.9.

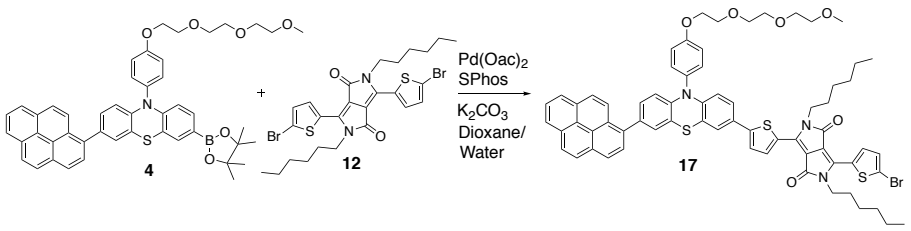

Scheme 2.9: Suzuki-Miyaura cross-coupling between DPP **12** and phenothiazine **4** in an attempt to form product **17**.

During the reaction the color changed from purple to blue-purple, which is a normal color for the mono-substituted dithiophenyl-DPP.[6] The crude material showed seven different spots on TLC. After four rounds of silica gel chromatography columns there was only a small amount of material left and still three spots on TLC. The same observation as for the previous described Suzuki on DPP was also seen in this reaction, the dehalogenated compound **16** was formed. This indicates that the Suzuki-Miyaura cross coupling on dithiophene-DPP compounds is challenging.

A change of methodology had to be done in order to synthesize target molecule **MEL3** with respectable yields. Both Stille cross-coupling[102,103] and direct arylation[104,105] on dithiophene-DPP-units have been described in the literature. Due to the highly toxic organotin agent used in Stille,[86] the direct arylation was the first choice.

2.2.8 Direct Arylation of the DPP-Unit

The procedure for the Pd-catalyzed direct arylation of the DPP compound was inspired by Bohra *et al*.[106] The method uses pivalic acid and K_2CO_3, as presented in Scheme 2.10

The DPP **9** was reacted in excess (1.2 eq.), to prevent di-substitution by the benzaldehyde. After 14 hours at 120 °C, the ratio between the mono-substituted **13** and the di-substituted DPP **15** of the crude material was 3:1, respectively. This means that an even larger excess of DPP is necessary to inhibit the di-substitution.

The DPP unit is as previous mentioned poorly soluble in many organic solvents. Therefore, only a limited selection of eluents are possible. This makes the purification with gel column chromatography challenging, and resulted in four columns where some product was isolated each time. The first column (Hexane/EtOAc/DCM)

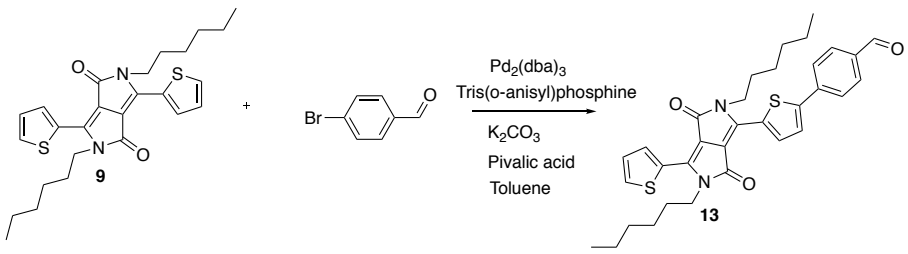

Scheme 2.10: Direct arylation between the DPP-unit **9** and benzaldehyde, to yield the DPP-based aldehyde **13**.

was performed to remove the starting material. The two aldehyde compounds were not eluted before addition of DCM. In theory this would result in isolation of all starting material. Unfortunately, the starting material was not soluble in the eluent-system, which resulted in DPP starting material **9** in all collected fractions. However, the largest amount of starting material was isolated during this column. The following three columns were able to isolate some of the three compounds each time. This direct alkylation gave the mono-substituted DPP-benzaldehyde **13** in a yield of 68% with high purity.

The exact same reaction conditions were used to couple the phenothiazine donor group **2** and the product **13** from the previous described reaction, as shown in Scheme 2.12.

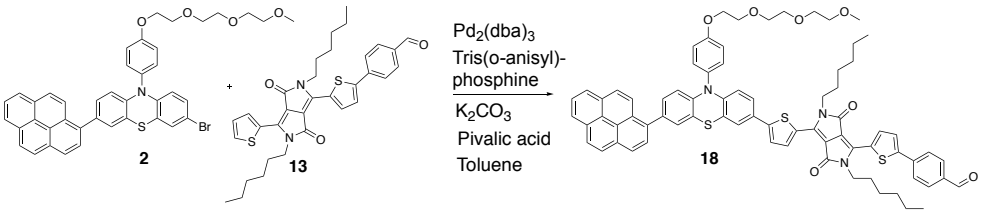

Scheme 2.11: The DPP-based aldehyde **13** was bound to the phenothiazine donor compound **2** in a direct arylation to form compound **18**.

After 12 hours at 120 °C the color changed from blue-purple to blue. The likely unfortunate by-product of this reaction could be the coupling of phenothiazine to a pyrene-group on another donor compound. This could result in the wanted product **18**, but with a double donor group couplet in series. After three silica gel chromatography columns, TLC-analysis indicated that there were still three compounds left. A ^{1}H NMR-analysis registered only one aldehyde peak, which is the functional-group who reacts in the next reaction, a Knoevenagel condensation.

The compound was therefore not further purified. The product **18** was synthesized in a 73% yield with a purity of 79%. HRMS was inconclusive, possibly due to its size and solubility properties.

2.2.9 Knoevenagel Condensation to Dye MEL3

A Knoevenagel condensation gave the target dye **MEL3**, as shown in Scheme 2.12.

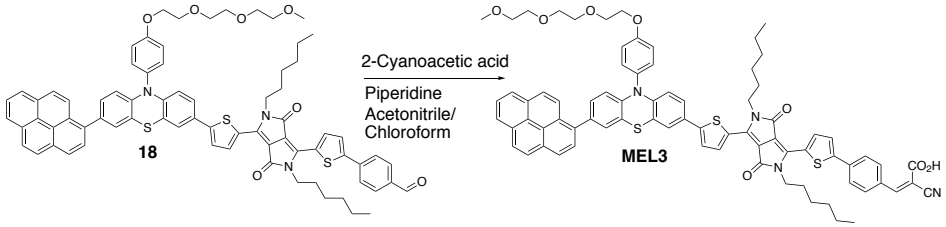

Scheme 2.12: Knoevenagel condensation to yield dye **MEL3**.

The starting material, 44.0 mg, was not soluble in the limited amount of acetonitrile. After one hour at reflux, additional solvent was added, but compound **18** was still not dissolved. Chloroform was added in a ratio of 1:3,[107] resulting in completely dissolved mixture. The reaction was followed by TLC, and full conversion was achieved after seven hours. Silica gel chromatography column gave 46.4 mg assumed product **MEL3**.

NMR spectroscopy for this molecule **MEL3** was inconclusive, meaning that HRMS and IR spectroscopy are the two most important analysis methods, in this case, for determining whether the dye is formed or not. The HRMS-analysis confirmed that the target dye **MEL3** was synthesized. IR spectroscopy had all the expected peaks for the target **MEL3**, but also an extra adsorption band. This signal is from the S=O stretch, indicating that the molecule is oxidized. Oxidation of the sulfur on phenothiazine S-5 have been seen during previous work in the research group at NTNU. There were also two other sulfur-atoms present on the thiophenes. The oxidized dye would have another molecular formula with corresponding molecular weight. The oxidized molecular weight was not found with HRMS-analysis, nor the dioxidized or trioxidized. It is therefore possible that there is more that differs between the by-product and the dye **MEL3** than oxidation of sulfur.

In TLC-analysis, only one spot was seen. This indicates that the by-product is an acid, due to the large difference in polarity compared to if it was not an acid. In the attempts to get a decent NMR spectra, the product **MEL3** was run in the

magnetic field of the NMR and solvents was removed in *vacuo* multiple times. This could have been unfortunate for the molecule, due to large exposure to light and air. The IR and MS analysis were both taken after this attempts of NMR-analysis. It is therefore not known whether the **MEL3** has been synthesized pure and unfortunately reacted during the analysis, or if the product was impure after the Knoevenagel reaction and purification. Since HRMS did not work for the predecessor molecule, it is also possible that the by-product was formed during the direct arylation. However, the HRMS and IR together indicated that the target dye **MEL3** is synthesized, but an unknown acid containing by-product is also present.

2.3 Photophysical Properties of the Dyes

This section presents UV-Vis absorption properties of sensitizers **MEL1-3**, **AFB-43** synthesized by Buene and the literature dye, **Dyenamo Blue**. All dyes are displayed in Figure 2.3. The obtained spectra for the the photophysical properties of the dyes are displayed in Figure 2.4, and summarized in Table 2.3.

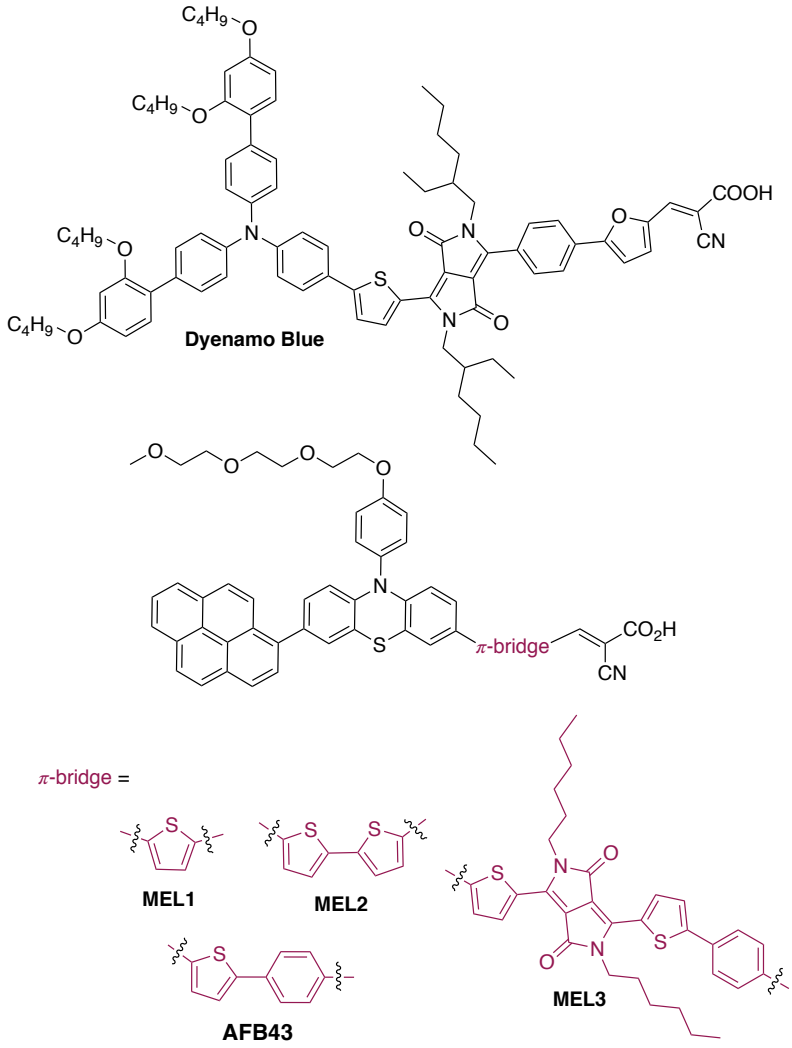

Figure 2.3: The literature dye **Dyenamo Blue**, previously synthesized dye **AFB-43** by Buene and the dyes in the **MEL**-series.

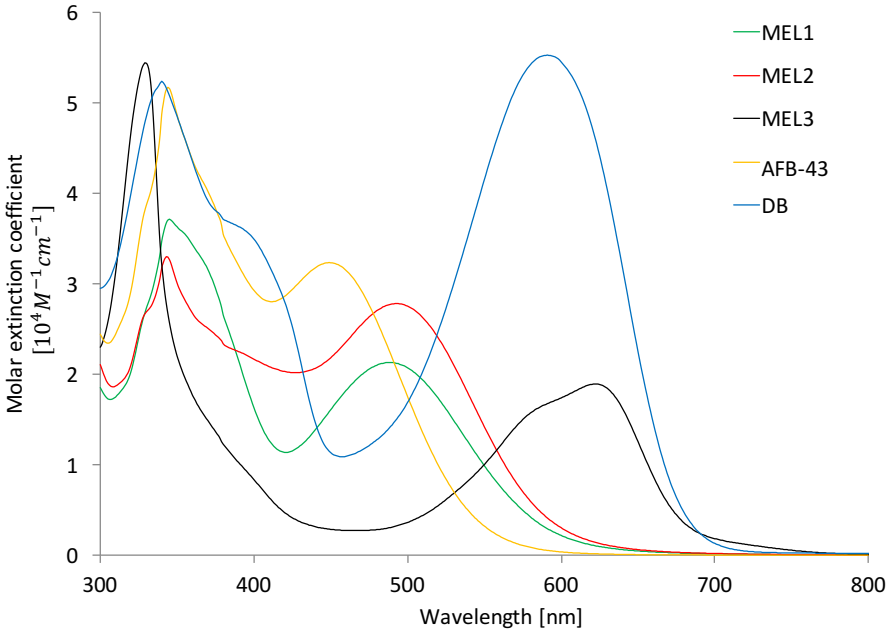

Figure 2.4: Recorded UV-Vis adsorption spectra of the dyes **MEL1-3** and **AFB-43** compared to the literature dye **Dyenamo Blue**.

The target dye **MEL1** had an adsorption maxima at 482 nm with a corresponding molar extinction coefficient, ε, of 21 401 $M^{-1}cm^{-1}$. The closely related dye **MEL2** showed a maxima adsorption of 497 with the corresponding ε-value of 27 838 $M^{-1}cm^{-1}$. Buenes dye **AFB-43** produced a lower adsorption, 452 nm, than **MEL1** and **MEL2**, but with a higher ε-value, 32 262 $M^{-1}cm^{-1}$. The DPP-dye **MEL3** had a more red-shifted adsorption spectra with a maxima of 622 nm and molar extinction coefficient of 18 928 $M^{-1}cm^{-1}$. The literature dye **Dyenamo Blue** had a lower adsorption maxima, 589 nm, but significant higher ε-value, 55 265 $M^{-1}cm^{-1}$, as shown in Table 2.3.

All the tested dyes had an adsorption maxima in the visible region, 400 - 700 nm. As displayed in Figure 2.4, two peaks are present for each dye. The peaks at 300-370 are corresponding to the π-π^* electronic transitions. The longer wavelengths at 380-600 nm are ascribed to the intramolecular charge transfer (ICT) from the donor to the acceptor.[108] This ensures efficient charge-separation in the excited state.

As expected the sensitizers with DPP-based π-bridges had more red-shifted adsorption maxima than the dyes with thiophene-based π-bridges. The sensitizer

Table 2.3: Photophysical properties of dyes **MEL1-3**, **AFB-43** and **Dyenamo Blue**.

Dye	Adsorption λ_{abs}[nm][a]	ε [$M^{-1}cm^{-1}$][b]	E_{0-0} [eV][c]
MEL1	492	21 401	2.08
MEL2	497	27 838	2.09
MEL3	622	18 928	1.81
AFB-43	452	32 262	2.29
Dyenamo Blue	589	55 265	1.83

[a] Absorption maximum of the most red shifted peak, measured in $CHCl_3$ ($2 \cdot 10^{-5}$ M).
[b] Molar extinction coefficient.
[c] Band gap energy.

AFB-43 has one thiophene and one phenyl, that blue-shifts the adsorption maxima. This can be due to the larger dihedral angel of the phenyl-thiophene bond, which decreases the orbital overlap.[109] This observation can be related to the phenyl in **MEL3**, and an even more red-shifted adsorption maxima could possibly occur if the phenyl was not present or replaced by a five membered heterocycle. A research done on phenyl-DPP based dyes looked at the difference of attaching the three aromatic compounds furan, phenyl and thiophene.[110] The combination of phenyl-DPP and thiophene showed the lowest conversion efficiency of all the three dyes. This supports that the phenyl-thiophene bond is not well suited for dyes to be used in DSSCs.

The band gap energy, E_{0-0}, was calculated according to the equation in Section 1.2.4: Energic Consideration of Dyes in DSSC. The result of the estimated band gap energy showed the same trend as previously described for adsorption, due to the dependence of these two values. The only exception was for the dyes **MEL1** and **MEL2**, where **MEL1** has a lower band gap energy than **MEL2**, although **MEL2** had a slightly more red-shifted adsorption maxima.

All the adsorption tested sensitizers showed a relatively high molar extinction coefficient, ε, of above 18 000 $M^{-1}cm^{-1}$. The literature dye **Dyenamo Blue** had a significant higher ε-value than the rest. The molar extinction coefficient is a measure of how strongly a molecule can absorb light at a particular wavelength, and can be increased by extending the π-conjugation of the π-bridge.[111] A dye with good light absorption-properties, high ε-value, can have less dye-molecules attached to the TiO_2. If fewer molecules are required for harvesting a certain amount of light energy, the thickness of the TiO_2-layer can be reduced.[112] A thin TiO_2-layer is desirable due to better electron and electrolyte diffusion through the semiconduc-

tor due to lower resistance, which lowers the charge recombination.[113]

Based on the photophysical properties of the dyes, the literature dye **Dyenamo Blue** is expected to outperform the dyes in the **MEL**-series, due to its red-shifted adsorption maxima and high molar extinction coefficient. The expected best dye to use in DSSCs of the **MEL**-series could be **MEL3** due to its large red-shifted adsorption maxima. **MEL3** has the lowest ε-value, but still higher than the literature dye **N719**, which is around 13 000 $M^{-1}cm^{-1}$.

The product **MEL3** is assumed to be impure, as discussed in Section 2.2.9: Knoevenagel Condensation to Dye **MEL3**. This can also be seen in Figure 2.4, as a double signal. It was used a 0.02 mM solution of the dyes to measure the photophysical properties, but if the product-mixture contains more than one molecule, this will result in a smaller signal with a lower extinction coefficient. This indicates that the dye **MEL3** is even more suited as a dye to use in DSSCs than expected from the measurements presented in this section.

None of these dyes cover large parts of the solar spectrum, displayed in Figure 2.5.[114] The TiO_2 can be co-sensitized with two different dyes to obtain a broad spectral response in the visible wavelengths.[115] The co-sensitization can also reduce charge recombination.[116]

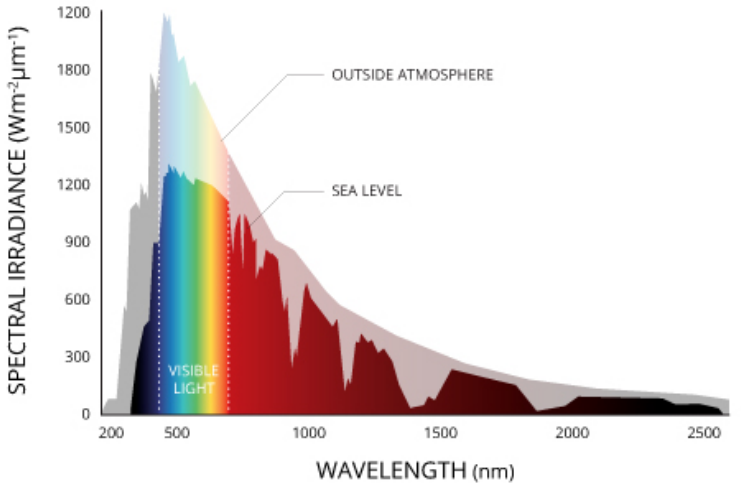

Figure 2.5: Solar spectrum at sea level and outside atmosphere. The solar radiation that reaches the earth contains most visible and infrared light.[114]

As presented in Figure 2.5, most energy can be harvested at wavelengths of around 500 nm. The dye **MEL2** has an absorption maxima at 497 nm, which is close to

the maxima of the solar spectra. The adsorption around 600 nm is close to zero, and in order to get a wider light absorption range the dyes **MEL2** and **MEL3** can be co-sensitized. The **MEL3** related dye **Dyenamo Blue** has been co-sensitized with dye **D35**. In this research the **Dyenamo Blue** had an efficiency of 5.6%, and increased to 7.3% when co-sensitizing with **D35** in a ratio of 1:1.[117] In another study the two same dyes were used with a ratio of 3:4 and resulted in an efficiency of 10.7%.[118] Due to assumed impurities in **MEL3**, the relative amounts of **MEL2** and **MEL3** for co-sensitization will not be discussed.

The other two dyes **MEL1** and **AFB-43** could also be used for co-sensitization with **MEL3**. **MEL1** has a lower extinction coefficient and slightly lower adsorption maxima, and will probably be outperformed by **MEL2**. The dye **AFB-43** has a significantly lower adsorption maxima and this dye combined with the **MEL3** dye will have a low adsorption around 530 nm, as displayed in Figure 2.4. The **MEL2** and **MEL3** dyes are assumed to perform best as co-sensitizers.

Chapter 3

Structure Elucidation

By investigation of ^{1}H, ^{13}C, COSY, HSQC and HMBC NMR spectra, IR and HRMS, the identities of the synthesized compounds were verified. The dyes **MEL1**, **MEL2** and **MEL3** were also characterized using UV-Vis spectroscopy. The spectroscopic data were analyzed using the literature by Silverstein *et al*.[119]

3.1 NMR

Figure 3.1 shows an overview of some connectivities used to elucidate the structure of new compounds. Assigned ^{1}H and ^{13}C are presented in Table 3.1 - 3.8, while NMR spectra used in stucture elucidation are given in Appendix under each specific compound. Most of the molecules have also been substantiated by MS and have been analyzed by IR spectroscopy.

All spectra contain residual signals from the used deuterated solvent. These, and signals remaining from solvents used in the synthesis were identified using litterature by Fulmer *et al*.[120] The solvent signals are not disscussed further. If other significant impurities are presented in the spectra, they will be commented.

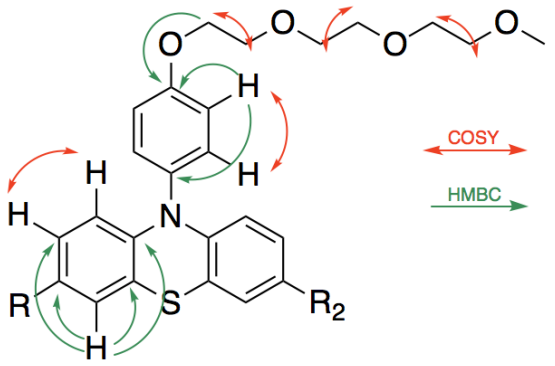

Figure 3.1: An overview of some COSY and HMBC connectivities used to elucidate the structure of new compounds.

For compounds containing pyrene, quaternary carbons in pyrene will not be assigned. No further reaction will be done directly on the pyrene group, and structure elucidation of pyrene is not crucial for further work with pyrene containing compounds. In order to identify different carbons and hydrogen of pyrene, the 2-D INADEQUATE NMR experiment can be used.[121] The method is useful for determining which signals arise from neighboring carbons. This method is mainly used in case of compounds with similar structures, such as pyrene.[122] The disadvantage of this experiment is the insensitivity, due to the low natural abundance of the NMR active ^{13}C isotope.

3.2 IR

IR spectra can be found in Appendix under each specific compound. Some bonds in the IR spectra are characteristic and shared for many of the synthesized molecules. All molecules have shown a weak absorption around 3200-2700 cm^{-1} resulting from aromatic C-H stretching. Aromatic C-H in-plane bending appear around 1300 - 1000 cm^{-1} and out-of-plane around 900 - 675 cm^{-1}. Other absorption bonds will be presented under each specific compound.

3.3 Spectroscopic Identification of 4

NMR, IR and HRMS analysis of compound **4** is shown in Appendix C: Spectroscopic Data - Compound **4**. HRMS concluded molecular formula $C_{47}H_{47}BNO_6S$ with exact mass 764.3217, which corresponded with the calculated mass at 764.7533.

Some characteristic signals of the functional groups on **4** were displayed in the IR spectrum. The peak 1140 is consistent with symmetric and asymmetric C-O-C streching of aliphatic ether.

The assigned ^{1}H and ^{13}C NMR signals of **4** are shown in Figure 3.2 and Table 3.1. This section contains a walk-through of the structure elucidation of the NMR analysis of compound **4**, apart from the quaternary carbon in the pyrene group.

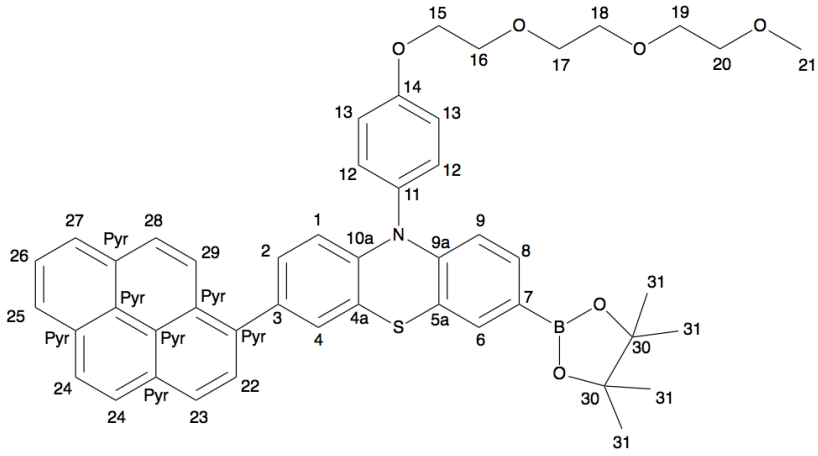

Figure 3.2: Assigned protons and carbons for compound **4**.

Table 3.1: ^{1}H (600 MHz) and ^{13}C NMR (150 MHz) shifts for compound **4** (DMSO-d_6). The position of carbons and protons are shown in Figure 3.2.

Position	**^{13}C NMR [ppm]**	**^{1}H NMR [ppm]**
1	116.2	6.30
2	129.7	7.19
3	135.3	-
4	128.3	7.30 - 7.26
4a	119.4	-
5a	118.0	-
6	132.8	7.26
7	122.7	-
8	134.4	7.23
9	115.4	6.19
9a	146.7	-
10a	143.1	-
11	132.5	-
12	132.3 (2C)	7.45 (2H)
13	117.3 (2C)	7.30 (2H)
14	158.9	-
15	67.9	4.23 (2H)
16	69.3	3.81 (2H)
17	70.4	3.63 (2H)
18	70.3	3.58 - 3.56 (2H)
19	70.1	3.55 - 3.53 (2H)
20	71.7	3.45 - 3.44 (2H)
21	58.5	3.24 (3H)
22	124.9	8.12
23	128.0	8.18
24	127.8 (2C)	8.21 (2H)
25	125.4	8.29
26	126.9	8.09
27	128.1	8.33-8.31
28	127.9	7.97
29	125.5	8.33-8.31
Pyr	136.1	-
Pyr	131.4	-
Pyr	130.8	-
Pyr	130.5	-
Pyr	125.8	-
Pyr	124.5	-
Pyr	124.6	-
30	84.0	-
31	25.1	1.27

The ^{1}H NMR singlet at 3.24 ppm, with intensity 3, was produced by the aliphatic ether-proton H-21. The protons did not couple to any other protons, as shown in Figure 3.3. As the figure displays, protons with chemical shift 3.45 - 3.44 ppm (H-20) and 3.55 - 3.53 ppm (H-19) couple with each other (green square). The same is observed for protons H-18 (3.58 - 3.56 ppm) and H-17 (3.63 ppm) (red square), and H-16 (3.81 ppm) and H-15 (4.23 ppm) (blue square).

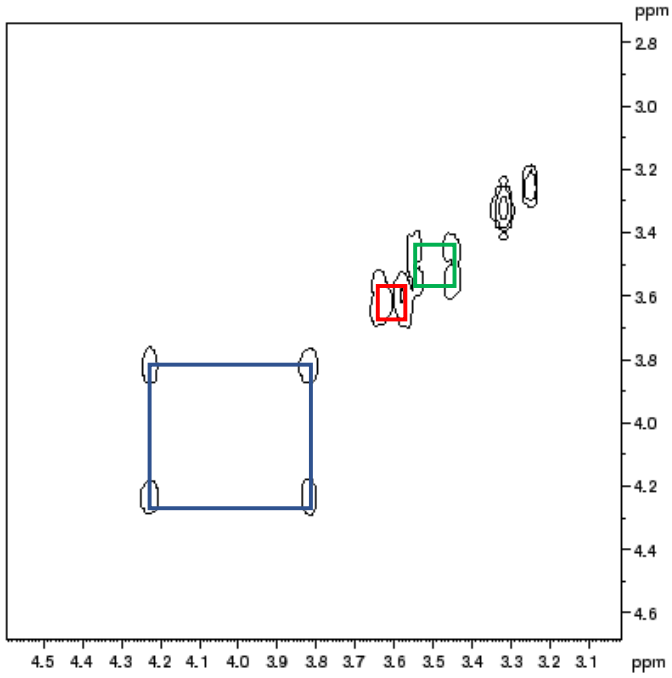

Figure 3.3: COSY of aliphatic ether chain in compound **4**.

As displayed in Figure 3.4, proton H-21 belongs to carbon with signal 58.5 ppm, H-20 to carbon at 71.7, and further on. This will not be explained for any other of the connecting protons and carbons in compound **4**.

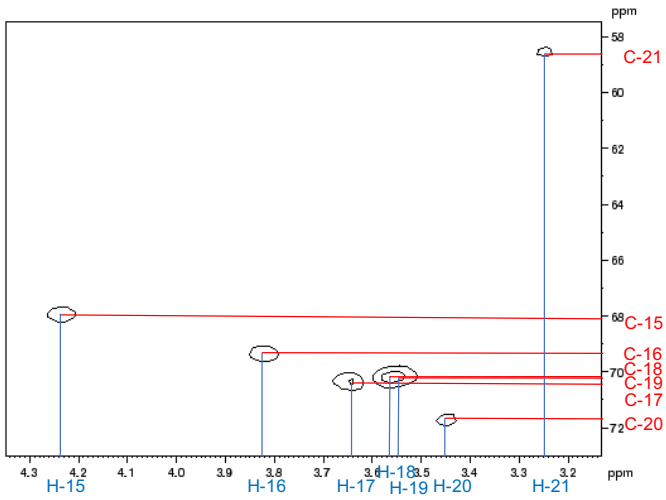

Figure 3.4: HSQC of aliphatic ether chain in compound **4**.

From COSY NMR spectra the ethylene-fragments and the one CH_3 group have been identified. Combining COSY and HMBC makes it possible to determine the order of the aliphatic ether chain, as shown in Figure 3.5, where coupling between carbon and neighboring protons are displayed.

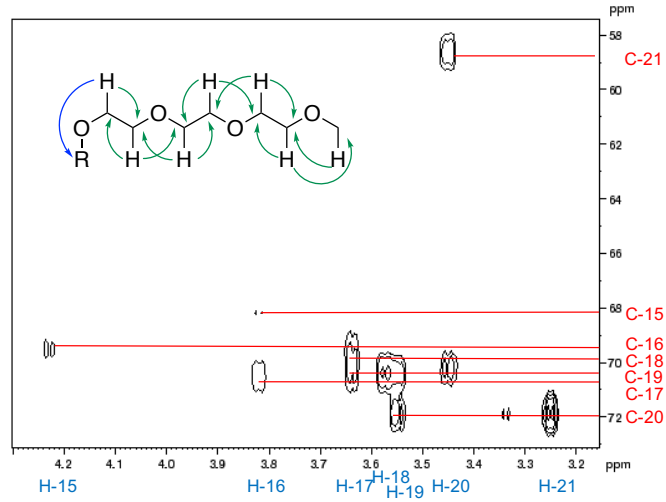

Figure 3.5: HMBC of aliphatic ether chain in compound **4**. Only one H shown where two or three H in the same position are equivalent.

The blue arrow in Figure 3.5 shows the coupling between H-15 and C-14, which is displayed in the HMBC NMR spectra in Appendix. Both H-12 and H-13 couple with C-14, as shown in Figure 3.6, but H-12 has a stronger correlation, which is normal for the meta position in phenyl compounds.

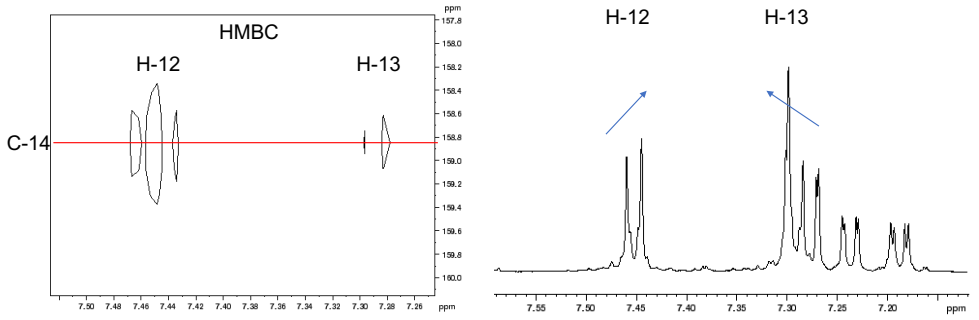

Figure 3.6: HMBC coupling between H-12, H-13 and C-14 and ^{1}H NMR of H-12 and H-13 in compound **4**.

As shown in Figure 3.6 the H-12 and H-13 are pointing at each other, which is an indication that they couple with each other. The use of coupling constants is preferable, but due to overlap in the ^{1}H NMR spectrum, the accurate coupling constants for H-13 could not be found. C-11 is coupling with both H-12 and H-13, but strongest to H-13. As expected, no correlation between C-11 and the phenothiazine proton is observed. H-4 is coupling with a carbon of chemical shift of 136.1 ppm, which is one of the pyrene-carbons, as displayed in Figure 3.7. This indicates that H-4 is on the left side of phenothiazine. Coupling between H-2 and

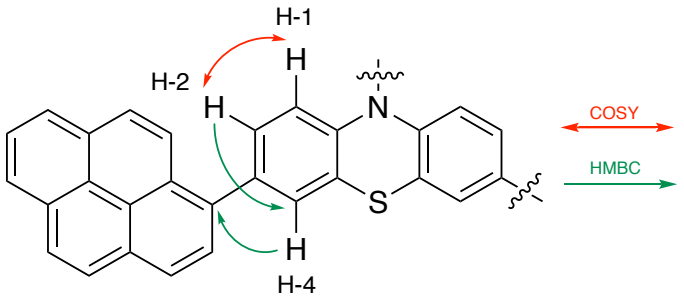

Figure 3.7: Proton-proton coupling between H-1 and H-2 (COSY) and proton-carbon coupling between H-4 and a pyrene-carbon and between H-2 and C-4 (HMBC) in compound **4**.

C-4 is suggested in HMBC NMR spectra, and further coupling between H-2 and H-1 is seen in COSY NMR spectra.

To verify the suggested structure displayed in Figure 3.7 the multiplicities and their coupling constants can be used for assigning H-1, H-2 and H-4. H-2 is a doublet of doublets, and has coupling-constants 8.5 Hz and 2.1 Hz, as shown in Figure 3.8. H-1 is a doublet with coupling-constant 8.42, which corresponds to the coupling-constant of H-2. The other coupling-constant of H-2 most likely corresponds to H-4, but the coupling-constant of H-4 can not be determined, due to the overlapping with the signal of H-13.

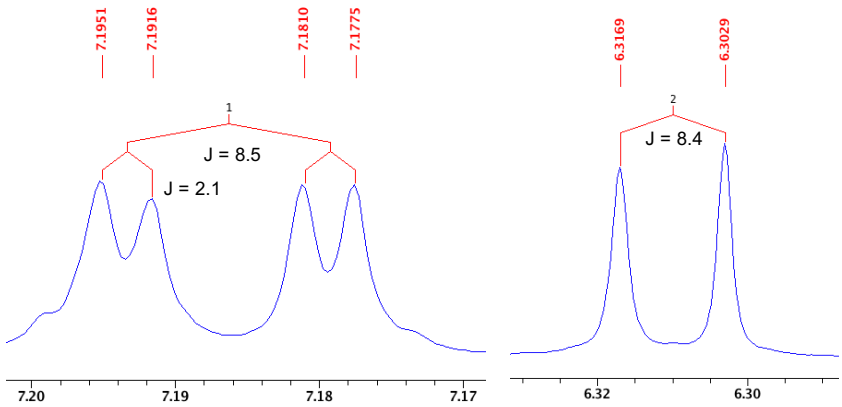

Figure 3.8: ^{1}H NMR of H-1 and H-2 signals in compound **4**.

The quaternary carbons C-3, C-4a and C-10a were assigned using HMBC. All of them coupled with the protons in the left ring of phenothiazine. C-3 was coupling with H-29 in the pyrene ring. C-10a was expected to have the highest chemical shift, due to having a nitrogen as the closest neighbor. The correlation between C-10a and the protons H-2 and H-4 was also stronger than between C-10a and H-1 due to meta-coupling,[119] as displayed in Figure 3.9. H-1 is in meta position with respect to C-4a, and a strong coupling between them is seen in the HMBC NMR spectra.

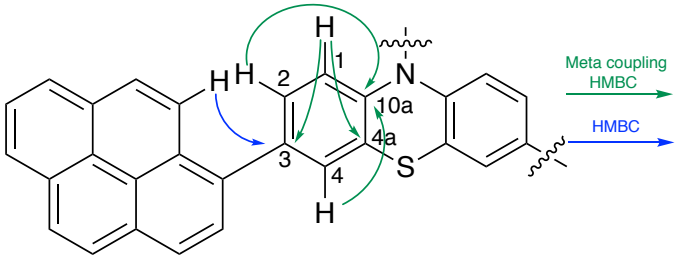

Figure 3.9: ^{1}H NMR of H-1 and H-2 signals in compound **4**.

The same can be done for the right side of the phenothiazine, so this will not be explained any futher. Connected to the right side of phenothiazine is the pinacolborane-group. H-31 had an intensity of 12 (3·4), and coupled to C-30.

For the pyrene-group, some fragments can be found using COSY NMR. The following fragments were found; H-22 and H-23, H-28 and H-29, H-26 couplet to both H-25 and H-27, as shown in Figure 3.10 as red arrows. A singlet of intensity 2 was seen for the two protons H-24, due to their identical environment. To connect all fragments HMBC NMR was used. The green arrows in Figure 3.10 give a summary of some of the couplings. A quaternary carbon with chemical shift 125.9 ppm coupled to both H-24 and H-25, which indicates that they are close to each other. The same observation was seen for the quaternary carbon with δ_c 124.9 ppm to H-27 and H-28, and between the quaternary carbon with δ_c 136.1 ppm to H-29 and H-22.

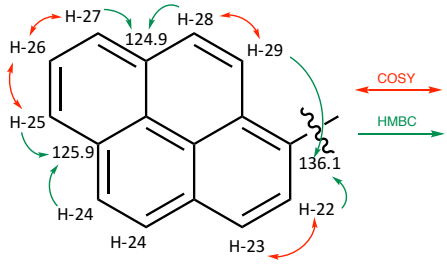

Figure 3.10: ^{1}H NMR of respectively H-1 and H-2 in compound **4**.

3.4 Spectroscopic Identification of 5

NMR, IR and HRMS analysis of compound **5** is shown in Appendix D: Spectroscopic Data - Compound **5**. HRMS predicted molecular formula $C_46H_38NO_5S_2$ with exact mass 748.2191, the calculated mass is 747.9182.

The IR spectrum in appendix displays some characteristic signals of the functional groups on compound **5**. The peak 1140 is consistent with symmetric and asymmetric C-O-C streching of aliphatic ether. The strong signal on 1654 cm^{-1} correspond to C=O stretching in aldehyde.

The assigned ^1H and ^{13}C NMR signals of **5** is shown in Figure 3.11 and Table 3.2.

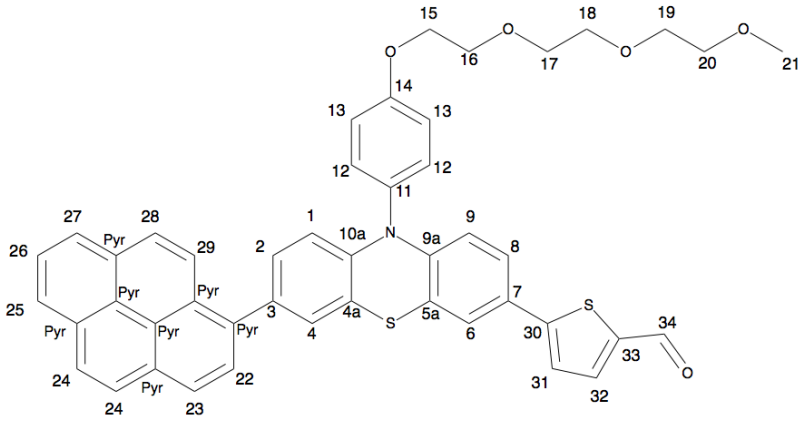

Figure 3.11: Assigned protons and carbons for compound **5**.

Table 3.2: ^{1}H (600 MHz) and ^{13}C NMR (150 MHz) shifts for compound **5** (DMSO-d_6). The position of carbons and protons are shown in Figure 3.11.

Position	**^{13}C NMR [ppm]**	**^{1}H NMR [ppm]**
1	116.2	6.34
2	130.0	7.21
3	135.5	-
4	124.4	7.56
4a	118.8	-
5a	119.9	-
6	128.5	7.34
7	127.4	-
8	126.1	7.39
9	116.3	6.21
9a	145.1	-
10a	142.9	-
11	132.5	-
12	132.3 (2C)	7.49 (2H)
13	117.3 (2C)	7.30 (2H)
14	159.0	-
15	68.0	4.23 (2H)
16	69.4	3.81 (2H)
17	70.4	3.64 - 3.62 (2H)
18	70.3	3.58 - 3.56 (2H)
19	70.1	3.55 - 3.53 (2H)
20	71.8	3.45 - 3.44 (2H)
21	58.5	3.24 (3H)
22	125.0	8.13
23	128.2	8.18
24	127.8 (2C)	8.21 (2H)
25	125.4	8.29
26	126.9	8.09
27	128.1	8.34 - 8.31
28	127.9	7.97
29	125.5	8.34 - 8.31
Pyr	136.1	-
Pyr	131.4	-
Pyr	130.9	-
Pyr	130.6	-
Pyr	125.8	-
Pyr	124.6	-
Pyr	124.5	-
30	152.1	-
31	124.8	7.63
32	139.9	7.99
33	141.5	-
34	184.2	9.86

3.5 Spectroscopic Identification of 6

NMR, IR and HRMS analysis of compound **6** is shown in Appendix E: Spectroscopic Data - Compound **6**. HRMS analysis confirms product **6** with a molecular formula $C_{50}H_{39}NO_5S_3$ with exact mass 830.2069 ($[M+H]^+$) and calculated mass is 830.0418.

The IR specra shows similar peaks as explained in Section 3.4. The assigned ^1H and ^{13}C NMR signals of **6** is shown in Figure 3.12 and Table 3.3.

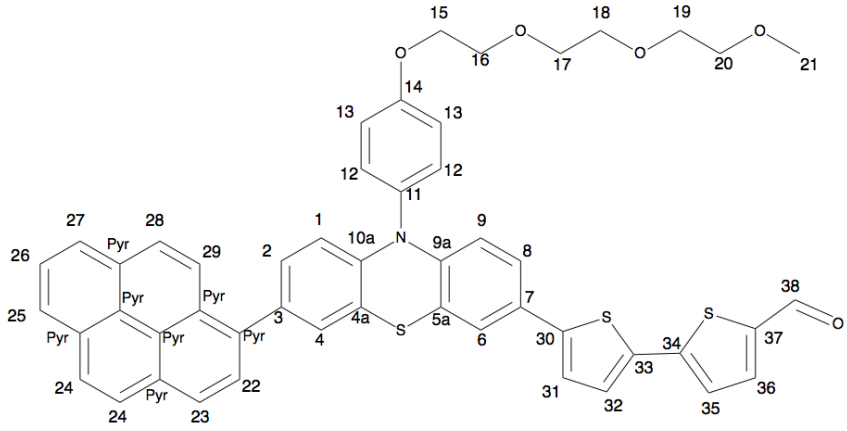

Figure 3.12: Assigned protons and carbons for compound **6**.

Table 3.3: ^1H (600 MHz) and ^{13}C NMR (150 MHz) shifts for compound **6** (DMSO-d_6). The position of carbons and protons are shown in Figure 3.12.

Position	**^{13}C NMR [ppm]**	**^1H NMR [ppm]**
1	116.2	6.34
2	129.9	7.21
3	135.3	-
4	124.9	7.49
4a	118.9	-
5a	119.9	-
6	128.5	7.34
7	127.9	-
8	125.2	7.31 - 7.27
9	116.4	6.21
9a	144.1	-
10a	143.1	-

11	132.6	-
12	132.3 (2C)	7.49 - 7.47 (2H)
13	117.4 (2C)	7.31 - 7.27 (2H)
14	159.0	-
15	68.0	4.23 (2H)
16	69.4	3.82 (2H)
17	70.4	3.65 - 3.63 (2H)
18	70.3	3.58 - 3.56 (2H)
19	70.1	3.55 - 3.54 (2H)
20	71.8	3.46 - 3.44 (2H)
21	58.5	3.24 (3H)
22	125.0	8.13
23	128.2	8.18
24	127.8 (2C)	8.21 (2H)
25	125.4	8.29
26	126.9	8.09
27	128.1	8.34 - 8.31
28	127.9	7.97
29	125.5	8.34 - 8.31
Pyr	136.1	-
Pyr	131.4	-
Pyr	130.9	-
Pyr	130.6	-
Pyr	125.8	-
Pyr	124.6	-
Pyr	124.5	-
30	144.5	-
31	123.7	7.49 - 7.47
32	128.7	7.59
33	133.9	-
34	146.0	-
35	125.4	7.54
36	139.7	8.00
37	141.5	-
38	184.2	9.88

3.6 Spectroscopic Identification of MEL1

NMR, IR and HRMS analysis of compound **MEL1** is shown in Appendix F: Spectroscopic Data - Compound **MEL1**.

HRMS-analysis shows that the molecular ion found was decarboxylated, this is a common fragmentation for acids.[123,124] This confirms that the product consist of **MEL1**, with a predicted molecular formula $C_46H_38NO_5S_2$, with exact mass 771.2351 ([M-COO+H]). The corresponding calculated mass was 770.9548.

The IR spectrum in appendix displayed some characteristic signals of the functional groups on compound **MEL1**. C≡N stretching is shown as a weak peak at 2164 cm^{-1}. The strong peak at 1574 is consistent with C=O stretching of the carboxylic acid. C-O-C streching of the aliphatic ether is shown as a peak at 1102 cm^{-1}.

The assigned ^1H and ^{13}C NMR signals are shown in Figure 3.13 and Table 3.4.

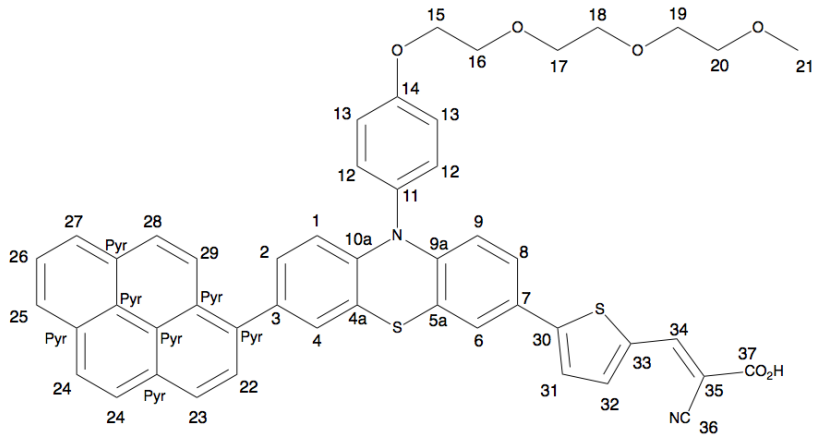

Figure 3.13: Assigned protons and carbons for compound **MEL1**.

Table 3.4: ^1H (600 MHz) and ^{13}C NMR (150 MHz) shifts for compound **MEL1** (DMSO-d_6). The position of carbons and protons are shown in Figure 3.13.

Position	^{13}C NMR [ppm]	^1H NMR [ppm]
1	116.3	6.34
2	130.0	7.21
3	135.4	-
4	128.5	7.33

4a	118.9	-
5a	119.9	-
6	124.1	7.49 - 7.47
7	127.7	-
8	125.7	7.32 - 7.29
9	116.4	6.23
9a	144.7	-
10a	143.0	-
11	132.5	-
12	132.3 (2C)	7.49 - 7.47 (2H)
13	117.4 (2C)	7.32 - 7.29 (2H)
14	159.0	-
15	68.0	4.23 (2H)
16	69.4	3.82 (2H)
17	70.4	3.64 - 3.62 (2H)
18	70.3	3.58 - 3.56 (2H)
19	70.1	3.55 - 3.53 (2H)
20	71.8	3.45 - 3.44 (2H)
21	58.5	3.24 (3H)
22	125.0	8.13
23	128.2	8.18
24	127.9 (2C)	8.21 - 8.20 (2H)
25	125.4	8.29
26	126.9	8.09
27	128.1	8.34 - 8.31
28	127.8	7.97
29	125.5	8.34 - 8.31
Pyr	136.1	-
Pyr	131.4	-
Pyr	130.9	-
Pyr	130.6	-
Pyr	125.8	-
Pyr	124.6	-
Pyr	124.5	-
30	149.2	-
31	124.4	7.57
32	138.4	7.77
33	135.4	-
34	143.0	8.21 - 8.20
35	163.7	-

Position number 36 and 37 are not assigned. Number 37 did not show in the ^{1}H or ^{13}C NMR spectra, but the δ_H are expected to be in the range of 9 - 12 ppm and a δ_C between 180 - 200 ppm. The shift for carbon number 36 is probably overlapping with another carbon, and is expected to be around 120 - 140 ppm. The exact δ_C could not be found, due to no H-C coupling in the HMBC NMR spectrum.

3.7 Spectroscopic Identification of MEL2

NMR, IR and HRMS analysis of compound **MEL2** is shown in Appendix G: Spectroscopic Data - Compound **MEL2**.

HRMS analysis displayed the same phenomenon that was found for the dye **MEL1**, decarboxylation, and suggest the product **MEL2** with molecule formula $C_{53}H_{40}N_2O_6S_3$, exact mass 853.2228 ([M-COO+H]). Calculated mass was 853.0784.

The IR spectrum in appendix shows simlilar trends as described for **MEL1**.

The assigned ^{1}H and ^{13}C NMR signals of **MEL2** is shown in Figure 3.14 and Table 3.5.

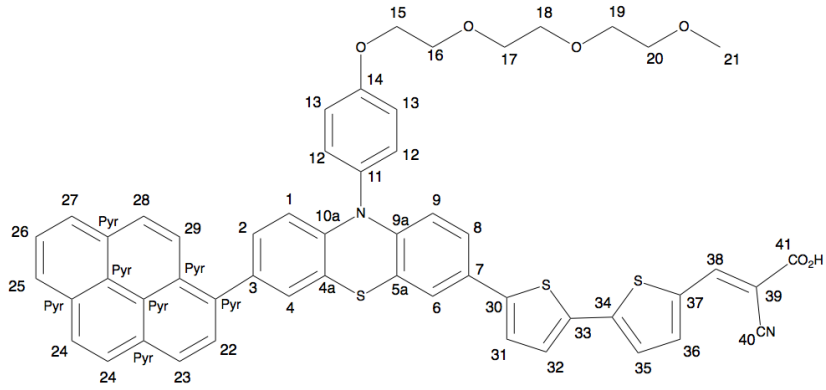

Figure 3.14: Assigned protons and carbons for compound **MEL2**.

Table 3.5: ^{1}H (600 MHz) and ^{13}C NMR (150 MHz) shifts for compound **MEL2** (DMSO-d_6). The position of carbons and protons are shown in Figure 3.14.

Position	**^{13}C NMR [ppm]**	**^{1}H NMR [ppm]**
1	116.2	6.33
2	129.9	7.20
3	135.2	-
4	128.5	7.33
4a	118.9	-
5a	119.8	-
6	123.6	7.49 - 7.47
7	128.0	-
8	125.1	7.31 - 7.27
9	116.4	6.20

9a	144.7	-
10a	143.0	-
11	132.6	-
12	132.4 (2C)	7.49 - 7.47 (2H)
13	117.4 (2C)	7.31 - 7.27 (2H)
14	159.0	-
15	68.0	4.23 (2H)
16	69.4	3.82 (2H)
17	70.4	3.65 - 3.63 (2H)
18	70.3	3.58 - 3.56 (2H)
19	70.1	3.55 - 3.54 (2H)
20	71.8	3.46 - 3.44 (2H)
21	58.5	3.25 (3H)
22	125.0	8.13
23	128.2	8.18
24	127.9 (2C)	8.21-8.20 (2H)
25	125.4	8.29
26	126.9	8.09
27	128.1	8.33 - 8.31
28	127.9	7.98
29	125.5	8.33 - 8.31
Pyr	136.1	-
Pyr	131.4	-
Pyr	130.9	-
Pyr	130.6	-
Pyr	125.8	-
Pyr	124.6	-
Pyr	124.5	-
31/32	124.9/125.0	7.49-7.47 (2H)
35	127.9	7.52
36	134.2	7.77
38	143.1	8.21 - 8.20
39	163.4	-

The Carbons at position number 30, 33, 34, 37 and 40 were not assigned, due to large overlap in the ^{13}C NMR spectra. As described in Section 3.6, the acidic carbon and proton number 40 did not show in the ^{13}C or ^{1}H NMR spectra.

3.8 Spectroscopic Identification of 13

NMR, IR and HRMS analysis of compound **13** is shown in Appendix L: Spectroscopic Data - Compound **13**. HRMS predicted molecular formula $C_33H_36N_2O_3S_2$ with exact mass 573.2246, which corresponded well with the calculated mass at 572.7791.

The IR spectrum in appendix displayed some characteristic signals of the functional groups on compound **13**. The strong signal on 1654 cm^{-1} correspond to C=O stretching in aldehyde. Amide C=O stretch also appear within the same region as for aldehyde C=O stretch. Amide C-N stretch is shown in the spectra as a medium peak at 1211 cm^{-1}.

The assigned ^{1}H and ^{13}C NMR signals of **13** is shown in Figure 3.15 and Table 3.6. Assigned protons and carbons 20 - 25 in the figure and table were combined, due to overlapping signals.

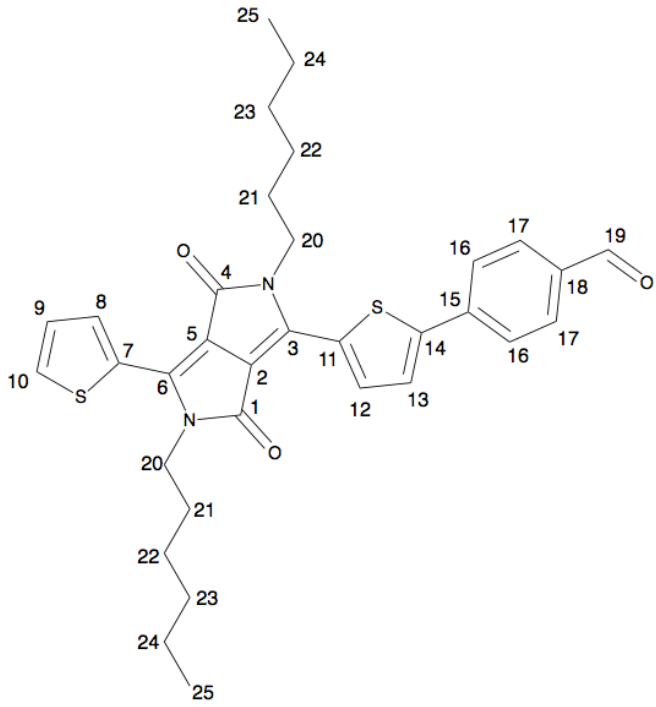

Figure 3.15: Assigned protons and carbons for compound **13**.

Table 3.6: ^{1}H (600 MHz) and ^{13}C NMR (150 MHz) shifts for compound **13** ($CDCl_3$). The position of carbons and protons are shown in Figure 3.15.

Position	**^{13}C NMR [ppm]**	**^{1}H NMR [ppm]**
1	161.4	-
2	108.3	-
3	139.0	-
4	161.4	-
5	108.3	-
6	140.5	-
7	129.7	-
8	135.6	8.97
9	128.7	7.31 - 7.29
10	131.1	7.66
11	130.7	-
12	136.3	8.94
13	126.3	7.60
14	147.3	-
15	138.7	-
16	126.4	7.84
17	130.6	7.94
18	136.0	-
19	191.2	10.03
20	42.3 (2C)	4.13 - 4.07 (4H)
21	30.0 (2C)	1.81 - 1.73 (4H)
22	26.6 (2C)	1.49 - 1.41 (4H)
23	31.4 (2C)	1.36 - 1.32 (4H)
24	22.6 (2C)	1.36 - 1.32 (4H)
25	14.0 (2C)	0.91 - 0.88 (6H)

3.9 Spectroscopic Identification of 15

NMR, IR and HRMS analysis of compound **15** is shown in Appendix M: Spectroscopic Data - Compound **15**. HRMS predicted molecular formula $C_{40}H_{40}N_2O_4S_2$ with exact mass 677.2508. The calculated mass was 676.8850.

The IR spectrum for this compound showed similar signals as compound **13**.

The assigned ^{1}H and ^{13}C NMR signals of **15** is shown in Figure 3.16 and Table 3.7.

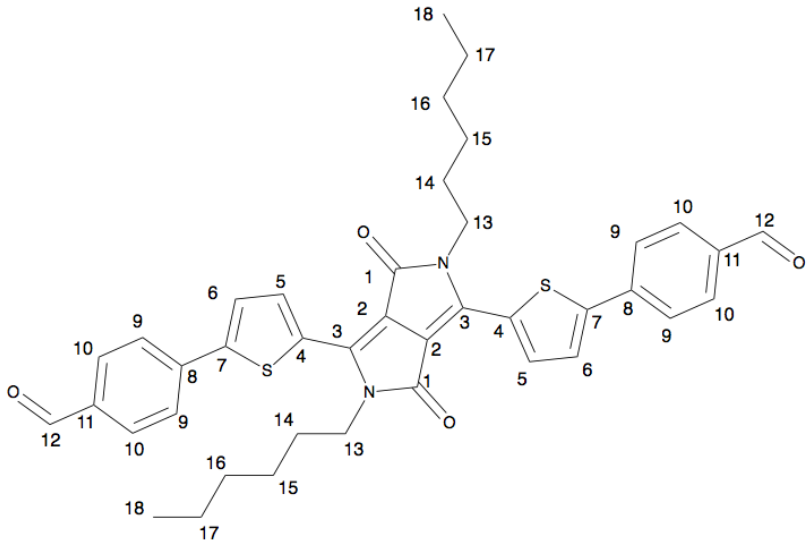

Figure 3.16: Assigned protons and carbons for compound **15**.

Table 3.7: ^{1}H (600 MHz) and ^{13}C NMR (150 MHz) shifts for compound **15** ($CDCl_3$). The position of carbons and protons are shown in Figure 3.16.

Position	**^{13}C NMR [ppm]**	**^{1}H NMR [ppm]**
1	161.3	-
2	108.8	-
3	139.4	-
4	130.5	-
5	136.6	8.98
6	126.4	7.62
7	147.8	-
8	138.6	-
9	126.5	7.85
10	130.6	7.95
11	136.0	-
12	191.2	10.04
13	42.4 (2C)	4.13 (4H)
14	30.0 (2C)	1.83 - 1.76 (4H)
15	26.6 (2C)	1.49 - 1.46 (4H)
16	31.4 (2C)	1.38 - 1.33 (4H)
17	22.6 (2C)	1.38 - 1.33 (4H)
18	14.0 (2C)	0.90 (6H)

3.10 Spectroscopic Identification of 18

NMR, IR and HRMS analysis of compound **18** is shown in Appendix N: Spectroscopic Data - Compound **18**.

The IR spectrum presents a strong peak at 1658 cm^{-1}, indicating a C=O stretching of aldehyde. Amide C=O stretch also appear within the same region. Amide C-N stretch is shown in the spectra as a medium peak at 1214 cm1. C-O-C stretchig of the aliphatic ether is shown as a weak peak at 1105 cm^{-1}.

The assigned ^{1}H and ^{13}C NMR signals of **18** is shown in Figure 3.17 and Table 3.8.

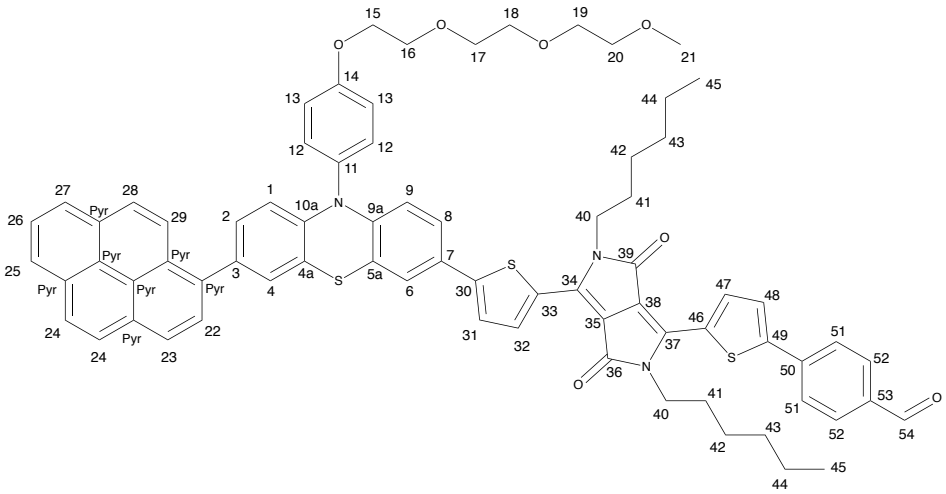

Figure 3.17: Assigned protons and carbons for compound **18**.

Table 3.8: ^{1}H (600 MHz) and ^{13}C NMR (150 MHz) shifts for compound **18** ($CDCl_3$). The position of carbons and protons are shown in Figure 3.17.

Position	**^{13}C NMR [ppm]**	**^{1}H NMR [ppm]**
1	115.8	6.36
2	129.3	7.12
3	135.9	-
4	128.5	7.33
4a	119.0	-
5a	120.4	-
6	123.7	7.29
7	127.3	-
8	125.0	7.19
9	115.9	6.25
9a	145.1	-
10a	143.0	-
11	132.9	-
12	132.0 (2C)	7.41 (2H)
13	116.9 (2C)	7.21 (2H)
14	158.9	-
15	67.9	4.26 (2H)
16	69.8	3.95 (2H)
17	71.0	3.81 - 3.79 (2H)
18	70.3	3.74 - 3.72 (2H)
19	70.7	3.70 - 3.68 (2H)
20	72.0	3.59 - 3.57 (2H)
21	59.1	3.40 (3H)
22	127.5	8.03
23	124.9	8.20 - 8.18
24	127.4 (2C)	8.08 (2H)
25	125.0	8.16
26	125.0	8.01
27	124.9	8.20 - 8.18
28	127.2	7.91
29	124.7	8.20 - 8.18
Pyr	136.2	-
Pyr	131.5	-
Pyr	131.0	-
Pyr	128.8	-
Pyr	126.0	-
Pyr	125.5	-
Pyr	125.1	-

30	140.5	-
31	123.8	7.35
32	137.5	9.01
33	149.8	-
34	127.6	-
35/38	115.8/115.9	-
36/39	161.2/161.5	-
37	130.9	-
40	42.3 (2C)	4.14 - 4.09 (4H)
41	30.1 (2C)	1.82 - 1.75 (4H)
42	26.6 (2C)	1.48 - 1.42 (4H)
43	31.4 (2C)	1.38 - 1.29 (4H)
44	29.8 (2C)	1.38 - 1.29 (4H)
45	14.1 (2C)	0.91 - 0.88 (6H)
46	147.0	-
47	135.9	8.91
48	126.4	7.60
49	138.0	-
50	138.8	-
51	126.4 (2C)	7.83 (2H)
52	130.6 (2C)	7.93 (2H)
53	147.0	-
54	191.4	10.03

3.11 Spectroscopic Identification of MEL3

IR and HRMS analysis of compound **MEL3** is shown in Appendix N: Spectroscopic Data - Compound **MEL3**. HRMS predicted molecular formula $C_{76}H_{71}N_4O_6S_3$ with exact mass 1231.4536. This corresponds to the decarboxylated molecular ion, which is normal for cyano-acrylic acids. The calculated mass is 1231.4536.

The IR spectra displays strong peaks at 2916 - 2850 cm^{-1} and 1701 - 1652 cm^{-1}, which can correspond to O-H stretching and C=O stretching in a carboxylic acid. The weak peaks at 2214-2013 is consistent with the C≡N stretching. The medium peak at 1081 cm^{-1} suggest the C-N stretching of the alkylated amide. Strong peaks at 1423 - 1307 cm^{-1} were found, and indicates the presence of S=O streching.

NMR-analysis was inconclusive for this compound.

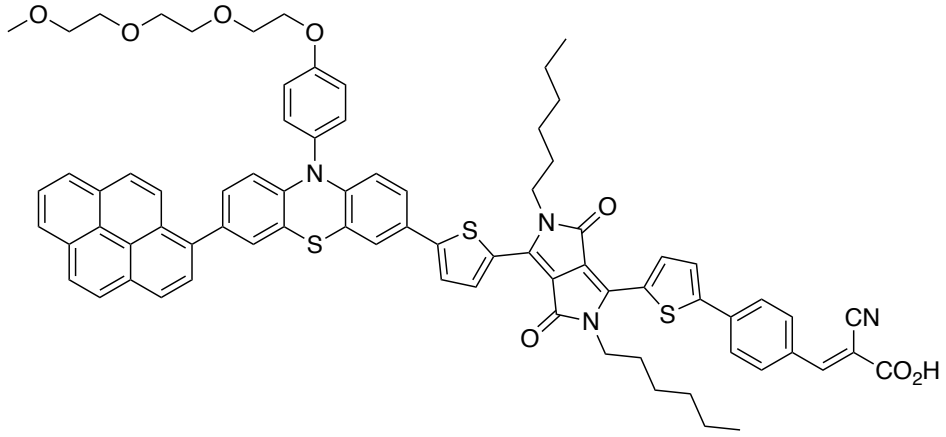

Figure 3.18: Compound **MEL3**.

Chapter 4

Conclusion and Further Work

4.1 Conclusion

The overall goal for this master thesis was to investigate the synthesis, chemistry and photophysical properties of phenothiazine-based dyes with various π-bridges. UV-Vis spectroscopy showed a large red-shifted adsorption maxima and corresponding low band gap energy for the extended π-conjugated dye **MEL3**. The DPP-dye **MEL3** has presumably better photophysical properties, especially extinction coefficient, than measured, due to impurities of the dye. Dye **MEL2** had the highest measured extinction coefficient of the dyes in the **MEL**-series. Dye **AFB-43** with both thiophene and phenyl in the π-bridge, had the most blue-shifted adsorption maxima. This can be due to the thiophene-phenyl bond that has a larger dihedral angle, and decreases the orbital overlap. Sensitizer **MEL3** also contains the thiophene-phenyl bond, and exchanging the phenyl with another aryl can possibly red-shift the adsorption maxima even more. The incorporation of the DPP-unit leads to sensitizers that adsorb other parts of the visible light spectra and can be used in co-sensitization. The two dyes suggested as the best combination for the co-sensitization are **MEL2** and **MEL3**.

The synthesis of the novel dyes **MEL1** and **MEL2** are given in Scheme 4.1. They were formed in a successful four-step linear synthesis. The first step toward these sensitizers gave the mono-substituted product in a yield of 54%. Due to the symmetry of phenothiazine **1**, this is considered as a high yield. In the following synthesis no further difficulties were met, and the reactions had yields ranging from 55 - 94%. The sensitizers **MEL1** and **MEL2** were synthesized in a total yield of

44% and 20%, respectively.

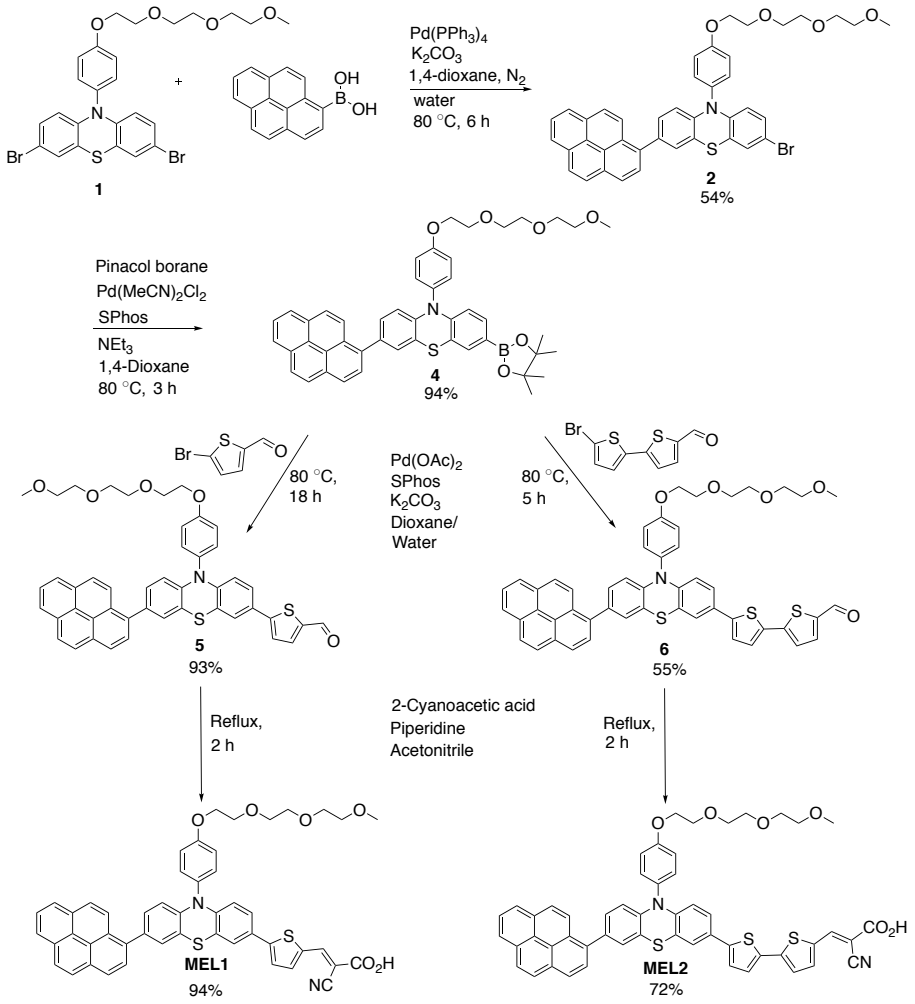

Scheme 4.1: Four-step synthesis route to **MEL1** and **MEL2**.

The first step towards the blue sensitizer **MEL3** was the alkylation, as displayed in Scheme 4.2. An investigation regarding the reaction temperature, time and purification method was performed in order to lower the yield of the by-products, namely mono-alkylated **8**, *N,O*-dialkylated **10** and *O,O*-dialkylated **11**. Long reaction time, 14 hours or more, was necessary to decrease the yield of mono-alkylated **8**. A high reaction-temperature, 140 °C, proved important for lowering the formation of *N,O*-dialkylated **10**. The two purification methods studied, were crystallization and silica gel chromatography column. Re-crystallization showed to

be superfluous, since pure product **9** precipitates from cold DMF. Crystallization was a more efficient purification method in large scales, while chromatography columns was a better choice for small scales. Product **9** was isolated in a yield of 52%.

The main synthetic challenge for this thesis has been the coupling between dithiophene-DPP unit and an aryl compound. A varied selection of Suzuki-Miyaura cross-coupling conditions were tested, and only a small amount of the dehalogenated product **13** was made. The synthetic route was changed, from a seven-step Suzuki-based to a five-step direct arylation-based strategy. This allows direct coupling from the alkylated DPP **9** to form compound **13** in 68% yield, followed by another direct arylation to form molecule **18** in 73% yield with a purity of 79%. The last step formed the target dye **MEL3**. Due to uncertainties regarding the impurities, the yield is uncertain.

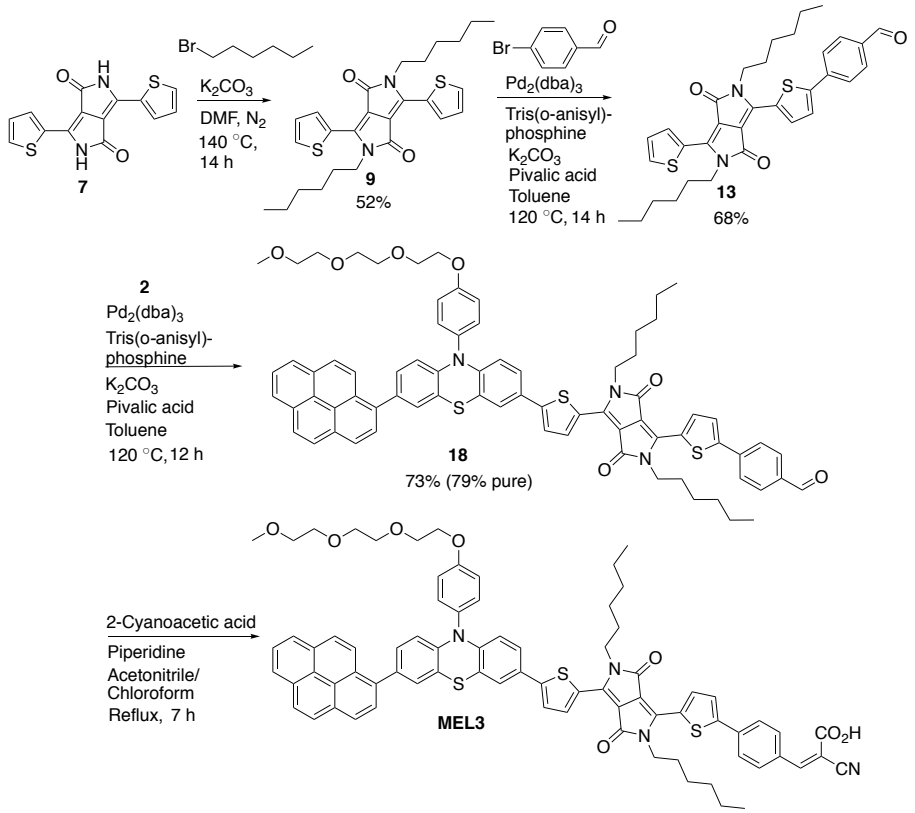

Scheme 4.2: Five-step synthesis route to **MEL3**.

4.2 Further Work

The synthesis of the novel dyes **MEL1** and **MEL2** worked out well and the main focus for the further work will be regarding dye **MEL3**. The synthetic route for the target molecule **MEL3** is still in need of optimization. The purification of the alkylation is one of the greatest weaknesses. Due to a limited selection of solvents that dissolves the DPP-based molecules it is also a limited selection of eluent-systems that can be used. It has been reported that alkyl-chains with the branching-point away from nitrogen have increased the solubility in many organic solvents. This could increase the yield in the alkylation step, as well as all the following DPP-containing steps. The direct arylation was successfully, but further optimization can be done, especially concerning the equivalents of starting material to tune the reaction towards the mono-substituted product.

The presence of a thiophene-phenyl p-linker has shown to decrease the efficiency of the dyes in DSSCs. Exchanging or eliminating the phenyl between the anchoring group and the DPP-unit in dye **MEL3** can red-shift the adsorption maxima more and thus a smaller band gap energy can be obtained. A five membered heteroaryl is preferable instead of the phenyl. The phenyl can also be left out, by binding the cyanoacrylic acid directly to the thiophene. This can be done by a formylation of the alkylated DPP group **9**, as displayed in Scheme 4.3. After the formylation is the DPP-unit no longer symmetric, and an easier direct arylation is expected.

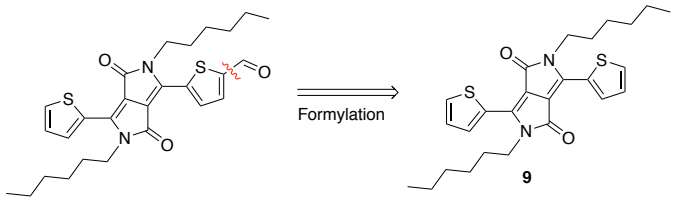

Scheme 4.3: Formylation of the DPP-unit to yield a dye with the anchoring group direct couplet to the thiophene on the DPP-unit.

There was some challenges regarding the analysis in the end of the synthetic-route towards **MEL3**. A blend of the target dye **MEL3** and an oxidized by-product were detected. An isolation of compound **MEL3** is therefore necessary in order to do further testing of **MEL3** as a sensitizer in DSSCs.

DSSCs can be fabricated for the dyes in the **MEL**-series. The iodine-electrolyte is well tested within the research group. With the incorporation of DPP it is probably

possible to use a cobalt electrolyte system, which is non-toxic and allows for higher open-circuit voltage.

Further investigation of the DPP-unit for use in DSSCs has potential due to the promising measured photophysical properties. Fabrication of co-sensitized DSSC with **MEL3** and **MEL2** can increase the efficiency due to a broad spectral response in the visible wavelengths.

Chapter 5

Experimental

5.1 General Methods

The reagents and solvents used were commercially available from Sigma Aldrich. A magnetic stirrer was used in all reactions, and an oil bath was used in cases of heating above 23 °C. All reactions were run under inert atmosphere (N_2), with degased solvents and under dry conditions (except Suzuki-Miyaura cross-coupling).

5.1.1 Chromatography

All reactions were monitored with thin layer chromatography, TLC (Merck, F_{254}, silica on aluminum plates). UV-light (254 nm and 365 nm) was used for visualization of the TLC-plates in case of non-colored substances. Most of the compounds had to be purified with column chromatography, with silica gel (40-60 μm) as a stationary phase and an eluent system as described for each reaction. For flash column, N_2 gas was used.

5.1.2 Nuclear Magnetic Resonance

^{1}H NMR (400/600 MHz) and ^{13}C NMR (100/150 MHz) were used to confirm the identity of the product, and were recorded at 22 °C on a Bruker spectrometer. The solvent used was DMSO-d_6 or $CDCl_3$, and calibration of the spectra was done by

using the signal of DMSO at 2.50 ppm (^{1}H) and 39.52 ppm (^{13}C), or that of TMS (0 ppm) in $CDCl_3$. Chemical shifts are reported as δ (ppm) and coupling constants as J (Hz).

5.1.3 Mass spectrometry

Synapt G2-S Q-TOF instrument form Waters^{TM} was used to determinate accurate mass in positive and negative mode. Samples were ionized by ACPI (Atmospheric-Pressure Chemical Ionization) and analyzed using an ASAP (Atmospheric Solids Analysis Probe). Waters^{TM} Software (Masslynx V4.1 SCN871) was used to calculate exact mass and spectrum processing.

5.1.4 Infrared absorption

Infrared absorption (IR) spectra were recorded with a FTIR Thermo Nicolet Nexus FT-IR Spectrometer using a Smart Endurance reflection cell. Reported frequencies were in the range of 4000 - 400 cm^{-1}.

5.1.5 Melting point

Stuart automatic melting point SMP40 or Gallenkamp Melting Point apparatus were used to determine the melting points.

5.1.6 UV-Vis spectroscopy

UV-Vis spectroscopy was performed using a Hitachi U-1900 spectrometer with light-path 10 mm. Wavelengths in the region 300-900 nm were reported. The adsorption maxima were presented with wavelength [nm], λ, and their corresponding molar extinction coefficients [$M^{-1}cm^{-1}$], ε.

5.2 Synthesis

5.2.1 3-Bromo-10-(4-(2-(2-(2-methoxyethoxy)ethoxy)ethoxy)-phenyl)-7-(pyren-1-yl)-10*H*-phenothiazine (2)[91]

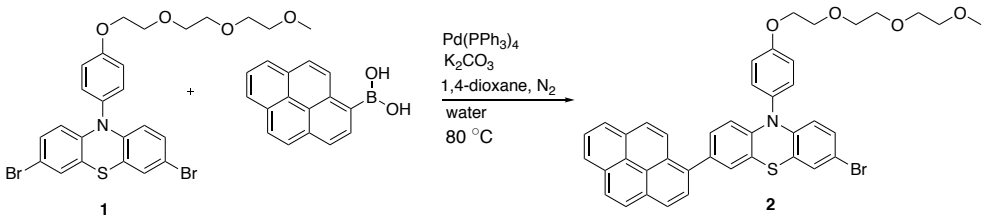

Compound **1** (500 mg, 0.84 mmol), pyrene-1-boronic acid (227 mg, 0.92 mmol), $Pd(PPh_3)_4$ (1.90 mg, 0.01 mmol), K_2CO_3 (431 mg, 3.36 mmol), 1,4-dioxane (3.00 mL) and water (3.00 mL) were stirred for 6 hours at 80 °C. The reaction was then quenched with water (40 mL) and extracted with EtOAc (120 mL). The organic phase was washed with water (40 mL) and dried with anhydrous Na_2SO_4. The solvent was filtered and removed *in vacuo*. Silica gel column chromatography was performed two times (95 g silica, EtOAc/pentane, 1:1, 79 g silica, EtO_2) where product was collected both times to yield compound **2**, 324 mg (0.45 mmol, 54%), as a yellow solid.

^{1}H NMR (600 MHz, DMSO-d_6) δ: 8.32 - 8.26 (m, 3H), 8.20 (s, 2H), 8.16 - 8.06 (m, 3H), 7.94 (d, J = 7.9, 1H), 7.43 (d, J = 8.9, 2H), 7.30 - 7.25 (m, 4H), 7.18 (dd, J = 8.5, J = 2.1, 1H), 7.11 (dd, J = 8.8, J = 2.3, 1H), 6.32 (d, J = 8.5, 1H), 6.08 (d, J = 8.8, 1H), 4.20 (t, J = 8.9, 2H), 3.80 (t, J = 8.9, 2H), 3.63 - 3.61 (m, 2H), 3.56 - 3.52 (m, 4H), 3.44 - 3.42 (m, 2H), 3.23 (s, 3H). The spectroscopic data corresponded well with that reported in the specialization project.[91]

5.2.2 10-(4-(2-(2-(2-Methoxyethoxy)ethoxy)ethoxy) phenyl)-3,7-di(pyren-1-yl)-10*H*-phenothiazine (3)[91]

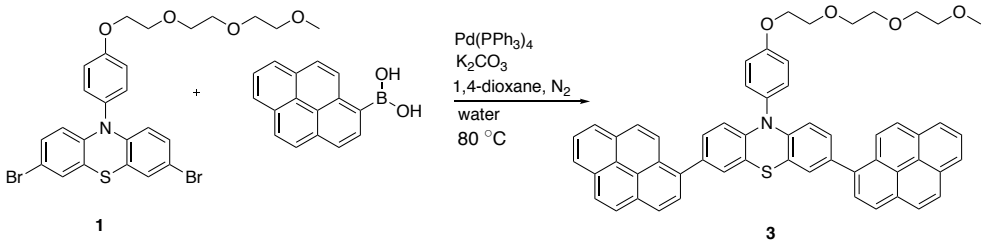

1 3

Product **3** was isolated from the synthesis described in Section 5.2.1.

^{1}H NMR (400 MHz, DMSO-d_6) δ: 8.36 - 8. 29 (m, 3H), 8.22 (s, 2H), 8.19 (d, J = 4.2, 2H), 8.10 (t, J = 7.6, 1H), 8.00 (d, J = 7.9, 1H), 7.60 (d, J = 8.9, 1H), 7.38 (d, J = 2.0, 1H), 7.34 (d, J = 9.0, 1H), 7.26 (dd, J = 8.5, J = 2.2, 1H), 6.43 (d, J = 8.5, 1H), 4.26 (t, J = 4.8, 2H), 3.84 (t, J = 4.2, 2H), 3.66 - 3.63 (m, 2H), 3.60 - 3.55 (m, 4H), 3.46 - 3.43 (m, 2H), 3.25 (s, 3H). The spectroscopic data corresponded well with that reported in the specialization project.[91]

5.2.3 10-(4-(2-(2-(2-Methoxyethoxy)ethoxy)ethoxy)phenyl)-3-(pyren-1-yl)-7-(4,4,5,5-tetramethyl-1,3,2-dioxaborolan-2-yl)-10*H*-phenothiazine (4)

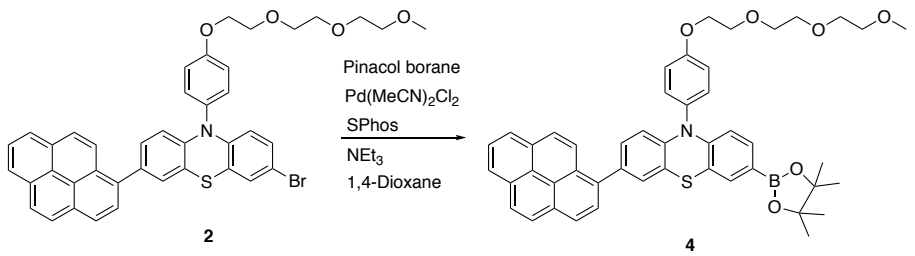

Compund (**2**) (270 mg, 0.38 mmol), $Pd(MeCN)_2Cl_2$ (1.00 mg, 0.02 mmol), SPhos (20.0 mg, 0.49 mmol), pinacol borane (72.3 mg, 0.57 mmol) and dry dioxane and NEt_3 were stirred for 3 hours at 80 °C. The reaction was cooled to room temperature before it was filtrated through a thin pad of Celite (SiO_2, EtOAc). The product **4** was not purified further, due to its unstability on silica. Drying gave 270 mg (0.35 mmol, 94%) of a yellow solid, mp. 59.7 - 62.2 °C.

^{1}H NMR (600 MHz, DMSO-d_6) δ: 8.33 - 8.31 (m, 2H), 8.29 (d, J = 7.5, 1H), 8.21 (s, 2H), 8.17 (d, J = 9.3, 1H), 8.12 (d, J = 9.3, 1H), 8.09 (t, J = 7.6, 1H), 7.97 (d, J = 7.9, 1H), 7.45 (d, J = 8.9, 2H), 7.30 - 7.26 (m, 4H), 7.23 (dd, J = 8.3, J = 1.4, 1H), 7.19 (dd, J = 8.4, J = 2.2, 1H), 6.30 (d, J = 8.4, 1H), 6.19 (d, J = 8.3, 1H), 4.23 (t, J = 4.7, 2H), 3.81 (t, J = 4.6, 2H), 3.64 - 3.61 (m, 2H), 3.58 - 3.56 (m, 2H), 3.55 - 3.53 (m, 2H), 3.45 -3.44 (m, 2H), 3.24 (s, 3H); ^{13}C NMR (150 MHz, DMSO-d_6) δ: 158.9, 146.7, 143.1, 136.1, 135.3, 134.4, 132.8, 132.5, 132.3 (2C), 131.4, 130.8, 130.5, 129.7, 128.3, 128.1, 128.0, 127.9, 127.8 (2C), 126.9, 125.8, 125.5, 125.4, 124.9, 124.6, 124.5, 122.7, 119.4, 118.0, 117.3 (2C), 116.2, 115.4, 84.0, 71.7, 70.4, 70.3, 70.1, 69.3, 67.9, 58.5; IR (neat, cm^{-1}) ν: 3038 (w), 1606 (w), 1507 (m), 1348 (m), 1140 (s), 846 (m), 670 (m), 549 (w); HRMS (APCI/ASAP+, m/z): found 764.3217 ([M+H]$^+$, calculated $C_{47}H_{47}BNO_6S$, 764.7533).

5.2.4 5-(10-(4-(2-(2-(2-Methoxyethoxy)ethoxy)ethoxy) phenyl)-7-(pyren-1-yl)-10*H*-phenothiazin-3-yl) thiophene-2-carbaldehyde (5)

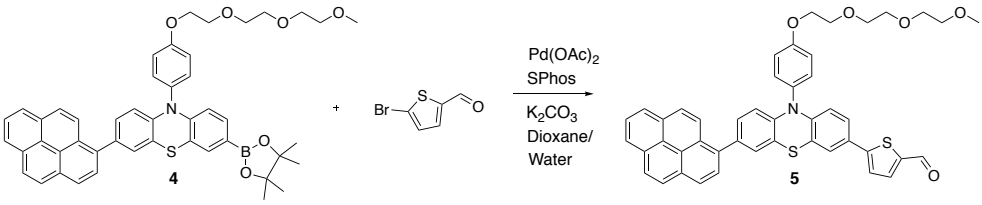

Compound **4** (190 mg, 0.25 mmol), 5-bromothenaldehyde (43.2 mg, 0.23 mmol), $Pd(OAc)_2$ (1.52 mg, 0.01 mmol), SPhos (5.57 mg, 0.01 mmol), K_2CO_3 (125 mg, 0.90 mmol), 1,4-dioxane (1.30 mL) and water (1.30 mL) were stirred for 18 hours at 80 °C. The reaction was then added water (40 mL) and extracted with EtOAc (3·40 mL). The organic phase was washed with water (40 mL) and dried with anhydrous Na_2SO_4. The solvent was filtered and removed *in vacuo*. Two Silica gel chromatography columns (39 g silica, Et_2O:EtOAc, 1:10, R_f = 0.45, 39 g silica, EtOAc, R_f = 0.37), where product was isolated from both columns, gave the product **5** as a yellow solid, 157 mg (0.21 mmol, 93%), mp. 123.1 - 123.9 °C.

^{1}H NMR (600 MHz, DMSO-d_6) δ: 9.86 (s, 1H), 8.34 - 8.31 (m, 2H), 8.29 (d, J = 7.5, 1H), 8.21 (s, 2H), 8.18 (d, J = 9.4, 1H), 8.13 (d, J = 9.3, 1H), 8.09 (t, J = 7.6, 1H), 7.99 (d, J = 4.0, 1H), 7.97 (d, J = 7.9, 1H), 7.63 (d, J = 4.0, 1H), 7.56 (d, J = 2.2, 1H), 7.49 (d, J = 8.8, 2H), 7.39 (dd, J = 8.7, J = 2.2, 1H), 7.34 (d, J = 2.1, 1H) 7.30 (d, J = 8.9, 2H), 7.21 (dd, J = 8.4, J = 2.1, 1H), 6.34 (d, J = 8.4, 1H), 6.2 (d, J = 8.7, 1H), 4.23 (t, J = 4.3, 2H), 3.81 (t, J = 4.6, 2H), 3.64 - 3.62 (m, 2H), 3.58 - 3.56 (m, 2H), 3.55 - 3.53 (m, 2H), 3.45 -3.44 (m, 2H), 3.24 (s, 3H); ^{13}C NMR (150 MHz, DMSO-d_6) δ: 184.2, 159.0, 152.1, 145.1, 142.9, 141.5, 139.8, 136.1, 135.5, 132.5, 132.3 (2C), 131.4, 130.9, 130.6, 130.0, 128.5, 128.2, 128.1, 127.9, 127.8 (2C), 127.4, 126.9, 126.1, 125.8, 125.5, 125.4, 125.0, 124.8, 124.6, 124.5, 124.4, 119.9, 118.8, 117.3 (2C), 116.3, 116.2, 71.8, 70.4, 70.3, 70.1, 69.4, 68.0, 58.5; IR (neat, cm^{-1}) ν: 3036 (w), 2869 (w), 1654 (m/s), 1431 (s), 1303 (m), 1223 (s), 1102 (m), 1055 (m), 799 (m), 682 (w/m), 552 (w); HRMS (APCI/ASAP+, m/z): found 748.2191 ([M+H]$^+$, calculated $C_{46}H_{37}NO_5S_2$, 747.9182).

5.2.5 5'-(10-(4-(2-(2-(2-Methoxyethoxy)ethoxy)ethoxy) phenyl)-7-(pyren-1-yl)-10*H*-phenothiazin-3-yl)- [2,2'-bithiophene]-5-carbaldehyde (6)

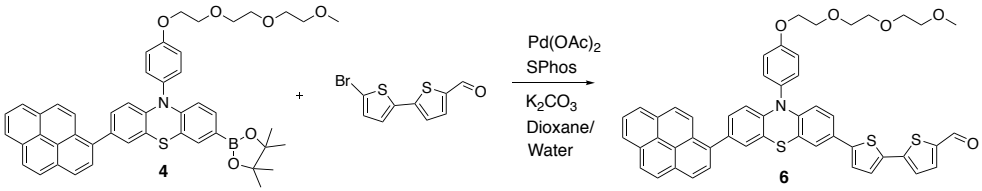

Compound **6** was made with the same approach as previously described for compound **5** (Section 5.2.4). Compound **4** (150 mg, 0.20 mmol) and the other reagents were stirred for 5 hours. Silica gel column chromatography was used two times (38 g silica, EtOAc, R_f = 0.42) and compound **6** was isolated after both columns, resulting in product **6** as a yellow solid, 80.8 mg (0.1 mmol, 55%), mp. 119.1 - 120.6 °C.

^{1}H NMR (600 MHz, DMSO-d_6) δ: 9.88 (s, 1H), 8.34 - 8.31 (m, 2H), 8.29 (d, J = 7.3, 1H), 8.21 (s, 2H), 8.18 (d, J = 9.4, 1H), 8.13 (d, 9.2, 1H), 8.09 (t, J = 7.6, 1H), 7.99 (d, J = 4.0, 1H), 7.98 (d, J = 7.9, 1H), 7.59 (d, J = 3.9, 1H), 7.53 (d, J = 3.6, 1H), 7.49 - 7.47 (m, 4H), 7.34 (d, J = 2.1, 1H), 7.31 - 7.27 (m, 3H), 7.21 (dd, J = 8.4, J = 2.1, 1H), 6.34 (d, J = 8.4, 1H), 6.21 (d, J = 8.6, 1H), 4.23 (t, J = 4.5, 2H), 3.82 (t, J = 4.6, 2H), 3.65 - 3.63 (m, 2H), 3.58 - 3.56 (m, 2H), 3.55 - 3.54 (m, 2H), 3.46 - 3.44 (m, 2H), 3.25 (s, 3H); ^{13}C NMR (150 MHz, DMSO-d_6) δ: 184.2, 159.0, 146.0, 144.5, 144.1, 143.1, 141.5, 139.7, 136.1, 135.3, 133.9, 132.6, 132.3 (2C), 131.4, 130.9, 130.6, 129.9, 128.7, 128.5, 128.2, 128.1, 127.9 (2C), 127.8 (2C), 126.9, 125.8, 125.5, 125.4 (2C), 125.2, 125.0, 124.9, 124.6, 124.5, 123.7, 119.9, 118.9, 117.4 (2C), 116.4, 116.2, 71.8, 70.4, 70.3, 70.1, 69.4, 68.0, 58.5; IR (neat, cm^{-1}) ν: 2923 (w), 1654 (s), 1606 (w), 1505 (m), 1444 (s), 1224 (s), 1102 (m), 791 (m), 551 (w); HRMS (APCI/ASAP+, m/z): found 830.2069 ([M+H]$^+$, calculated $C_{50}H_{39}NO_5S_3$, 830.0418).

5.2.6 (e)-2-Cyano-3-(5-(10-(4-(2-(2-(2-methoxyethoxy) ethoxy)ethoxy)phenyl)-7-(pyren-1-yl)-10*H*-phenothiazin-3-yl)thiophen-2-yl)acrylic acid (MEL1)

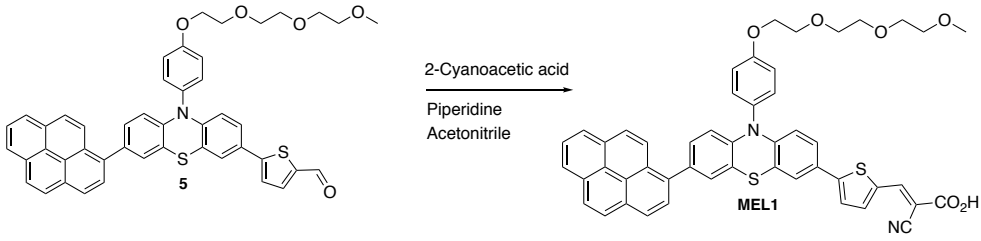

Compound **5** (150 mg, 0.20 mmol), 2-cyanoacetic acid (162 mg, 1.90 mmol), piperidine (0.20 mL, 1.14 mmol) and acetonitrile (22 mL) were stirred for 2 hours at reflux (84 °C). After reaching room temperature, the reaction was quenched with acidic water (120 mL, 2M HCl), and stirred for 15 min. The mixture was extracted with chloroform (100 mL) and dried over anhydrous Na_2SO_4. The solvent was filtered and removed *in vacuo*. Silica gel column chromatography (38 g silica, gradient DCM - DCM:MeOH, 5:1) gave product **MEL1** as a red solid, 153 mg (0.19 mmol, 94%), mp. 172.7 - 173.4 °C.

^{1}H NMR (600 MHz, DMSO-d_6) δ: 8.34 - 8.31 (m, 2H), 8.29 (d, J = 7.4, 1H), 8.21 - 8.20 (m, 3H), 8.18 (d, J = 9.4, 1H), 8.13 (d, J = 9.2, 1H), 8.09 (t, J = 7.6, 1H), 7.97 (d, J = 7.8, 1H), 7.77 (d, J = 3.7, 1H), 7.6 (d, J = 3.91, 1H), 7.49- 7.47 (m, 3H), 7.33 (d, J = 2.1, 1H), 7.32 - 7.29 (m, 3H), 7.21 (dd, J = 8.4, J = 2.0, 1H), 6.34 (d, J = 8.4, 1H), 6.23 (d, J = 8.7, 1H), 4.23 (t, J = 4.2, 2H), 3.82 (t, J = 4.4, 2H), 3.64 - 3.62 (m, 2H), 3.58 - 3.56 (m, 2H), 3.55 - 3.53 (m, 2H), 3.45 -3.44 (m, 2H), 3.24 (s, 3H). ^{13}C NMR (150 MHz, DMSO-d_6) δ: 163.7, 159.0, 149.2, 144.7, 143.0 (2C), 138.4, 136.1, 135.4 (2C), 132.5, 132.3 (2C), 131.4, 130.9, 130.6, 130.0, 128.5, 128.2, 128.1, 127.9 (2C), 127.8, 127.7, 126.9, 125.8, 125.7, 125.5, 125.4, 125.0, 124.6, 124.5, 124.4, 124.1, 119.9, 118.9, 117.4 (2C), 116.4, 116.3, 71.8, 70.4, 70.3, 70.1, 69.4, 68.0, 58.5. IR (neat, cm^{-1}) ν: 3035 (w), 2915 (w), 2849 (w), 2164 (w), 1710 (w), 1574 (m/s), 1472 (m/s), 1304 (s), 1242 (s), 1102 (m), 1060 (m), 939 (w), 800 (m/s), 719 (w/m), 617 (w), 547 (w). HRMS (APCI/ASAP+, m/z): found 771.2351 ([M-COO+H], calculated $C_{48}H_{38}N_2O_4S_2$, 770.9548)

5.2.7 (e)-2-Cyano-3-(5'-(10-(4-(2-(2-(2-methoxyethoxy) ethoxy)ethoxy)phenyl)-7-(pyren-1-yl)-10*H*-phenothiazin-3-yl)-[2,2'-bithiophen]-5-yl)acrylic acid (MEL2)

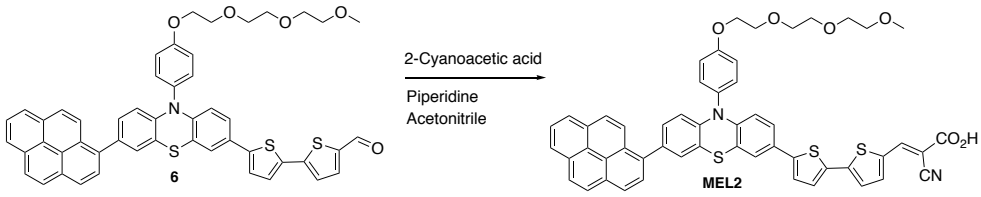

The dye **MEL2** was made with the same reaction conditions as dye **MEL1**. Compound **6** (79 mg, 0.10 mmol) and the other reagents were stirred for 2 hours. Purification by silica gel column chromatography (40 g silica, DCM - DCM:Metanol, 10:1) gave dye **MEL2** as a red solid, 58.3 mg (0.06 mmol, 72%), mp. 171.4 - 172.1 °C.

^{1}H NMR (600 MHz, DMSO-d_6) δ: 8.33 - 8.31 (m, 2H), 8.29 (d, J = 7.26, 1H), 8.21 (s, 3H), 8.18 (d, J = 9.4, 1H), 8.13 (d, 9.3, 1H), 8.09 (t, J = 7.6, 1H), 7.98 (d, J = 7.9, 1H), 7.77 (broad, 1H), 7.52 (d, J = 3.8, 1H), 7.49 - 7.47 (m, 5H), 7.33 (d, J = 2.1, 1H), 7.31 - 7.27 (m, 3H), 7.20 (dd, J = 8.4, J = 2.1, 1H), 6.33 (d, J = 8.4, 1H), 6.20 (d, J = 8.6, 1H), 4.23 (t, J = 4.5, 2H), 3.82 (t, J = 4.6, 2H), 3.65 - 3.63 (m, 2H), 3.58 - 3.56 (m, 2H), 3.55 - 3.54 (m, 2H), 3.46 - 3.44 (m, 2H), 3.25 (s, 3H); ^{13}C NMR (150 MHz, DMSO-d_6) δ: 159.0, 144.0, 136.1, 135.2, 134.2, 132.6, 132.4 (2C), 131.4, 130.9, 130.6, 129.9, 128.5, 128.2, 128.1, 128.0, 127.9 (3C), 126.9, 125.8, 125.5, 125.4 (2C), 125.1, 125.0 (2C), 124.9, 124.6, 124.5, 123.6, 119.8, 118.9, 117.4 (2C), 116.4, 116.2, 71.8, 70.4, 70.3, 70.1, 69.4, 68.0, 58.5; IR (neat, cm^{-1}) ν: 2916 (w), 2207 (w), 1711 (m), 1505 (m), 1440 (m), 1241 (s), 1052 (m), 791 (m/s), 549 (w), 447 (w). HRMS (APCI/ASAP+, m/z): found 853.2228 ([M-COO+H], calculated $C_{52}H_{41}N_2O_4S_3$, 853.0784).

5.2.8 2,5-Dihexyl-3,6-di(thiophen-2-yl)-2,5-dihydropyrrolo [3,4-c]pyrrole-1,4-dione (9)[125]

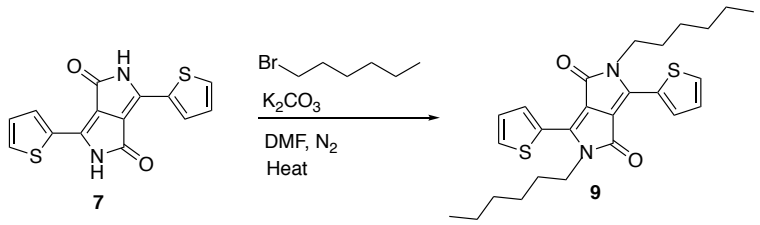

Table 5.1: Summary of alkylation reactions and purification. Hx is short for hexane. All purifications and yields in this table are from the first purification step, and some of them were purified further.

Entry	Scale [mg]	Heat [°C]	Time [h]	Crude [%] 8[a]	Crude [%] 10[b]	Purification Cryst[c]	Purification Chrom.[d]	Yield [%]
1	100	120	3	27	18	-	$CHCl_3$:Hx 7:3	11
2	750	120	25	2	22	DMF (DCM/Hx)	-	9
3	150	120	25	4	19	-	-	-
4	100	120	24	7	20	-	-	-
5	100	120	24	6	18	DMF	-	31
6	100	120	24	7	9	-	Hx:EtOAc 9:1	46
7	100	140	24	7	5	-	-	-
8	1000	140	24	6	4	DMF	-	31
9	1000	140	21	6	3	-	Hx:EtOAc 9:1	10
10	2000	140	14	4	2	DMF	-	43
11	2000	155	20	7	3	DMF	-	46

[a] *N*-monoalkylated **8**.
[b] *N,O*-dialkylated **10**.
[c] Crystallization (re-crystallization).
[d] Silica gel chromatography column.

The alkylation reactions were performed with varying different reaction conditions or purification methods, as shown in Table 5.1. Compound **7** and K_2CO_3 (10 eq.) were dissolved in DMF and heated. $Bu_4N^+HSO_4^-$ (0.05 eq.) was also present in experiment entry 1-4. After approximately 30 minutes 1-bromohexane (10 eq.) was added to the mixture. After full convertion the reaction was removed from the heat, and allowed to reach room temperature. Silica gel column chromatography or crystallization (or re-crystallization) were used as purification methods, as shown in Table 5.1. With eluent system $CHCl_3$:hexane was the R_f value 0.18 and 0.14 for the *N,N*-dialkylated **9** and *N,O*-dialkylated **10**, and 0.25 and 0.21 in hexane:EtOAc, respectively. Product **9** was isolated as dark pink/gold crystals.

Among others, entry 10 displayed in Table 5.1, were purified further. Silica gel column chromatography (104 g silica, hexane:EtOAc, 9:1) was used as a purification method after the DMF crystallization. Product **9** was isolated as a dark pink solid, 281 mg (0.60 mmol, 9%), and resulted in a total yield of 52%.

^{1}H NMR (400 MHz, $CDCl_3$) δ: 8.95 (dd, J = 3.9, J = 1.0, 2H), 7.66 (dd, J = 5.0, J = 1.0, 2H), 7.31 (t, J = 9.0, 2H), 4.10 (t, J = 8.0, 4H), 1.77 (quintet, J = 7.8, 4H), 1.46 - 1.41 (m, 4H), 1.38 - 1.37 (m, 8H), 0.91 (t, J = 7.0, 6H). The spectroscopic data corresponded well with that reported previously.[125]

5.2.9 2-Hexyl-4-(hexyloxy)-3,6-di(thiophen-2-yl)pyrrolo[3,4] pyrrol-1(2*H*)-one (10)[77]

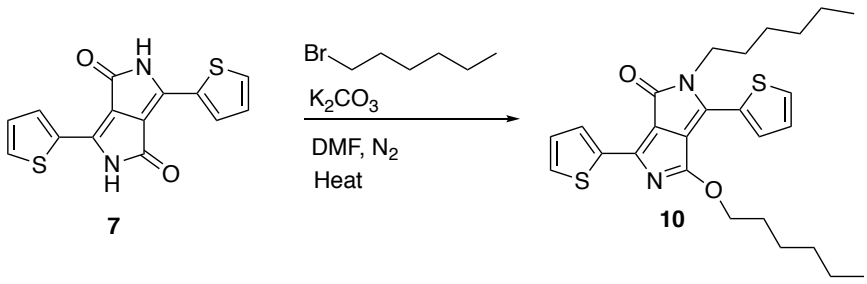

Product **10** was isolated, 43.8 mg (0.09 mmol), as a pink solid from the synthesis described in Section 5.2.8.

^{1}H NMR (400 MHz, $CDCl_3$) δ: 8.47 (dd, J = 3.8, J = 0.9, 1H), 8.28 (dd, J = 3.8, J = 0.8, 1H), 7.73 (dd, J = 5.1, J = 0.8, 1H), 7.51 (dd, J = 5.0, J = 0.8, 1H), 7.29 - 7.27 (m, 1H), 7.22 (dd, J = 3.7, J = 1.1, 1H), 4.61 (t, J = 6.5, 2H), 4.00 (t, J = 7.8, 2H), 1.91 - 1.84 (m, 2H), 1.77 - 1.70 (m , 2H), 1.40 - 1.30 (m, 12H), 0.96 - 0.88 (m, 6H). The spectroscopic data corresponded well with that reported previously.[77]

5.2.10 3,6-bis(5-Bromothiophen-2-yl)-2,5-dihexyl-2,5- dihydropyrrolo [3,4]pyrrole-1,4-dione (12)[126]

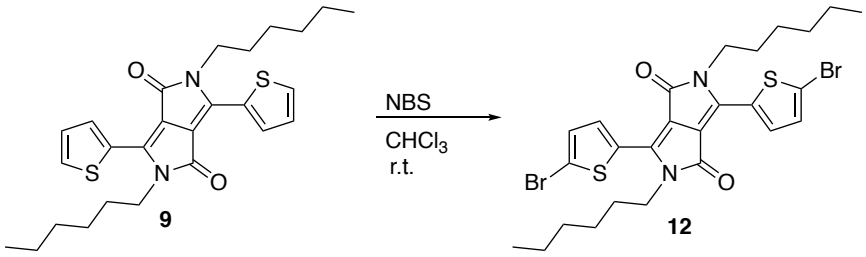

Compound **9** (700 mg, 1.49 mmol) and NBS (558 mg, 3.14 mmol) were dissolved in degassed $CHCl_3$ (10 mL) and acetic acid (10 mL). The reaction was stirred for 15 hours, before it was quenched with water (16 mL). The water phase was extracted with DCM (3·16 mL) and the organic phase was washed with water (16 mL) and brine (16 mL). The organic phase was dried over Na_2SO_4, and filtered. DCM was removed *in vacuo*.

The same experiment was run with a 500 mg and 200 mg scale. All three experiments with a 99% yield of compound **12**.

^{1}H NMR (400 MHz, $CDCl_3$) δ: 8.67 (d, J = 4.2, 2H), 7.24 (d, J = 4.2, 2H), 3.98 (t, J = 7.7, 4H), 1.71 (quintet, J = 7.5, 4H), 1.41 (quintet, J = 7.6, 4H), 1.34 - 1.32 (m, 8H), 0.98 (t, J = 6.8, 6H). The spectroscopic data corresponded well with that reported previously.[100]

5.2.11 Attempted Synthesis of 4-(5-(4-(5-Bromothiophen-2-yl)-2,5-dihexyl-3,6-dioxo-2,3,5,6-tetrahydropyrrolo[3,4]pyrrol-1-yl)thiophen-2-yl)benzaldehyde (14)

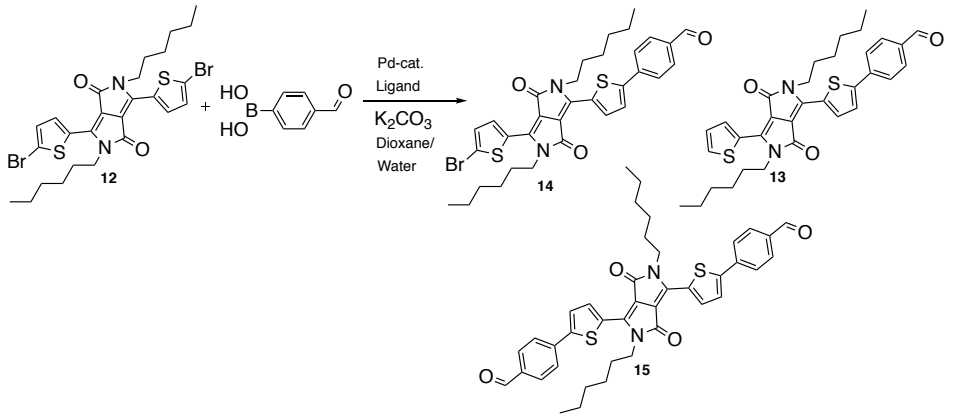

A summary of the different experiments are shown in Table 5.2, with varied catalysts and ligands. Compound **12** , 4-formylphenylboronic acid (1 eq.), K_2CO_3 (3 eq.), Pd-catalyst, ligand, dioxane and water were stirred at 80 °C. The reaction mixture was extracted with chloroform before the solvent was removed *in vacuo*. Experiment Entry 1 was an attempt to get the disubstituted product **15** and had 3 eq. of 4-formylphenylboronic acid and more catalyst and ligand, as shown in Table 5.2. An unknown compound was also formed, it is not included in the table, but it is the remaining amount of the 100% in the crude material. Only one thing is certain about the unknown compound, it is not the homo-couplet benzaldehyde.

Table 5.2: Summary of suzuki cross coupling experiments on DPP, with varied catalyst and ligand. One unknown compound was also present, but is not included in this table.

Entry	Time [h]	Catalyst	(Eq.)	Ligand	(Eq.)	Crude [%] S[a]	13	15
1	26	$Pd(OAc)_2$	(0.06)	SPhos	(0.10)	61	8	8
2	17	$Pd(OAc)_2$	(0.03)	SPhos	(0.06)	100	0	0
3	17	$Pd(OAc)_2$	(0.04)	SPhos	(0.08)	76	6	17
4	1	$Pd(OAc)_2$	(0.04)	XPhos	(0.08)	70	18	10
5	48	$Pd(dppf)Cl_2$	(0.06)	-	-	63	0	0
6	5	$Pd(PPh_3)_4$	(0.03)	-	-	94	0	6

[a] Starting material, 4-formylphenylboronic acid. Detected by ^1H NMR analysis.

5.2.12 Attempted Synthesis of 3-(5-Bromothiophen-2-yl)-2,5-dihexyl-6-(5-(10-(4-(2-(2-(2-methoxyethoxy)ethoxy)ethoxy)phenyl)-7-(pyren-1-yl)-10*H*-phenothiazin-3-yl)thiophen-2-yl)-2,5-dihydro-pyrrolo[3,4]pyrrole-1,4-dione (17)

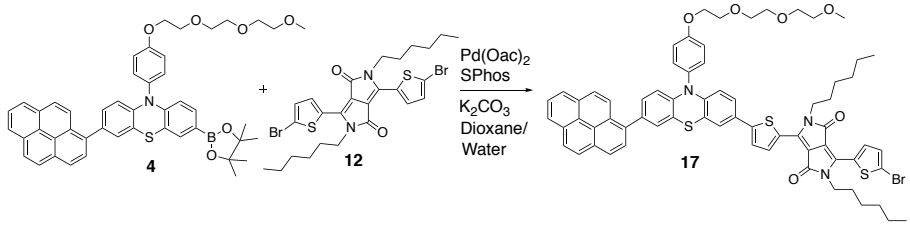

Compound **4** (50.0 mg, 0.08 mmol), compound **12** (55,9 mg, 0.07 mmol), K_2CO_3 (33.1 mg, 0.24 mmol), Pd(dppf)Cl_2 (1.75 mg, 0.01 mmol), 1,4-dioxane (2.00 mL) and water (2.00 mL) were stirred for 1 hour at 80 °C. The color changed from purple to dark blue-purple during the reaction. The reaction was quenched with water (10 mL) and extracted with EtOAc (3·40 mL). The organic phase was washed with water (40 mL) and dried with anhydrous Na_2SO_4. The solvent was filtered and removed *in vacuo*. TLC showed seven spots and following eluent systems were used in silica gel column chromatography; chloroform, Et_2O, EtOAc, EtOAc:Hexane (4:1). After the four different silica gel chromatography columns, TLC showed three different spots (R_f = 0, 0.31, 0.57, Et_2O). The exact same reaction was done with a reaction time of 26 hours, which resulted in the same amounts of spots on TLC.

5.2.13 4-(5-(2,5-Dihexyl-3,6-dioxo-4-(thiophen-2-yl)-2,3,5,6-tetrahydropyrrolo[3,4]pyrrol-1-yl)thiophen-2-yl) benzaldehyde (13)

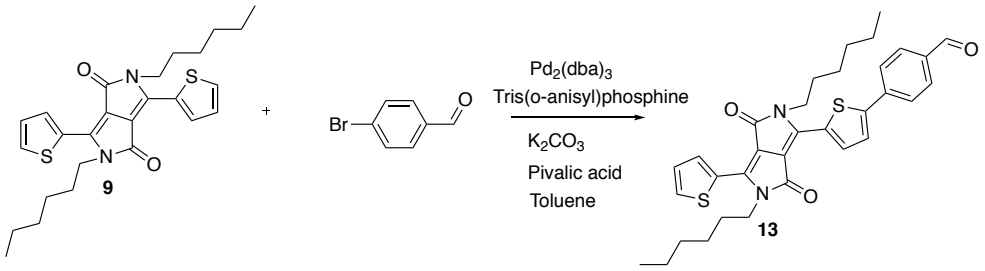

Compound **9** (150 mg, 0.32 mmol), 4-bromobenzaldehyde (42.1 mg, 0.27 mmol), $Pd_2(dba)_3$ (24.4 mg, 0.03 mmol), tris(o-anisyl)phosphine (18.8 mg, 0.05 mmol), K_2CO_3 (95.6 mg, 0.29 mmol), pivalic acid (5.45 mg, 0.05 mmol) and dry toluene (2.50 mL) were stirred for 14 hours at 120 °C. The reaction was then cooled with water (40 mL) and extracted with chloroform (3·80 mL). The organic phase was washed with water (40 mL) and dried with anhydrous Na_2SO_4. The solvent was filtered and removed *in vacuo*. In total four silica gel chromatography columns were used. First one column (39 g silica, gradient hexane:EtOAc, 9:1, - hexane:EtOAc:DCM, 130:20:50) followed by three more (39 g silica, chloroform, R_f 0.80) isolated some product **13** after each column. In total 118.7 mg (0.18 mmol, 68%) was collected of product **13** as a dark purple solid, mp. 211.5 - 212.9 °C.

^{1}H NMR (600 MHz, $CDCl_3$) δ: 10.03 (s, 1H), 8.97 (dd, J = 3.8, J = 1.0, 1H), 8.94 (d, J = 4.1, 1H), 7.94 (d, J = 8.3, 2H), 7.84 (d, J = 8.1, 2H), 7.66 (dd, J = 5.0, J = 1.3, 1H), 7.60 (d, J = 4.1, 1H), 7.31 - 7.29 (m, 1H), 4.13 - 4.07 (m, 4H), 1.81 - 1.73 (m, 4H), 1.49 - 1.41 (m, 4H), 1.36 - 1.32 (m, 8H), 0.91 - 0.88 (m, 6H); ^{13}C NMR (150 MHz, $CDCl_3$) δ: 191.2, 161.4 (2C), 147.3, 140.5, 139.0, 138.7, 136.3, 136.0, 135.6, 131.1, 130.7, 130.6, 129.7, 128.7, 126.4, 126.3, 108.3 (2C), 42.3 (2C), 31.4 (2C), 30.0 (2C), 26.6 (2C), 22.6 (2C), 14.0 (2C); IR (neat, cm^{-1}) ν: 2953 (w), 2854 (w), 1704 (m), 1653 (s), 1599 (m), 1556 (m/s), 1460 (w), 1401(m), 1336 (w), 1211 (m), 1170 (w), 1101 (w), 834 (m), 730 (m), 465 (w); HRMS (APCI/ASAP+, m/z): found 573.2246 ($[M+H]^+$, calculated $C_{33}H_{36}N_2O_3S_2$, 572.7791).

5.2.14 4-(5-(2,5-Dihexyl-3,6-dioxo-4-(thiophen-2-yl)-2,3,5,6-tetrahydropyrrolo[3,4]pyrrol-1-yl)thiophen-2-yl) benzaldehyde (15)

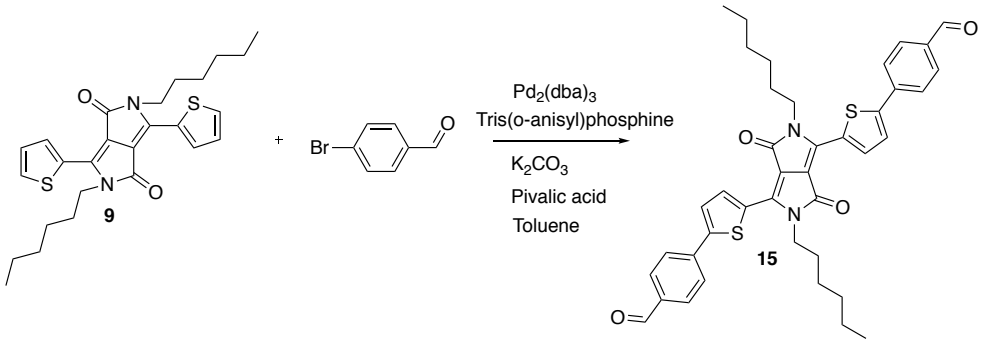

Following the reaction described in Section 5.2.13, compound **15** was also performed. Silica gel column chromatography (39 g silica, chloroform, R_f = 0.68) gave product **15** as a blue solid, 20.0 mg (0.03 mmol, 11%), mp. 290.7 - 292.0 °C.

^{1}H NMR (600 MHz, $CDCl_3$) δ: 10.04 (s, 2H), 8.98 (d, J = 4.1, 2H), 7.95 (d, J = 8.2, 4H), 7.85 (d, J = 8.2,4H), 7.62 (d, J = 4.1, 2H), 4.13 (t, J = 7.8, 4H), 1.83 - 1.78 (m, 4H), 1.49 - 1.46 (m, 4H), 1.38 - 1.33 (m, 8H), 0.90 (t, J = 7.0, 6H); ^{13}C NMR (150 MHz, $CDCl_3$) δ: 191.2 (2C), 161.3 (2C), 147.8 (2C), 139.4 (2C), 138.6 (2C), 136.6 (2C), 136.0 (2C), 130.6 (2C), 130.5 (2C), 126.5 (2C), 126.4 (2C), 108.8 (2C), 42.4 (2C), 31.4 (2C), 30.0 (2C), 26.6 (2C), 22.6 (2C), 14.0 (2C); IR (neat, cm^{-1}) ν: 2953 (w), 2727 (w), 1701 (m), 1651 (s), 1551 (m/s), 1401 (m), 1305 (w), 1238 (m), 1023 (w), 805 (m/s), 728 (m), 468 (w); HRMS (APCI/ASAP+, m/z): found 677.2508 ($[M+H]^+$, calculated $C_{40}H_{40}N_2O_4S_2$, 676.8850).

5.2.15 4-(5-(2,5-Dihexyl-4-(5-(10-(4-(2-(2-(2-methoxyethoxy) ethoxy)ethoxy)phenyl)-7-(pyren-1-yl)-10*H*-phenothiazin-3-yl)thiophen-2-yl)-3,6-dioxo-2,3,5,6-tetrahydropyrrolo [3,4]pyrrol-1-yl)thiophen-2-yl)benzaldehyde (18)

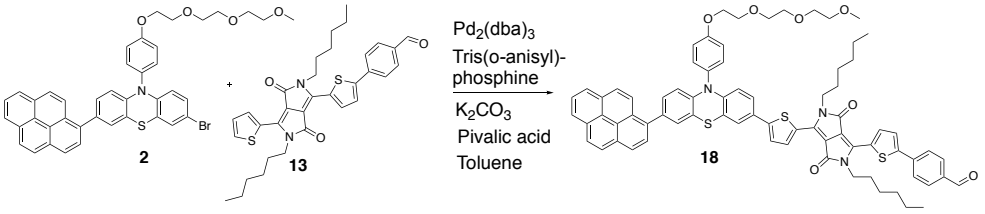

Compound **2** (44.0 mg, 0.08 mmol), compound **13** (45.9 mg, 0.06 mmol), $Pd_2(dba)_3$ (5.86 mg, 0.01 mmol), Tris(o-anisyl)phosphine (4.51 mg, 0.01 mmol), K_2CO_3 (22.9 mg, 0.07 mmol), pivalic acid (1.31 mg, 0.01 mmol) and dry toluene (1.00 mL) were stirred for 12 hours at 120 °C. The reaction was then quenched with water (10 mL) and extracted with chloroform (3·25 mL). The organic phase was washed with water (40 mL) and dried with anhydrous Na_2SO_4. The solvent was filtered and removed *in vacuo*. Silica gel column chromatography (two times 39 g silica, $CHCl_3$, 38 g silica, Et_2O) yielded product **18** as a blue solid, 56.8 mg (0.05 mmol, 73%, 79 % pure). mp. 98.1 - 100.0 °C.

^{1}H NMR (600 MHz, $CDCl_3$) δ: 10.03 (s, 1H), 9.01 (d, J = 4.2, 1H), 8.91 (d, J = 4.2, 1H), 8.20 - 8.28 (m, 3H), 8.16 (d, J = 7.5, 1H), 8.08 (s, 2H), 8.03 (d, J = 9.2, 1H), 8.01 (t, J = 7.6, 1H), 7.93 (d, J = 8.4, 2H), 7.91 (d, J = 7.8, 1H), 7.83 (d, J = 8.3, 2H), 7.60 (d, J = 4.2, 1H), 7.41 (d, J = 8.8, 2H), 7.35 (d, J = 4.2, 1H), 7.33 (d, J = 2.1, 1H), 7.29 (d, J = 2.0, 1H), 7.21 (d, J = 8.9, 2H), 7.19 (dd, J = 8.7, J = 2.1, 1H), 7.12 (dd, J = 8.4, J = 2.0, 1H), 6.36 (d, J = 8.4, 1H), 6.25 (d, J = 8.7, 1H), 4.26 (t, J = 4.8, 2H), 4.14 - 4.09 (m, 4H), 3.95 (t, J = 4.8, 2H), 3.81 - 3.79 (m, 2H), 3.74 - 3.72 (m, 2H), 3.70 - 3.68 (m, 2H), 3.59 - 3.57 (m, 2H), 3.40 (s, 3H), 1.82 - 1.75 (m, 4H), 1.48 - 1.42 (m, 4H), 1.38 - 1.29 (m, 8H), 0.91 - 0.88 (m, 6H); ^{13}C NMR (150 MHz, $CDCl_3$) δ: 191.4, 161.5, 161.2, 158.9, 149.8, 147.0 (2C), 145.1, 143.0, 140.5, 138.8, 138.0, 137.5, 136.2, 135.9 (2C), 132.9, 132.0 (2C), 131.5, 131.0, 130.9, 130.6 (2C), 129.3, 128.8, 128.5, 127.6, 127.5, 127.4 (2C), 127.3, 127.2, 126.4 (3C), 126.0, 125.5, 125.1, 125.0 (3C), 124.9 (2C), 124.7, 123.8, 123.7, 120.4, 119.0, 116.9 (2C), 115.9, 115.8, 72.0, 71.0, 70.7, 70.3, 69.8, 67.9, 59.1, 42.3 (2C), 31.4 (2C), 30.1 (2C), 29.8 (2C), 26.6 (2C), 14.1 (2C); IR (neat, cm^{-1}) ν: 3037 (m), 2955 (s), 2855 (m), 1658 (s), 1731 (w), 1600 (m), 1555 (m), 1431 (m), 1310 (m), 1214(m), 1105 (w), 833 (w), 730 (w), 479 (w).

5.2.16 (z)-3-(5-(4-(2-((2-Azaneylidene)-3-methyl)-3-hydroperoxy-32-prop-1-en-1-yl)phenyl)thiophen-2-yl)-2,5-dihexyl-6-(5-(10-(4-(2-(2-(2-methoxyethoxy)ethoxy)ethoxy)phenyl)-7-(pyren-1-yl)-10*H*-phenothiazin-3-yl)thiophen-2-yl)-2,5-dihydropyrrolo[3,4-c]pyrrole-1,4-dione (MEL3)

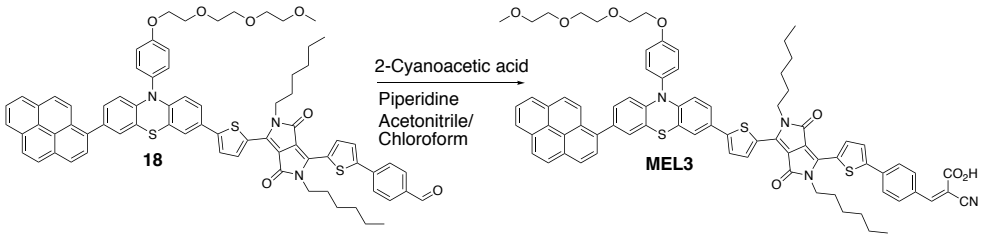

Compound **18** (44.0 mg, 0.04 mmol), 2-cyanoacetic acid (61.9 mg, 0.73 mmol) and acetonitrile (6.50 mL) were stirred for 1 hours at reflux (84 °C). Acetonitrile (13.0 mL), $CHCl_3$ (6.50 mL) and piperidine (0.06 mL, 0.44 mmol) were added and the reaction mixture was stirred for 7 hours, then allowed to reach room temperature. The reaction was quenched with acidic water (120 mL, 2M HCl), and stirred for 30 minutes. The mixture was extracted with $CHCl_3$ (3·30 mL) and dried over anhydrous Na_2SO_4. The solvent was filtered and removed *in vacuo*. Silica gel column chromatography (38 g silica, gradient DCM - DCM:MeOH, 5:1) gave product **MEL3** as a blue solid, 46.4 mg (0.04 mmol, 88%), mp. 133.2 - 134.7 °C.

IR (neat, cm^{-1}) ν: 3037 (m), 2916 (s), 2850 (s), 2214 (w), 1701 (s), 1652 (m/s), 1555 (m), 1423 (s), 1307 (s), 1242 (s), 1081 (m/s), 941 (m), 844 (m), 743 (s), 666 (m/s), 555 (m), 428 (w); HRMS (APCI/ASAP+, m/z): found 1231.4536 ([M-COO+H]$^+$, calculated $C_{76}H_{71}N_4O_6S_3$, 1231.5844).

Bibliography

[1] A. Hagfeldt, G. Boschloo, L. Sun, L. Kloo, H. Pettersson, "Dye-Sensitized Solar Cells", *Chemical Reviews* **2010**, *110*, 6595–6663.

[2] M. Freitag, J. Teuscher, Y. Saygili, X. Zhang, F. Giordano, P. Liska, J. Hua, S. M. Zakeeruddin, J.-E. Moser, M. Grätzel, A. Hagfeldt, "Dye-Sensitized Solar Cells for Efficient Power Generation under Ambient Lighting", *Nature Photonics* **2017**, *11*, 372–378.

[3] B. O'Regan, M. Grätzel, "A Low-Cost, High-Efficiency Solar Cell Based on Dye-Sensitized Colloidal TiO_2 Films", *Nature* **1991**, *353*, 737–740.

[4] ITRI Dye Sensitized Solar Cell, `https://www.itri.org.tw/eng/Content/MsgPic01/Contents.aspx?SiteID=1&MmmID=620651711540203650&MSid=621024012624321275`, Accessed: 2019-05-15.

[5] J.-H. Yum, T. W. Holcombe, Y. Kim, K. Rakstys, T. Moehl, J. Teuscher, J. H. Delcamp, M. K. Nazeeruddin, M. Grätzel, "Blue-Coloured Highly Efficient Dye-Sensitized Solar Cells by Implementing the Diketopyrrolopyrrole Chromophore", *Scientific Reports* **2013**, *3*, 2446.

[6] S. Qu, W. Wu, J. Hua, C. Kong, Y. Long, H. Tian, "New Diketopyrrolopyrrole (DPP) Dyes for Efficient Dye-Sensitized Solar Cells", *The Journal of Physical Chemistry C* **2010**, *114*, 1343–1349.

[7] J. Manina Cole, Y. Gong, J. McCree-Grey, P. Evans, S. Holt, "Modulation of N3 and N719 dye. TiO_2 Interfacial Structures in Dye-Sensitized Solar Cells as Influenced by Dye Counter Ions, Dye De-

protonation Levels, and Sensitizing Solvent", *ACS Applied Energy Materials* **2018**, *1*, 2821–2831.

[8] C.-P. Lee, R. Y.-Y. Lin, L.-Y. Lin, C.-T. Li, T.-C. Chu, S.-S. Sun, J. T. Lin, K.-C. Ho, "Recent Progress in Organic Sensitizers for Dye-Sensitized Solar Cells", *RSC Advances* **2015**, *5*, 23810–23825.

[9] BP, Statistical Review of World Energy, **2019**, `https://www.bp.com/en/global/corporate/energy-economics/statistical-review-of-world-energy.html` (visited on 06/07/2019).

[10] IEA, Renewables 2018, **2019**, `https://www.iea.org/renewables2018/` (visited on 06/07/2019).

[11] Y. Hao, Y. Saygili, J. Cong, A. Eriksson, W. Yang, J. Zhang, E. Polanski, K. Nonomura, S. M. Zakeeruddin, M. Grtzel, A. Hagfeldt, G. Boschloo, "Novel Blue Organic Dye for Dye-Sensitized Solar Cells Achieving High Efficiency in Cobalt-Based Electrolytes and by Co-Sensitization", *ACS Applied Materials & Interfaces* **2016**, *8*, 32797–32804.

[12] J. Nelson, *The Physics of Solar Cells*, Imperial College Press, **2003**.

[13] T. Markvart, *Solar Electricity, 2. Ed.* Wiley, **2009**.

[14] B. Gregg, M. C. Hanna, "Comparing Organic to Inorganic Photovoltaic Cells: Theory, Experiment, and Simulation", *Journal of Applied Physics* **2003**, *93*, 3605.

[15] M. R. Travino, *Dye-Sensitized Solar Cells and Solar Cell Performance*, Nova Science Publishers, Incorporated, **2011**.

[16] A. Tiwari, G Tiwari, S., *Handbook of Solar Energy, Theory, Analysis and Applications*, **2016**.

[17] T. Saga, "Advances in Crystalline Silicon Solar Cell Technology for Industrial Mass Production", *NPG Asia Materials* **2010**, *2*, 96–102.

[18] S. Chandra, "Recent Trends in High Efficiency Photo-Electrochemical Solar Cell Using Dye-Sensitised Photo-Electrodes and Ionic Liquid Based Redox Electrolytes", *Physical Science* **2012**, *82*, 5–19.

[19] F. Capasso, "The Channeling Avalanche Photodiode: A Novel Ultra-Low-Noise Interdigitated p-n Junction Detector", *IEEE Transactions on Electron Devices* **1982**, *29*, 1388–1395.

[20] A. Hagfeldt, G. Boschloo, L. Sun, L. Kloo, H. Pettersson, "Dye-Sensitized Solar Cells", *Chemical Reviews* **2010**, *110*, 6595–6663.

[21] M. Barberio, F. Stranges, A. Imbrogno, F. Xu, "Growth of Core-Shell Quantum Dots/Titanium Dioxide Hybrid Films as Photoanode for Graetzel Cells", *Surface and Coatings Technology* **2015**, *271*, 259 –264.

[22] M. Urbani, M. Grtzel, M. K. Nazeeruddin, T. Torres, "Meso-Substituted Porphyrins for Dye-Sensitized Solar Cells", *Chemical Reviews* **2014**, *114*, 12330–12396.

[23] T. W. Hamann, R. A. Jensen, A. B. F. Martinson, H. Van Ryswyk, J. T. Hupp, "Advancing Beyond Current Generation Dye-Sensitized Solar Cells", *Energy Environ. Sci.* **2008**, *1*, 66–78.

[24] P. Gu, D. Yang, X. Zhu, H. Sun, P. Wangyang, J. Li, H. Tian, "Influence of Electrolyte Proportion on the Performance of Dye-Sensitized Solar Cells", *AIP Advances* **2017**, *7*, 105219.

[25] L.-C. Tseng, M. Kuo, R.-H. Lee, "An Imidazolium Iodide-Containing Hyperbranched Polymer Ionic Liquid that Improves the Performance of Dye-Sensitized Solar Cells", *Journal of Polymer Research* **2016**, *23*, 157.

[26] J.-H. Yum, E. Baranoff, F. Kessler, T. Moehl, S. Ahmad, T. Bessho, A. Marchioro, E. Ghadiri, J.-E. Moser, C. Yi, M. Nazeeruddin, M. Grtzel, "A Cobalt Complex Redox Shuttle for Dye-Sensitized Solar Cells with High Open-Circuit Potentials", *Nature Communications* **2012**, *3*, 631.

[27] J. Cong, D. Kinschel, Q. Daniel, M. Safdari, E. Gabrielsson, H. Chen, P. H. Svensson, L. Sun, L. Kloo, "Bis(1,1-bis(2-pyridyl)ethane) copper(i/ii) as an Efficient Redox Couple for Liquid Dye-Sensitized Solar Cells", *Journal of Materials Chemistry A* **2016**, *4*, 14550–14554.

[28] P. Qin, "The Study of Organic Dyes for p-Type Dye-Sensitized Solar Cells", *Doctoral Thesis Kungliga Tekniska högskolan* **2010**, 2–4.

[29] T. T. T. Pham, S. K. Saha, D. Provost, Y. Farr, M. Raissi, Y. Pellegrin, E. Blart, S. Vedraine, B. Ratier, D. Aldakov, F. Odobel, J. Boucl, "Toward Efficient Solid-State *p*-Type Dye-Sensitized Solar Cells: The Dye Matters", *The Journal of Physical Chemistry C* **2017**, *121*, 129–139.

[30] J. Lim, M. Lee, S. K. Balasingam, J. Kim, D. Kim, Y. Jun, "Fabrication of Panchromatic Dye-Sensitized Solar Cells Using Pre-Dye

coated TiO_2 Nanoparticles by a Simple Dip Coating Technique", *RSC Advances* **2013**, *3*, 4801–4805.

[31] G. A. T. Tractz, A. Viomar, B. V. Dias, C. A. d. Lima, E. P. Banczek, M. T. d. Cunha, S. R. M. Antunes, P. R. P. Rodrigues, "Recombination Study of Dye Sensitized Solar Cells with Natural Extracts", *Journal of the Brazilian Chemical Society* **2019**, *30*, 371 –378.

[32] J. R. Mann, M. K. Gannon, T. C. Fitzgibbons, M. R. Detty, D. F. Watson, "Optimizing the Photocurrent Efficiency of Dye-Sensitized Solar Cells through the Controlled Aggregation of Chalcogenoxanthylium Dyes on Nanocrystalline Titania Films", *The Journal of Physical Chemistry C* **2008**, *112*, 13057–13061.

[33] S.-R. Li, C.-P. Lee, H.-T. Kuo, K.-C. Ho, S.-S. Sun, "High-Performance Dipolar Organic Dyes with an Electron-Deficient Diphenylquinoxaline Moiety in the π-Conjugation Framework for Dye-Sensitized Solar Cells", *Chemistry A European Journal* **2012**, *18*, 12085–12095.

[34] F. Ambrosio, N. Martsinovich, A. Troisi, "What Is the Best Anchoring Group for a Dye in a Dye-Sensitized Solar Cell?", *The Journal of Physical Chemistry Letters* **2012**, *3*, 1531–1535.

[35] L. Zhang, J. M. Cole, "Anchoring Groups for Dye-Sensitized Solar Cells", *ACS Applied Materials & Interfaces* **2015**, *7*, 3427–3455.

[36] Y. Hao, Y. Saygili, J. Cong, A. Eriksson, W. Yang, J. Zhang, E. Polanski, K. Nonomura, S. M. Zakeeruddin, M. Grtzel, A. Hagfeldt, G. Boschloo, "Novel Blue Organic Dye for Dye-Sensitized Solar Cells Achieving High Efficiency in Cobalt-Based Electrolytes and by Co-Sensitization", *ACS Applied Materials & Interfaces* **2016**, *8*, 32797–32804.

[37] Dyenamo, Dyenamo-Developed Blue Dye for High-Performing Esthetic DSSC Devices, Improved Version of DN-F10 (Dyenamo Blue), **2019**, `https://dyenamo.se/dyenamo_dyes.php` (visited on 05/12/2019).

[38] X.-F. Zang, Z.-S. Huang, H.-L. Wu, Z. Iqbal, L. Wang, H. Meier, D. Cao, "Molecular Design of the Diketopyrrolopyrrole-Based Dyes with Varied Donor Units for Efficient Dye-Sensitized Solar Cells", *Journal of Power Sources* **2014**, *271*, 455 –464.

[39] H. Tian, X. Yang, R. Chen, Y. Pan, L. Li, A. Hagfeldt, L. Sun, "Phenothiazine Derivatives for Efficient Organic Dye-Sensitized Solar Cells", *Chemical Communications* **2007**, 3741–3743.

[40] V. Venkatraman, M. Foscato, V. R. Jensen, B. K. Alsberg, "Evolutionary *de novo* Design of Phenothiazine Derivatives for Dye-Sensitized Solar Cells", *Journal of Materials Chemistry A* **2015**, *3*, 9851–9860.

[41] A. F. Buene, N. Boholm, A. Hagfeldt, B. H. Hoff, "Effect of Furan π-Spacer and Triethylene Oxide Methyl Ether Substituents on Performance of Phenothiazine Sensitizers in Dye-Sensitized Solar Cells", *New Journal of Chemistry* **2019**.

[42] A. F. Buene, E. E. Ose, A. G. Zakariassen, A. Hagfeldt, B. H. Hoff, "Auxiliary Donors for Phenothiazine Sensitizers for Dye-Sensitized Solar Cells - How Important are They Really?", *Journal of Materials Chemistry A* **2019**, *7*, 7581–7590.

[43] D. G. Farnum, G. Mehta, G. G. Moore, F. P. Siegal, "Attempted Reformatskii Reaction of Benzonitrile, 1,4-Diketo-3,6-diphenylpyrrolo [3,4-C]pyrrole. A Lactam Analogue of Pentalene.", *Tetrahedron Letters* **1974**, *15*, 2549 –2552.

[44] T. Beyerlein, B. Tieke, S. Forero-Lenger, W. Brtting, "Red Electroluminescence from a 1,4-Diketopyrrolo[3,4-c]pyrrole (DPP)-Based Conjugated Polymer", *Synthetic Metals* **2002**, *130*, 115 –119.

[45] A. Tang, C. Zhan, J. Yao, E. Zhou, "Design of Diketopyrrolopyrrole (DPP)-Based Small Molecules for Organic-Solar-Cell Applications", *Advanced Materials* **2017**, *29*.

[46] O. Wallquist, R. Lenz, "20 Years of DPP Pigments - Future Perspectives", *Macromolecular Symposia* **2002**, *187*, 617–630.

[47] B. Tieke, A. R. Rabindranath, K. Zhang, Y. Zhu, "Conjugated Polymers Containing Diketopyrrolopyrrole Units in the Main Chain", *Beilstein Journal of Organic Chemistry* **2010**, *6*, 830–845.

[48] S. Qu, H. Tian, "Diketopyrrolopyrrole (DPP)-Based Materials for Organic Photovoltaics", *Chemical Communications* **2012**, *48*, 3039–3051.

[49] Y. Zhu, PhD thesis, Universität zu Köln, **2006**.

[50] H. Zhao, J. Long, X. Luo, B. Zhao, S. Tan, "2-Ethynyl-6-methylthieno [3,2-b]thiophene as an Efficient π-Spacer for Porphyrin-Based Dyes", *Dyes and Pigments* **2015**, *122*, 168 –176.

[51] H. Jia, X. Ju, M. Zhang, Z. Ju, H. Zheng, "Effects of Heterocycles Containing Different Atoms as π-Bridges on the Performance of Dye-Sensitized Solar Cells", *Physical Chemistry Chemical Physics* **2015**, *17*, 16334–16340.

[52] F. A. Carey, R. Sundberg, *Advanced Organic Chemistry. Part B: Reactions and Synthesis. Fourth Edition*, *Vol. 6*, **2001**.

[53] S. Kotha, M. Meshram, C. Chakkapalli, "Synergistic Approach to Polycycles Through Suzuki-Miyaura Cross Coupling and Metathesis as Key Steps", *Beilstein Journal of Organic Chemistry* **2018**, *14*, 2468–2481.

[54] M. Grzybowski, D. T. Gryko, "Diketopyrrolopyrroles: Synthesis, Reactivity, and Optical Properties", *Advanced Optical Materials* **2015**, *3*, 280–320.

[55] C. F. Lima, J. E. Rodriguez-Borges, L. M. Santos, "Exploring the Selectivity of the Suzuki-Miyaura Cross-Coupling Reaction in the Synthesis of Arylnaphthalenes", *Tetrahedron* **2011**, *67*, 689–697.

[56] H. Lakmini, I. Ciofini, A. Jutand, C. Amatore, C. Adamo, "Pd-Catalyzed Homocoupling Reaction of Arylboronic Acid: Insights from Density Functional Theory", *The Journal of Physical Chemistry A* **2008**, *112*, 12896–12903.

[57] O. Hammerich, B. Speiser, *Organic Electrochemistry*, CRC Press, **2015**.

[58] L. Kürti, B. Czak, *Strategic Applications of Named Reactions in Organic Synthesis*, Elsevier, **2005**.

[59] M. Garca-Melchor, A. A. C. Braga, A. Lleds, G. Ujaque, F. Maseras, "Computational Perspective on Pd-Catalyzed C-C Cross-Coupling Reaction Mechanisms", *Accounts of Chemical Research* **2013**, *46*, 2626–2634.

[60] A. J. J. Lennox, G. C. Lloyd-Jones, "Transmetalation in the Suzuki-Miyaura Coupling: The Fork in the Trail", *Angewandte Chemie International Edition* **2013**, *52*, 7362–7370.

[61] M. Perez-Rodriguez, A. A. C. Braga, M. Garcia-Melchor, M. H. Perez-Temprano, J. A. Casares, G. Ujaque, A. R. de Lera, R. Alvarez, F. Maseras, P. Espinet, "C-C Reductive Elimination in Palladium Complexes, and the Role of Coupling Additives. A DFT Study Supported by Experiment", *Journal of the American Chemical Society* **2009**, *131*, 3650–3657.

[62] N. Miyaura, A. Suzuki, "Palladium-Catalyzed Cross-Coupling Reactions of Organoboron Compounds", *Chemical Reviews* **1995**, *95*, 2457–2483.

[63] I. J. S. Fairlamb, "Regioselective (Site-Selective) Functionalisation of Unsaturated Halogenated Nitrogen, Oxygen and Sulfur Hetero-

cycles by Pd-Catalysed Cross-Couplings and Direct Arylation Processes", *Chemical Society Reviews* **2007**, *36*, 1036–1045.

[64] C. Mollar, M. Besora, F. Maseras, G. Asensio, M. Medio-Simn, "Competitive and Selective Csp^3-Br versus Csp^2-Br Bond Activation in Palladium-Catalysed Suzuki Cross-Coupling: An Experimental and Theoretical Study of the Role of Phosphine Ligands", *Chemistry A European Journal* **2010**, *16*, 13390–13397.

[65] C. Morton, R. Riggs, D. Smith, N. Westwood, P Lightfoot, A. Slawin, "Synthetic Studies Related to Diketopyrrolopyrrole (DPP) Pigments. Part 2: The Use of Esters in Place of Nitriles in Standard DPP Syntheses: Claisen-Type Acylations and Furopyrrole Intermediates", *Tetrahedron* **2005**, *61*, 727–738.

[66] A. F. Littke, C. Dai, G. C. Fu, "Versatile Catalysts for the Suzuki Cross-Coupling of Arylboronic Acids with Aryl and Vinyl Halides and Triflates under Mild Conditions", *Journal of the American Chemical Society* **2000**, *122*, 4020–4028.

[67] G. A. Molander, B. Biolatto, "Palladium-Catalyzed SuzukiMiyaura Cross-Coupling Reactions of Potassium Aryl- and Heteroaryltrifluoroborates", *The Journal of Organic Chemistry* **2003**, *68*, 4302–4314.

[68] C. A. Tolman, "Steric Effects of Phosphorus Ligands in Organometallic Chemistry and Homogeneous Catalysis", *Chemical Reviews* **1977**, *77*, 313–348.

[69] R. Martin, S. L. Buchwald, "Palladium-Catalyzed SuzukiMiyaura Cross-Coupling Reactions Employing Dialkylbiaryl Phosphine Ligands", *Accounts of Chemical Research* **2008**, *41*, 1461–1473.

[70] K. L. Billingsley, S. L. Buchwald, "An Improved System for the Palladium-Catalyzed Borylation of Aryl Halides with Pinacol Borane", *The Journal of Organic Chemistry* **2008**, *73*, 5589–5591.

[71] M. Murata, T. Oyama, S. Watanabe, Y. Masuda, "Palladium-Catalyzed Borylation of Aryl Halides or Triflates with Dialkoxyborane: A Novel and Facile Synthetic Route to Arylboronates", *The Journal of Organic Chemistry* **2000**, *65*, PMID: 10813911, 164–168.

[72] K. C. Lam, T. B. Marder, Z. Lin, "Mechanism of the Palladium-Catalyzed Borylation of Aryl Halides with Pinacolborane", *Organometallics* **2010**, *29*, 1849–1857.

[73] W. K. Chow, O. Y. Yuen, P. Y. Choy, C. M. So, C. P. Lau, W. T. Wong, F. Y. Kwong, "A Decade Advancement of Transition Metal-

Catalyzed Borylation of Aryl Halides and Sulfonates", *RSC Advances* **2013**, *3*, 12518–12539.

[74] Z.-S. Huang, H. Meier, D. Cao, "Phenothiazine-Based Dyes for Efficient Dye-Sensitized Solar Cells", *Journal of Materials Chemistry C* **2016**, *4*, 2404–2426.

[75] X. Li, X. Zhang, J. Hua, H. Tian, "Molecular Engineering of Organic Sensitizers with *o,p*-Dialkoxyphenyl-Based Bulky Donors for Highly Efficient Dye-Sensitized Solar Cells", *Molecular Systems Design Engineering* **2017**, *2*, 98–122.

[76] T. I. Crowell, D. W. Peck, "Kinetic Evidence for a Schiff Base Intermediate in the Knoevenagel Condensation1", *Journal of the American Chemical Society* **1953**, *75*, 1075–1077.

[77] B. Zhao, K. Sun, F. Xue, J. Ouyang, "Isomers of Dialkyl Diketo-Pyrrolo-Pyrrole: Electron-Deficient Units for Organic Semiconductors", *Organic Electronics* **2012**, *13*, 2516 –2524.

[78] S. Stas, S. Sergeyev, Y. Geerts, "Synthesis of Diketopyrrolopyrrole (DPP) Derivatives Comprising Bithiophene Moieties", *Tetrahedron* **2010**, *66*, 1837–1845.

[79] S. Frebort, Z. Elias, A. Lycka, S. Lunak, J. Vynuchal, L. Kubac, R. Hrdina, L. Burgert, "O- and N-alkylated Diketopyrrolopyrrole Derivatives", *Tetrahedron Letters* **2011**, *52*, 5769 –5773.

[80] D. Z. Mijin, M. M. Misic-Vukovic, S. D. Petrovic, "Alkylation of N-Substituted 2-Phenylacetamides", *ChemInform* **2005**, *36*.

[81] K. J. Hoffmann, P. H. Carlsen, "Study of an Efficient and Selective Bromination Reaction of Substituted Thiophenes", *Synthetic Communications* **1999**, *29*, 1607–1610.

[82] J. C. Lewis, A. M. Berman, R. G. Bergman, J. A. Ellman, "Rh(I)-Catalyzed Arylation of Heterocycles via CH Bond Activation: Expanded Scope through Mechanistic Insight", *Journal of the American Chemical Society* **2008**, *130*, 2493–2500.

[83] D. J. Schipper, K. Fagnou, "Direct Arylation as a Synthetic Tool for the Synthesis of Thiophene-Based Organic Electronic Materials", *Chemistry of Materials* **2011**, *23*, 1594–1600.

[84] S. I. Gorelsky, D. Lapointe, K. Fagnou, "Analysis of the Concerted Metalation-Deprotonation Mechanism in Palladium-Catalyzed Direct Arylation Across a Broad Range of Aromatic Substrates", *Journal of the American Chemical Society* **2008**, *130*, 10848–10849.

[85] S. I. Gorelsky, D. Lapointe, K. Fagnou, "Analysis of the Palladium-Catalyzed (Aromatic) CH Bond Metalation-Deprotonation Mechanism Spanning the Entire Spectrum of Arenes", *The Journal of Organic Chemistry* **2012**, *77*, 658–668.

[86] H. Bohra, M. Wang, "Direct CH Arylation: A Greener Approach Towards Facile Synthesis of Organic Semiconducting Molecules and Polymers", *Journal of Materials Chemistry A* **2017**, *5*, 11550–11571.

[87] B. Biswas, M. Sugimoto, S. Sakaki, "CH Bond Activation of Benzene and Methane by M(η^2-O_2CH)$_2$ (M = Pd or Pt). A Theoretical Study", *Organometallics* **2000**, *19*, 3895–3908.

[88] M. Lafrance, K. Fagnou, "Palladium-Catalyzed Benzene Arylation: Incorporation of Catalytic Pivalic Acid as a Proton Shuttle and a Key Element in Catalyst Design", *Journal of the American Chemical Society* **2006**, *128*, 16496–16497.

[89] S. I. Gorelsky, "Reactivity and Regioselectivity of Palladium-Catalyzed Direct Arylation in Noncooperative and Cooperative Processes", *Organometallics* **2012**, *31*, 4631–4634.

[90] Y. Gao, J. Bai, Y. Sui, Y. Han, Y. Deng, H. Tian, Y. Geng, F. Wang, "High Mobility Ambipolar Diketopyrrolopyrrole-Based Conjugated Polymers Synthesized via Direct Arylation Polycondensation: Influence of Thiophene Moieties and Side Chains", *Macromolecules* **2018**, *51*, 8752–8760.

[91] M. Løberg, "Synthesis Towards Blue Phenothiazine Dyes Containing Diketopyrrolopyrrole π-Bridge", *Specialization Project Thesis NTNU* **2018**.

[92] D. M. Knapp, E. P. Gillis, M. D. Burke, "A General Solution for Unstable Boronic Acids: Slow-Release Cross-Coupling from Air-Stable MIDA Boronates", *Journal of the American Chemical Society* **2009**, *131*, 6961–6963.

[93] M. Murata, T. Oyama, S. Watanabe, Y. Masuda, "Palladium-Catalyzed Borylation of Aryl Halides or Triflates with Dialkoxyborane: A Novel and Facile Synthetic Route to Arylboronates", *The Journal of Organic Chemistry* **2000**, *65*, 164–168.

[94] O. Vakuliuk, S. Ooi, I. Deperasinska, O. Staszewska-Krajewska, M. Banasiewicz, B. Kozankiewicz, O. Danylyuk, D. T. Gryko, "Unprecedented Rearrangement of Diketopyrrolopyrroles Leads to Struc-

turally Unique Chromophores", *Chemical Communications* **2017**, *53*, 11877.

[95] X. Zhao, G. Xue, G. Qu, V. Singhania, Y. Zhao, K. Butrouna, A. Gumyusenge, Y. Diao, K. R. Graham, H. Li, J. Mei, "A Chiral Organic Base Catalyst with Halogen-Bonding-Donor Functionality: Asymmetric Mannich Reactions of Malononitrile with N-Boc Aldimines and Ketimines", *Chemical Communications* **2017**, *50*, 6202–6209.

[96] P. Data, A. Kurowska, S. Pluczyk, P. Zassowski, P. Pander, R. Jedrysiak, M. Czwartosz,. Otulakowski, J. Suwinski, M. Lapkowski, A. Monkman, "Exciplex Enhancement as a Tool to Increase OLED Device Efficiency", *The Journal of Physical Chemistry C* **2016**, *120*.

[97] M. A. Naik, N. Venkatramaiah, C. Kanimozhi, S. Patil, "Influence of Side-Chain on Structural Order and Photophysical Properties in Thiophene Based Diketopyrrolopyrroles: A Systematic Study", *The Journal of Physical Chemistry C* **2012**, *116*, 26128–26137.

[98] T. Lei, J.-H. Dou, J. Pei, "Influence of Alkyl Chain Branching Positions on the Hole Mobilities of Polymer Thin-Film Transistors", *Advanced Materials* **2012**, *24*, 6457–6461.

[99] I. Kang, H.-J. Yun, D. S. Chung, S.-K. Kwon, Y.-H. Kim, "Record High Hole Mobility in Polymer Semiconductors via Side-Chain Engineering", *Journal of the American Chemical Society* **2013**, *135*, 14896–14899.

[100] S.-X. Sun, Y. Huo, M.-M. Li, X. Hu, H.-J. Zhang, Y.-W. Zhang, Y.-D. Zhang, X.-L. Chen, Z.-F. Shi, X. Gong, Y. Chen, H.-L. Zhang, "Understanding the Halogenation Effects in Diketopyrrolopyrrole-Based Small Molecule Photovoltaics", *ACS Applied Materials & Interfaces* **2015**, *7*, 19914–19922.

[101] Y. Kim, C. E. Song, A. Cho, J. Kim, Y. Eom, J. Ahn, S.-J. Moon, E. Lim, "Synthesis of Diketopyrrolopyrrole (DPP)-Based Small Molecule Donors Containing Thiophene or Furan for Photovoltaic Applications", *Materials Chemistry and Physics* **2014**, *143*, 825 –829.

[102] Y. Li, S. P. Singh, P. Sonar, "A High Mobility P-Type DPP-Thieno[3,2-b]thiophene Copolymer for Organic Thin-Film Transistors", *Advanced Materials* **2010**, *22*, 4862–4866.

[103] H. Maruo, Y. Sasaki, K. Harada, K. Suwa, K. Oyaizu, H. Segawa, K. Carter, H. Nishide, "Hole-Transporting Diketopyrrolopyrrole-Thiophene Polymers and Their Additive-Free Application for a Perov-

skite-Type Solar Cell with an Efficiency of 16.3%", *Polymer Journal* **2018**, *51*.

[104] S.-Y. Liu, W.-F. Fu, J.-Q. Xu, C.-C. Fan, H. Jiang, M. Shi, H.-Y. Li, J.-W. Chen, Y. Cao, H.-Z. Chen, "A Direct Arylation-Derived DPP-Based Small Molecule for Solution-Processed Organic Solar Cells", *Nanotechnology* **2013**, *25*, DOI 10.1088/0957-4484/25/1/014006.

[105] J.-R. Pouliot, B. Sun, M. Leduc, A. Najari, Y. Li, M. Leclerc, "A High Mobility DPP-Based Polymer Obtained via Direct (Hetero)-Arylation Polymerization", *Polymer Chemistry* **2015**, *6*, 278–282.

[106] H. Bohra, H. Chen, Y. Peng, A. Efrem, F. He, M. Wang, "Direct Arylation Polymerization Toward Efficient Synthesis of Benzo[1,2-c:4,5-c'] Dithiophene-4,8-dione Based Donor-Acceptor Alternating Copolymers for Organic Optoelectronic Applications", *Journal of Polymer Science Part A: Polymer Chemistry* **2018**, *56*, 2554–2564.

[107] L. Miu, S. Yan, H. Yao, Q. Chen, J. Zhang, Z. Wang, P. Cai, T. Hu, S. Ding, J. Chen, M. Liang, S. Yang, "Insight into the Positional Effect of Bulky Rigid Substituents in Organic Sensitizers on the Performance of Dye-Sensitized Solar Cells", *Dyes and Pigments* **2019**, *168*, 1 –11.

[108] Y. Hua, S. Chang, D. Huang, X. Zhou, X. Zhu, J. Zhao, T. Chen, W.-Y. Wong, W.-K. Wong, "Significant Improvement of Dye-Sensitized Solar Cell Performance Using Simple Phenothiazine-Based Dyes", *Chemistry of Materials* **2013**, *25*, 2146–2153.

[109] B. Chen, H. Nie, P. Lu, J. Zhou, A. Qin, H. Qiu, Z. Zhao, B. Z. Tang, "Conjugation Versus Rotation: Good Conjugation Weakens the Aggregation-Induced Emission Effect of Siloles", *Chemical Communications* **2014**, *50*, 4500–4503.

[110] S. Qu, B. Wang, F. Guo, J. Li, W. Wu, C. Kong, Y. Long, J. Hua, "New Diketo-Pyrrolo-Pyrrole (DPP) Sensitizer Containing a Furan Moiety for Efficient and Stable Dye-Sensitized Solar Cells", *Dyes and Pigments* **2012**, *92*, 1384 –1393.

[111] H. Choi, I. Raabe, D. Kim, F. Teocoli, C. Kim, K. Song, J.-H. Yum, J. Ko, M. K. Nazeeruddin, M. Grtzel, "High Molar Extinction Coefficient Organic Sensitizers for Efficient Dye-Sensitized Solar Cells", *Chemistry A European Journal* **2010**, *16*, 1193–1201.

[112] I. Sta, M. Jlassi, M. Hajji, M. F. Boujmil, R. Jerbi, M. Kandyla, M. Kompitsas, H. Ezzaouia, "Structural and Optical Properties of TiO_2 Thin Films Prepared by Spin Coating", *Journal of Sol-Gel Science and Technology* **2014**, *72*, 421–427.

[113] S. H. Kim, H. W. Kim, C. Sakong, J. Namgoong, S. W. Park, M. J. Ko, C. H. Lee, W. I. Lee, J. P. Kim, "Effect of Five-Membered Heteroaromatic Linkers to the Performance of Phenothiazine-Based Dye-Sensitized Solar Cells", *Organic Letters* **2011**, *13*, 5784–5787.

[114] F. Environmental, Solar Radiation and Photosynethically Active Radiation, **2014**, `https://www.fondriest.com/environmental-measurements/parameters/weather/solar-radiation/` (visited on 06/05/2019).

[115] S. Fan, X. Lu, H. Sun, G. Zhou, Y. J. Chang, Z.-S. Wang, "Effect of the Co-Sensitization Sequence on the Performance of Dye-Sensitized Solar Cells with Porphyrin and Organic Dyes", *Physical Chemistry Chemical Physics* **2016**, *18*, 932–938.

[116] J. Luo, Z. Wan, Y. Wang, C. Jia, "A Co-Sensitization Process for Dye-Sensitized Solar Cell: Enhanced Light-Harvesting Efficiency and Reduced Charge Recombination", *IOP Conference Series: Materials Science and Engineering* **2018**, *394*, 042018.

[117] P. Liu, L. Wang, K. M. Karlsson, Y. Hao, J. Gao, B. Xu, G. Boschloo, L. Sun, L. Kloo, "Molecular Engineering of D-π-A Type of Blue-Colored Dyes for Highly Efficient Solid-State Dye-Sensitized Solar Cells through Co-Sensitization", *ACS Applied Materials & Interfaces* **2018**, *10*, 35946–35952.

[118] Y. Hao, W. Yang, L. Zhang, R. Y. Jiang, E. Mijangos, Y. Saygili, L. Hammarström, A. Hagfeldt, G. Boschloo, "A Small Electron Donor in Cobalt Complex Electrolyte Significantly Improves Efficiency in Dye-Sensitized Solar Cells", *Nature Communications* **2016**.

[119] R. M. Silverstein, F. X. Webster, D. Kiemle, D. L. Bryce, *Spectrometric Identification of Organic Compounds*, **2014**.

[120] G. R. Fulmer, A. J. M. Miller, N. H. Sherden, H. E. Gottlieb, A. Nudelman, B. M. Stoltz, J. E. Bercaw, K. I. Goldberg, "NMR Chemical Shifts of Trace Impurities", *Organometallics* **2010**, *29*, 2176–2179.

[121] R. M. Silverstein, G. C. Bassler, "Spectrometric Identification of Organic Compounds", *Journal of Chemical Education* **1962**, *39*.

[122] D. W. Bohman, Z. Li, D. Li, N. L. Owen, “The Analysis of Mixtures Using the 2-D INADEQUATE NMR Technique”, *Journal of Molecular Structure* **1999**, *480-481*, 125 –132.

[123] S. Grossert, P. D Fancy, R. L White, “Fragmentation Pathways of Negative Ions Produced by Electrospray Ionization of Acyclic Dicarboxylic Acids and Derivatives”, *Canadian Journal of Chemistry* **2011**, *83*, 1878–1890.

[124] D. P. Demarque, A. E. M. Crotti, R. Vessecchi, J. L. C. Lopes, N. P. Lopes, “Fragmentation Reactions Using Electrospray Ionization Mass Spectrometry: an Important Tool for the Structural Elucidation and Characterization of Synthetic and Natural Products”, *Natural Product Reports* **2016**, *33*, 432–455.

[125] S. P. Mishra, A. K. Palai, M. Patri, “Synthesis and Characterization of Soluble Narrow Band Gap Conducting Polymers Based on Diketopyrrolopyrrole and Propylenedioxythiophenes”, *Synthetic Metals* **2010**, *160*, 2422 –2429.

[126] C. Kanimozhi, N. Yaacobi-Gross, E. K. Burnett, A. L. Briseno, T. D. Anthopoulos, U. Salzner, S. Patil, “Use of Side-Chain for Rational Design of n-Type Diketopyrrolopyrrole-Based Conjugated Polymers: What Did We Find Out?”, *Physical Chemistry Chemical Physics* **2014**, *16*, 17253–17265.

Appendix

A Spectroscopic Data - Compound 2

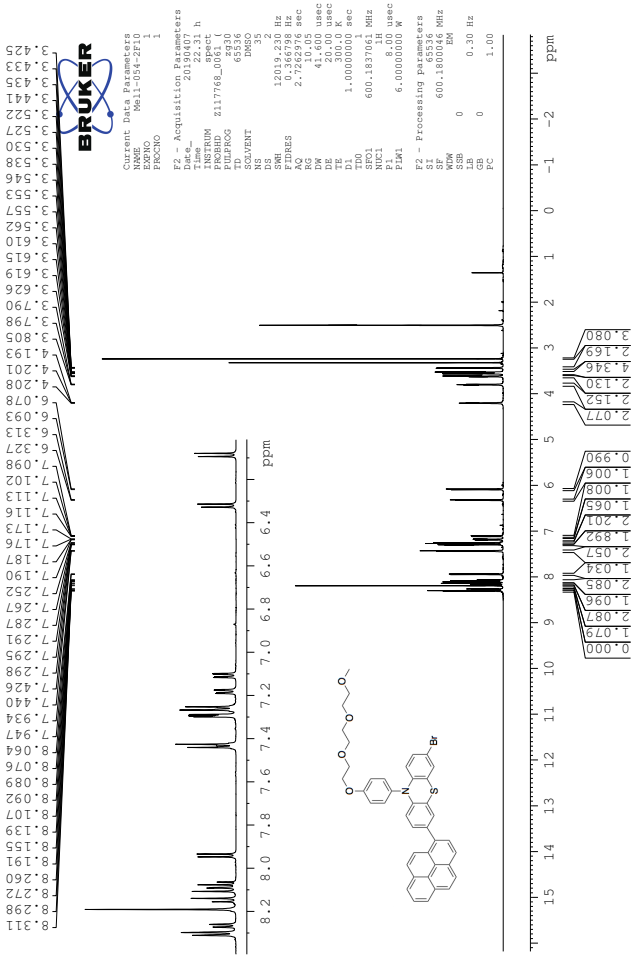

Figure 1: ^{1}H NMR spectrum of compound **2**.

B Spectroscopic Data - Compound 3

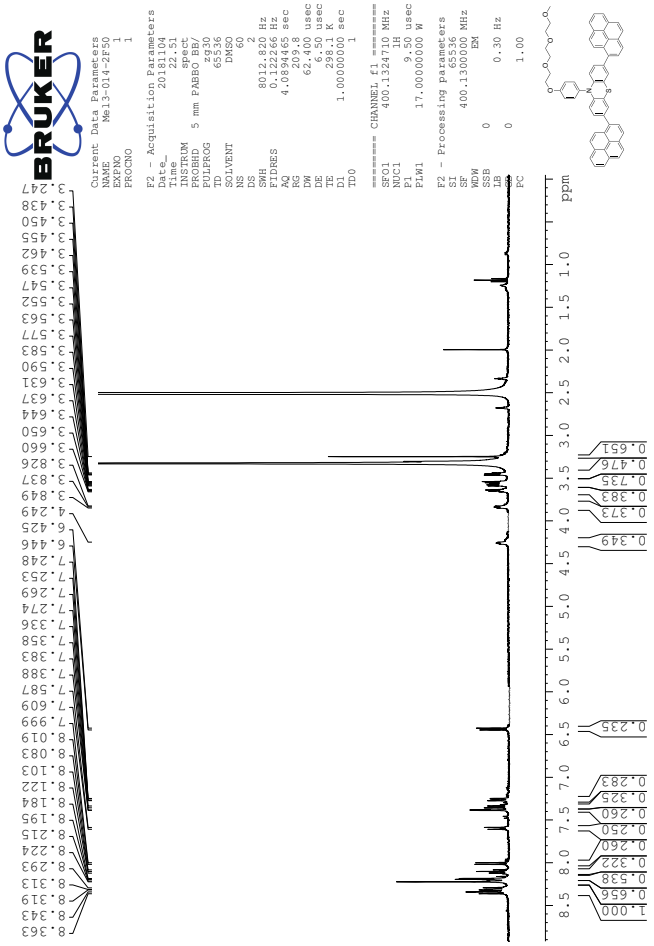

Figure 2: ^{1}H NMR spectra of compound **3**.

C Spectroscopic Data - Compound 4

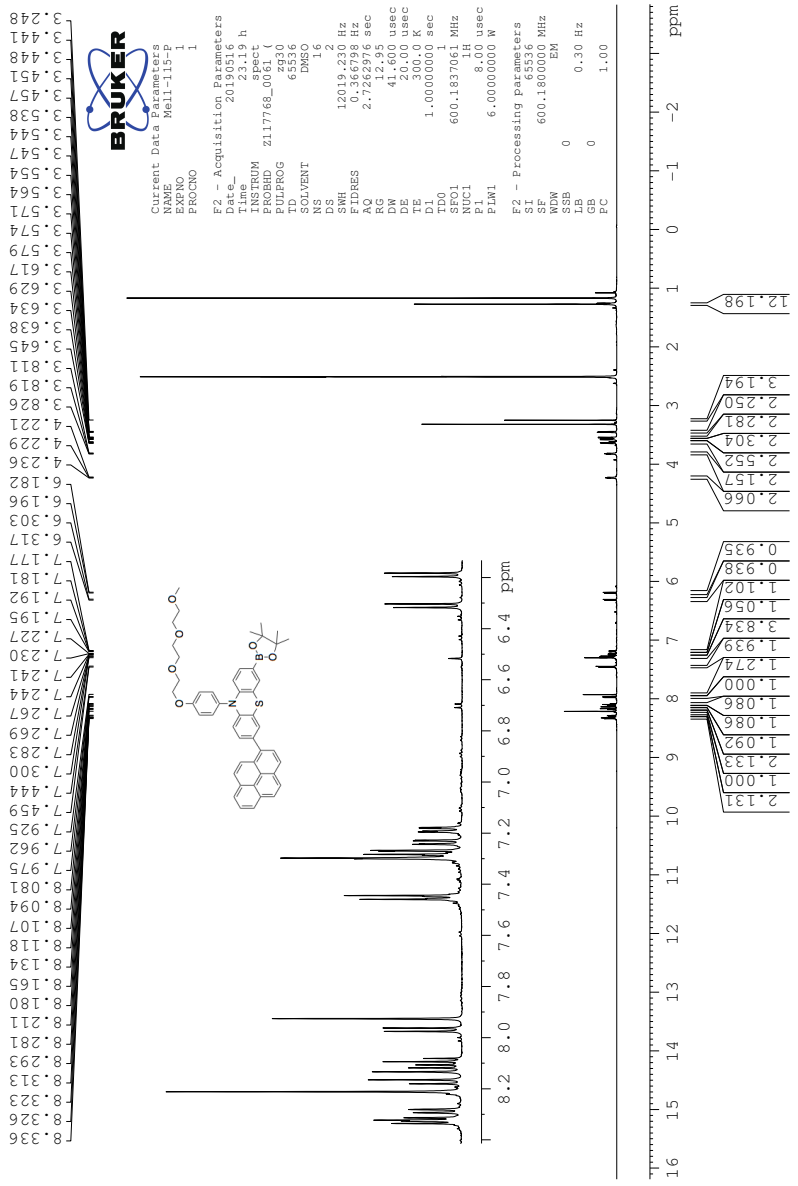

Figure 3: ^{1}H NMR spectra of compound **4**.

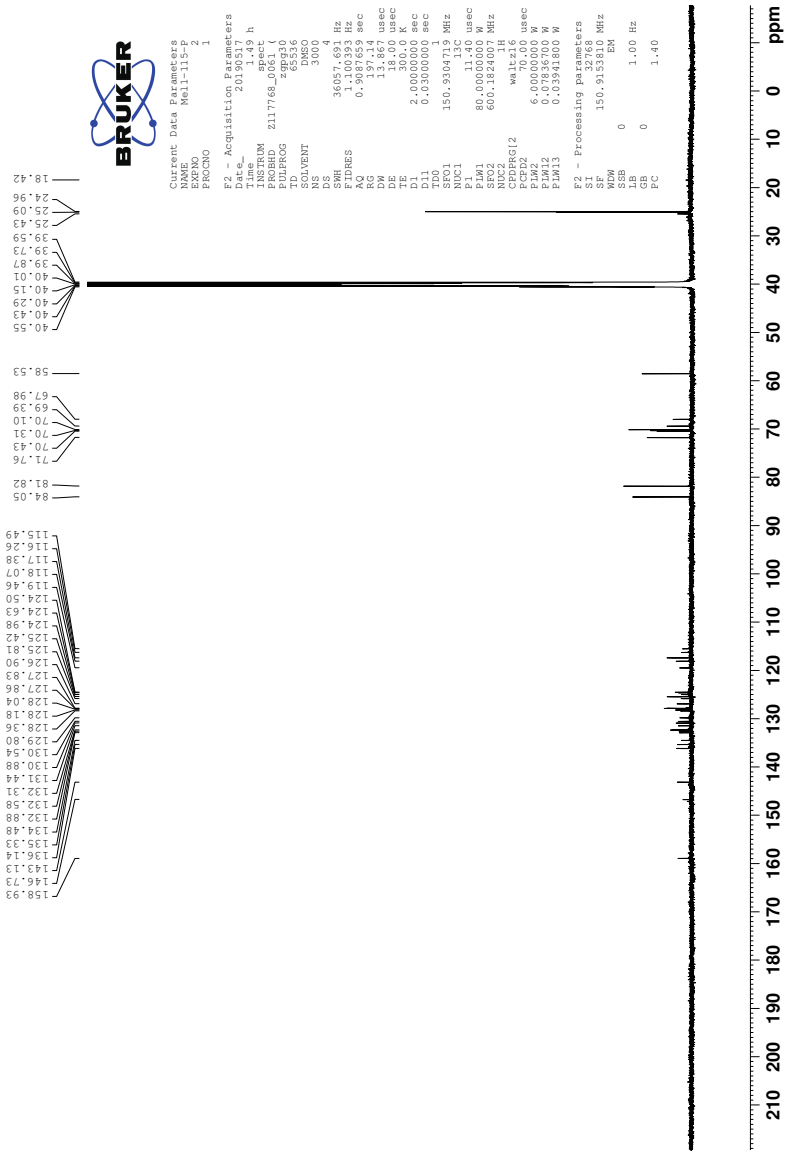

Figure 4: ^{13}C NMR spectra of compound **4**.

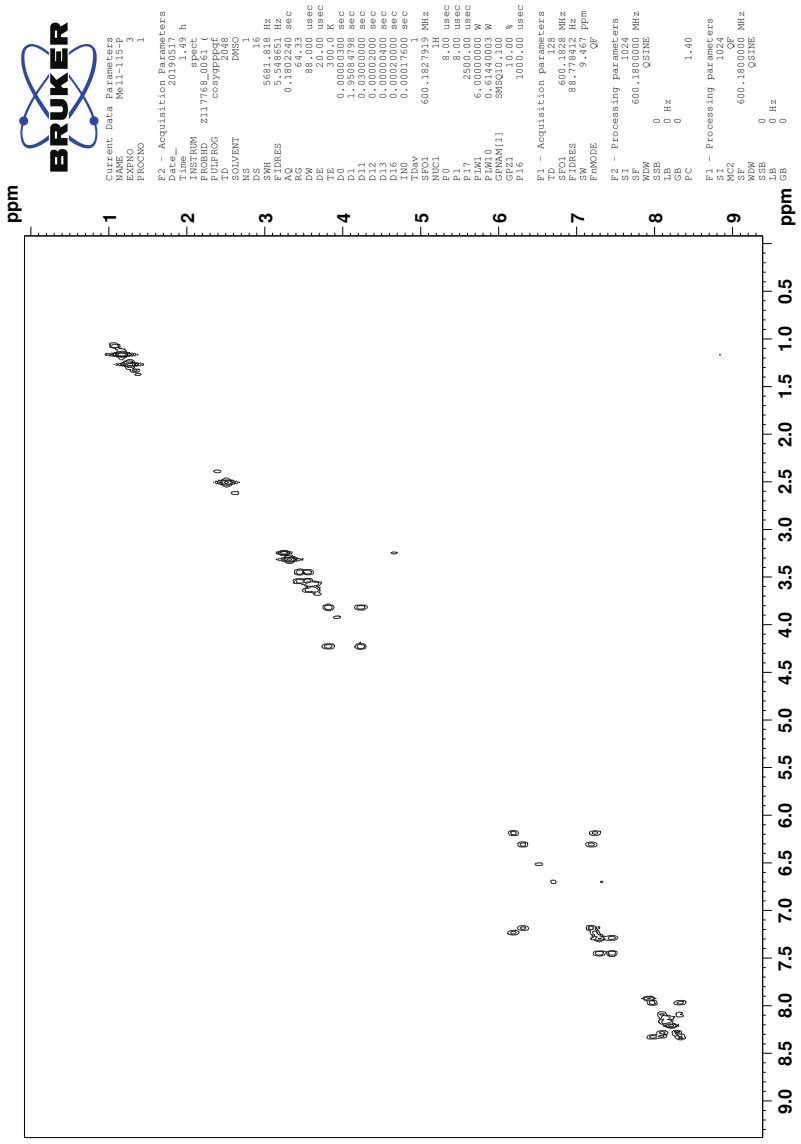

Figure 5: COSY NMR spectra of compound **4**.

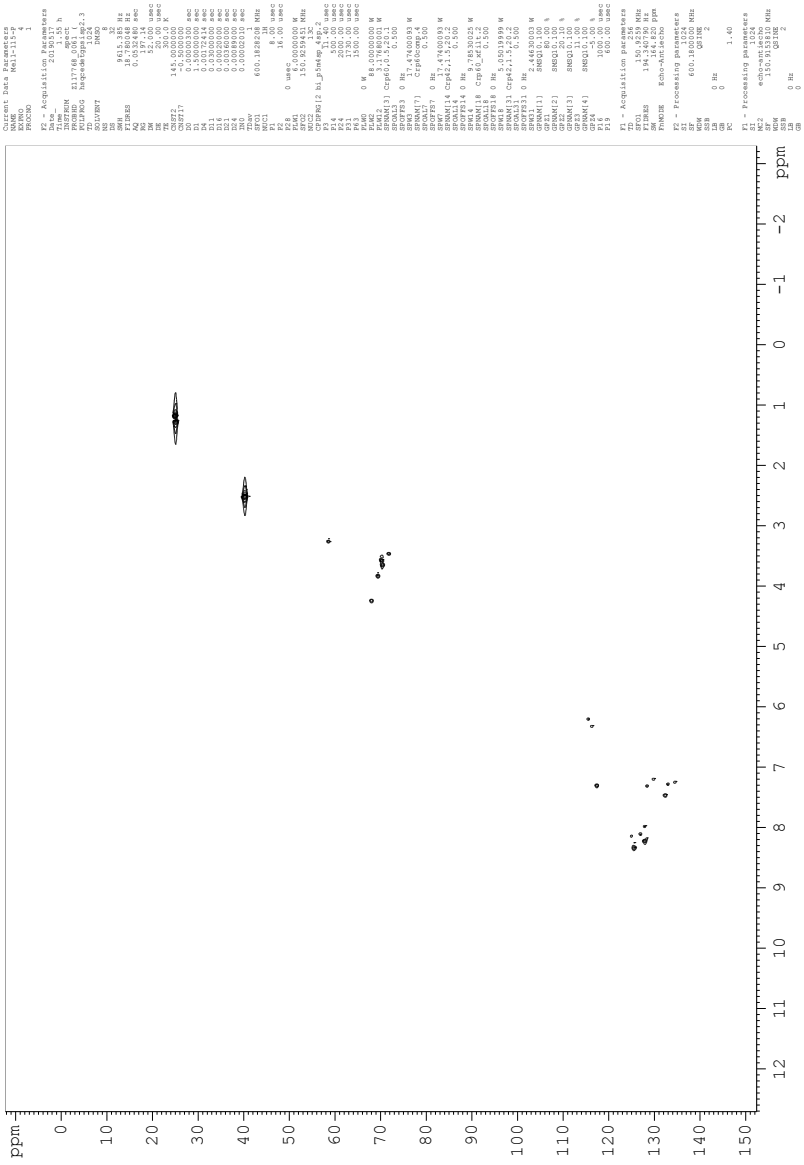

Figure 6: HSQC NMR spectra of compound **4**.

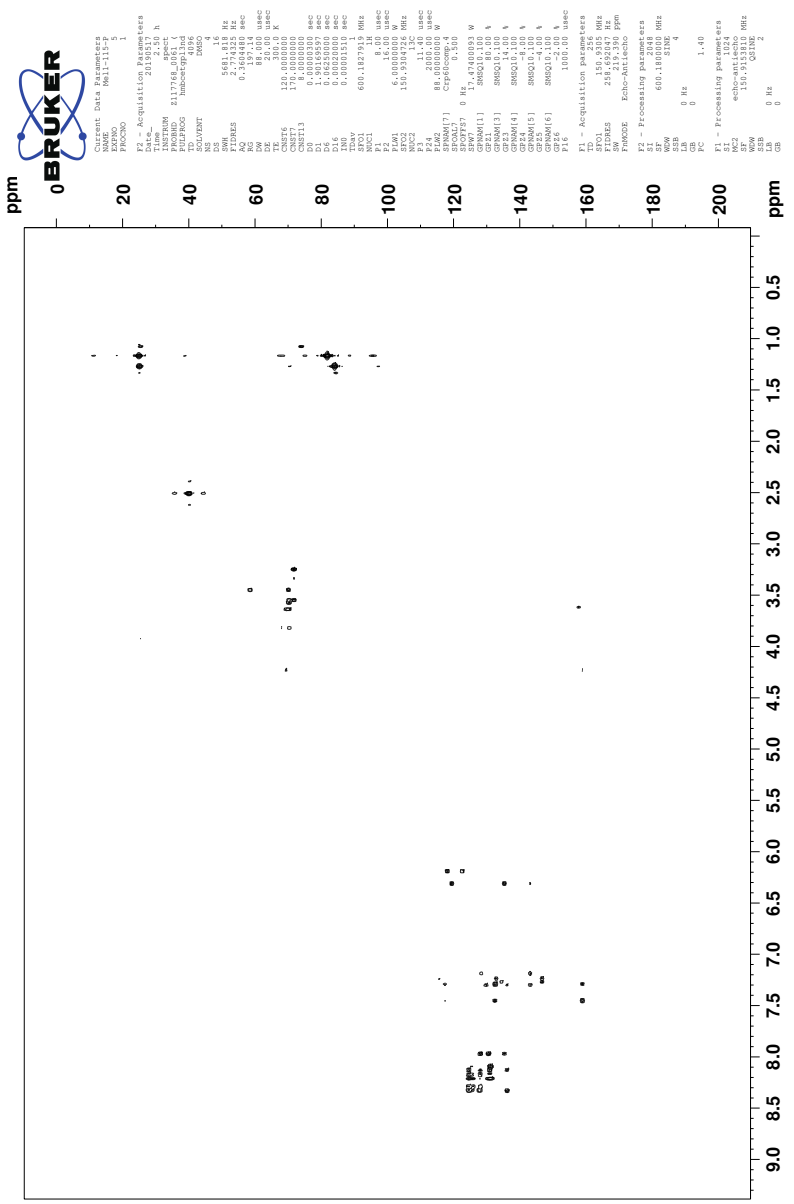

Figure 7: HMBC NMR spectra of compound **4**.

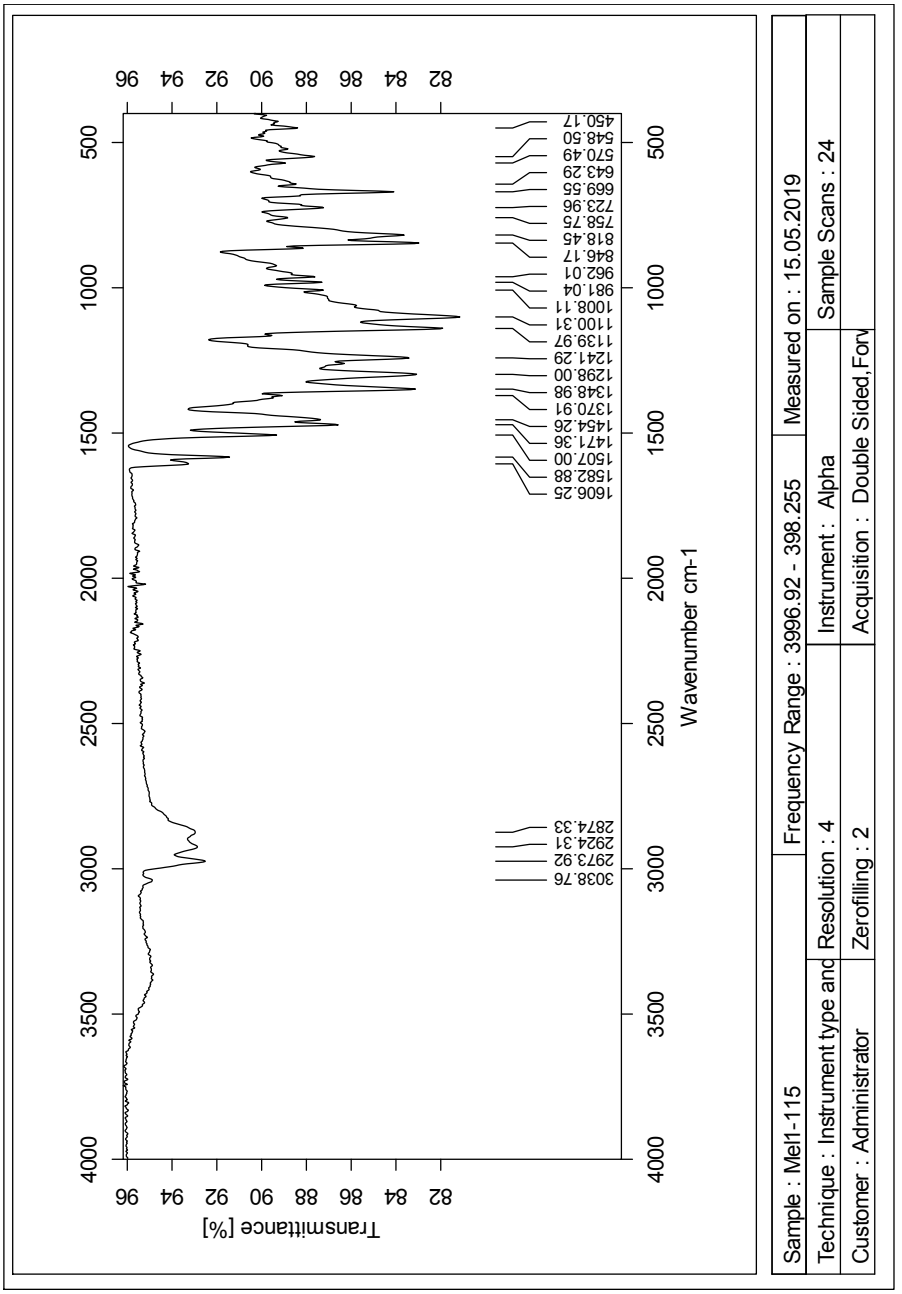

Figure 8: IR spectra of compound **4**.

Elemental Composition Report **Page 1**

Single Mass Analysis
Tolerance = 2.0 PPM / DBE: min = -50.0, max = 50.0
Element prediction: Off
Number of isotope peaks used for i-FIT = 3

Monoisotopic Mass, Even Electron Ions
15419 formula(e) evaluated with 15 results within limits (all results (up to 1000) for each mass)
Elements Used:
C: 0-100 H: 0-150 11B: 0-1 N: 0-10 O: 0-10 S: 0-4
2019-480 297 (5.790) AM2 (Ar,35000.0,0.00,0.00); Cm (280:300)
1: TOF MS ASAP+

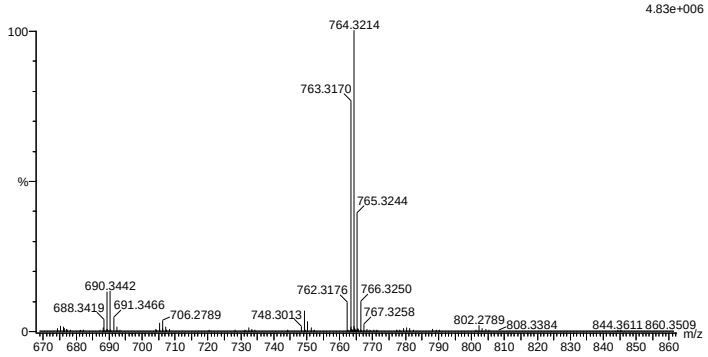

Minimum:				-50.0				
Maximum:		5.0	2.0	50.0				
Mass	Calc. Mass	mDa	PPM	DBE	i-FIT	Norm	Conf(%)	Formula
764.3214	764.3215	-0.1	-0.1	22.5	774.8	0.938	39.16	C39 H43 11B N7 O9
	764.3211	0.3	0.4	16.5	779.2	5.312	0.49	C39 H51 11B N3 O8 S2
	764.3217	-0.3	-0.4	17.5	774.6	0.790	45.40	C40 H50 N3 O10 S
	764.3217	-0.3	-0.4	25.5	775.9	2.058	12.77	C47 H47 11B N O6 S
	764.3217	-0.3	-0.4	12.5	782.0	8.131	0.03	C32 H51 11B N9 O6 S3
	764.3219	-0.5	-0.7	7.5	783.4	9.566	0.01	C33 H58 N5 O7 S4
	764.3219	-0.5	-0.7	15.5	783.1	9.263	0.01	C40 H55 11B N3 O3 S4
	764.3223	-0.9	-1.2	26.5	779.3	5.447	0.43	C48 H46 N O8
	764.3205	0.9	1.2	26.5	779.6	5.747	0.32	C45 H46 N7 O S2
	764.3204	1.0	1.3	7.5	782.6	8.758	0.02	C31 H55 11B N5 O10 S3
	764.3224	-1.0	-1.3	13.5	779.2	5.319	0.49	C33 H50 N9 O8 S2
	764.3224	-1.0	-1.3	21.5	778.8	4.927	0.73	C40 H47 11B N7 O4 S2
	764.3226	-1.2	-1.6	16.5	781.3	7.452	0.06	C41 H54 N3 O5 S3
	764.3226	-1.2	-1.6	24.5	780.9	7.025	0.09	C48 H51 11B N O

Figure 9: Mass spectra of compound **4**.

D Spectroscopic Data - Compound 5

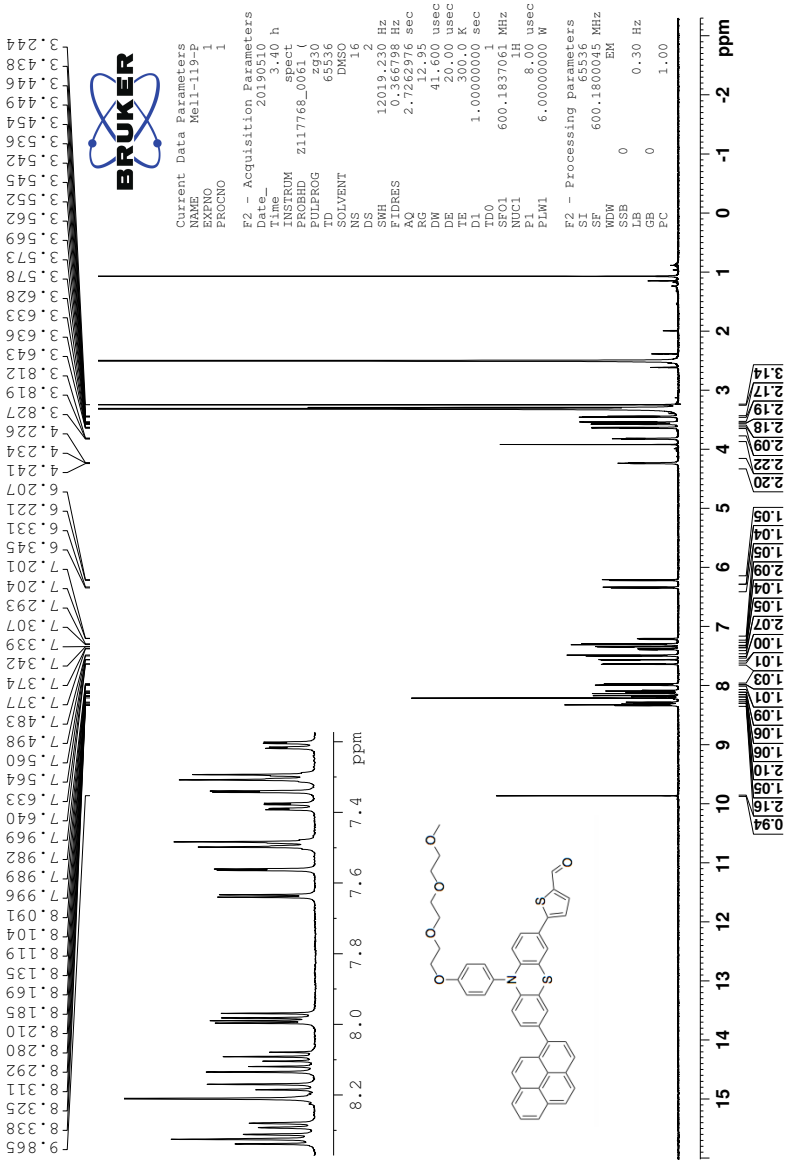

Figure 10: ^{1}H NMR spectra of compound **5**.

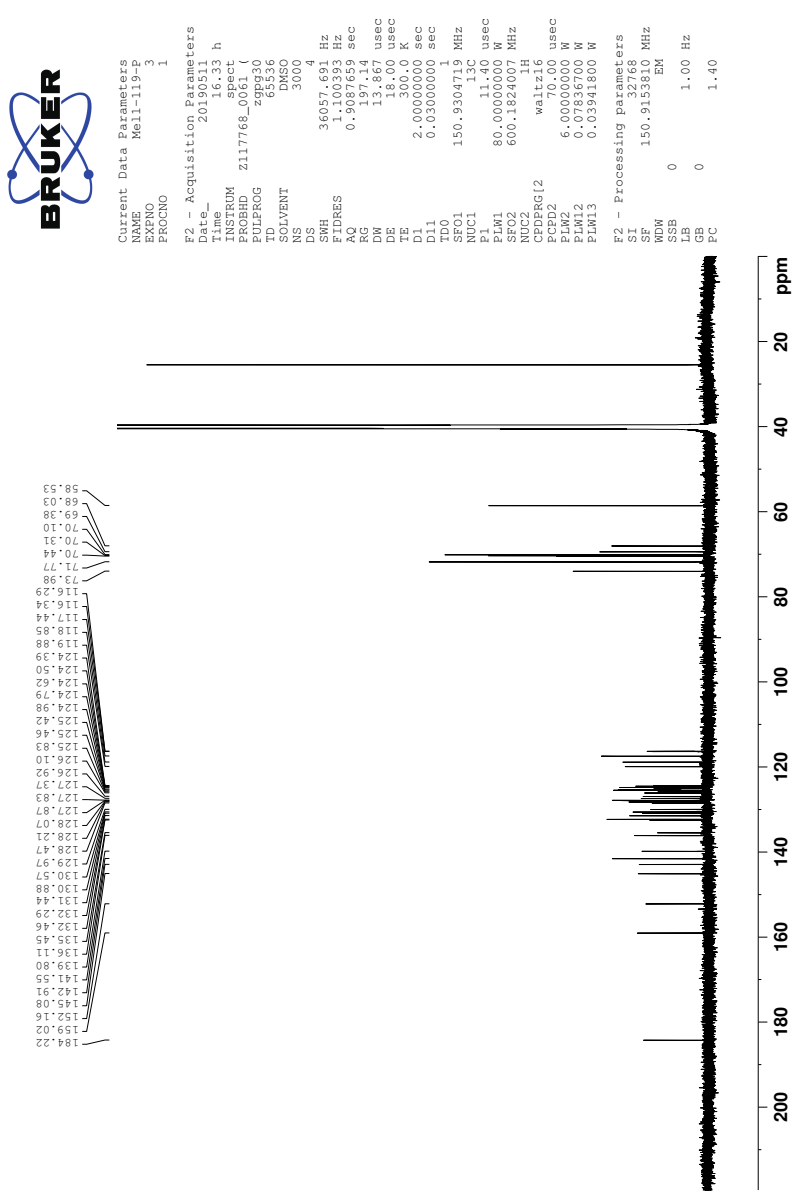

Figure 11: ^{13}C NMR spectra of compound **5**.

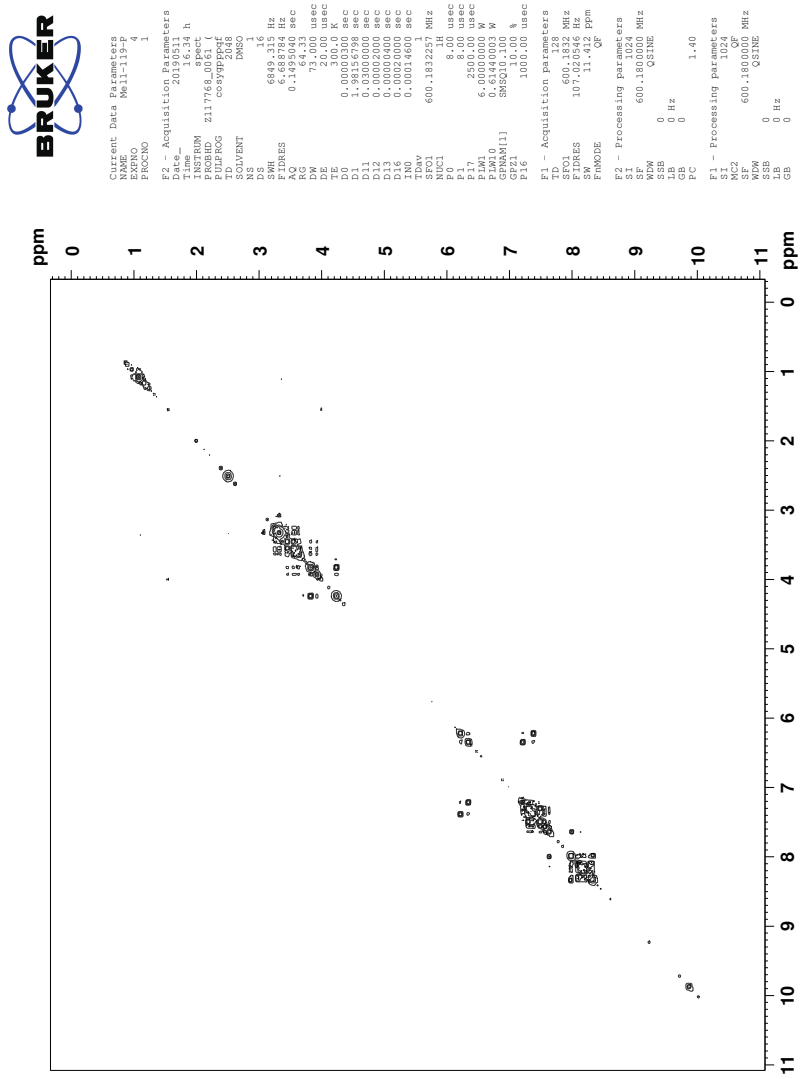

Figure 12: COSY NMR spectra of compound **5**.

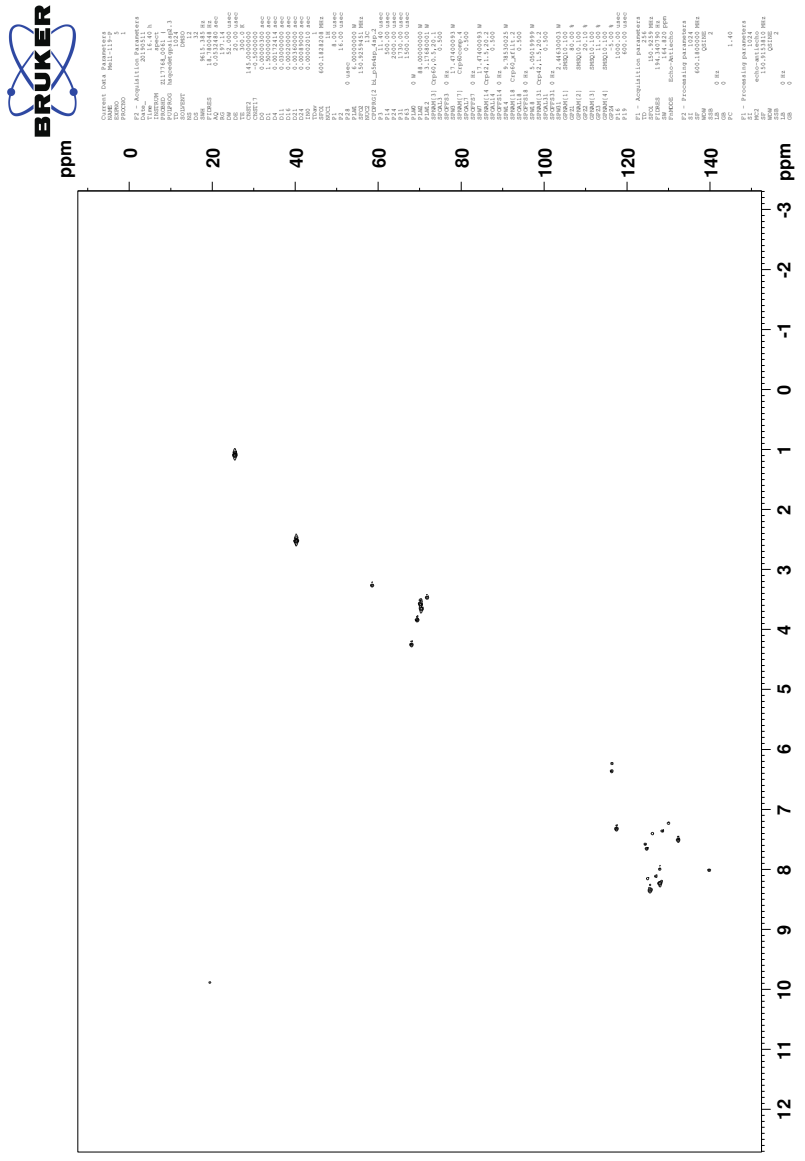

Figure 13: HSQC NMR spectra of compound **5**.

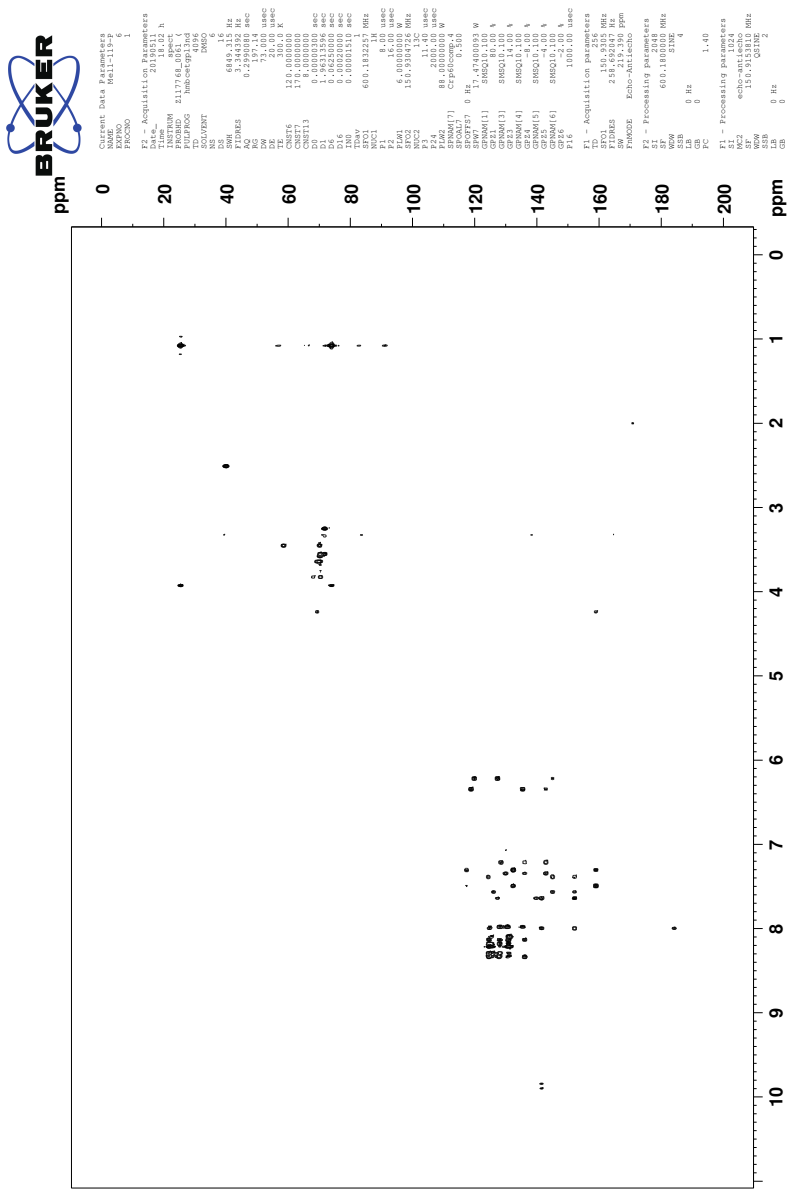

Figure 14: HMBC NMR spectra of compound **5**.

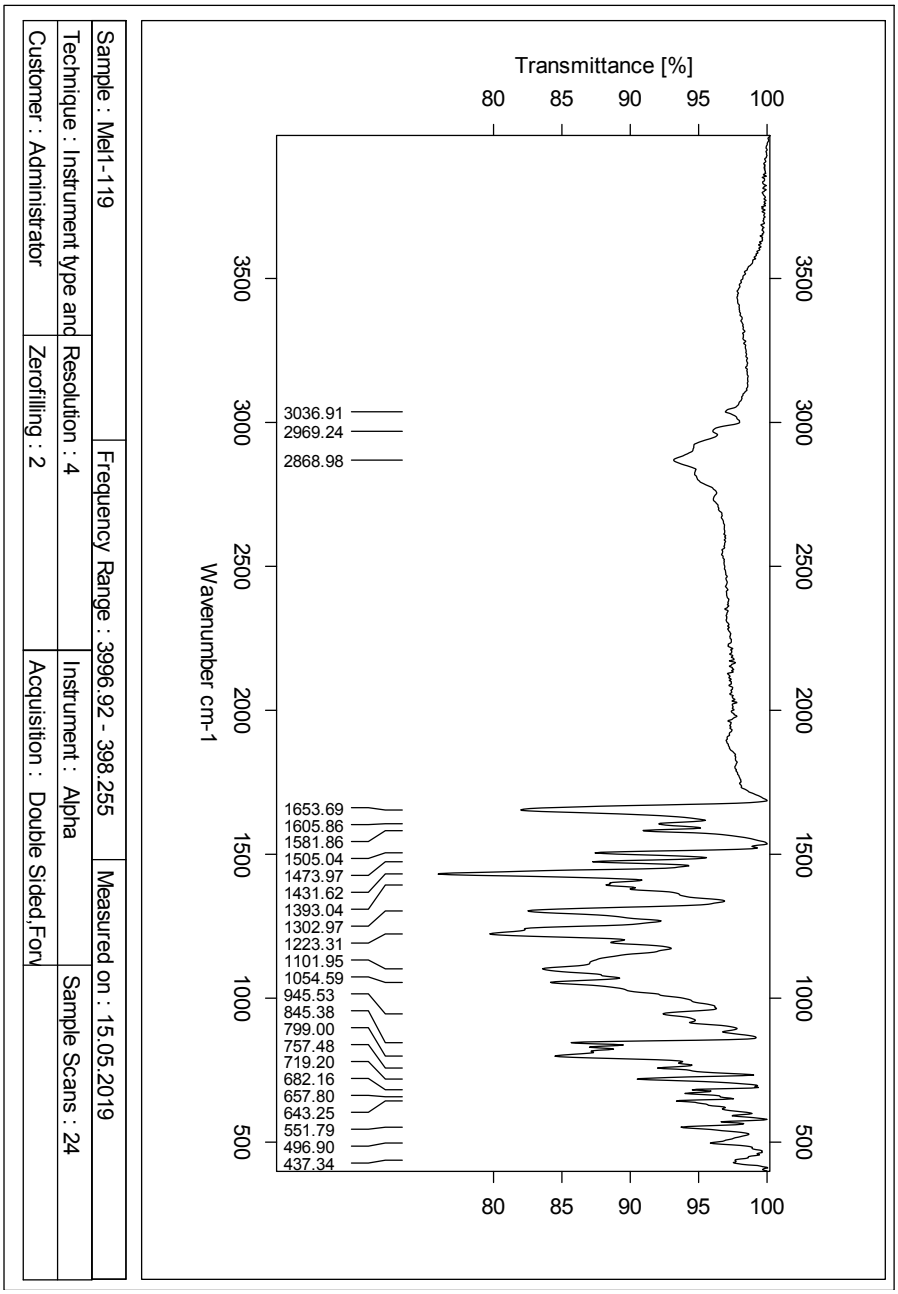

Figure 15: IR spectra of compound **5**.

Elemental Composition Report **Page 1**

Single Mass Analysis
Tolerance = 2.0 PPM / DBE: min = -50.0, max = 50.0
Element prediction: Off
Number of isotope peaks used for i-FIT = 3

Monoisotopic Mass, Even Electron Ions
7663 formula(e) evaluated with 11 results within limits (all results (up to 1000) for each mass)
Elements Used:
C: 0-100 H: 0-150 N: 0-10 O: 0-10 S: 0-4
2019-483 297 (5.791) AM2 (Ar,35000.0,0.00,0.00); Cm (279:300)
1: TOF MS ASAP+

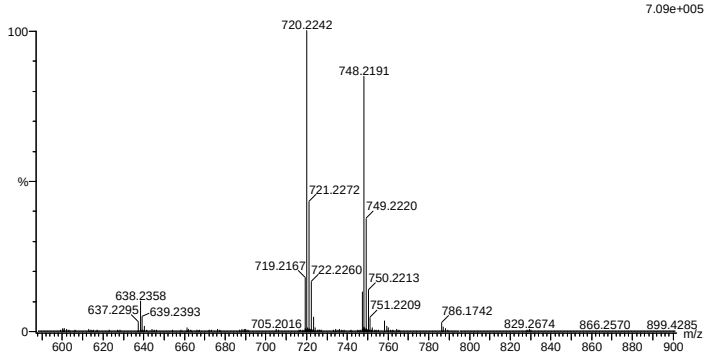

Minimum:				-50.0				
Maximum:		5.0	2.0	50.0				
Mass	Calc. Mass	mDa	PPM	DBE	i-FIT	Norm	Conf(%)	Formula
748.2191	748.2200	-0.9	-1.2	27.5	779.9	14.924	0.00	C47 H42 N S4
	748.2205	-1.4	-1.9	33.5	776.9	11.868	0.00	C47 H34 N5 O S2
	748.2191	0.0	0.0	28.5	774.9	9.848	0.01	C46 H38 N O5 S2
	748.2196	-0.5	-0.7	34.5	778.7	13.694	0.00	C46 H30 N5 O6
	748.2183	0.8	1.1	29.5	777.5	12.498	0.00	C45 H34 N O10
	748.2198	-0.7	-0.9	24.5	777.8	12.742	0.00	C39 H38 N7 O3 S3
	748.2185	0.6	0.8	19.5	778.5	13.480	0.00	C38 H42 N3 O7 S3
	748.2190	0.1	0.1	25.5	765.0	0.000	99.99	C38 H34 N7 O8 S
	748.2192	-0.1	-0.1	15.5	781.3	16.262	0.00	C31 H42 N9 O5 S4
	748.2183	0.8	1.1	16.5	775.9	10.923	0.00	C30 H38 N9 O10 S2
	748.2178	1.3	1.7	10.5	782.2	17.197	0.00	C30 H46 N5 O9 S4

Figure 16: Mass spectra of compound **5**.

E Spectroscopic Data - Compound 6

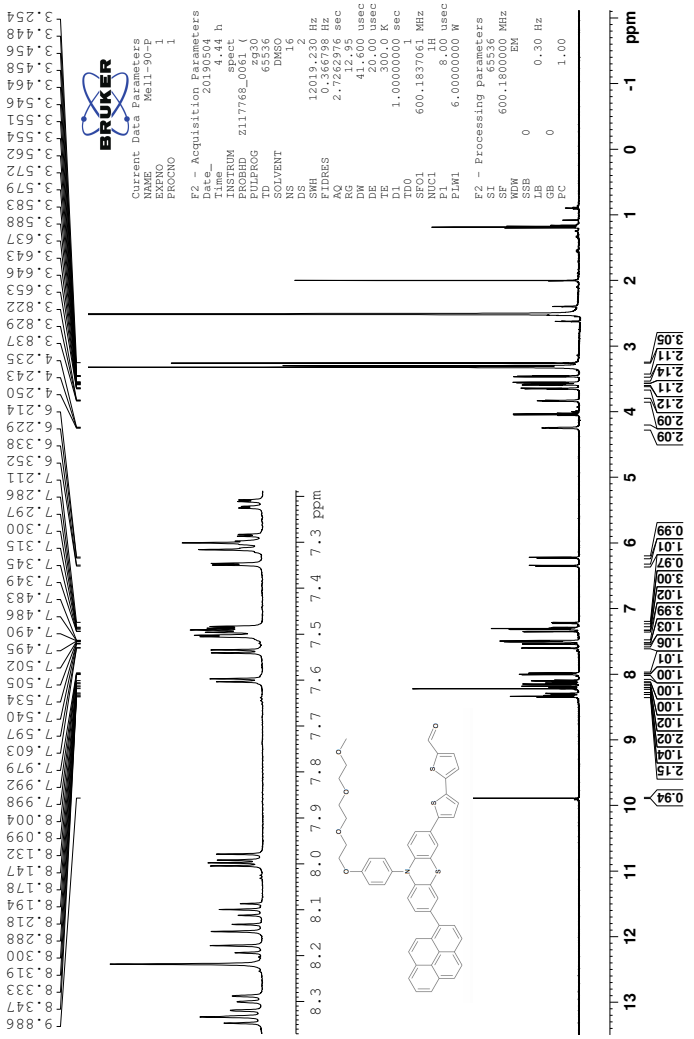

Figure 17: ^{1}H spectrum of compound **6**.

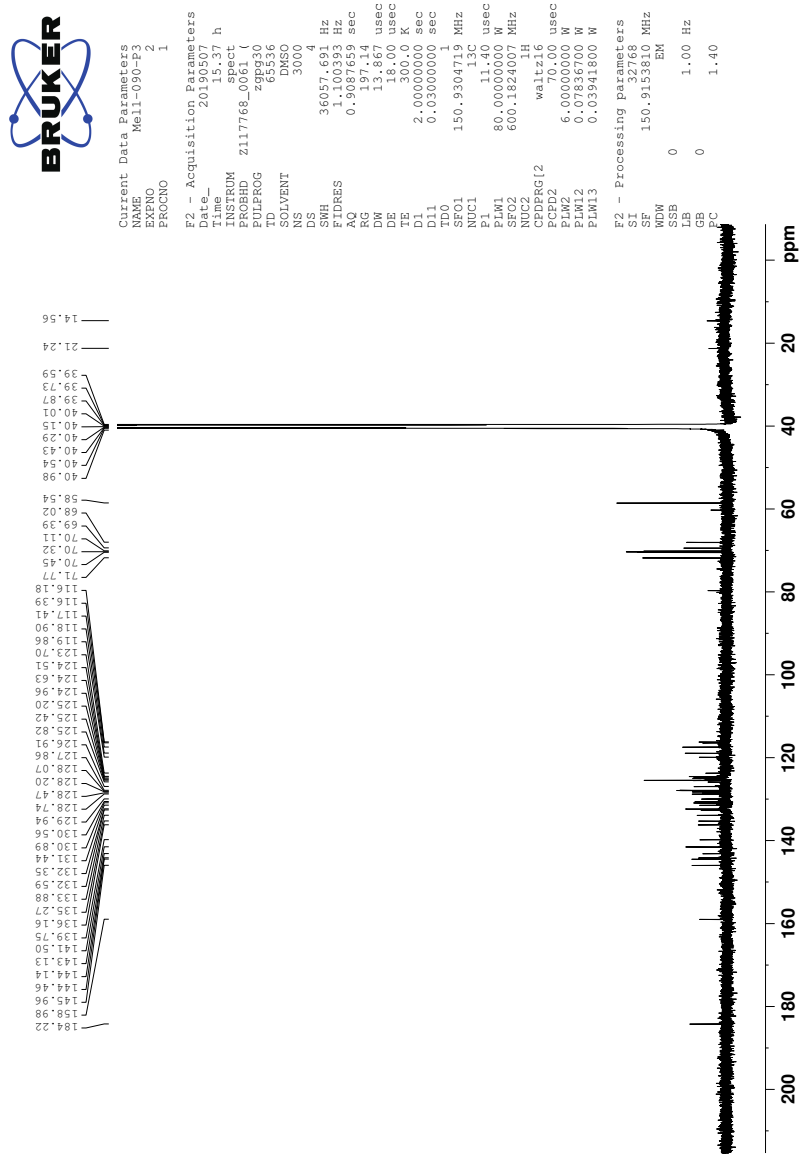

Figure 18: ^{13}C NMR spectra of compound **6**.

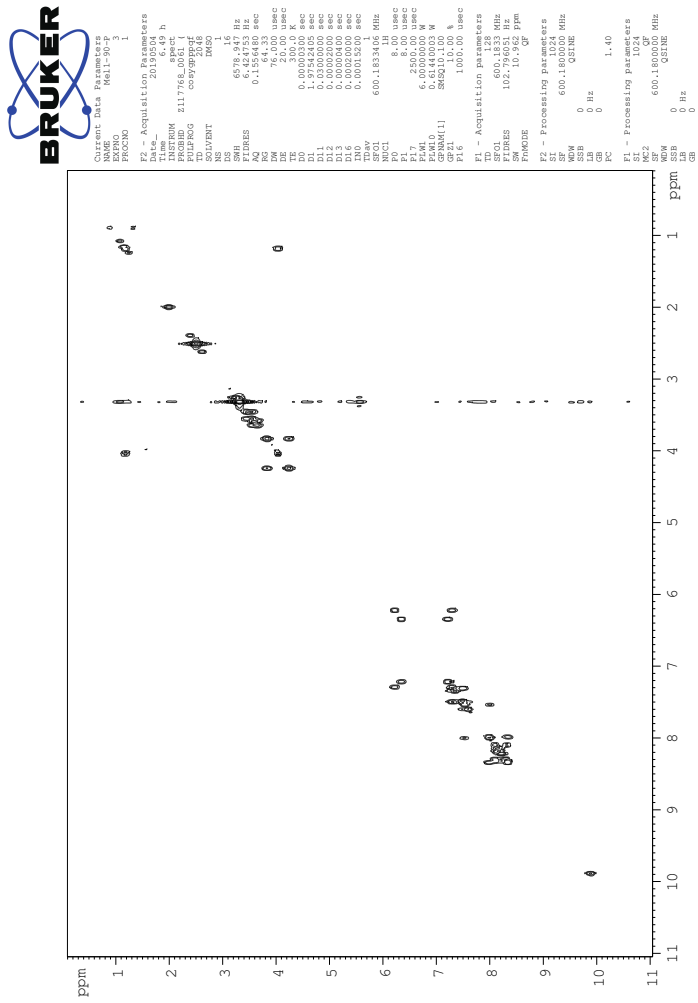

Figure 19: COSY NMR spectra of compound **6**.

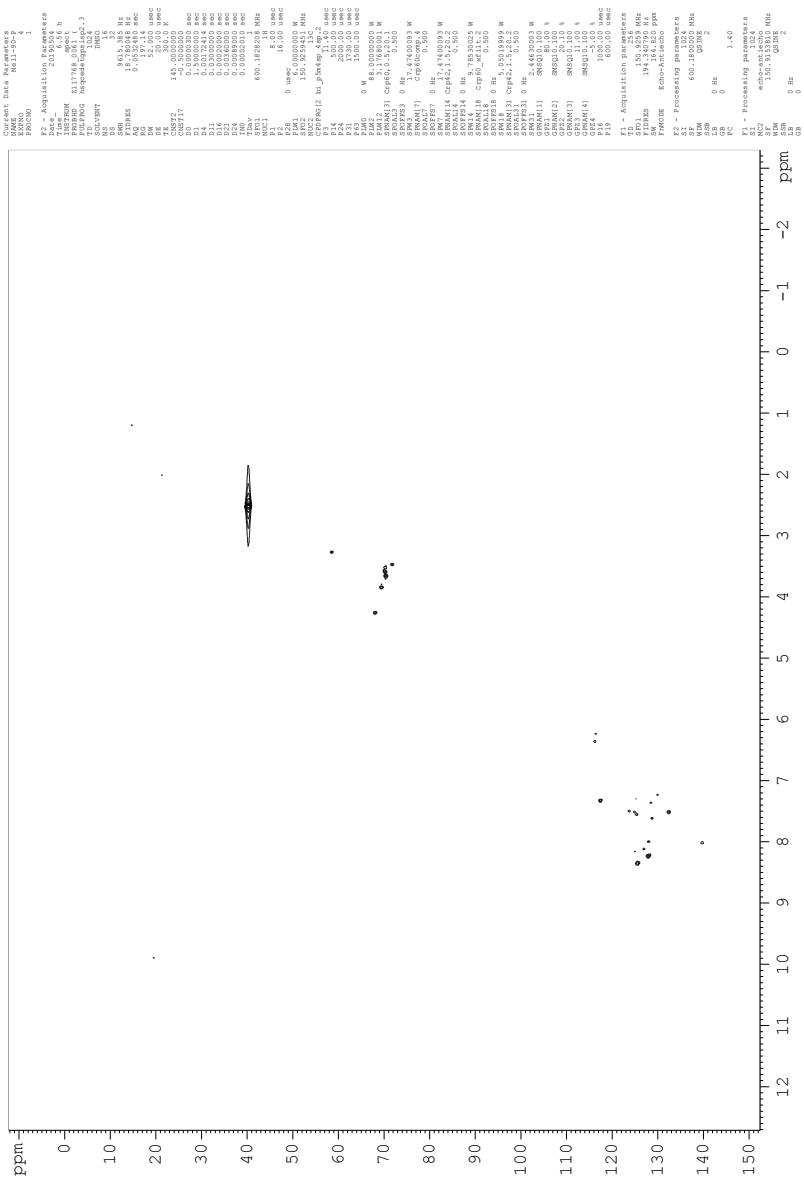

Figure 20: HSQC NMR spectra of compound **6**.

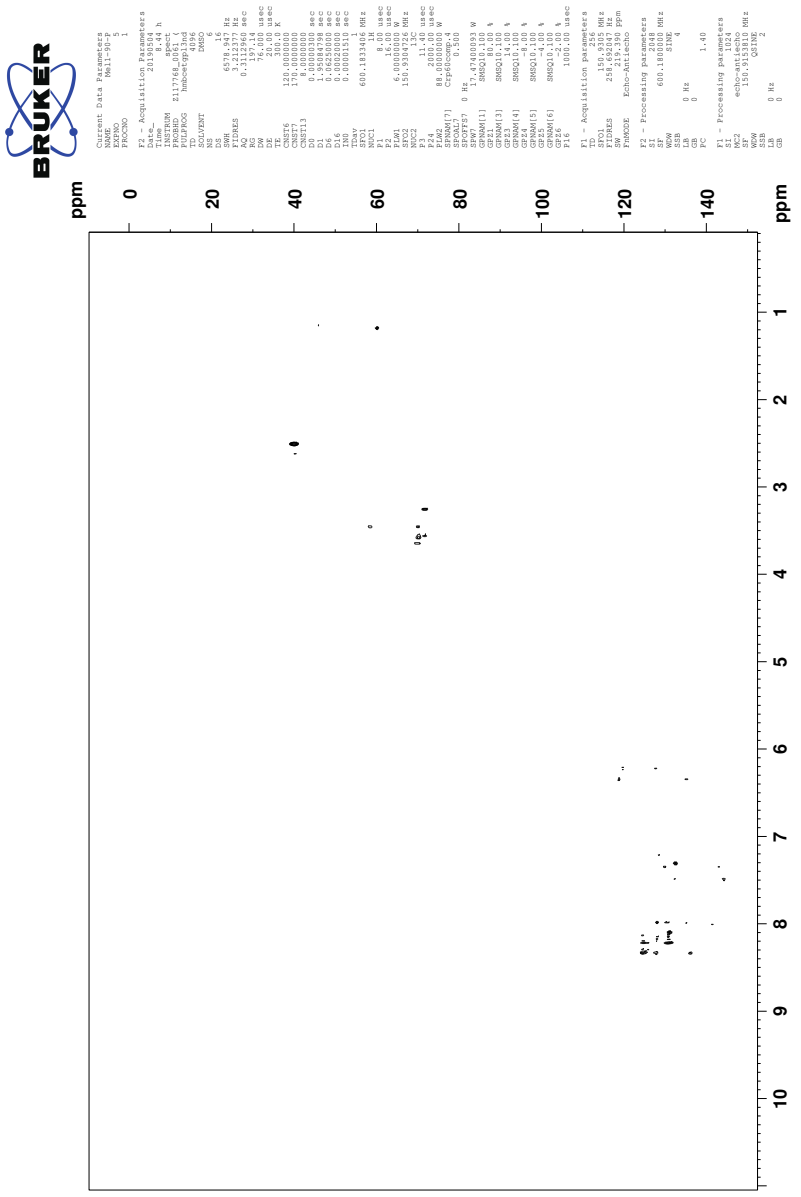

Figure 21: HMBC NMR spectra of compound **6**.

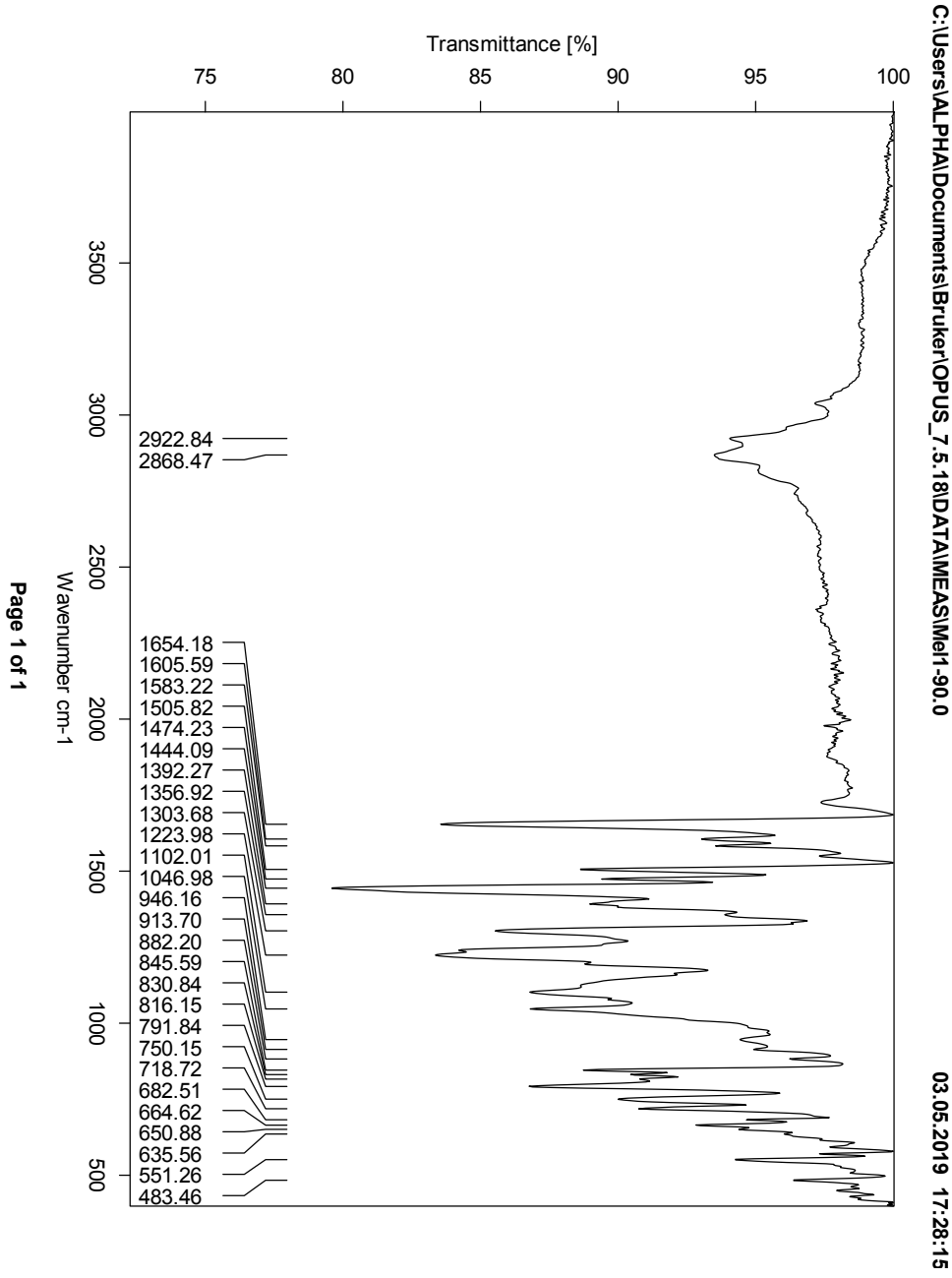

Figure 22: IR spectra of compound **6**.

Elemental Composition Report **Page 1**

Single Mass Analysis
Tolerance = 2.0 PPM / DBE: min = -50.0, max = 50.0
Element prediction: Off
Number of isotope peaks used for i-FIT = 3

Monoisotopic Mass, Even Electron Ions
7663 formula(e) evaluated with 10 results within limits (all results (up to 1000) for each mass)
Elements Used:
C: 0-100 H: 0-150 N: 0-10 O: 0-10 S: 0-4
2019-438 139 (1.549) AM2 (Ar,35000.0,0.00,0.00); Cm (135:139)
1: TOF MS ES+

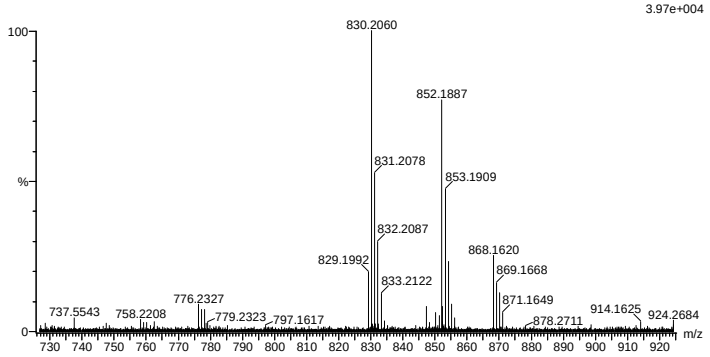


```
Minimum:                              -50.0
Maximum:                5.0    2.0    50.0

Mass       Calc. Mass  mDa    PPM    DBE    i-FIT   Norm   Conf(%) Formula

830.2060   830.2069    -0.9   -1.1   31.5   521.9   0.816  44.24   C50 H40 N O5 S3
           830.2075    -1.5   -1.8   27.5   522.5   1.363  25.60   C43 H40 N7 O3
                                                                   S4
           830.2062    -0.2   -0.2   22.5   523.1   2.015  13.33   C42 H44 N3 O7
                                                                   S4
           830.2048    1.2    1.4    41.5   523.4   2.325  9.77    C54 H32 N5 O S2
           830.2067    -0.7   -0.8   28.5   524.2   3.128  4.38    C42 H36 N7 O8
                                                                   S2
           830.2060    0.0    0.0    32.5   525.3   4.165  1.55    C49 H36 N O10 S
           830.2044    1.6    1.9    35.5   526.6   5.512  0.40    C54 H40 N S4
           830.2060    0.0    0.0    19.5   526.7   5.607  0.37    C34 H40 N9 O10
                                                                   S3
           830.2073    -1.3   -1.6   37.5   526.9   5.783  0.31    C50 H32 N5 O6 S
           830.2053    0.7    0.8    47.5   528.8   7.745  0.04    C54 H24 N9 O2
```

Figure 23: Mass spectra of compound **6**.

F Spectroscopic Data - Compound MEL1

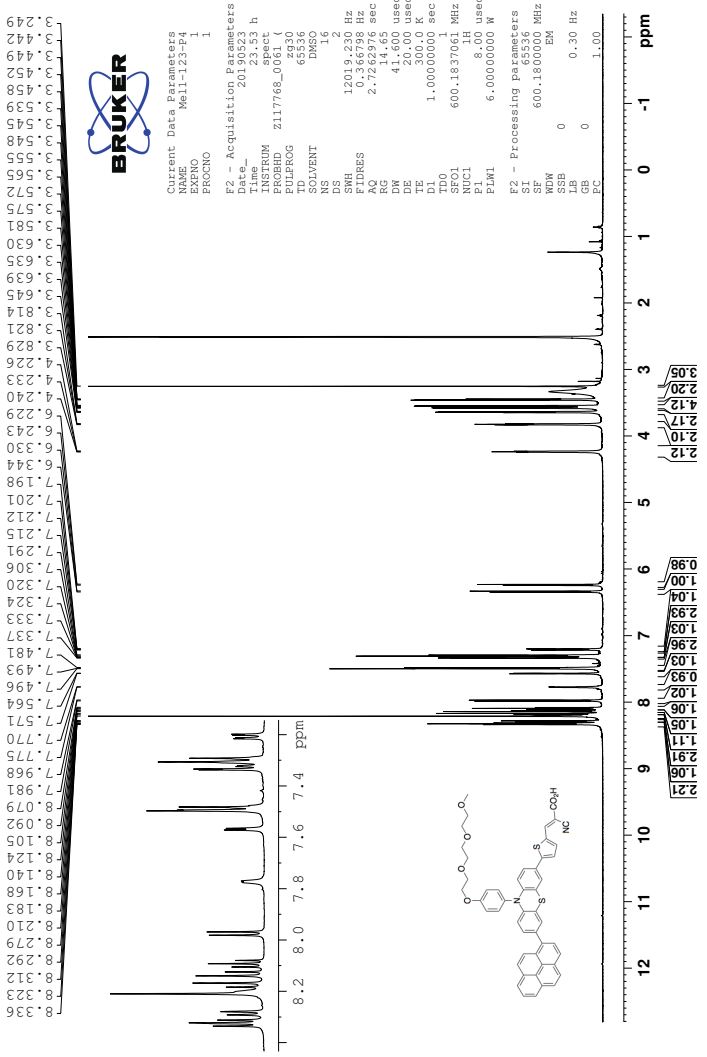

Figure 24: ^{1}H spectrum of compound **MEL1**.

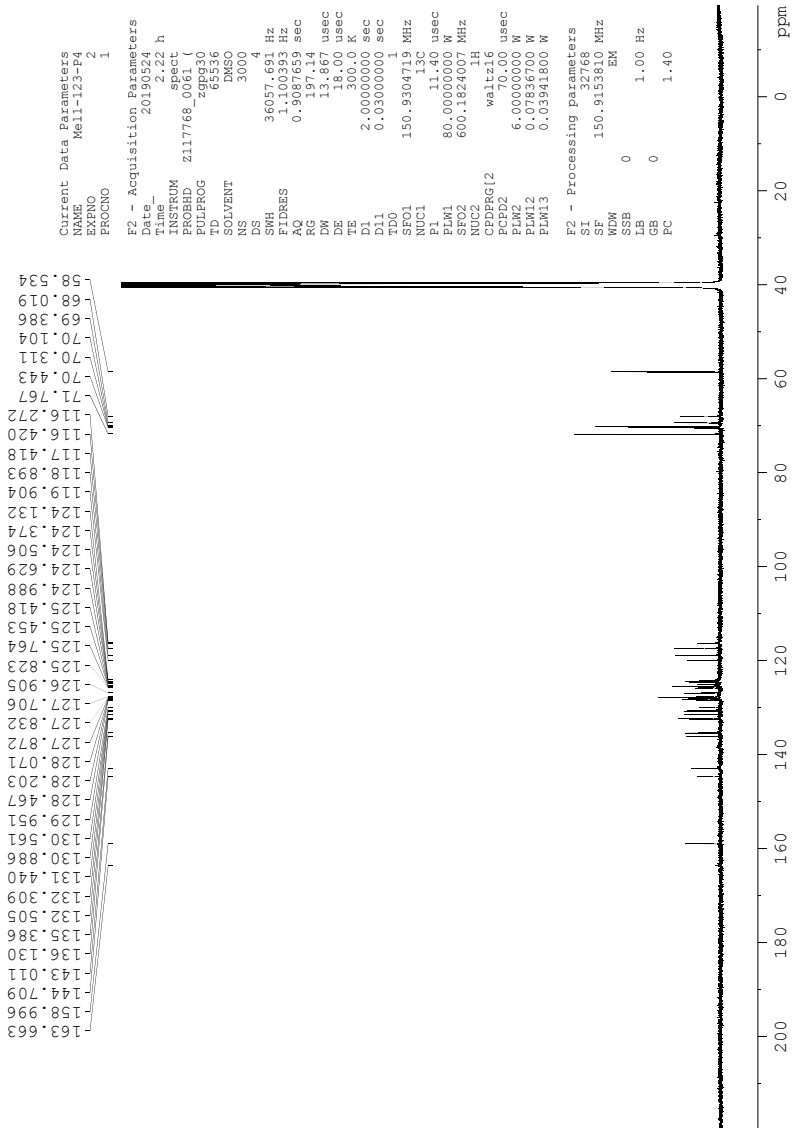

Figure 25: ^{13}C NMR spectra of compound **MEL1**.

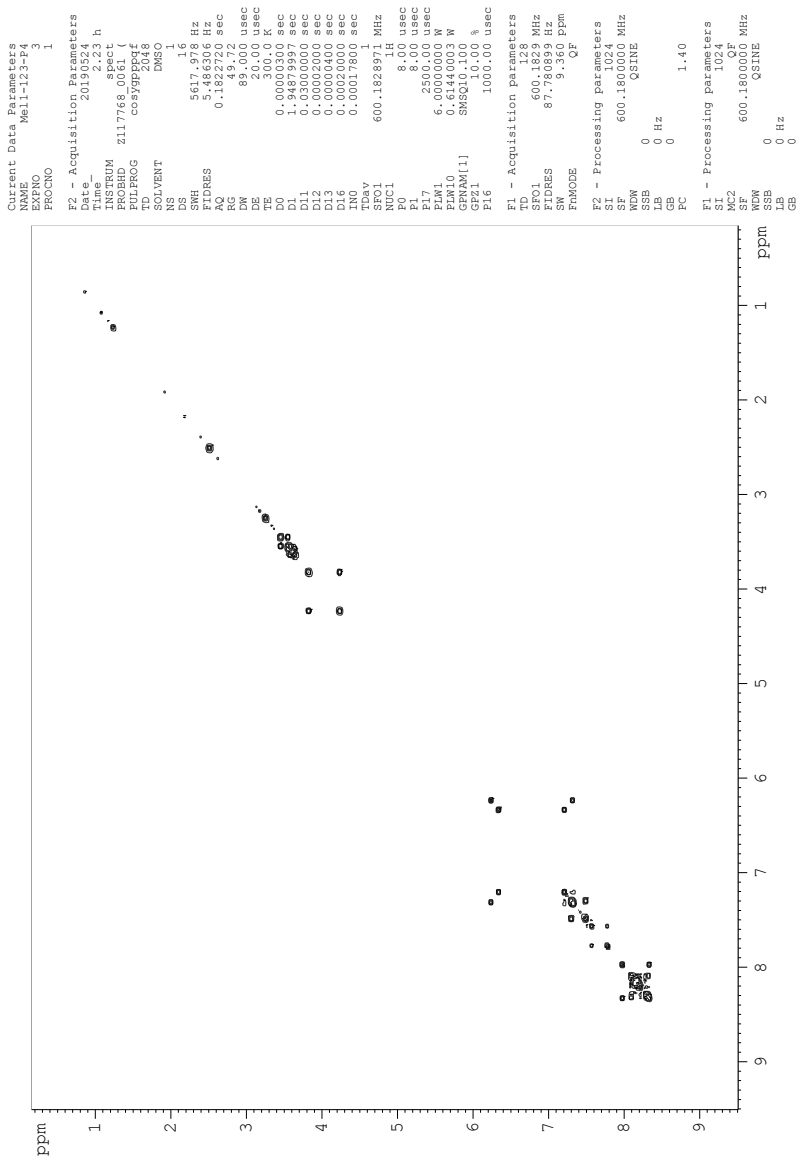

Figure 26: COSY NMR spectra of compound **MEL1**.

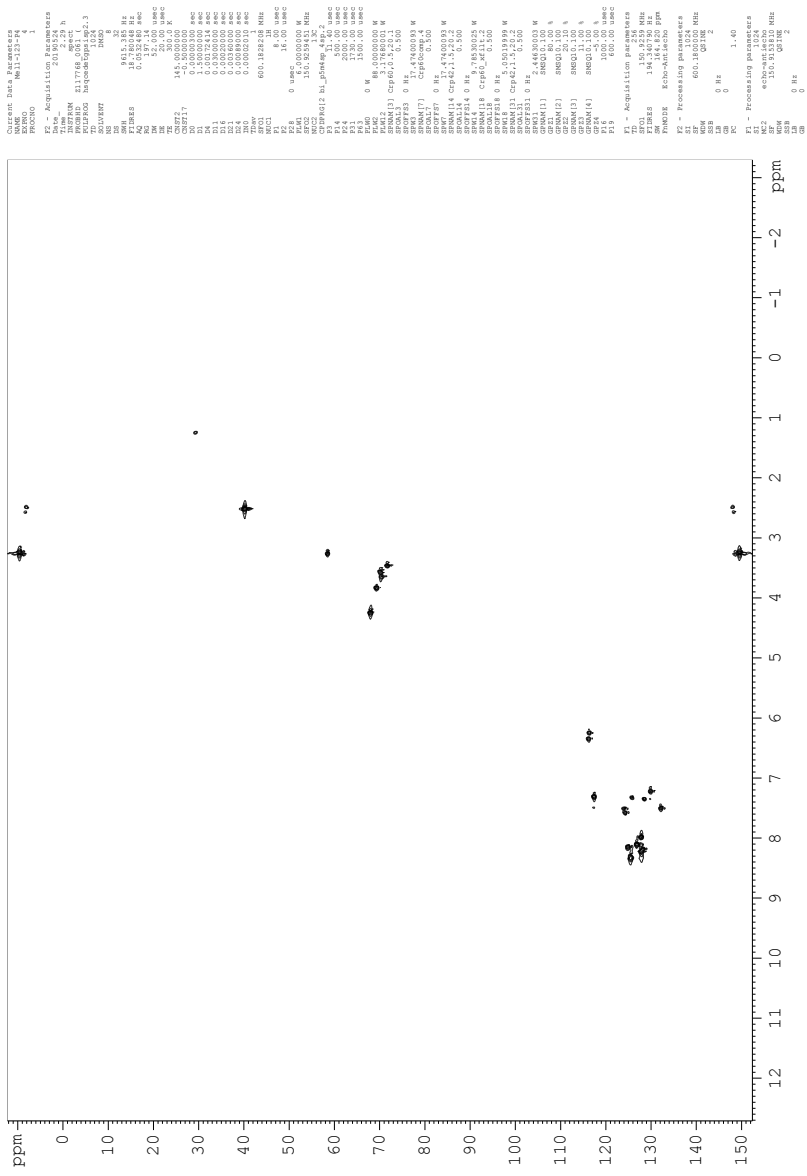

Figure 27: HSQC NMR spectra of compound **MEL1**.

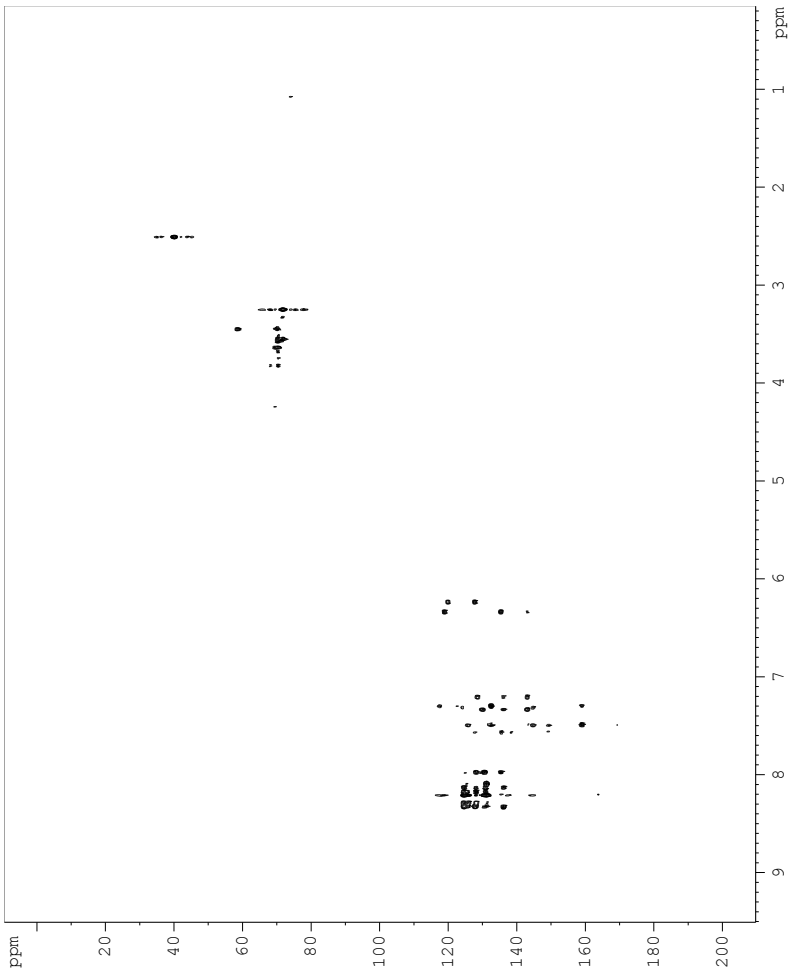

Figure 28: HMBC NMR spectra of compound **MEL1**.

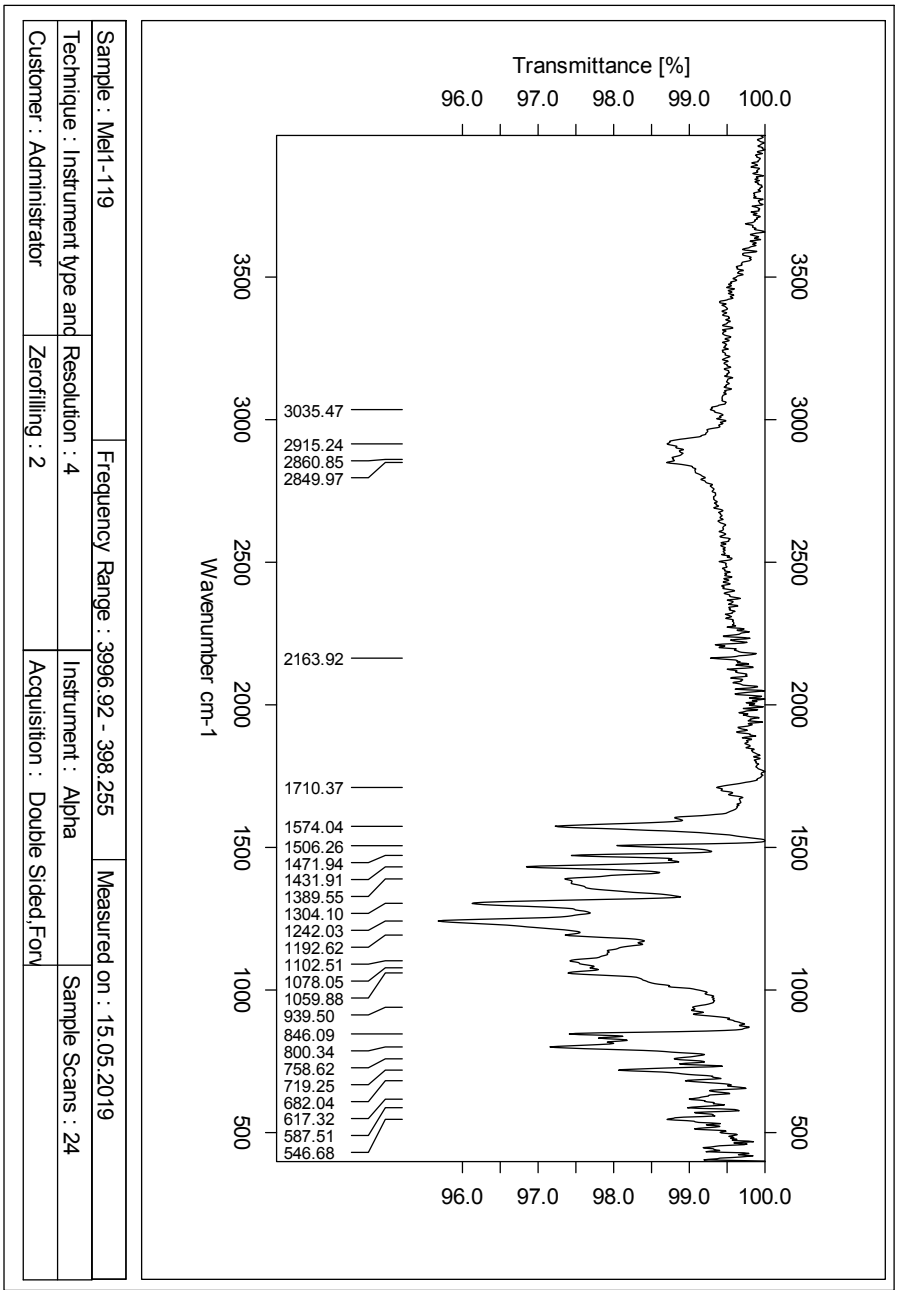

Figure 29: IR spectra of compound **MEL1**.

Elemental Composition Report **Page 1**

Single Mass Analysis
Tolerance = 1.0 PPM / DBE: min = -50.0, max = 50.0
Element prediction: Off
Number of isotope peaks used for i-FIT = 3

Monoisotopic Mass, Even Electron Ions
7773 formula(e) evaluated with 6 results within limits (all results (up to 1000) for each mass)
Elements Used:
C: 0-100 H: 0-150 N: 0-10 O: 0-10 S: 0-4
2019-484 297 (5.791) AM2 (Ar,35000.0,0.00,0.00); Cm (281:302)
1: TOF MS ASAP+

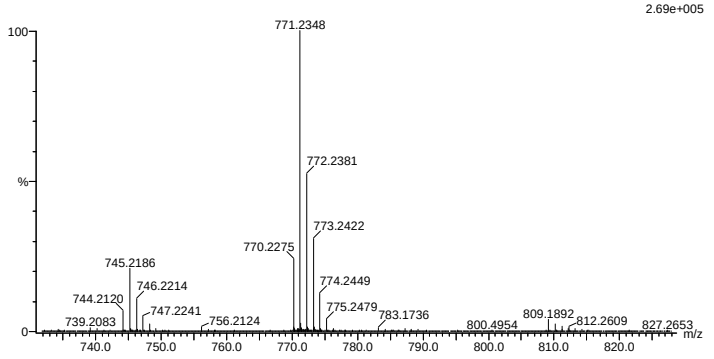

Minimum:				-50.0				
Maximum:		5.0	1.0	50.0				
Mass	Calc. Mass	mDa	PPM	DBE	i-FIT	Norm	Conf(%)	Formula
771.2348	771.2351	-0.3	-0.4	30.5	659.2	1.706	18.16	C48 H39 N2 O4 S2
	771.2343	0.5	0.6	31.5	657.9	0.462	62.99	C47 H35 N2 O9
	771.2349	-0.1	-0.1	27.5	661.5	4.009	1.81	C40 H35 N8 O7 S
	771.2345	0.3	0.4	21.5	659.4	1.956	14.15	C40 H43 N4 O6 S3
	771.2352	-0.4	-0.5	17.5	661.1	3.647	2.61	C33 H43 N10 O4 S4
	771.2343	0.5	0.6	18.5	663.3	5.871	0.28	C32 H39 N10 O9 S2

Figure 30: Mass spectra of compound **MEL1**.

G Spectroscopic Data - Compound MEL2

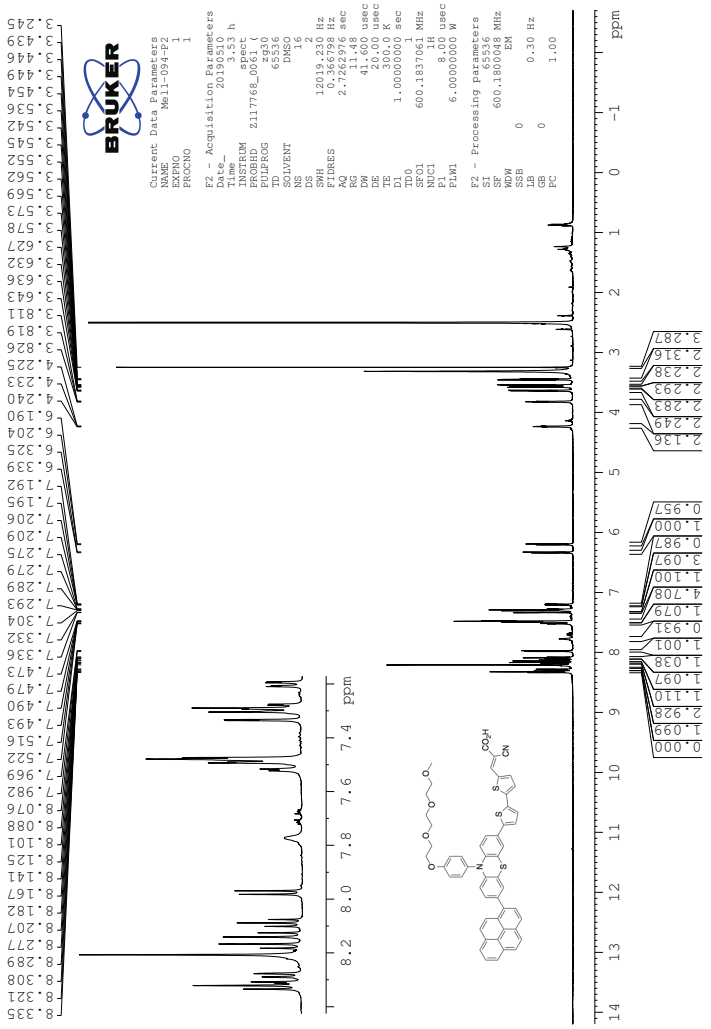

Figure 31: ^{1}H spectrum of compound **MEL2**.

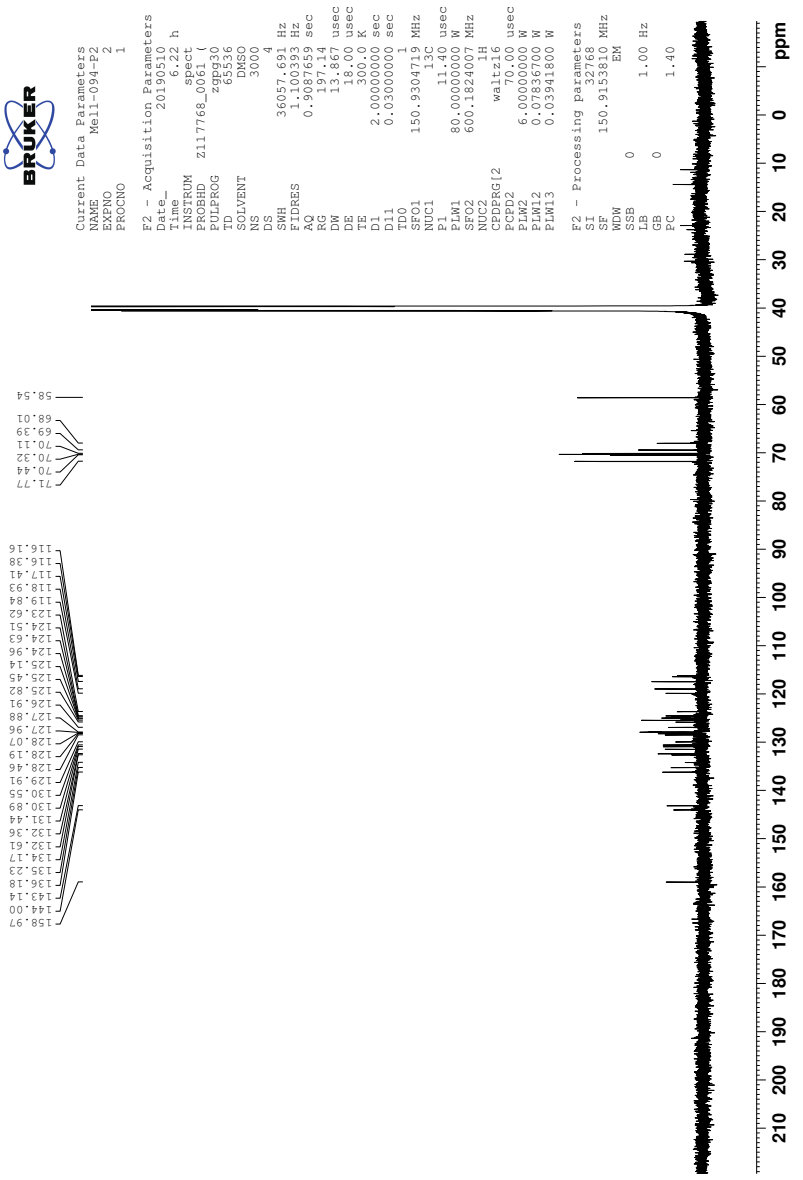

Figure 32: ^{13}C NMR spectra of compound **MEL2**.

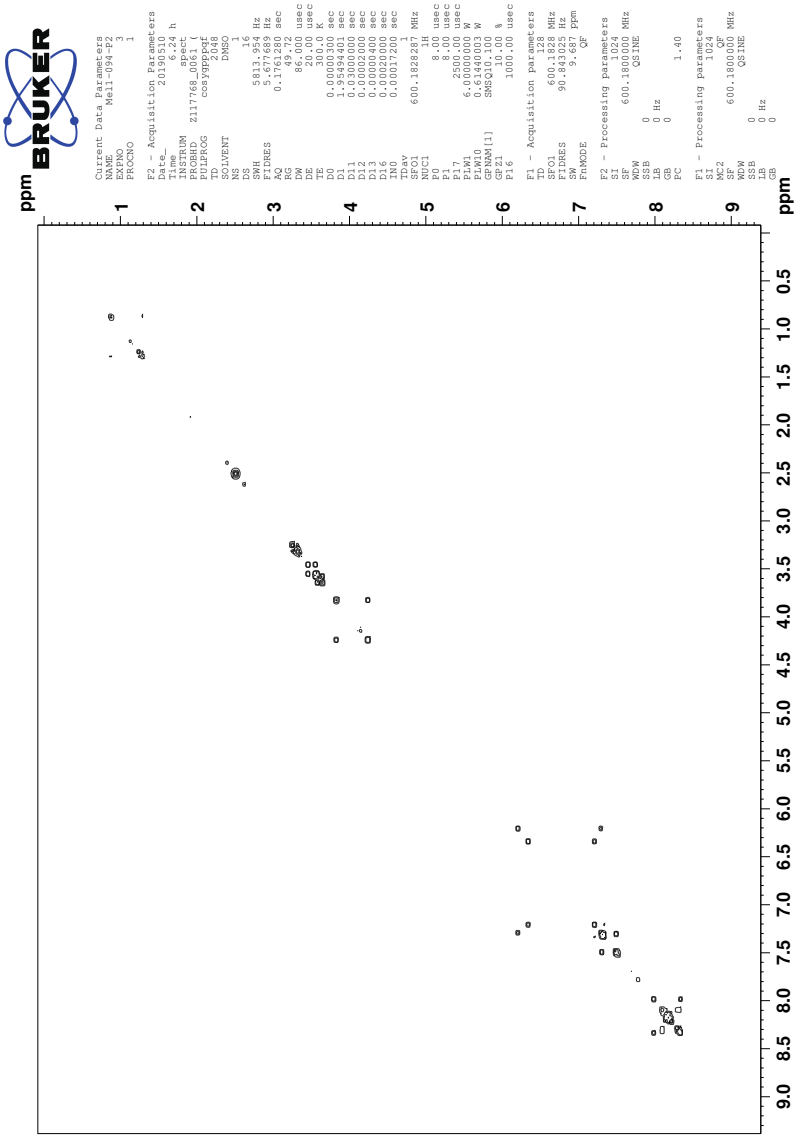

Figure 33: COSY NMR spectra of compound **MEL2**.

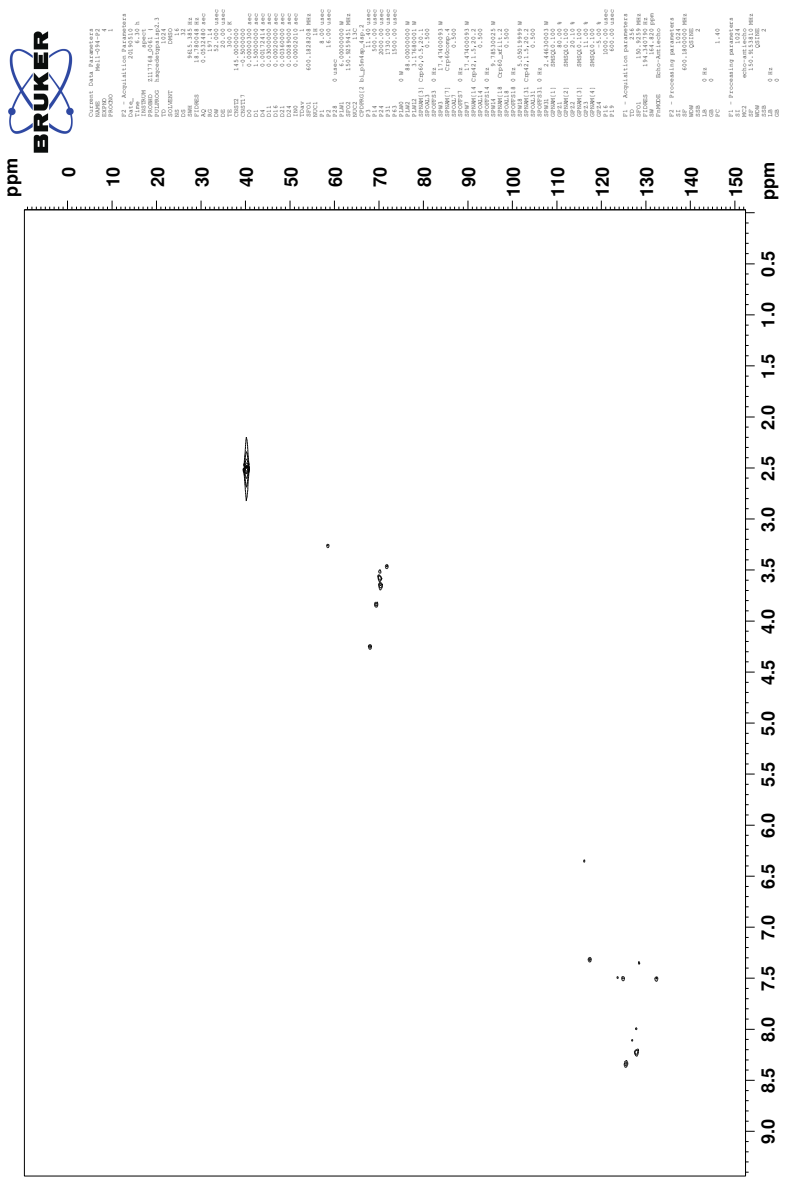

Figure 34: HSQC NMR spectra of compound **MEL2**.

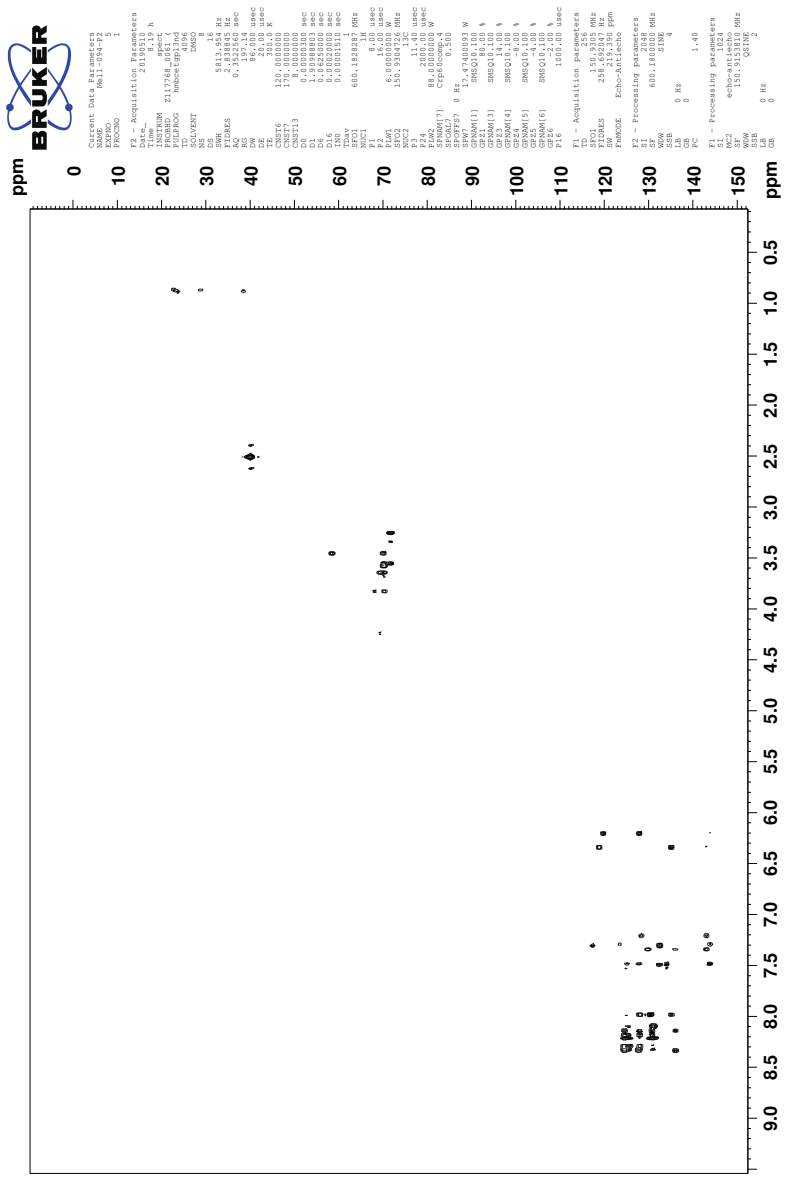

Figure 35: HMBC NMR spectra of compound **MEL2**.

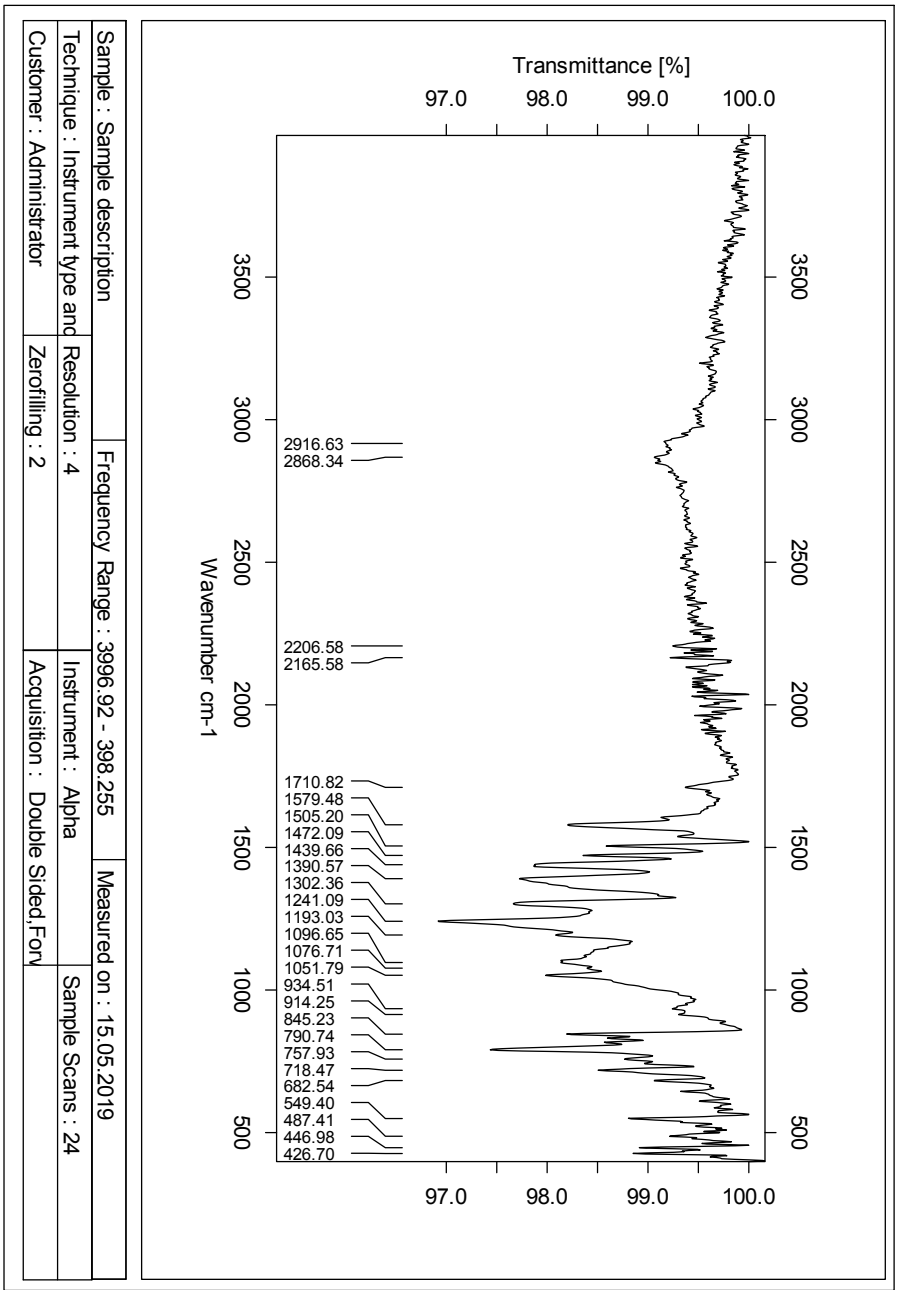

Figure 36: IR spectra of compound **MEL2**.

Elemental Composition Report **Page 1**

Single Mass Analysis
Tolerance = 2.0 PPM / DBE: min = -50.0, max = 50.0
Element prediction: Off
Number of isotope peaks used for i-FIT = 3

Monoisotopic Mass, Even Electron Ions
7755 formula(e) evaluated with 13 results within limits (all results (up to 1000) for each mass)
Elements Used:
C: 0-100 H: 0-150 N: 0-10 O: 0-10 S: 0-4
2019-479 289 (5.635) AM2 (Ar,35000.0,0.00,0.00); Cm (281:301)
1: TOF MS ASAP+

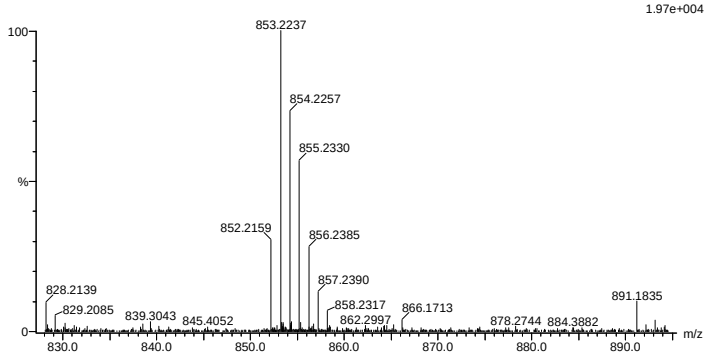

Minimum:				-50.0				
Maximum:		5.0	2.0	50.0				
Mass	Calc. Mass	mDa	PPM	DBE	i-FIT	Norm	Conf(%)	Formula
853.2237	853.2235	0.2	0.2	42.5	445.3	2.160	11.53	C60 H37 O2 S2
	853.2240	-0.3	-0.4	48.5	444.2	1.060	34.63	C60 H29 N4 O3
	853.2226	1.1	1.3	43.5	444.6	1.468	23.03	C59 H33 O7
	853.2247	-1.0	-1.2	44.5	445.9	2.801	6.08	C53 H29 N10 O S
	853.2242	-0.5	-0.6	38.5	445.9	2.764	6.31	C53 H37 N6 S3
	853.2228	0.9	1.1	33.5	446.2	3.132	4.36	C52 H41 N2 O4 S3
	853.2233	0.4	0.5	39.5	446.2	3.059	4.70	C52 H33 N6 O5 S
	853.2253	-1.6	-1.9	29.5	446.7	3.589	2.76	C48 H41 N2 O9 S2
	853.2235	0.2	0.2	29.5	446.7	3.609	2.71	C45 H41 N8 O2 S4
	853.2227	1.0	1.2	30.5	447.5	4.430	1.19	C44 H37 N8 O7 S2
	853.2222	1.5	1.8	24.5	447.2	4.051	1.74	C44 H45 N4 O6 S4
	853.2220	1.7	2.0	21.5	448.6	5.465	0.42	C36 H41 N10 O9 S3
	853.2254	-1.7	-2.0	16.5	448.3	5.210	0.55	C33 H45 N10 O9 S4

Figure 37: Mass spectra of compound **MEL2**.

H Spectroscopic Data - Compound 9

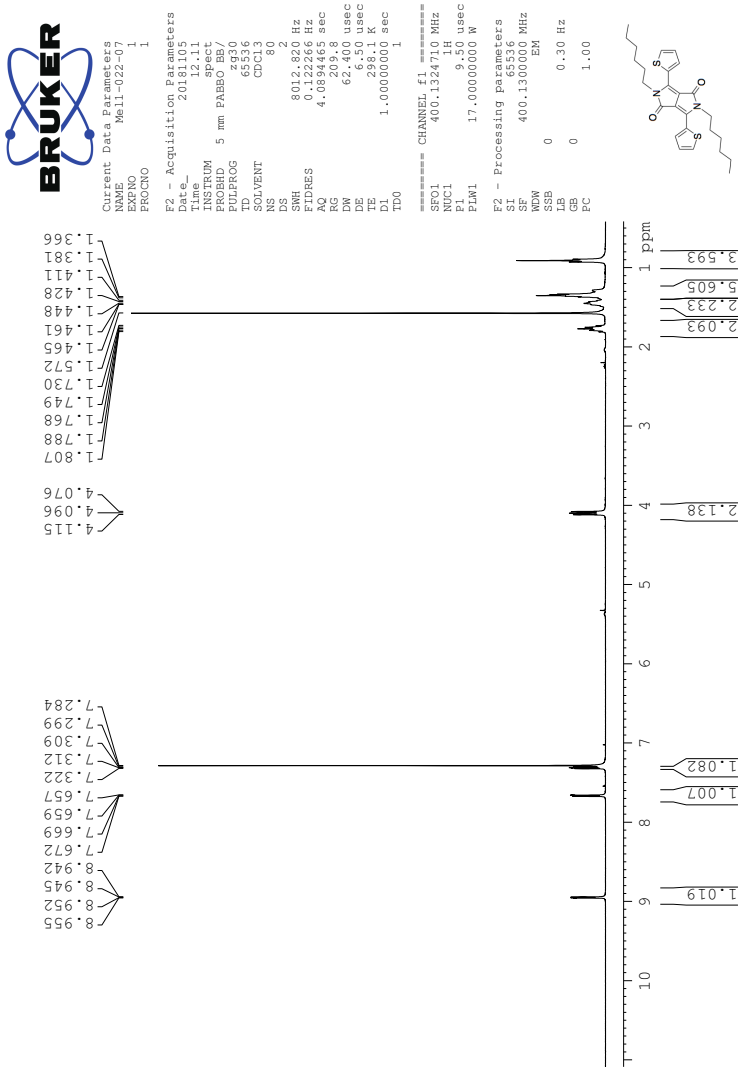

Figure 38: ^{1}H NMR spectra of compound **9**.

I Spectroscopic Data - Compound 10

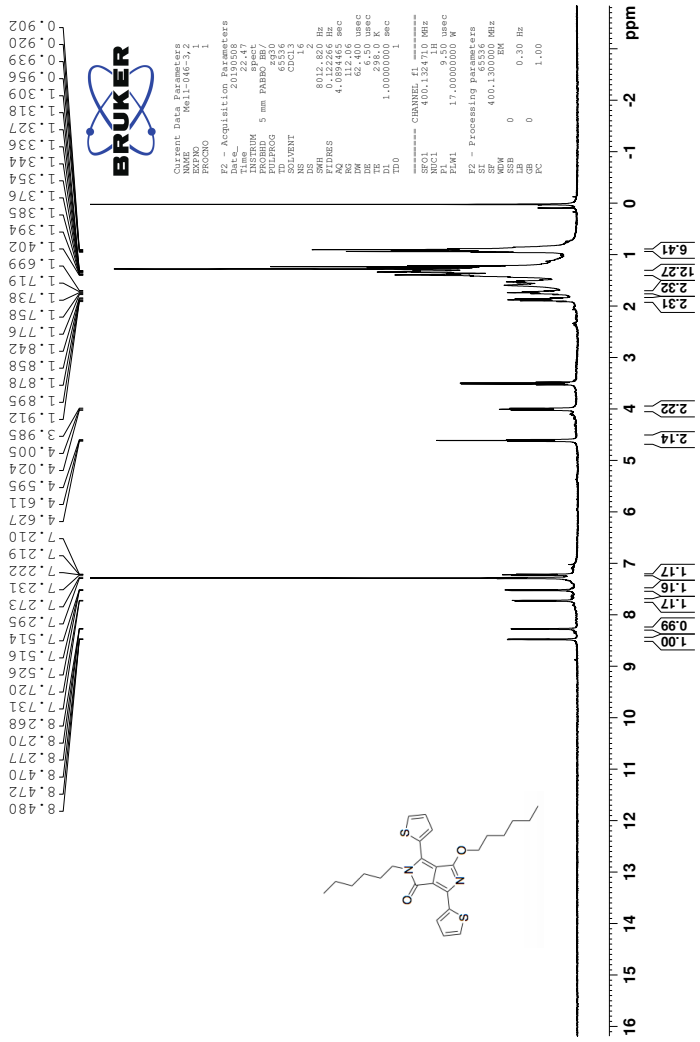

Figure 39: ^{1}H NMR spectra of compound **10**.

J Spectroscopic Data - Compound 12

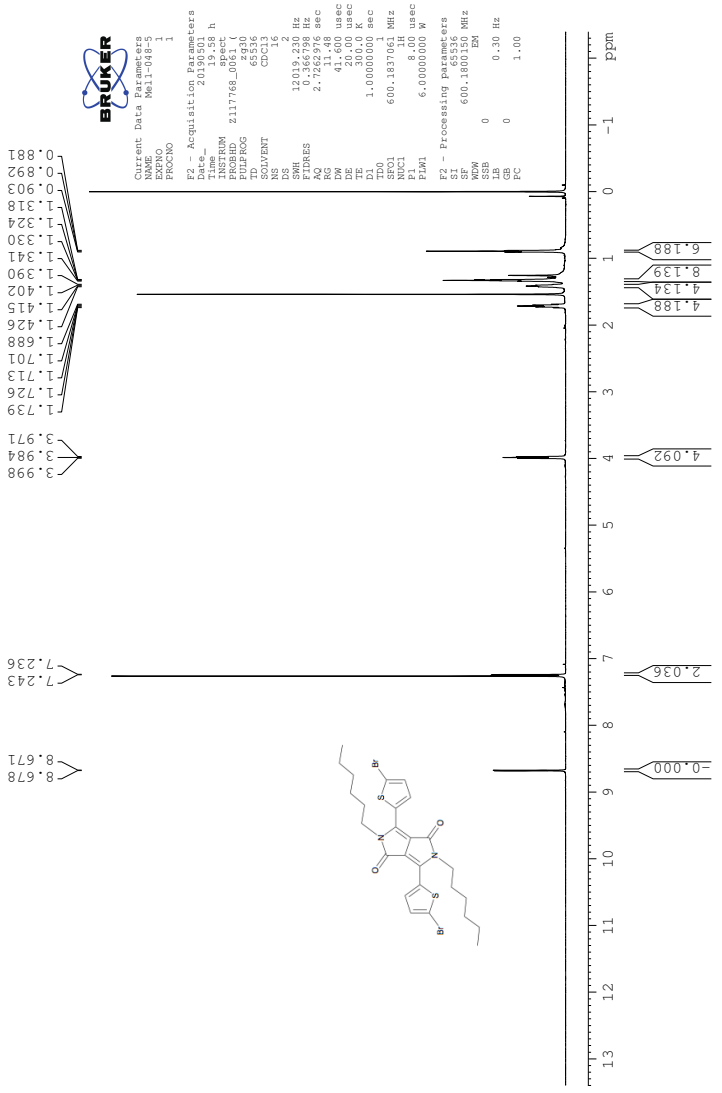

Figure 40: ^{1}H NMR spectra of compound **12**.

K Spectroscopic Data - Compound 16

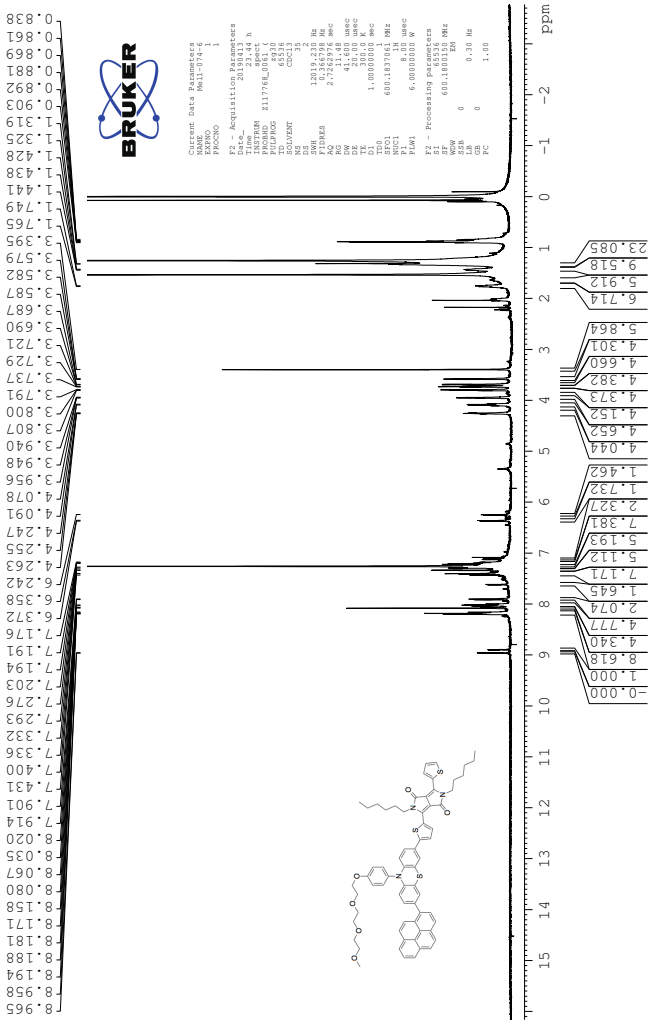

Figure 41: ^{1}H NMR spectra of the impure compound **16**.

L Spectroscopic Data - Compound 13

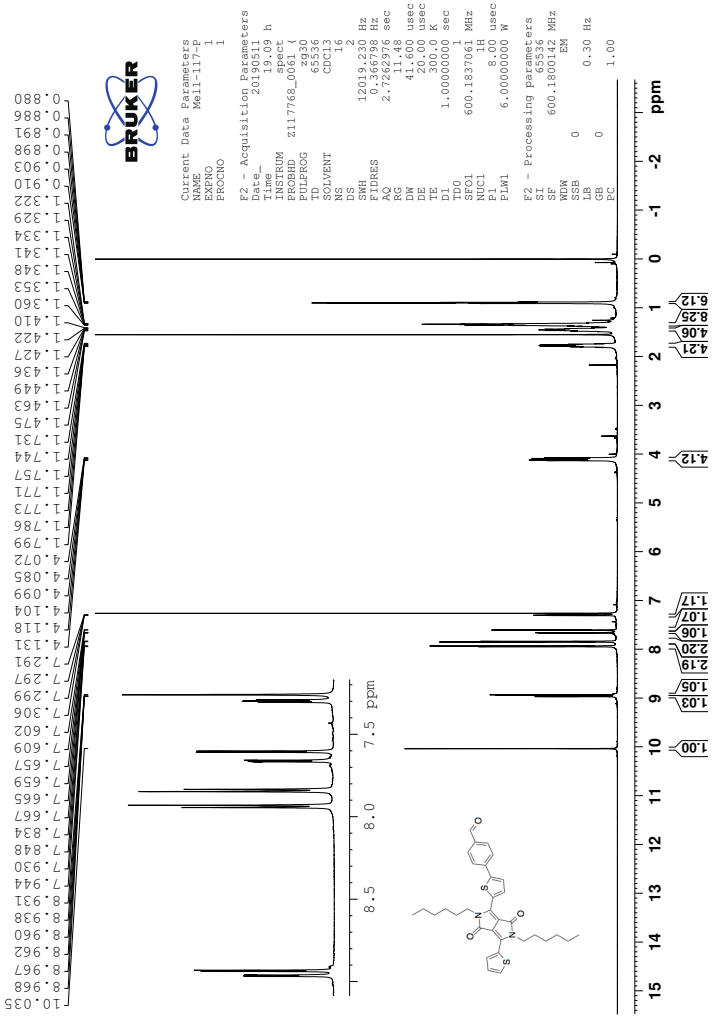

Figure 42: ^{1}H spectrum of compound **13**.

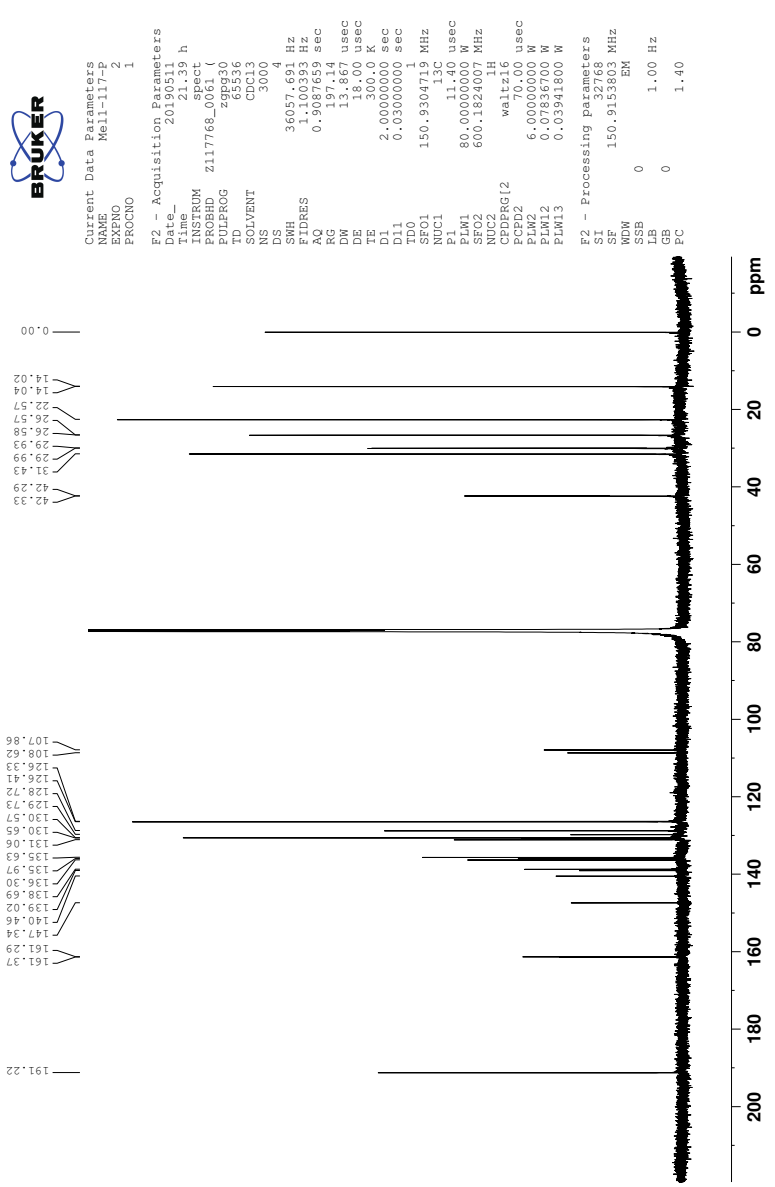

Figure 43: ^{13}C NMR spectra of compound **13**.

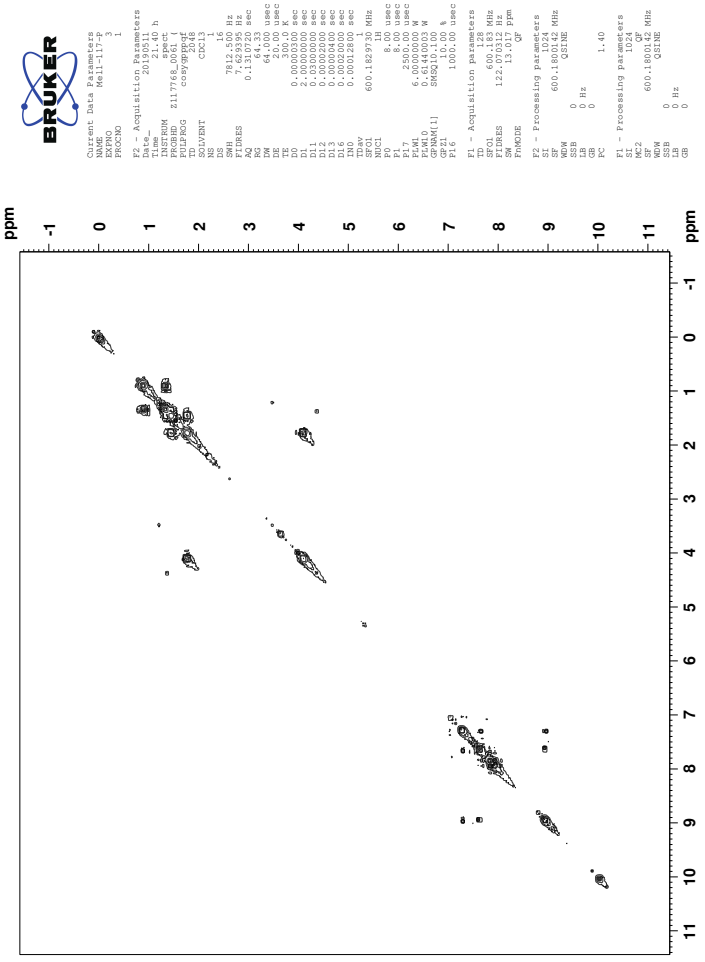

Figure 44: COSY NMR spectra of compound **13**.

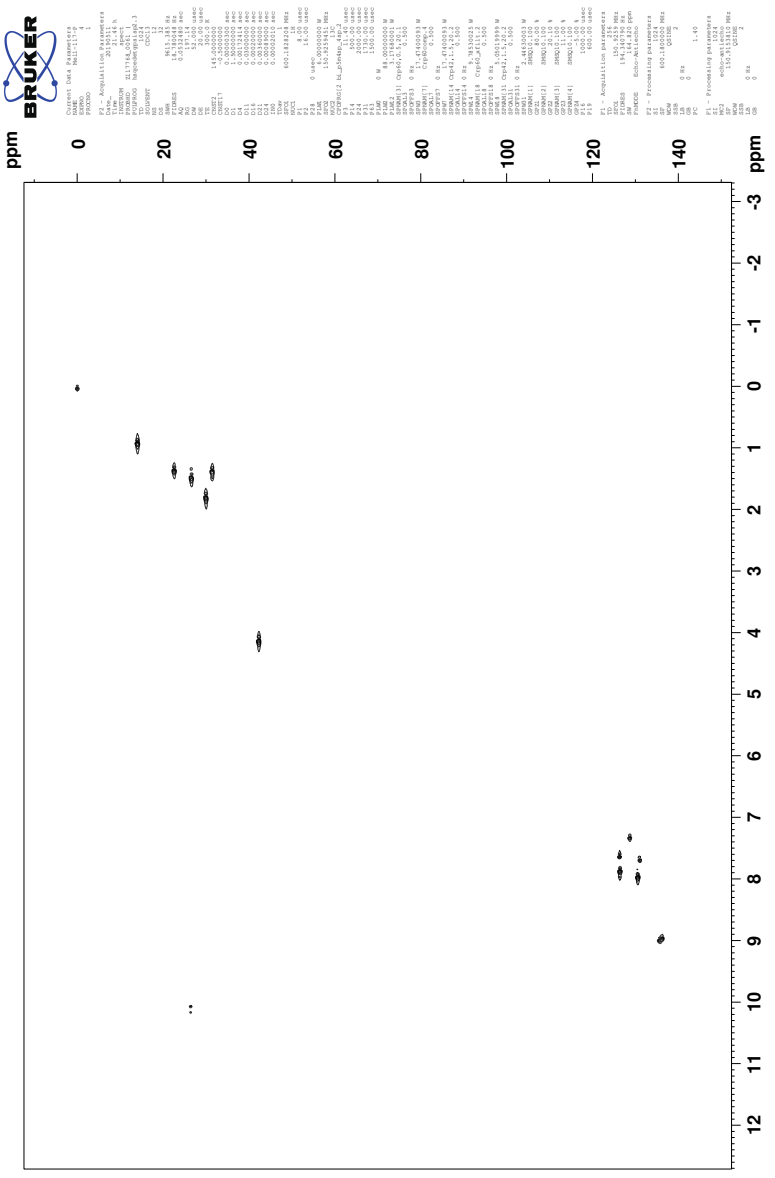

Figure 45: HSQC NMR spectra of compound **13**.

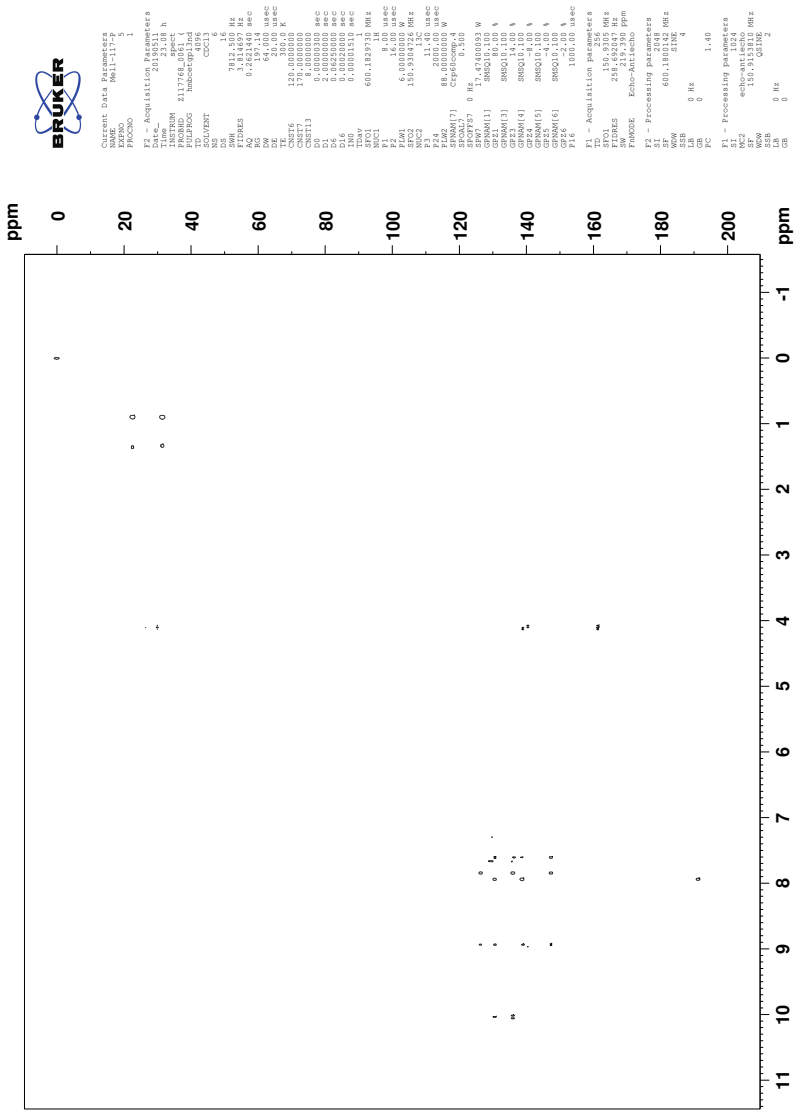

Figure 46: HMBC NMR spectra of compound **13**.

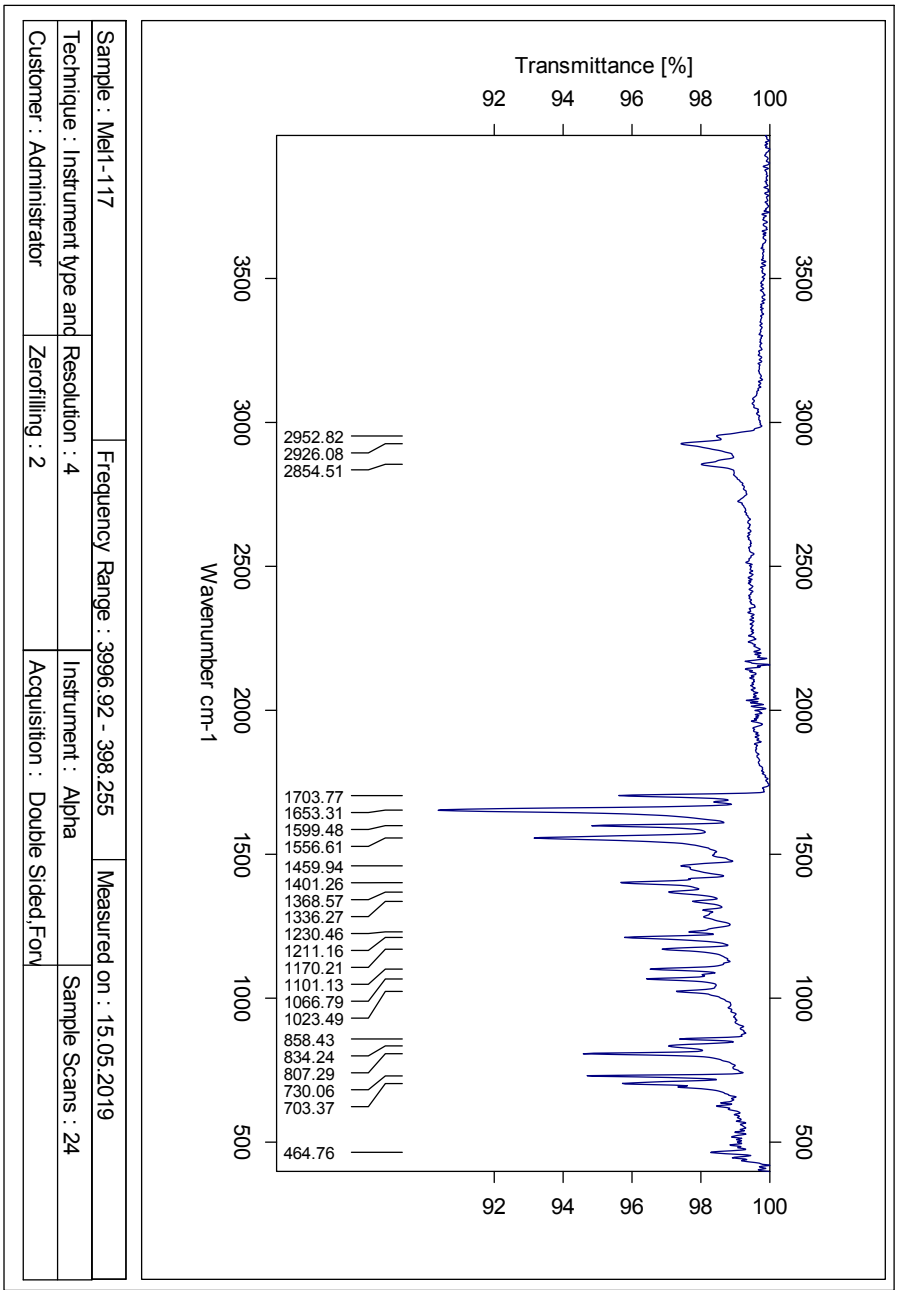

Figure 47: IR spectra of compound **13**.

Elemental Composition Report **Page 1**

Single Mass Analysis
Tolerance = 2.0 PPM / DBE: min = -50.0, max = 50.0
Element prediction: Off
Number of isotope peaks used for i-FIT = 3

Monoisotopic Mass, Even Electron Ions
7466 formula(e) evaluated with 9 results within limits (all results (up to 1000) for each mass)
Elements Used:
C: 0-100 H: 0-150 N: 0-10 O: 0-10 S: 0-4
2019-481 239 (4.652) AM2 (Ar,35000.0,0.00,0.00); Cm (225:239)
1: TOF MS ASAP+

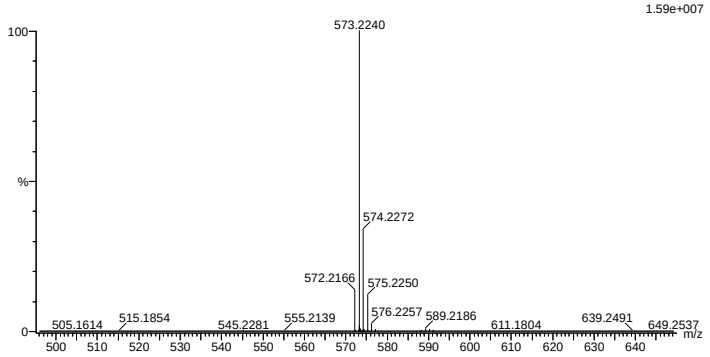

Minimum:				-50.0				
Maximum:		5.0	2.0	50.0				
Mass	Calc. Mass	mDa	PPM	DBE	i-FIT	Norm	Conf(%)	Formula
573.2240	573.2244	-0.4	-0.7	13.5	1112.8	0.087	91.71	C25 H33 N8 O6 S
	573.2230	1.0	1.7	8.5	1115.5	2.824	5.94	C24 H37 N4 O10 S
	573.2246	-0.6	-1.0	16.5	1116.5	3.761	2.33	C33 H37 N2 O3 S2
	573.2237	0.3	0.5	4.5	1121.5	8.850	0.01	C17 H37 N10 O8 S2
	573.2239	0.1	0.2	7.5	1122.2	9.500	0.01	C25 H41 N4 O5 S3
	573.2237	0.3	0.5	17.5	1123.4	10.667	0.00	C32 H33 N2 O8
	573.2250	-1.0	-1.7	22.5	1124.2	11.471	0.00	C33 H29 N6 O4
	573.2246	-0.6	-1.0	3.5	1125.2	12.515	0.00	C18 H41 N10 O3 S4
	573.2233	0.7	1.2	-1.5	1126.1	13.378	0.00	C17 H45 N6 O7 S4

Figure 48: Mass spectra of compound **13**.

M Spectroscopic Data - Compound 15

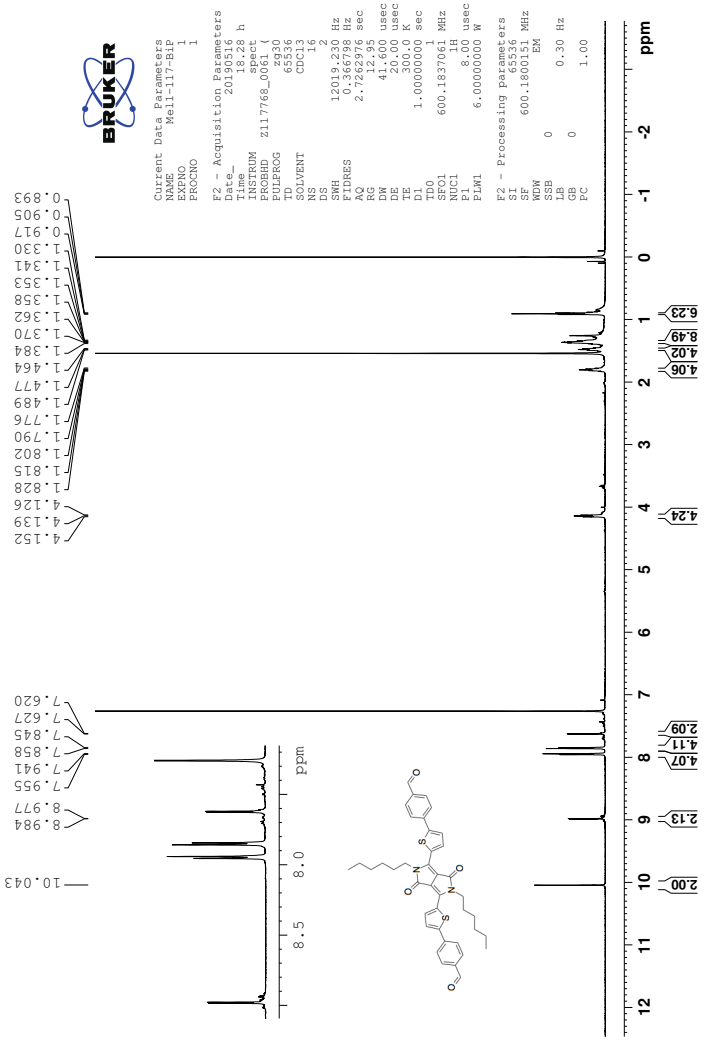

Figure 49: ^{1}H spectrum of compound **15**.

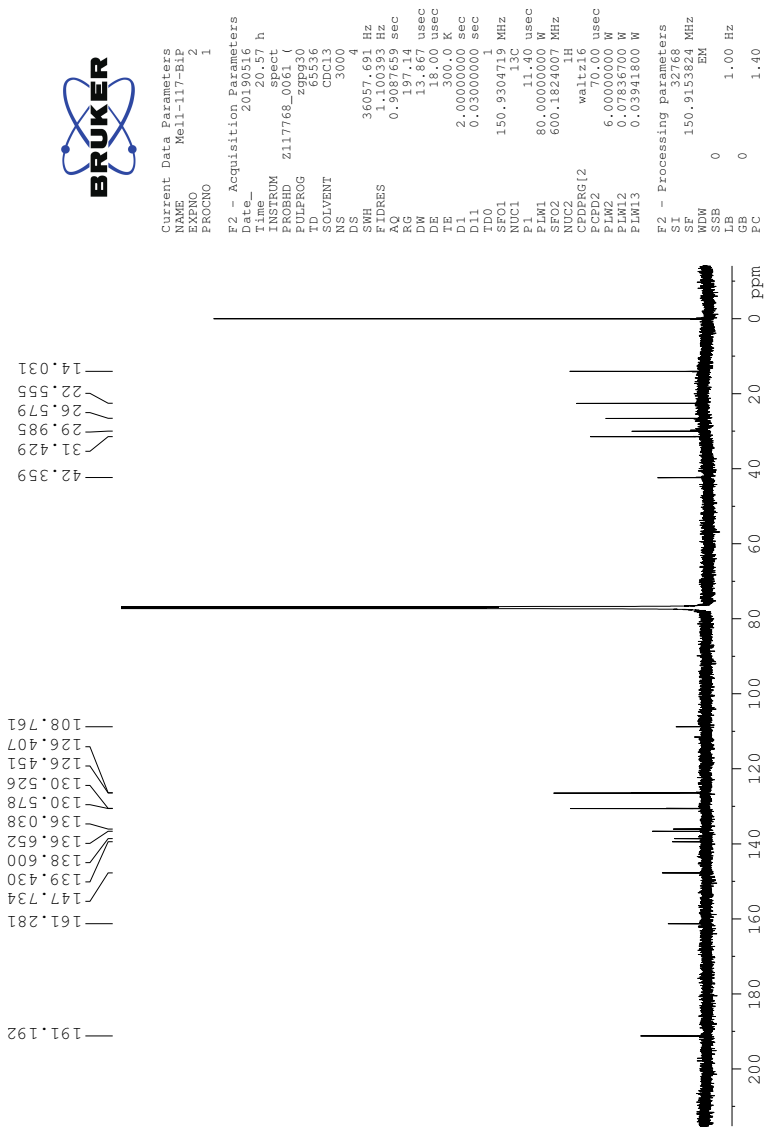

Figure 50: ^{13}C NMR spectra of compound **15**.

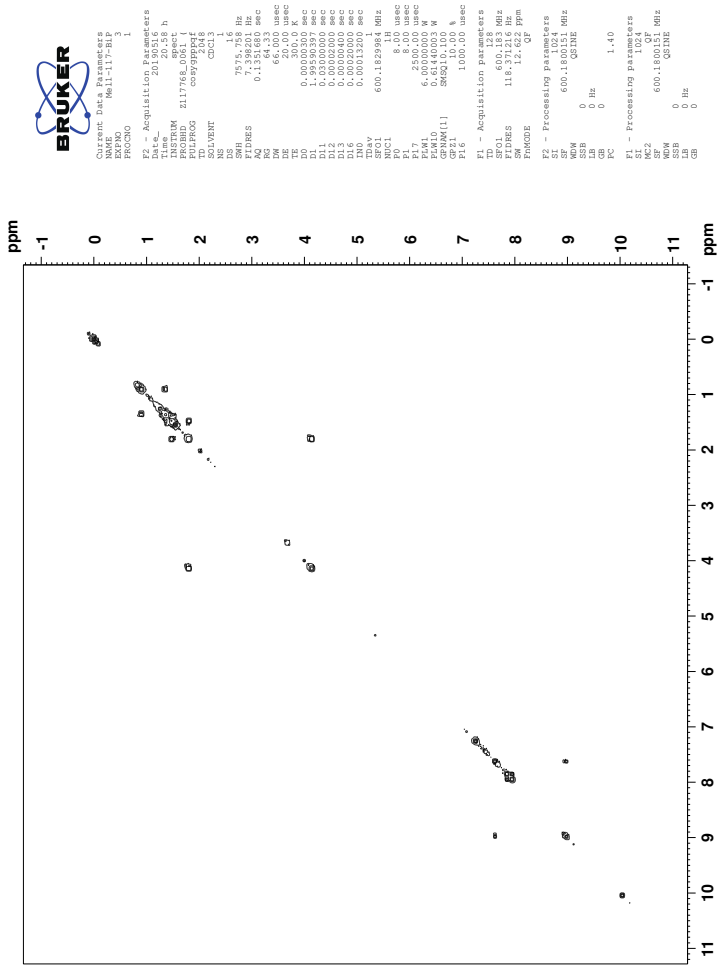

Figure 51: COSY NMR spectra of compound **15**.

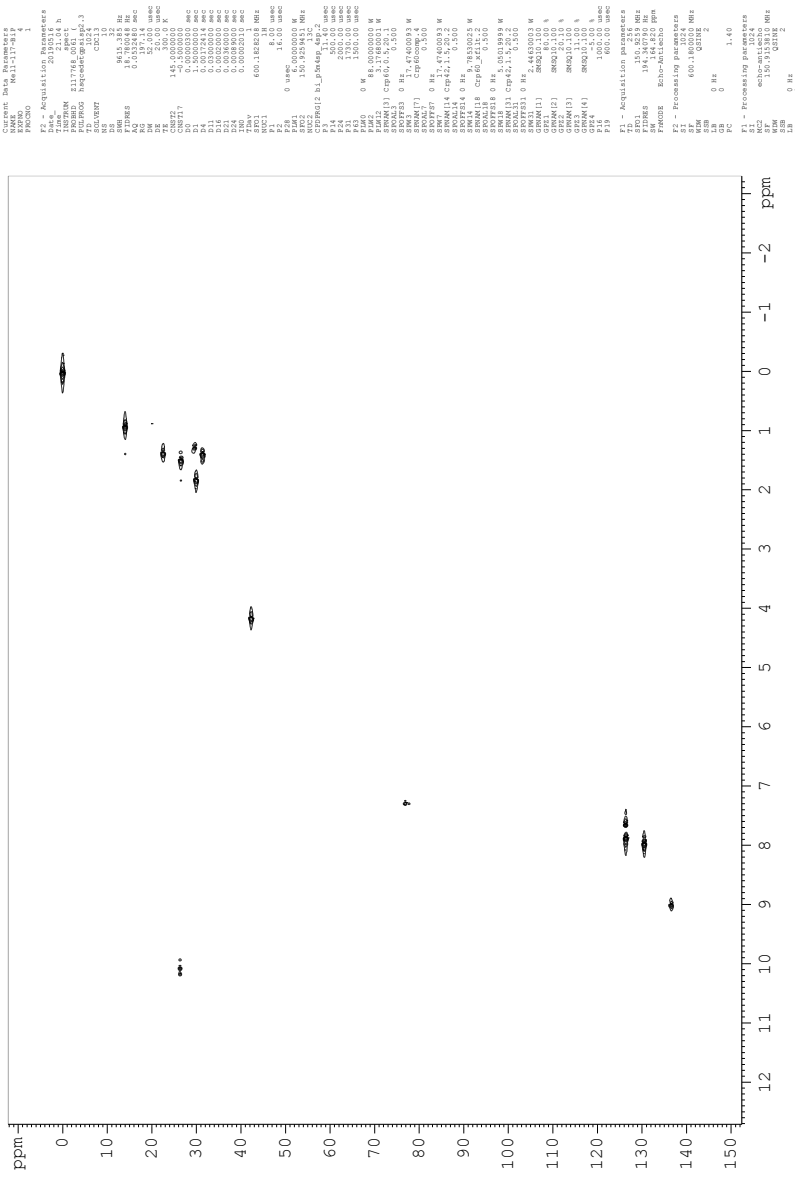

Figure 52: HSQC NMR spectra of compound **15**.

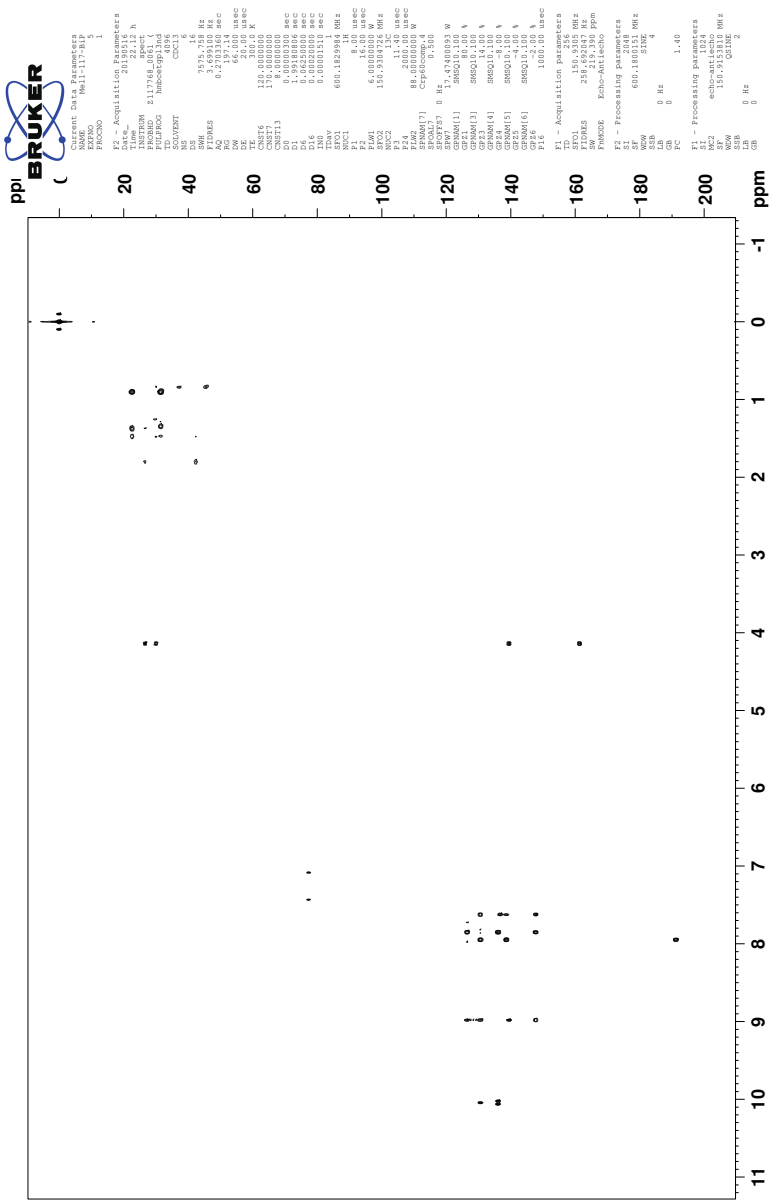

Figure 53: HMBC NMR spectra of compound **15**.

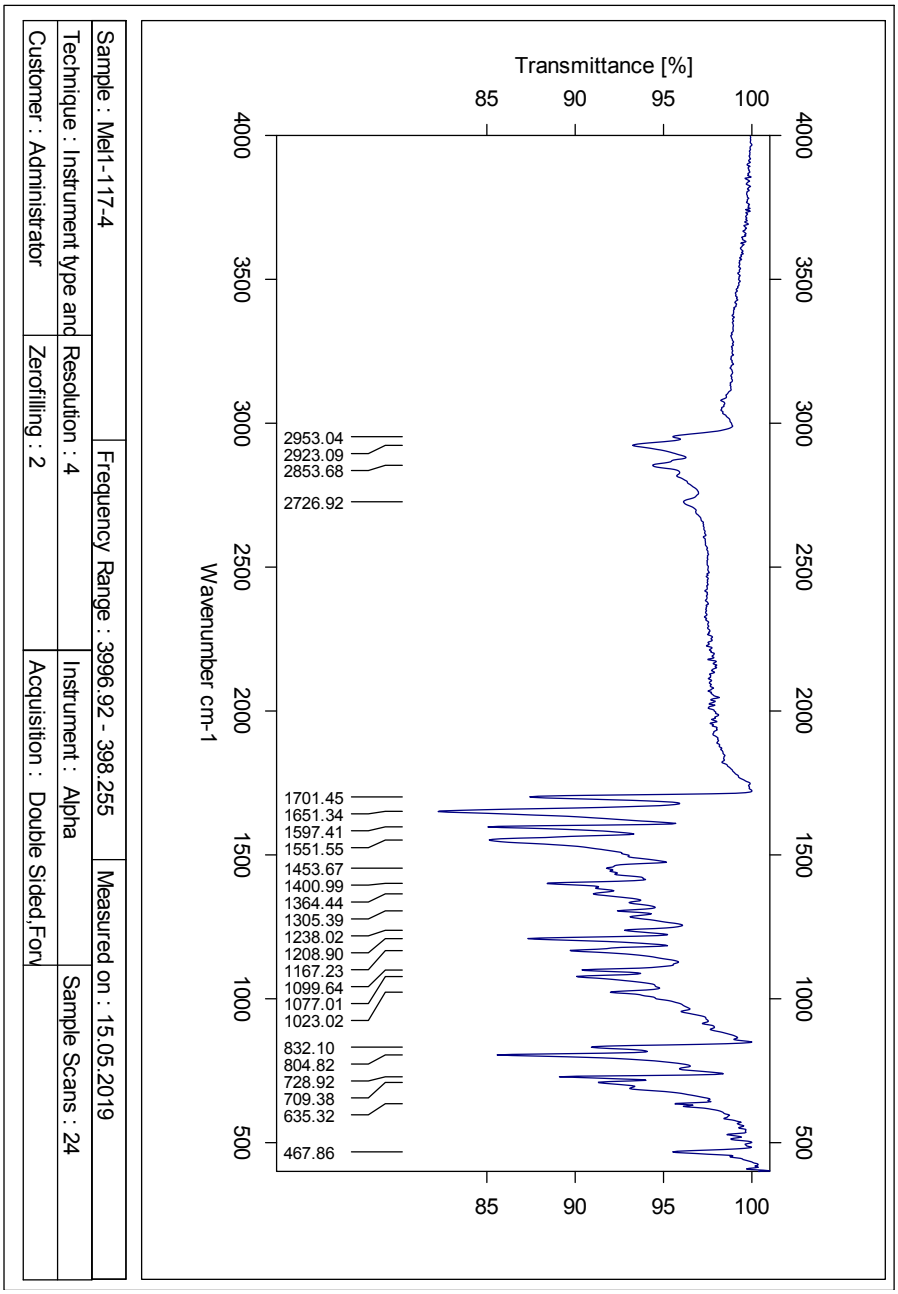

Figure 54: IR spectra of compound **15**.

Elemental Composition Report **Page 1**

Single Mass Analysis
Tolerance = 2.0 PPM / DBE: min = -50.0, max = 50.0
Element prediction: Off
Number of isotope peaks used for i-FIT = 3

Monoisotopic Mass, Even Electron Ions
7730 formula(e) evaluated with 10 results within limits (all results (up to 1000) for each mass)
Elements Used:
C: 0-100 H: 0-150 N: 0-10 O: 0-10 S: 0-4
2019-482 300 (5.842) AM2 (Ar,35000.0,0.00,0.00); Cm (283:302)
1: TOF MS ASAP+

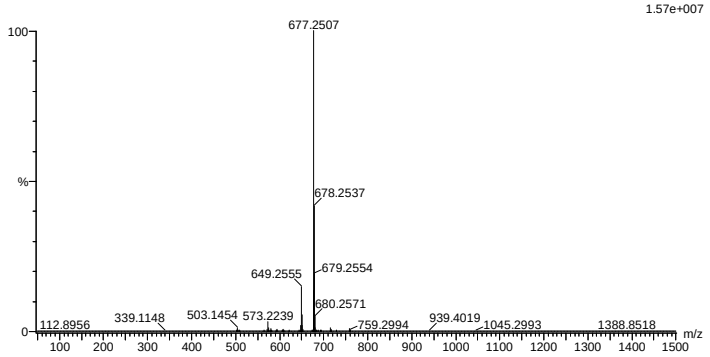

Minimum:				-50.0				
Maximum:		5.0	2.0	50.0				
Mass	Calc. Mass	mDa	PPM	DBE	i-FIT	Norm	Conf(%)	Formula
677.2507	677.2514	-0.7	-1.0	30.5	958.8	0.761	46.71	C48 H37 O2 S
	677.2508	-0.1	-0.1	21.5	959.2	1.180	30.74	C40 H41 N2 O4 S2
	677.2499	0.8	1.2	22.5	960.4	2.417	8.92	C39 H37 N2 O9
	677.2512	-0.5	-0.7	27.5	961.0	2.990	5.03	C40 H33 N6 O5
	677.2506	0.1	0.1	18.5	961.2	3.156	4.26	C32 H37 N8 O7 S
	677.2515	-0.8	-1.2	17.5	961.5	3.495	3.03	C33 H41 N8 O2 S3
	677.2501	0.6	0.9	12.5	962.5	4.470	1.15	C32 H45 N4 O6 S3
	677.2499	0.8	1.2	9.5	964.7	6.661	0.13	C24 H41 N10 O9 S2
	677.2508	-0.1	-0.1	8.5	966.1	8.078	0.03	C25 H45 N10 O4 S4
	677.2495	1.2	1.8	3.5	967.0	9.030	0.01	C24 H49 N6 O8 S4

Figure 55: Mass spectra of compound **15**.

N Spectroscopic Data - Compound 18

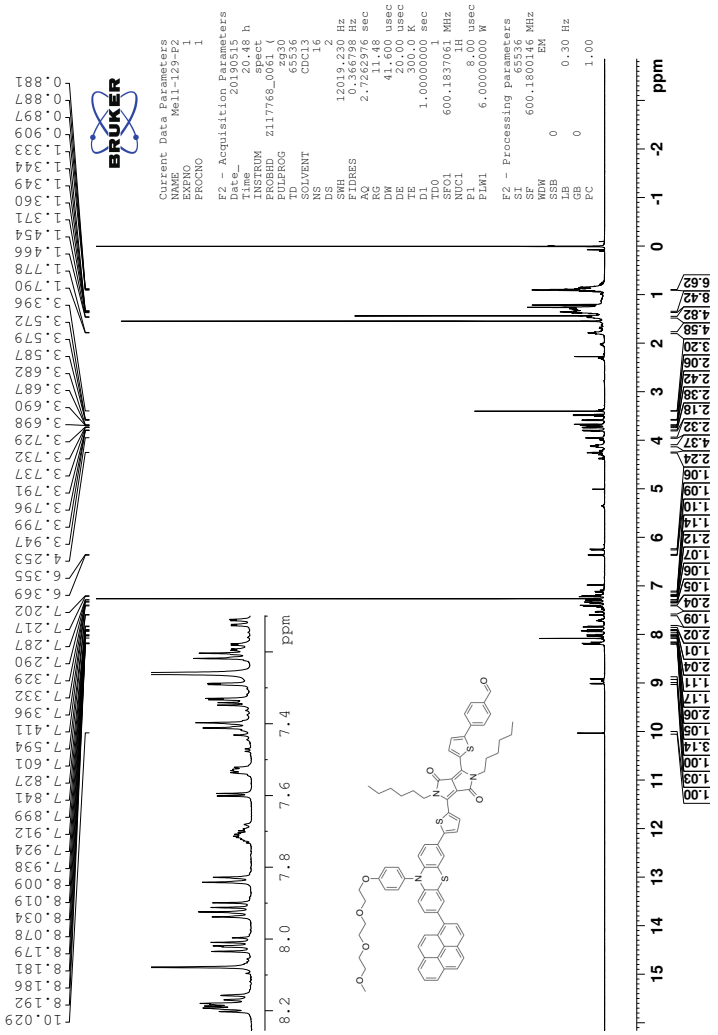

Figure 56: ^{1}H spectrum of compound **18**.

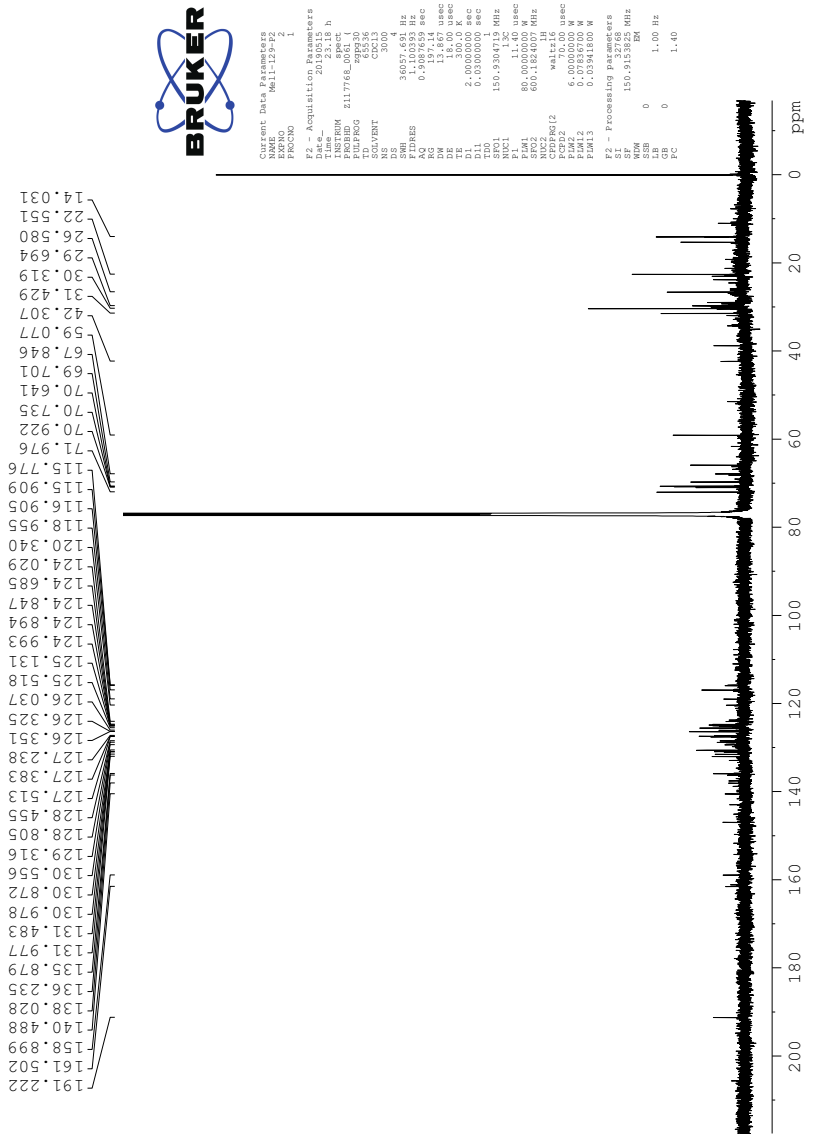

Figure 57: ^{13}C NMR spectra of compound **18**.

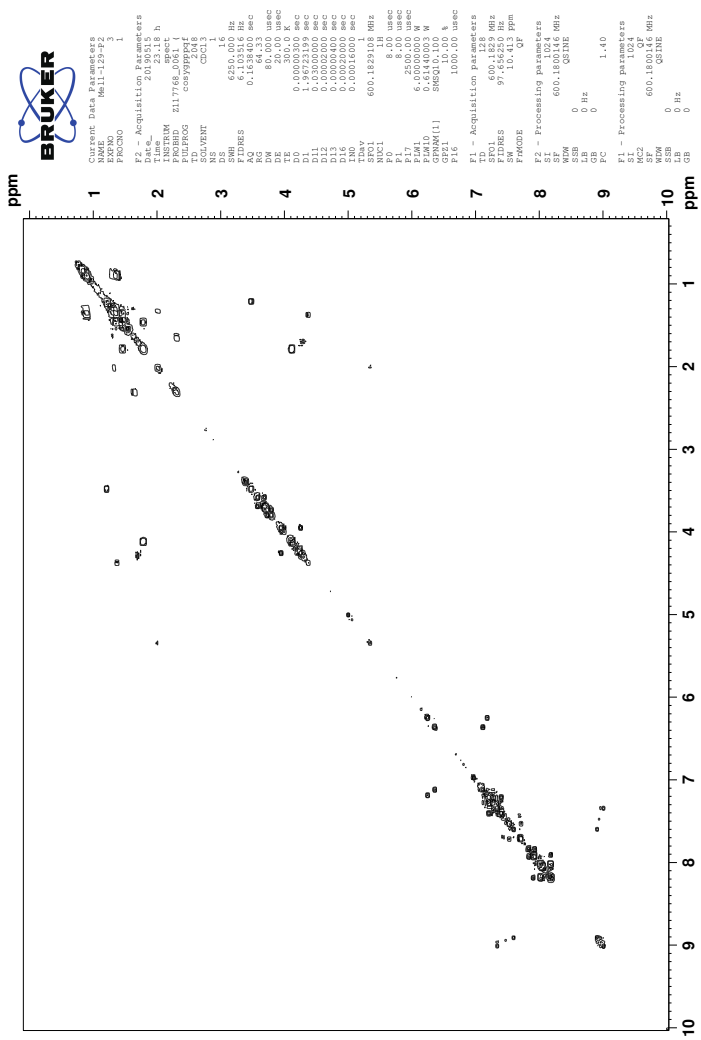

Figure 58: COSY NMR spectra of compound **18**.

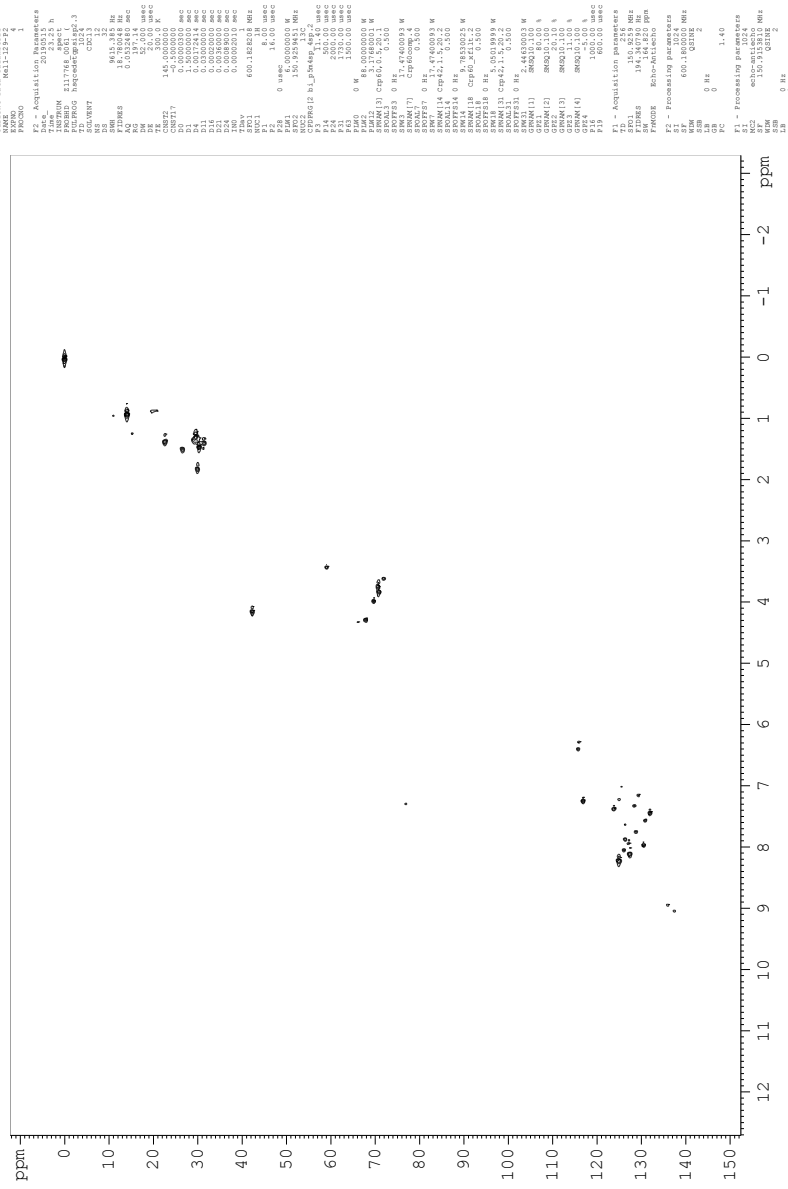

Figure 59: HSQC NMR spectra of compound **18**.

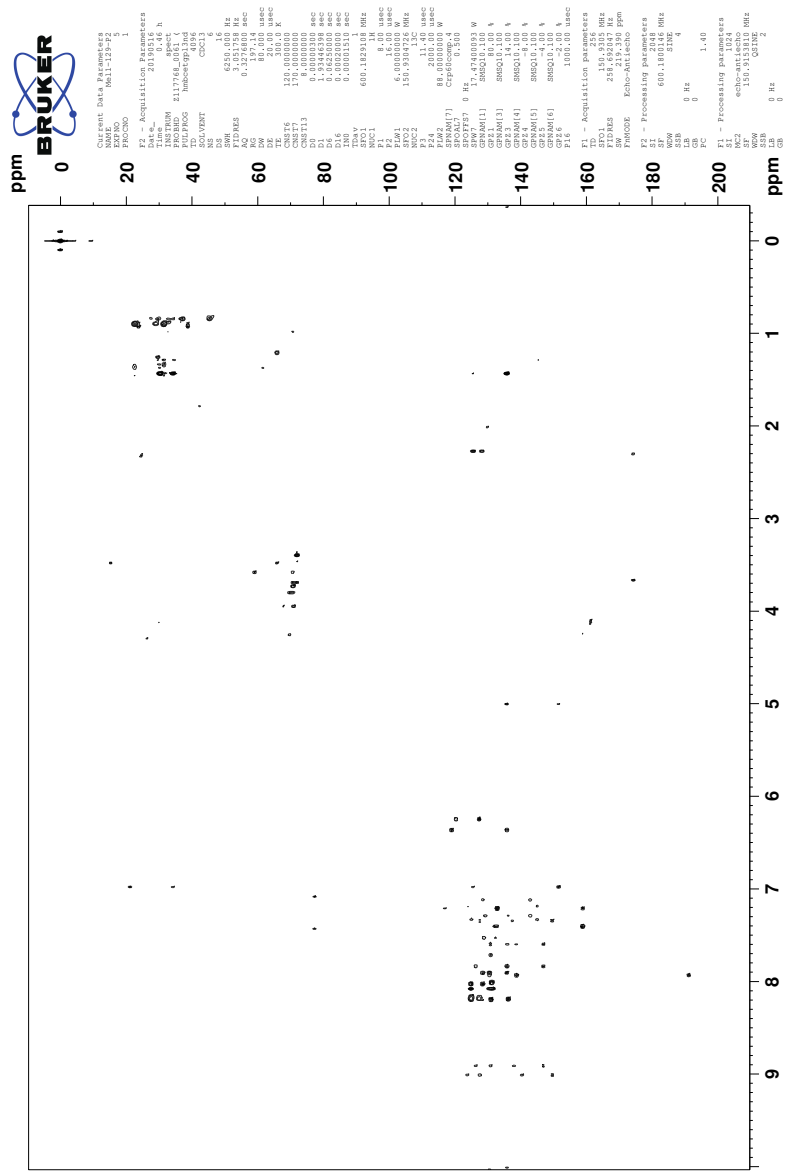

Figure 60: HMBC NMR spectra of compound **18**.

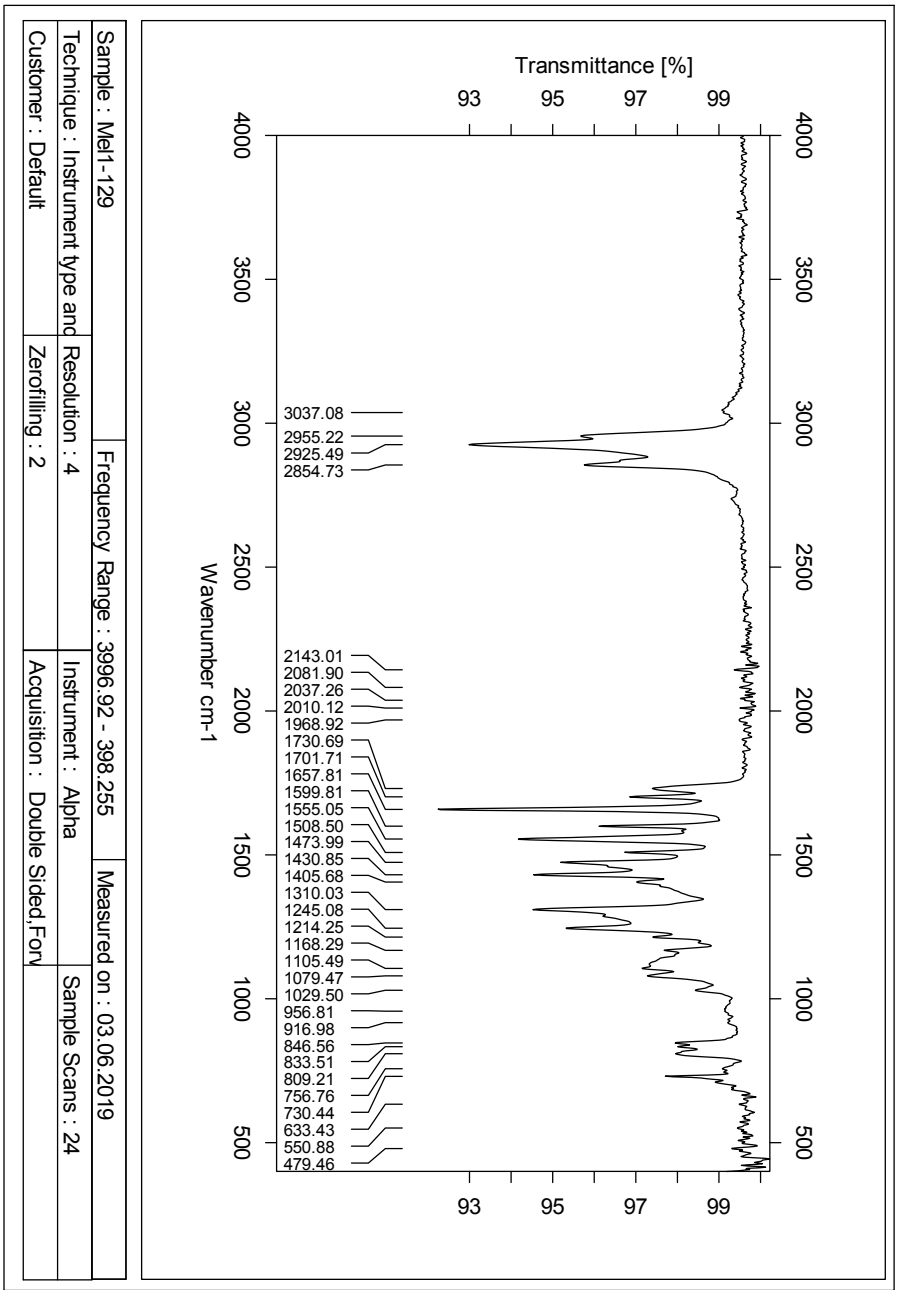

Figure 61: IR spectra of compound **18**.

O Spectroscopic Data - Compound MEL3

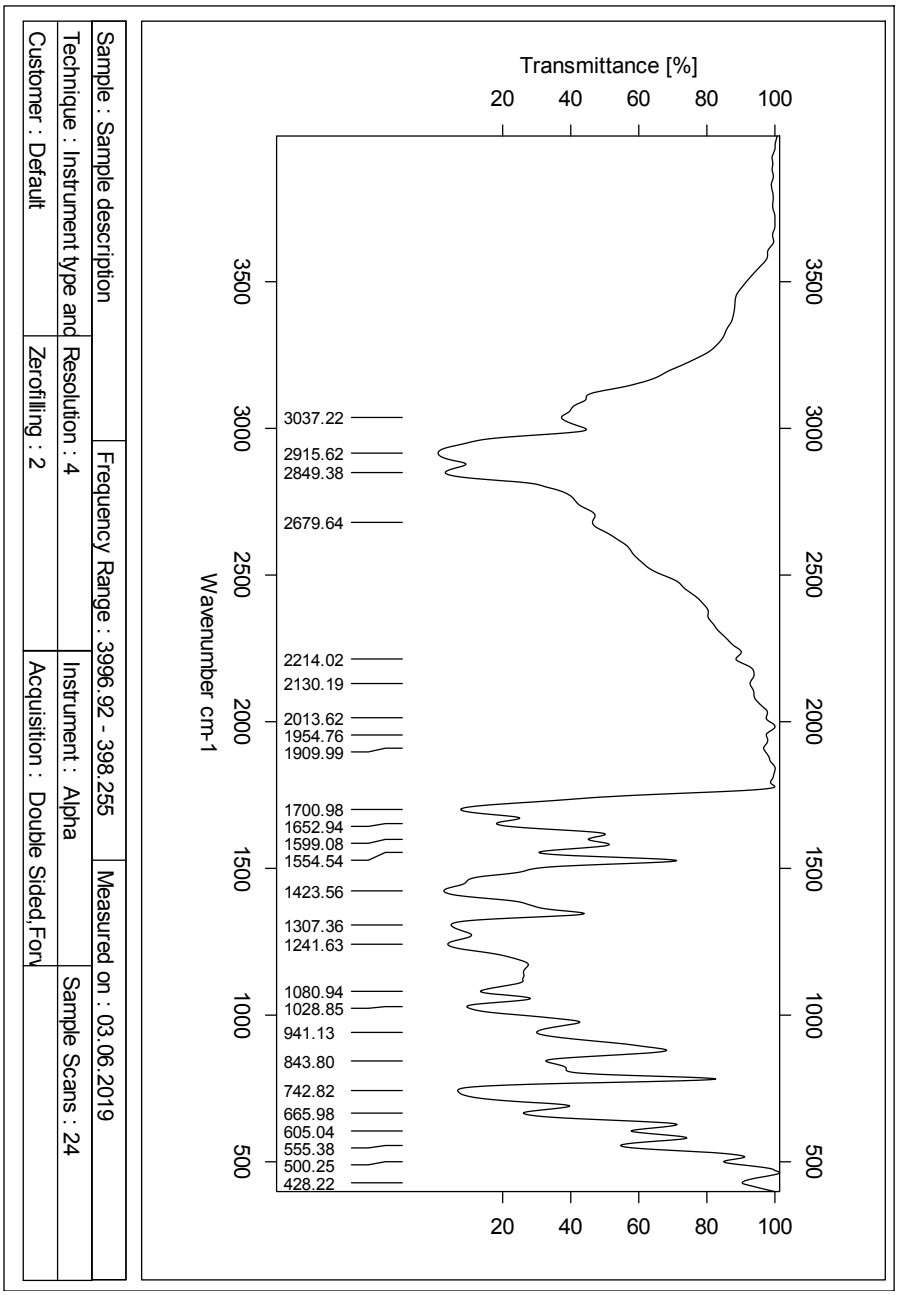

Figure 62: IR spectra of compound **MEL3**.

Elemental Composition Report **Page 1**

Single Mass Analysis
Tolerance = 2.0 PPM / DBE: min = -50.0, max = 50.0
Element prediction: Off
Number of isotope peaks used for i-FIT = 3

Monoisotopic Mass, Even Electron Ions
3956 formula(e) evaluated with 2 results within limits (all results (up to 1000) for each mass)
Elements Used:
C: 2-100 H: 0-150 N: 0-6 O: 0-10 S: 0-3
2019_556_20190605re 28 (0.321) AM2 (Ar,35000.0,0.00,0.00); ABS; Cm (17:28)
1: TOF MS ES+

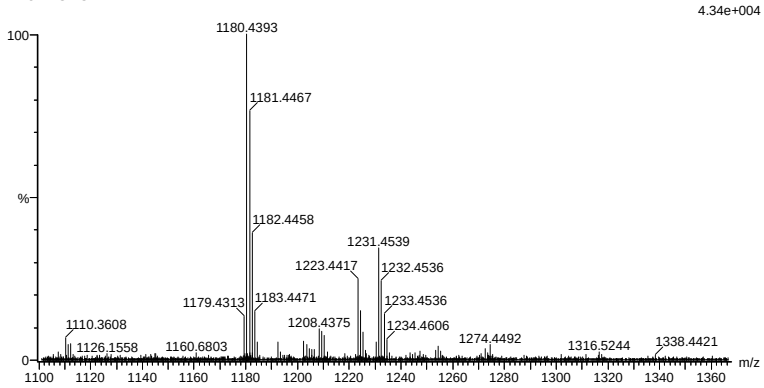

Minimum:				-50.0				
Maximum:		5.0	2.0	50.0				
Mass	Calc. Mass	mDa	PPM	DBE	i-FIT	Norm	Conf(%)	Formula
1231.4539	1231.4536	0.3	0.2	43.5	308.6	1.287	27.61	C76 H71 N4 O6 S3
	1231.4522	1.7	1.4	38.5	307.7	0.323	72.39	C75 H75 O10 S3

Figure 63: Mass spectra of compound **MEL3**.

Monica Eian Løberg

Synthesis of Phenothiazine Dyes

NTNU
Kunnskap for en bedre verden